CONTINUOUS L-DOPA SECRETION BY AAV GENE THERAPY TO IMPROVE THE TREATMENT OF PARKINSON'S DISEASE

Antunes, Andre Saraiva Leao Marcelo

Awarding institution:
King's College London

CONTINUOUS L-DOPA SECRETION BY AAV GENE THERAPY TO IMPROVE THE TREATMENT OF PARKINSON'S DISEASE

André Saraiva Leão Marcelo Antunes

A thesis submitted to King's College London

for the degree of Doctor of Philosophy

Department of Infectious Diseases
King's College London
School of Medicine

-April 2016-

“I have no doubt at all that science and peace will one day conquer ignorance and violence. The future belongs to those who serve mankind. The young scientists know many secrets, which we do not. Their morale must remain high. Laboratories must fill the world and you must, at the end of your lives, be able to say that you have done what you could”

Louis Pasteur

Abstract

Parkinson's disease (PD) is characterised by progressive degeneration of the dopaminergic neurons in the substantia nigra leading to severe motor complications. Standard oral treatment with L-DOPA provides powerful symptomatic relief, but disabling side effects eventually develop due to the pulsatile stimulation of the dopamine receptors. In this thesis, two gene therapy strategies were evaluated as potential treatments to diminish the fluctuations inherent to oral medication.

In the first project, I evaluated a proof-of-concept for AAV-mediated continuous L-DOPA synthesis in the periphery. I could show that, in healthy mice, hepatic L-DOPA production and release can be achieved by the delivery of tyrosine hydroxylase (*TH*) and GTP-cyclohydrolase-1 (*GCH1*), but to achieve plasma L-DOPA levels that approximate those achieved with oral treatment additional organs may need to be targeted. Therefore a tricistronic vector was generated that encoded *TH*, *GCH1* and 6-pyrovoyltetrahydopterin synthase (*PTPS*) under the control of a ubiquitous promoter to achieve L-DOPA synthesis in muscle and liver. Preclinical studies are currently ongoing to test the potential of this vector.

The second project builds on strong preclinical data generated in a rat model of PD and assesses safety and efficacy of an AAV vector harbouring *TH* and *GCH1* delivered to the brain of MPTP-lesioned non-human primates (NHP). I show that intervention is safe and leads to symptomatic improvement without worsening pre-established dyskinesia. However, it was discovered that vector production invariably leads to the formation of two vector species due to recombination between identical promoter sequences. Alternative vectors were designed with the goal to further improve transgene expression and clinical effect, and to avoid the generation of additional vector species. However, these did not prove to be superior in animal models of PD.

The data indicate that (1) AAV-mediated continuous L-DOPA delivery in the periphery is feasible but requires further optimisation and assessment in animal models to fully demonstrate proof-of-concept, (2) AAV-mediated continuous L-DOPA delivery has clinical relevance but may require improved vector design

and the achievement of stronger preclinical efficacy data to warrant progression to clinical trials.

Table of Contents

Index of Figures

Index of Tables

Abbreviations

3-MT	3-methoxytyramine
3-OMD	3-O-Methyldopa
6-OHDA	6-hydroxydopamine
AA	Amino acid residue
AADC	Aromatic l-amino acid decarboxylase
AAP	Assembly-activating protein
AAV	Adeno-associated virus
AC	Anterior commissure
AMD	Alpha-methyldopa
ANOVA	Analysis of variance
ARSA	Arylsulfatase A
AAVR	AAV receptor
AAVS1	AAV integration site 1
Ad	Adenovirus
ADA-SCID	Adenosine deaminase SCID
ADP	Adenosine diphosphate
AP	Anteroposterior
ATCC	American type culture collection
ATP	Adenosine triphosphate
BBB	Blood brain barrier
BH4	Tetrahydrobiopterin
bp	Base pairs
BSA	Bovine serum albumin
cAMP	Cyclic adenosine monophosphate
cDNA	Complementary DNA
CIP	Calf intestinal phosphatase
CMV	Cytomegalovirus
CNS	Central nervous system
COMT	Catechol-O-methyltransferase
CRISPR	Clustered regularly interspaced short palindromic repeats
DAT	Dopamine transporter
DBS	Deep brain stimulation

DHBA	2,3-Dihydroxybenzoic acid
dH_2O	Distilled water
ddH_2O	Double distilled water
DMEM	Dulbecco's modified eagle medium
DMSO	Dimethyl sulfoxide
DNA	Deoxyribonucleic acid
DOPAC	3,4-dihydroxyphenylacetic acid
dsAAV	Double-stranded AAV
DV	Dorsoventral
E1	E1 protein of papilloma virus
ED	Electrochemical detection
EDTA	1-(4-Aminobenzyl)ethlenediamine-N,N,N',N'-tetraacetic acid
EF1α	Elongation factor 1-alpha
ELISA	Enzyme-linked immunosorbent assay
EMCV	Encephalomyocarditis virus
FBS	Foetal bovine serum
FMDV	Foot-and-mouth disease virus
GABA	Gamma-aminobutyric acid
GAD	Glutamic acid decarboxylase
GCH1	GTP-cyclohydrolase-1
gcp	Genome containing particles
GDNF	Glial cell-derived neurotrophic factor
GFP	Green fluorescent protein
GMP	Good manufacturing practice
GPe	External segment of the globus pallidus
GPi	Internal segment of the globus pallidus
hAAT	Human alpha 1-antitrypsin promoter
HCR	Hepatic control region
HEK293T	Human embryonic kidney 293 cells
H&E	Haematoxylin and eosin staining
hFIX	Human clotting factor IX
hFIXco	Human clotting factor IX gene codon optimised
HPLC	High-performance liquid chromatography

HR	Homologous recombination
HRP	Horseradish peroxidase
HSPG	Heparate sulphate proteoglycan
HSV-1	Herpes simplex virus 1
HTRA2	High temperature requirement protein A2
HVA	Homovanillic acid
IHC	Immunohistochemistry
ILAS	Institute of laboratory animal sciences
IMS	Industrial methylated spirit
IRES	Internal ribosome entry site
ITR	Inverted terminal repeat
LB	Lysogeny broth
LCA	Leber's congenital amaurosis
L-DOPA	L-3,4-dihydroxyphenylalanine
LID	L-DOPA-induced dyskinesia
LPL	Human lipoprotein lipase
LRRK2	Leucine-rich repeat kinase 2
MAO	Monoamine oxidase
ML	Mediolateral
MLD	Metachromatic leukodystrophy
MOI	Multiplicity of infection
MPSIIIA	Mucopolysaccharidosis type IIIA
MPTP	1-methyl-4-phenyl-1,2,3,6-tetrahydropyridine
MWCO	Molecular weight cut off
mRNA	Messenger RNA
NCBI	National center for biotechnology information
NEB	New England Biolabs
NHP	Non-human primate
NGF	Nerve growth factor
NTN	Neuturin
NTP	Nucleoside triphosphate
OD	Optical density
ORF	Open reading frame

OSA	1-Octanesulfonic acid
OTCD	Ornithine transcarbamylase deficiency
PAGE	Poly-acrylamide gel electrophoresis
PAH	Phenylalanine hydroxylase
PBS	Phosphate buffered saline
PC	Posterior commissure
PCA	Perchloric acid
PCR	Polymerase chain reaction
PD	Parkinson's disease
PDGFR	Platelet-derived growth factor receptor
PEI	Polyethylinimine
PFA	Paraformaldehyde
PH	Peak height
PHR	Peak height ratio
PINK1	PTEN-induced putative kinase 1
PTEN	Phosphatase and tensin homolog
PTPS	6-Pyruvoyl-tetrahydropterin synthase
qPCR	Quantitative real-time PCR
rAAV	Recombinant AAV vectors
RE	Restriction endonuclease
RNA	Ribonucleic acid
RPE65	Retinal pigment epithelium-specific protein
RT	RT reverse transcriptase
SCID-X1	X-linked severe combined immunodeficiency
SDS	Sodium dodecyl sulphate
SEM	Standard error of the mean
SMA	Spinal muscular atrophy
SMN1	Survival of motor neuron 1
SNc	Substantia nigra pars compacta
ssDNA	Single-stranded DNA
STD	Standard
STN	Subthalamic nucleus
Str	Striatum

SURE	Stop Unwanted Rearrangement Events
SV40	Simian virus 40
SYN	Human synapsin promoter
TAE	Tris base, acetic acid and EDTA buffer
TALENs	Transcription activator-like effector nucleases
TEMED	N,N,N',N'-tetramethylethylenediamine
TH	Tyrosine hydroxylase
tTH	Truncated TH
UCLA	University of California, Los Angeles
UPDRS	Unified Parkinson's Disease Rating Scale
VA RNA	Viral associated RNA
VMAT2	Vesicular monoamine transporter 2
VP	Viral protein
VTA	Ventral tegmental area
WHX	Woodchuck hepatitis virus X protein
WPRE	Woodchuck Posttranscriptional Regulatory Element
WT	Wild type

Acknowledgements

First and foremost I would like to express my sincere gratitude to my supervisors Els Henckaerts and Michael Linden for giving me the opportunity to join the lab and for their support throughout these four years. To Els especially, whose guidance and motivation were always encouraging and allowed me to grow as a scientist.

I would like to thank my thesis committee, Chad Swanson, Mary Collins and Stuart Neil for their scientific advice and support. I also want to thank Chad Swanson for organising the PhD Journal Club; it certainly deepened my understanding of virology and my sense of critical thinking.

I am deeply grateful to all the present and past lab members for their help, feedback, discussions and all the fun in and outside the lab. Profound gratitude goes to Leti, who made me feel welcome in the lab and in London since the very beginning. I have learned from you more than I could have ever imagined, from Spanish swear words to molecular cloning and, above all, how to be a determined scientist, always striving for the best without ever stopping to laugh. To Martino, for all the scientific discussions, the Friday kindergarten moments, for introducing me to raviolone and for the gigantic help with the formatting of this thesis. It would certainly not have looked as good without your help. To Sarah, whose drive and determination have inspired me. To Julie, for being such a fun and lovely person to work with, be around and dance with at the Christmas parties. To Núria, for all the random favours you promptly did and all the chats we had across the bench. To Stina and Zoé, it was fun working with you. To Faisal, for the help with the countless AAV production cell factories. To Kam, for all the fun and jokes.

I would like to thank Mike McDonald for the immense support, the valuable scientific discussions, patience and trust. It was a pleasure working with you and I hope we stay in touch. I also want to thank Tomas Björklund for the discussions throughout these years and especially for welcoming me twice in his lab in Lund. To Patrick for his kindness and patience with me during my visits to Lund.

My gratitude also goes to Sarah Salvage, for her support and scientific feedback. To Atsuko Hikima, who has been an invaluable and tenacious collaborator, without whom I would not have achieved so much. A special thank

you to Carl Hobbs for his immense competence, contribution and help whenever I needed. Your willingness to help others with a smile upon your face is something I will pass on.

Special thanks to Fernanda Kyle. Your company and unconditional support throughout these years were crucial and words cannot express how grateful I am to you.

At last but not least, I would like to thank my family: my parents Ruth and Fernando, my brother Daniel and my aunt Thelma. Your presence in my life has been constant and your importance has never been reduced by the ocean that has separated us for most of the time in the past ten years. I am profoundly thankful to have you all in my life.

Chapter 1 Introduction

1.1 Gene Therapy

1.1.1 History and Development

The development of gene therapy began in the early 1960s with the realisation that exogenous DNA could be introduced into mammalian cells (Rabotti 1963; Borenfreund et al. 1970). Years later, the discovery that the polyomavirus SV40 integrated its DNA into the host cell genome during the process of neoplastic transformation led to the assumption that stable and functional gene transfer between two different systems must be possible (Sambrook et al. 1968). Rather prematurely, in the early 1970s, a first attempt of gene transfer to treat three young patients suffering from arginase deficiency was performed by injecting them with the wild-type cottontail rabbit papilloma virus (CRPV) under the mistaken assumption that the wild-type virus would encode the gene for arginase (Orth et al. 1967; Terheggen et al. 1975). Only years later, with the advent of recombinant DNA technology, the development of methods for gene delivery into eukaryotic cells and a better understanding of the genetic basis of many diseases did the field regain confidence in the potential of gene therapy to treat human diseases (Graham & van der Eb 1973; Maniatis et al. 1976; Wigler et al. 1978; Mulligan et al. 1979; Jackson et al. 1992). However, in 1980 another rather premature study was conducted in humans, in which blood was reinfused in thalassemia patients after it was transfected *in vitro* with plasmids containing the human globin and a viral thymidine kinase gene. This study, severely criticised by the scientific community, had not received permission from the UCLA Institutional Review Board and led to the sanctioning of the principal investigator by the NIH (Sun 1982). This episode prompted the discussion on the ethics and public policy aspects of gene therapy ultimately leading to the creation of a committee by the NIH to regulate the application of gene therapy in humans (Friedmann 1992; Sheridan 2011). The episode also preceded a 10-year gap in which no clinical trials of gene transfer were attempted. During this time researchers gained a better understating of the biology of different viruses and, more importantly, they learned how to modify

viral genomes and efficiently produce recombinant vectors (Shimotohno and Temin 1981; Doehmer et al. 1982; Mann, Mulligan, and Baltimore 1983; Miller, Law, and Verma 1985; Markowitz, Goff, and Bank 1988; Howley and Livingston 2009). The ability of retroviruses to efficiently transduce mammalian cells and integrate their genomes made them a strong candidate for gene therapy vectors. In 1990, the first gene therapy trial was approved. The therapy was tested in two young patients with severe combined immunodeficiency (ADA-SCID) who received a reinfusion of peripheral blood T cells transduced with a retroviral vector carrying the adenosine deaminase cDNA (Blaese et al. 1995). Although the therapeutic benefit to the patients was modest, the demonstration that gene therapy could be safely conducted led to an increased number of clinical trials for a broad range of inherited disorders and cancers. However, in 1999 the field had a major clinical setback after the death of a young patient due to vector-associated toxicity. A young man received a recombinant adenoviral vector to treat ornithine transcarbamylase deficiency (OTCD), the most common metabolic disorder of the urea cycle, and died 98 hours later due to an acute systemic inflammation and multi-organ failure caused by a strong immune response to the adenoviral vector (Raper et al. 2003). Not much later, in a gene therapy trial for X-linked severe combined immunodeficiency (X-linked SCID), 5 out of 20 treated children developed leukaemia, one of whom died, due to insertional mutagenesis caused by the Moloney murine leukaemia virus–based gammaretroviral vector (Cavazzana-Calvo et al. 2000; Gaspar et al. 2004; Howe et al. 2008; Hacein-Bey-Abina et al. 2008; Hacein-Bey-Abina et al. 2010; Gaspar et al. 2011). Notwithstanding this fatal case, the X-linked SCID trial was regarded as successful, with cure and survival rates similar to those associated with matched-sibling donor allogeneic hematopoietic stem cell transplantation. In the past decade a variety of gene delivery strategies have been developed and approved for clinical trials, some of them leading to the effective treatment of diseases such as haemophilia B (Nathwani et al. 2011), sickle-cell disease, beta-thalassemia (Negre et al. 2016), lipoprotein lipase deficiency (LPLD) (Ylä-Herttuala 2012) and inoperable melanoma (Goins et al. 2014).

Although gene therapy was first conceived as a strategy to treat hereditary monogenic disorders, the notion that gene therapy can be used to treat

degenerative and even infectious diseases in humans has now long been accepted in the scientific and public policy circles. Nowadays, medical conditions including cancer, cardiovascular diseases, infectious diseases and neurodegenerative disorders are also considered for gene therapy.

New technologies have expanded the potential of gene therapy with tools that allow for *in vivo* gene editing. Tools such as transcription activator–like effector nucleases (TALENs) have recently been used to successfully cure a new-born from leukaemia (Reardon 2015). Furthermore, the clustered regularly interspaced short palindromic repeat (CRISPR)-associated nuclease Cas9, although not yet tested in humans, holds great potential for future genetic therapies (Sterneckert et al. 2014).

1.1.2 Forms of Gene Delivery

The main goal of gene therapy is to safely achieve stable expression of a gene of interest in the appropriate tissue. In this pursuit, different strategies for gene delivery have been developed, each with particular characteristics as to which type of cells they target and for how long the transgene is expressed. Delivery of transgenes can be divided in two forms: non-viral and viral.

1.1.2.1 Non-viral Mediated Gene Delivery

Non-viral vectors for gene delivery generally consist of double-stranded DNA plasmids associated with cationic liposomes to allow passage through the cell membrane (Pedroso de Lima et al. 2001; Wong et al. 2007). However, physical methods, such as electroporation or propulsion, can also be used to deliver DNA into a cell (Gehl 2003). Non-viral vectors are cheap, easy to produce and generally trigger a minimal immune response, however they still face the problem of low efficiency of gene delivery and expression in a therapeutic context (Lechardeur et al. 2005).

1.1.2.2 Viral Mediated Gene Delivery

Viral vectors are the main tool for gene delivery in gene therapy strategies. The ability of viruses to efficiently transfer and express their genetic information in different hosts and tissues has been exploited and viral vectors have been engineered to package a modified genome carrying a gene of interest in place of the viral genes.

Viral vectors can be subdivided in two categories: integrating and non-integrating vectors. Integrating vectors insert their genetic material in the recipient's genome ensuring that their genes are passed on to future cell generations and are therefore used to transduce actively dividing cells. Non-integrating vectors, on the other hand, do not insert themselves in the recipient's genome and are generally used to transduce post-mitotic or non-dividing cells. While integrating vectors are stably inherited, their insertion into the human genome is never completely devoid of the risk of insertional mutagenesis.

To date different vectors for gene therapy have been developed which differ mainly in the mode and type of cells they transduce, their packaging capacity, gene expression profile and ability to elicit immune responses. These differences, together with the diversity of diseases that are potentially treatable by gene therapy, make it impossible to have one single vector that is suitable for all applications. The viral vectors most commonly used in gene therapy are derived from gammaretroviruses, lentiviruses, adenoviruses, adeno-associated viruses (AAV) and herpes simplex-1 viruses (HSV-1).

Because some of these viruses are pathogenic in their wild-type forms, their formation and replication in a therapeutic context is highly undesired. To avoid pathogenicity and increase their safety profile, mechanisms are employed during vector production to ensure the generation of replicative defective vectors. This can be achieved through the replacement of viral genes by the therapeutic transgene and the separation of *cis* and *trans* elements. *Cis* elements are the nucleic acid sequences that are biologically active, while *trans* elements are protein-coding sequences that act through the expressed proteins. This separation is a very important safety mechanism in vector production to impose a barrier for the formation of replication competent wild-type virus.

The popularity of AAV as a gene therapy vector has significantly grown in the last decades owing mainly to its ability to achieve long-term transgene expression, its low immunogenicity and the lack of pathogenicity associated to viral infection. Although a debate on the oncogenic potential of AAV has been recently sparked by a study linking AAV infection with the development of hepatocellular carcinoma (Nault et al. 2015), this study was resoundingly rejected by leading researchers in the fields of gene therapy and molecular genetics and more recent data refute the proposed link between AAV infection and hepatocellular carcinoma (Berns et al. 2015; Gil-Farina et al. 2016).

Since the study described in this thesis made use of AAV vectors, its biology and application in gene therapy will be discussed in further detail.

1.2 Adeno-Associated Virus

AAV belongs to the *Parvoviridae* family and is classified in the *Dependovirus* genus due to its dependence on helper functions provided by other DNA viruses such as adeno- or herpes virus to complete a productive replication cycle. AAV is a nonenveloped, small virus (25nm) with a linear single-stranded DNA (ssDNA) genome of 4.7kb. The viral genome can be either sense or antisense and contains two main open reading frames (ORF): *rep* and *cap.* The *rep* ORF codes for the non-structural proteins Rep78, Rep68, Rep52 and Rep40, while the *cap* ORF codes for the structural proteins VP1, VP2 and VP3 (Srivastava et al. 1983). Within the VP2 coding sequence, a cryptic ORF is present that codes for a protein involved in capsid assembly called assembly-activating protein (AAP) (Sonntag et al. 2010). The expression of a variety of proteins from such a limiting coding capacity is achieved by combining different promoters, alternative splicing and non-conventional start codons (Lusby et al. 1980; Marcus et al. 1981; Qiu et al. 2006).

The viral genome is further characterised by the presence of inverted terminal repeats (ITRs), 145bp imperfect palindromic sequences that flank the open reading frames and that self-anneal to form T-shaped hairpins. The ITRs provide all the *cis*-acting elements necessary for replication and packaging of the viral genome (Samulski et al. 1989) (Figure 1).

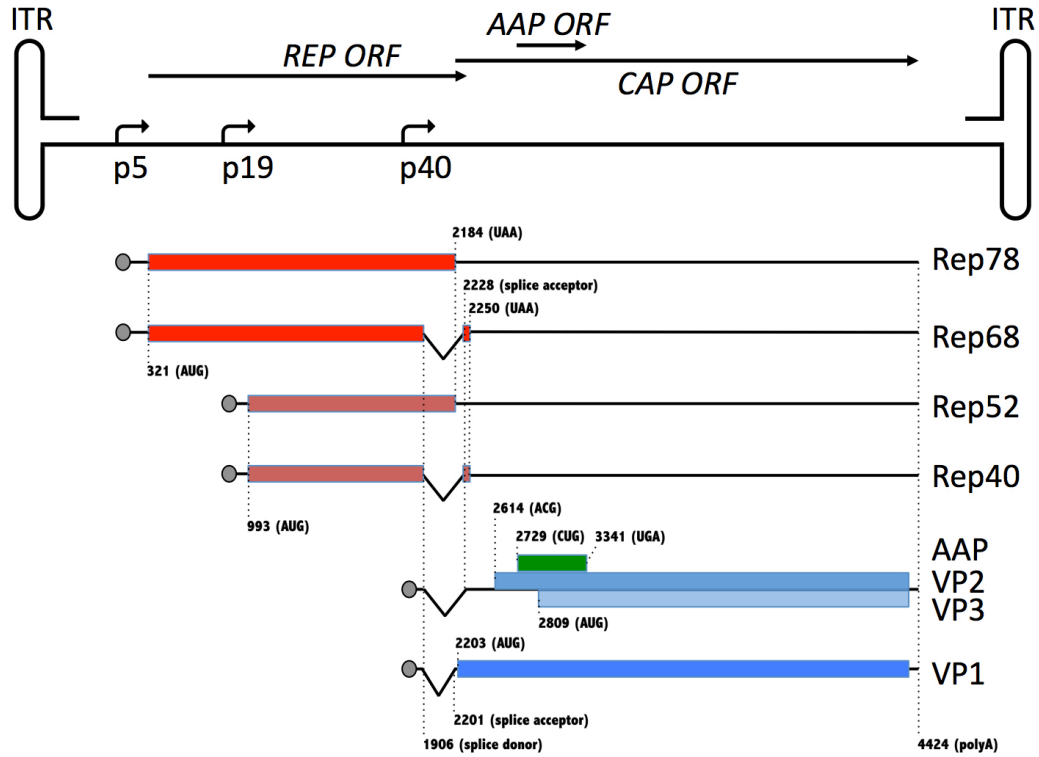

Figure 1: AAV genome, genes, transcriptional units and proteins.
There are three promoters, identified by their relative position in the genome: p5, p19 and p40. The p5 promoter controls the expression of the large Rep proteins Rep78 and the spliced variant Rep68. The p19 gives rise to the small Rep proteins Rep52 and Rep40. The p40 promoter controls the expression of the three capsid proteins VP1, VP2 and VP3, as well as of AAP. There is a single splice donor site and two splice acceptor sites, one of which (2228) is used most frequently. Alternative splicing and non-conventional start codons (for VP2 and AAP) allow the generation of 8 proteins (coloured boxes). All the AAV mRNAs use a single polyA tail located at the right end of the genome.

The 4.7kb genome is packaged in an icosahedral capsid formed by a total of 60 copies of VP1, VP2 and VP3, in a ratio of 1:1:10, respectively. The capsid proteins provide vital functions for the virus life cycle, such as host cell recognition and binding, entry and trafficking to the nucleus, release of the viral genome at the appropriate time and place, egress from the host cell, and escape from immune surveillance (Agbandje-McKenna & Kleinschmidt 2011). In total, 13 AAV serotypes have been isolated (AAV1-13), with AAV2 being the most extensively studied and best known. Among the differences between the 13 serotypes are the variations in their *cap* gene sequences that reflect their evolutionary relationship and phylogenetic proximity to each other. These variations play important roles in viral host cell binding, tissue tropism and determination of capsid antigenicity (Srivastava et al. 1983; Muramatsu et al. 1996; Chiorini et al. 1997; Rutledge et al. 1998; Chiorini et al. 1999; Gao et al. 2002; Gao et al. 2004;

Mori et al. 2004; Schmidt et al. 2006; Schmidt, Voutetakis, et al. 2008; Schmidt, Govindasamy, et al. 2008; Drouin & Agbandje-McKenna 2013).

1.2.1 AAV Life Cycle and Biological Barriers for Cell Transduction

AAV has a complex and tightly regulated life cycle characterised by the presence of a productive replicative and a latent phase. Under permissive conditions, such as co-infection with adeno- or herpes virus, the AAV DNA will undergo several rounds of replication before being packaged into newly formed capsids. Under non-permissive conditions, however, AAV will remain latent in the cell, either episomally or integrated in the host genome (Henckaerts & Linden 2010).

Infection begins with the attachment of the virus to the host cell surface. Following attachment, AAV interacts with the AAV receptor (AAVR) before being internalised through endocytosis and trafficked to the *trans*-Golgi network (Pillay et al. 2016).

The intricacies of AAV intracellular trafficking to the nucleus are not completely understood but AAV has been shown to co-localise with markers of early, late, recycling endosomes as well as lysosomes after internalisation and it is known that endosomal processing, which leads to conformational changes to the AAV capsid, is necessary for efficient AAV infection (Nonnenmacher & Weber 2011). Whether AAV uncoating occurs inside the nucleus or immediately prior to nuclear entry is still a matter of debate with existing evidence supporting both interpretations (Bartlett et al. 2000; Sanlioglu et al. 2000; Xiao et al. 2002; Lux et al. 2005). Following genome release, the single-stranded DNA must be converted into a double-stranded DNA genome for gene expression and replication. The essential elements required for AAV DNA replication are the viral ITRs, the large Rep proteins (Rep78 or Rep68) and a subset of helper-virus factors such as the adenoviral E1, E2A, E4orf6 proteins and the adenoviral non-coding VA1 RNA (Hauswirth and Berns 1977; Geoffroy and Salvetti 2005; Vogel et al. 2013).

The model for AAV replication was described several decades ago and it is often referred to as rolling hairpin replication (Kerr et al. 2005). It consists of a modified version of the plasmid rolling circle replication mechanism and

involves a strand displacement process. Replication of the AAV genome is shown in Figure 2 and begins with the synthesis of the second DNA strand with the self-annealed ITR on the 3' end of the genome functioning as a primer for unidirectional DNA synthesis. The extension from the 3' end results in a double-stranded molecule covalently attached at one side. The replication of the ITR that originally served as a primer is called terminal resolution and it requires the binding of Rep to a region of the ITR called Rep binding site (RBS) and subsequent nicking at the terminal resolution site (TRS) to generate a new free 3'-OH. DNA replication is resumed from the newly generated 3'-OH and the second ITR is copied. At the end of this process a double-stranded linear DNA molecule with palindromic ends is generated, which can fold back into T-shaped structures, thereby allowing a new round of replication by strand displacement to begin.

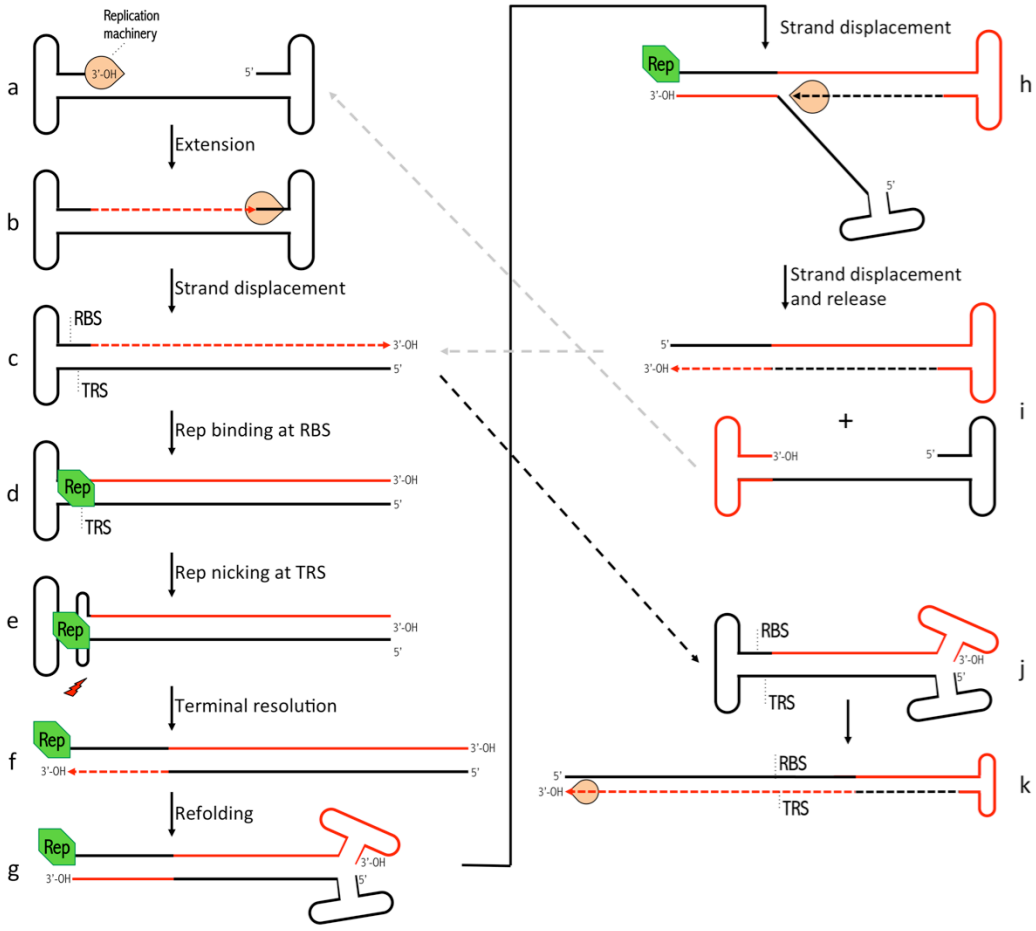

Figure 2: Rolling hairpin replication of AAV DNA.

The free 3'-OH provided by the self-annealed ITR (a) serves as the primer for DNA replication mediated by the cellular machinery (b). The right ITR is replicated by strand displacement, generating a double-stranded molecule covalently linked by the left ITR (c). Rep binds at the RBS in the left ITR (d) and nicks at the nearby TRS site (e) to allow the terminal resolution of the left ITR (f). The complementary ITR sequences at the right end of the genome fold back (g), freeing a new 3'-OH that can be used for another round of replication by strand displacement (h) that generates a new single-stranded AAV genome and a double-stranded molecule covalently linked by the right ITR (i). These molecules can then be used for another round of replication (grey arrows) or potentially could serve as packaging templates. If the refolding of the right ITR occurs prior to the terminal resolution of the left ITR (j) followed by replication by strand displacement, a dimeric replication intermediate can be formed (k). By subsequent RBS binding and TRS nicking the dimeric intermediate can re-enter the replication cycle.

Packaging occurs by inserting the newly synthesised AAV genomes into pre-assembled capsids, formed rapidly in the nucleus with help of the assembly activating protein (Sonntag et al. 2010). Packaging is known to be a slow reaction and the only *cis* acting elements necessary for this process are the AAV ITRs (McLaughlin et al. 1988). Experiments have demonstrated the interaction between Rep and capsids during genome packaging and that part of the capsid-associated Rep is covalently attached to the 5' end of replicated DNA (Wistuba et al. 1995; Prasad & Trempe 1995).

AAV encounters several biological barriers that appear to limit its ability to efficiently transduce certain tissues. The first one is the viral attachment and interaction with different factors present at the host cell surface. This step has a particular significance in defining tissue tropism and transduction efficiency of different serotypes. Successful AAV entry into the cell is greatly affected by attachment factor and co-receptor recognition. Heparan sulphate proteoglycan (HSPG) has been identified as one of the primary attachment factors for AAV2 and AAV3 (Summerford & Samulski 1998; Handa et al. 2000; Wong et al. 2015). In contrast, sialic acid has been identified as a primary attachment receptor for AAV4 and AAV5 (Kaludov et al. 2001; Walters et al. 2001). AAV7 and AAV8 were rescued from non-human primate tissues and their distinct tissue tropisms suggest that they use different cell surface receptors than other AAV serotypes (Summerford et al. 1999; Qing et al. 1999). AAV also requires co-receptors for efficient infection. For example, although both AAV2 and AAV3 use HSPG to attach to cells, AAV3 can transduce hematopoietic cells, which are not susceptible to transduction with AAV2, suggesting that co-receptors on the cell surface are required for infection and can influence the tropism of different AAV

serotypes. The integrin αVβ5 and the fibroblast growth factor receptor have been identified as co-receptors for AAV2. Similarly, platelet-derived growth factor receptor (PDGFR) has been identified as a co-receptor for AAV5 (Pilz et al. 2012). The abundance of AAV co-receptors on the surface of target cells and the activation of cellular pathways that trigger endocytosis can also be a rate-limiting factor in AAV infection (Duan, Yue, et al. 1998).

Viral trafficking, endosomal escape and nuclear import are interrelated processes and appear to be rate-limiting for many AAV serotypes. It has become increasingly recognised that following endocytosis, processing of AAV virions through the endosomal compartment is intricately linked to transduction. For example, when directly injected into the cytoplasm, AAV2 fails to accumulate in the nucleus, suggesting the necessity of endosomal processing for viral infection. Further, endosomal processing of AAV has been shown to lead to the externalisation of the phospholipase A2 catalytic domain, a functional domain relevant for viral infection (Sonntag et al. 2006). In addition, different serotypes might be distinctively affected by endosomal acidification depending on the stability of their capsid proteins (Ding et al. 2005; Nam et al. 2011; Horowitz et al. 2013).

The final steps for AAV transduction include viral uncoating and conversion of the single-stranded AAV genome to double-stranded DNA capable of expressing its genes. Although still an elusive matter, it is generally believed that AAV particles are transported into the nucleus prior to uncoating and that both processes represent rate-limiting steps for AAV infection (Seisenberger et al. 2001; Xiao et al. 2002).

In the absence of co-infection with a helper virus, AAV is not able to replicate and enters the latent phase of its life cycle by integrating into the host cell genome. Integration was first mapped to one locus in the human chromosome 19, termed *AAVS1*, and was shown to be a Rep dependent mechanism (Kotin & Siniscalco 1990; Kotin et al. 1991; Samulski et al. 1991; Surosky et al. 1997). More recently, several other integration hotspots were identified in the human genome but the AAVS1 locus remains by far the most frequently targeted by AAV (Hüser et al. 2014; Petri et al. 2015). A schematic representation of the AAV life cycle is shown in Figure 3.

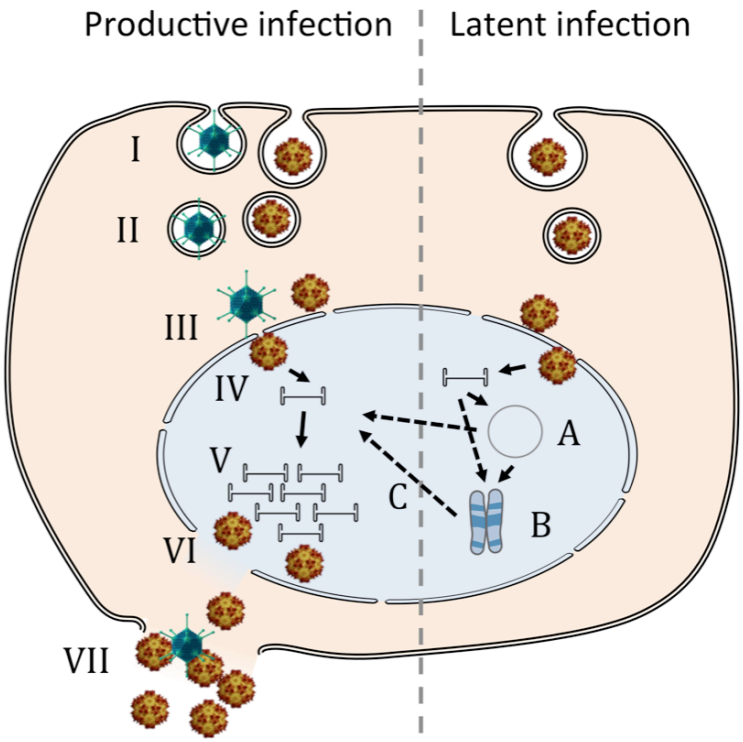

Figure 3: The AAV life cycle.
The AAV life cycle is divided between productive infection in the presence of helper virus (adenovirus in the picture) and latent infection in its absence. (I) The AAV particle enters the cell by receptor-mediated endocytosis and (II) is trafficked through the endosomal system to (III) the nuclear membrane. (IV) After translocation to the nucleus, the viral DNA is released and (V) undergoes several rounds of replication before being (VI) packaged in pre-formed capsids and (VII) egressing from the cell. In the absence of helper functions, the AAV particle reaches the nucleus where it can establish latency by (A) forming a stable circular episome or (B) by integrating into the human genome. In the event of helper virus superinfection, (C) the AAV genome can be rescued from its latent state and undergo productive replication. The relative sizes of the elements of this diagram are not in scale but are adapted for clarity.

1.3 Recombinant AAV Vectors

Integrated AAV has been shown to be rescued from the host genome upon infection with helper viruses (Hoggan, M. D., Thomas, G. F. and Johnson 1973). This observation suggested that rescue of the AAV genome from a plasmid should be possible if a helper virus was present. Indeed, when the AAV genome was cloned into a bacterial plasmid and exposed to a helper virus in culture cells, it was able to replicate and infect in a manner that was indistinguishable from wild-type virions. This breakthrough promoted rapid progress in the AAV field by facilitating the manipulation of its genome for the study of replication and

gene expression (Samulski et al. 1982; Laughlin et al. 1983). With this new tool to study AAV, it was quickly noticed that the ITRs were *cis*-acting elements, while the genes between them - later discovered to code for the Rep and Cap proteins - had a *trans*-acting function in AAV replication. This notion paved the way for the generation of recombinant AAV vectors (rAAV): by retaining the *cis*-acting ITRs and providing the *trans*-acting Rep and Cap functions by complementation, the whole AAV genome could be deleted (except for the ITRs) and a vector containing a foreign DNA sequence of up to 4.5kb could be produced (Figure 4).

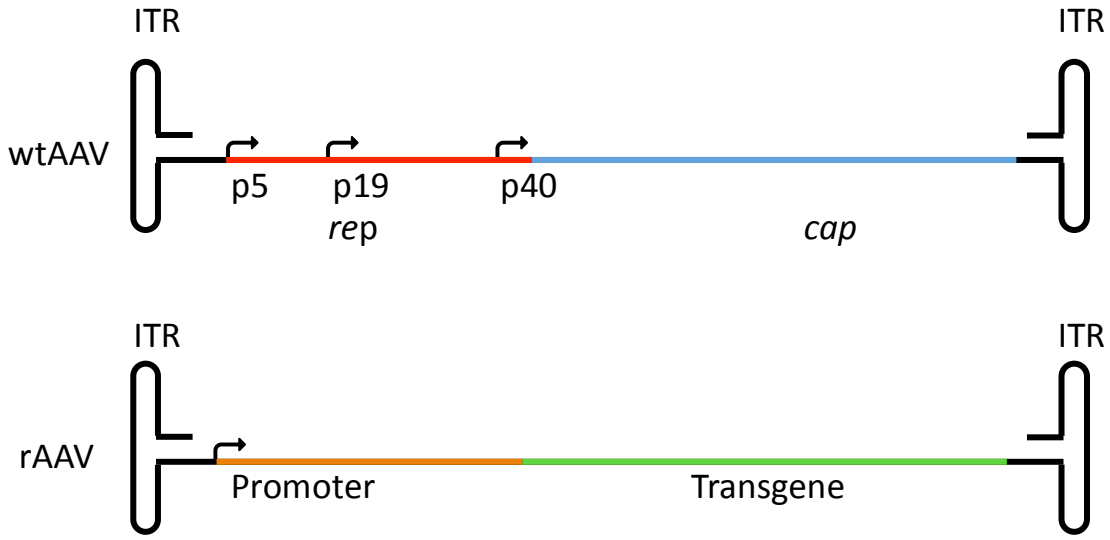

Figure 4: Genomic structures of wild-type and recombinant AAV.
rAAV is generated by removing the *trans*-acting elements *rep* and *cap* from the wild-type virus (top) and replacing them by a transgene cassette consisting of a promoter and a transgene (bottom). The only viral elements present in rAAV are the *cis*-acting ITRs, responsible for the packaging of the transgene cassette into AAV capsids. The *rep* and *cap* ORF are depicted in red and blue, respectively. The transgene cassette is depicted by the orange and green lines and they represent the promoter and the transgene under its control, respectively.

Because the rAAV generated by Rep and Cap *trans*-complementation are devoid of all wild-type genes, these vectors are unable to replicate or to integrate and their recombinant genomes form concatemers, which are able to stably express their transgenes in transduced cells. Also important for the development of rAAV were studies that analysed mutations in the adenovirus genome and identified the subset of adenoviral genes, including E1, E2A, E4orf6 and the VA RNA as necessary and sufficient to establish the helper functions required for AAV replication (Matsushita et al. 1998). This discovery led to the development

of plasmids harbouring helper function genes, which allowed for the production of rAAV using helper virus-free methods (Streck et al. 2005).

Another important advance in the generation of rAAV vectors was the development of double-stranded AAV vectors (dsAAV - also referred to as self-complementary AAV), which are able to achieve a more rapid onset of transgene expression (Wang et al. 2003). Double-stranded AAV is generated by mutating the TRS in one ITR, thereby abolishing the terminal resolution step of the AAV replication and resulting in a sense and antisense strand covalently linked (Figure 2j). The rapid transgene expression of dsAAV occurs because they bypass the rate-limiting second-strand synthesis step once the genome is uncoated in the cell (McCarty 2008). Gene therapy strategies have taken advantage of the rapid onset of transgene expression in dsAAV, however the packaging of a dimeric genome limits the loading capacity of dsAAV to half of the length of the ssAAV genome. This size restriction limits the application of dsAAV vectors for gene therapy but the ability of AAV to form concatemers *in vivo* has led to the development of dual vector strategies in order to overcome this size limitation (Yang et al. 1999; Yan et al. 2000; Ghosh & Duan 2007).

Concatemerisation of the AAV genome is important not only for dual vector strategies in gene therapy; it is also the underlying mechanism through which rAAV is able to stably express its transgenes. Concatemerisation occurs through intramolecular recombination of independent monomer circular vector genomes mostly in a head-to-tail configuration (Duan, Sharma, et al. 1998; Yang et al. 1999; Nakai et al. 2001).

1.3.1 Production of recombinant AAV

Production of rAAV vectors can be achieved in culture by supplying cells with (1) a plasmid containing a transgene cassette flanked by the AAV ITRs, (2) the AAV *rep* and *cap* coding sequences and (3) the helper functions. Several methods have been developed, which use different forms of delivery of each of these three elements necessary for rAAV production. The most common one consists of double or triple transfection of the human embryonic kidney derived cell line HEK293. Triple transfection is performed when the three items mentioned above

are provided in separate plasmids, however the combination of elements 2 and 3 into one single plasmid is also possible and allows for a double transfection for rAAV production. Transfection-based production commonly uses adherent cells, which can render the production of rAAV a laborious task when very high yields are desired. However, HEK293 cells have been adapted to suspension cultures and protocols have been optimised for the production of large-scale good manufacturing practices (GMP)-compliant vectors (Grieger et al. 2015). Alternative rAAV production methods consist of suspension cell culture systems of either insect cells, to which all three components mentioned above are provided by baculovirus infection or stable mammalian packaging (containing *rep* and *cap*) or producer (containing the transgene flanked by AAV ITRs) cell lines, to which certain components are provided by adenovirus infection. rAAV production protocols are continuously improving and the HEK293 transfection system has been optimised to yield enough vector for preclinical and clinical trials, however further advances in rAAV production protocol are still desired. Regardless of the production system adopted, the yield of rAAV is usually 10-fold lower than that of wtAAV, possibly due to differences between providing the *trans*-acting elements by complementation vs. within the AAV genome. Furthermore, the ratio between empty- and genome containing particles varies between different purification systems but it is usually higher for rAAV than for wtAAV (Aucoin et al. 2008).

High-yielding and scalable rAAV purification methods are of paramount importance for the application of rAAV in large-scale preclinical and clinical studies.

1.3.2 Purification of recombinant AAV

Traditional purification methods include density gradient centrifugation, most commonly using iodixanol or caesium chloride, and chromatography, such as ion-exchange, receptor-specific affinity purification and AVB sepharose affinity purification. Gradient centrifugation purification results in a smaller ratio of empty/genome containing particles due to the density difference between empty and full particles, which are separated during the centrifugation. The downside

of this method is the difficulty to adapt it for large-scale productions. The opposite is true for chromatography purification methods: while they are relatively easy to upscale, they do not distinguish between empty and full particles. Thus, if a small ratio of empty/full particles is desired in a large-scale production, a combination of both purification methods must be used. However, for the majority of routine laboratory research and preclinical studies, either purification method is suitable. In recent years, AVB sepharose affinity chromatography has gained increased popularity. In contrast to the other chromatography methods, its AAV affinity ligand - a 14kDa fragment from a single chain antibody expressed in yeast and conjugated to the sepharose - allows for one-step purification compatible with multiple AAV serotypes (Snyder, Richard O., Moullier 2011).

Accurate quantification of rAAV is important to ensure correct and reproducible dosing in both preclinical and clinical settings. Despite of its relevance there is no single method that is consistently used across laboratories to quantify rAAV. The most common method for AAV titration is based on real-time quantitative PCR (qPCR). It relies on the generation of a standard curve in which the copy numbers of the primer target sequence - generally the transgene - are known for each dilution point. This standard curve is then used to estimate the rAAV titre by linear regression. It is therefore extremely important to avoid contamination of the samples and to set up a negative control for the PCR reaction. Equally important is to make sure that DNAse treatment of the rAAV is done prior to titration as reminiscent DNA from the transfection can stick to the outside of the capsid and lead to an overestimation of the genome titre. The advantages of qPCR titration over other methods are its practicality, relatively low cost and speed in obtaining the results. Other genome titration methods, each with their up and down sides, are also available. ELISA, while a very sensitive method, is costly and cannot distinguish between empty and full capsids. Slot blot is the most reliable titration method but its disadvantage lies in the fact that it takes about two days to complete (Snyder, Richard O., Moullier 2011). Alkaline gel electrophoresis is a cheap method for AAV genome titration and is based on the quantification of the DNA loaded on a gel relative to a standard curve generated with known amounts of reference DNA. Another

advantage of the alkaline agarose gel method is that it also allows the visualisation of the DNA species. A standard curve based titration can also be done to quantify total particle titre in a preparation by running purified rAAV in a polyacrylamide gel (PAGE) alongside BSA samples of known concentration and quantifying the AAV VP3 protein (Kohlbrenner et al. 2012).

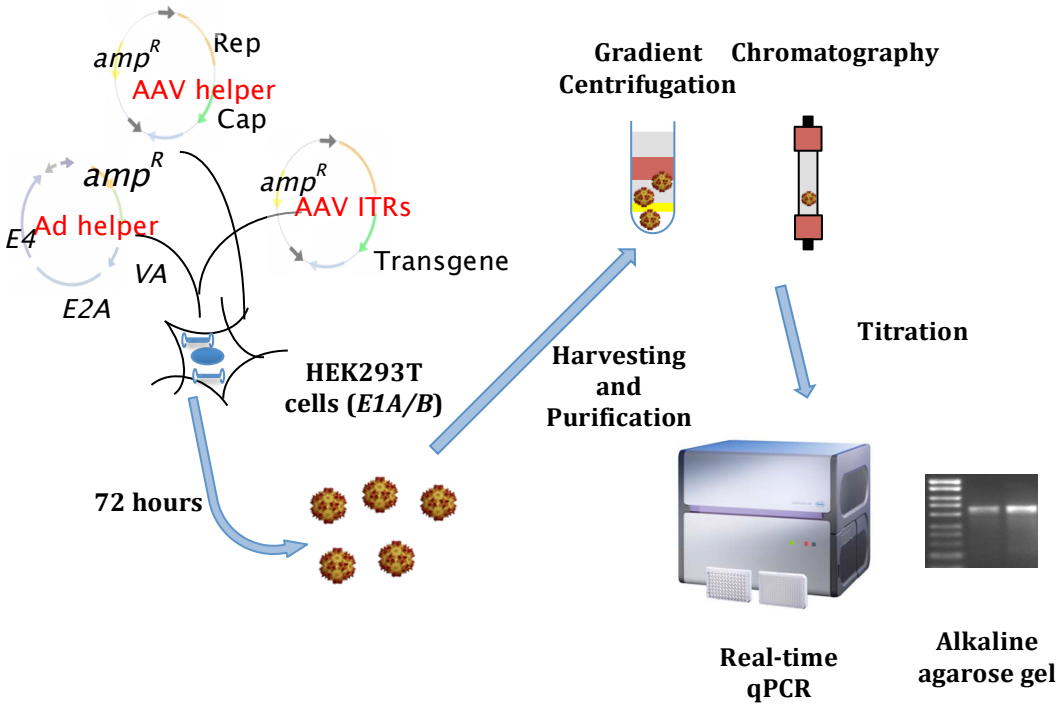

Figure 5: Recombinant AAV production process.
rAAV is generally produced by transfection of HEK293 cells with plasmids that provide the transgene flanked by AAV ITRs, helper virus functions and Rep and Cap proteins. While the ITR sequence and Rep are always from AAV2, the Cap protein used can vary and determines the serotype of the produced rAAV. The separation of the *trans*-acting elements (Rep and Cap) from the *cis*-acting ITRs is a security measure to avoid the generation of replication competent AAV. 72h post-transfection the virus can be harvested from the supernatant through protein precipitation and from the cells through freeze-and-thaw cycles to disrupt the cell membrane. Purification of rAAV is done either by density gradient centrifugation or chromatography, after which the titre is determined by real-time qPCR and/or alkaline agarose gel electrophoresis.

1.4 AAV as a Vector for Gene Therapy

AAV fulfils all pre-requisites of a good gene therapy vector: it is able to transduce both dividing and non-dividing cells, achieves long-term transgene expression and is well tolerated. In addition, the variety of serotypes isolated to date combined with an increasing number of platforms for capsid modification dramatically expanded AAV versatility and utility. Initially, most of the rAAV

vectors were based on AAV2 but nowadays most of the vectors used are pseudotyped i.e. they are packaged in a capsid of some serotype other than AAV2 but contain their transgenes flanked by AAV2 ITRs. The most commonly used pseudotyped vectors include AAV1, AAV5, AAV8, AAV9 and AAVrh10 because of their different capsid properties, tropism and biodistribution profiles (Zincarelli et al. 2008). In addition, emerging technologies allow the design of AAV vectors with enhanced tropism to certain organs or cell-types (Lisowski et al. 2014; Zinn & Vandenberghe 2014).

Accumulating evidence from studies using different serotypes show that in general AAV1, AAV6 and AAV9 are efficient in transducing muscle (Hauck & Xiao 2003; Rivière et al. 2006; Tabebordbar et al. 2015), AAV5, AAV9 and AAVrh10 present a broad distribution in the brain (Davidson et al. 2000; Lin et al. 2005; Meadows et al. 2015), while AAV8 is particularly efficient in liver, skeletal and cardiac muscle transduction (Wang et al. 2005; Nakai et al. 2005). Overall, AAV8 is the vector that most efficiently crosses the blood vessel barrier, leading to systemic gene transfer in liver, skeletal and cardiac muscles.

Interestingly, gender has shown to be a factor influencing AAV8-mediated transduction in the liver, with males being more permissible than females (Davidoff et al. 2003). It is clear that one serotype can have tropism for more than one tissue and thus, in order to achieve a higher degree of specificity and avoid transduction of undesired organs or cell types, vectors of a particular serotype are usually combined with a tissue-specific promoter. This strategy ensures that only particular cell-types are able to express the transgene delivered by AAV. The transduction profile of different serotypes after systemic delivery has been thoroughly evaluated in mice and overall it can be ranked as: AAV9 > AAV8 = AAVrh.10 > AAV7 > AAV6 > AAV1 > AAV5 > AAV2 > AAV3 (Zincarelli et al. 2008; Pañeda et al. 2009).

Not only mice but also larger animal models have shown long-term transgene expression following AAV administration. In dogs, AAV1-, AAV2-, AAV6-, AAV8- and AAV9-mediated gene transfer led to phenotype correction in haemophilia A and B, while AAV5 led to behavioural recovery in a NHP model of Parkinson's disease (Muramatsu et al. 2002; Sarkar et al. 2006; Niemeyer et al. 2009). Furthermore, successful transduction of NHP retina by AAV5 vectors has

provided strong support for the treatment of retinal degenerative retinopathies, such as Leber congenital amaurosis (Stieger et al. 2009).

1.4.1 Clinical Trials Using Recombinant AAV Vectors

To date, the most promising results from *in vivo* gene therapy trials have been achieved using AAV. Because AAV2 was the first serotype discovered, the greater knowledge about it serotype led to it being the first one to be used as a gene therapy vector. With the isolation of new serotypes and the characterisation of their different tropism profiles and transduction efficiencies, AAV2 was soon replaced in the clinic by serotypes that more closely fit the specific transduction profile required for each gene transfer approach. Challenges to the clinical use of AAV are generally tissue-specific and vary from immune responses against the vector to the optimal mode of gene delivery in each tissue.

Exciting progress has been made using AAV in diseases such as congenital blindness and haemophilia and gene therapy to treat these conditions are moving closer to clinical application.

1.4.1.1 AAV-Mediated Gene Transfer for the Treatment of Leber's Congenital Amaurosis

One of the most compelling examples of success in clinical gene transfer using AAV vectors are the trials for the treatment of the retinal degenerative disorder Leber's congenital amaurosis (LCA). This disease, characterised by early-onset blindness due to retinal degeneration, can result from mutations in 14 different genes. Following successful AAV-mediated expression of *RPE65*, one of the 14 possible genes affected, in animal models, three clinical trials for RPE65 deficiency were initiated in 2007 (Koenekoop). Very little immune response to the vector and the transgene product were observed and no serious adverse events among the >25 subjects injected was reported. Three years post-AAV injection, all three trials reported success as determined by psychophysical measures of visual function (visual acuity and visual fields), objective measures (such as pupillary light response or full field light sensitivity) and functional measures (such as the ability to navigate an obstacle course in dim light), with at

least some parameters improving in nearly all subjects (Bainbridge et al. 2008; Maguire et al. 2008; Hauswirth et al. 2008; Pierce & Bennett 2015). Demonstration of proof-of-concept in this disease has laid the groundwork for trials for a host of more common inherited retinal degenerative disorders, such as Leber's hereditary optic neuropathy, choroideraemia and age-related macular degeneration.

1.4.1.2 AAV-Mediated Gene Delivery for the Treatment of Haemophilia B

The clinical trials for the treatment of haemophilia B are another example of successful AAV gene therapies that have brought, alongside the cure of some patients, enormous advancement in the understanding of AAV tolerance and its interaction with the human immune system. Haemophilia B is a bleeding diathesis caused by mutations in the gene that codes for the blood coagulation factor IX. When left untreated, the disease leads to death in childhood or adolescence and current treatment by intravenous infusion of clotting factor concentrates remains unaffordable for the majority of the people affected. Haemophilia B is an attractive target for gene therapy approaches because the therapeutic window is wide. Increasing factor IX levels to >2% already leads to phenotype correction and levels up to 150% are still considered normal. In addition, endpoints are easy to measure and small and large animal models of the disease exist.

The first AAV clinical trial to treat haemophilia B was done using AAV2 at relatively low doses as a precaution prompted by the death of a young man seven years earlier, who received liver-directed gene therapy with an adenoviral vector (Gelsinger & Shamoo 2008). This haemophilia B trial showed clear efficacy in one subject, with circulating factor IX levels in the range of 10–12% of normal at the highest dose tested. However, elevated factor IX levels persisted for only ~10 weeks and were followed by a rise in transaminase levels. Further investigation demonstrated that the transaminase elevation and the decrease in factor IX levels were due to a selective $CD8^+$ T cell response against transduced hepatocytes triggered by the AAV capsid. A second subject showed no evidence of factor IX expression or transaminase elevation and this lack of response was

attributed to the presence of pre-existing neutralising antibodies against AAV, which blocked the transduction of the vector. These issues, not observed in any preclinical studies in animals, led to a better understanding of the AAV interaction with the immune system and to the optimisation of vectors and trial protocols (Manno et al. 2006). A subsequent clinical trial made use of a double-stranded AAV genome packaged in the liver-tropic capsid of AAV8 in order to achieve a more rapid and potent transgene expression using a smaller dose. A dose-dependent immune response was also observed when using AAV8 but this was addressed with a short course corticoid administration to the patients, which temporarily suppressed their immune system and assured a steady rise in factor IX plasma levels. Interestingly, no transaminase elevation has been observed since the corticoid treatment was terminated, indicating that capsid antigens presented at the surface of hepatocytes might be degraded over time (Nathwani et al. 2014). This second trial has exceeded all expectations and today, more than 6 years post-AAV administration, the six high-dose patients (out of 10 recruited) are still expressing FIX at ~5% of normal levels. At present, three other trials are ongoing for AAV gene therapy for the treatment of haemophilia B (High et al. 2014). Two of them have not reported any results yet and the third one has sent out a press release stating that AAV treatment has led to the cure of patients.

1.4.1.3 AAV-Mediated Gene Delivery to the CNS

The progress in the development of AAV gene therapies for the treatment of conditions affecting the CNS has been slower than for diseases affecting peripheral organs. Particularly challenging has been the issue of broad versus local delivery. To date, several early-stage clinical trials using AAV in the CNS have been carried out showing good vector tolerability and long-term transgene expression, however clear evidence of efficacy in controlled Phase II/III trials still remains to be shown (O'Connor & Boulis 2015).

For some conditions such as Parkinson's disease local delivery to specific brain areas can provide therapeutic relief of motor symptoms however most neurodegenerative disorders require a broad delivery to the CNS. In these cases,

access to large areas of the brain and the blood-brain-barrier (BBB) impose limitations for vector delivery. Some serotypes such as AAV9 and AAVrh10 have been shown to be able to cross the BBB, but systemic delivery of AAV must take into consideration potential problems of off-target transduction and neutralising antibodies (Inagaki et al. 2006; Wolf et al. 2015). In addition, the choice of AAV serotype, delivery techniques must be considered carefully. Overall, although much progress has been made in achieving widespread transduction of the CNS in animal models and several studies have confirmed the safety profile and tolerability of AAV gene therapy, its efficacy in the treatment of CNS disorders remains to be proven.

1.4.1.3.1 AAV Gene Therapy for Alzheimer's Disease

Alzheimer's disease is a progressive neurodegenerative disorder characterised by the loss of memory and cognitive functions and disease progression has been associated with accumulation of amyloid β plaques and the loss of cholinergic neurons. A Phase I clinical trial using AAV2 to express the nerve growth factor (NGF) in the brain showed that therapy was well tolerated, with post-mortem analysis of brain tissue identifying expression of NGF in an active form (Rafii et al. 2014). The data supported the initiation of a controlled Phase II trial to rigorously assess the effectiveness of AAV2-NGF, however it was eventually announced that the trial failed to meet its primary endpoints.

1.4.1.3.2 AAV Gene Therapy for Spinal Muscular Atrophy

Spinal muscular atrophy (SMA) is a motor neuron disease caused by the loss of the survival motor neuron 1 (*SMN1*) gene and is the leading genetic cause of infantile death. Because SMA is a monogenic disease, it is a good candidate for gene replacement strategies and a Phase I clinical study with AAV9 is currently ongoing with the aim to test safety and efficacy of intravenous AAV delivery for the correction of a disease affecting the CNS (Faravelli et al. 2015; Duque et al. 2015).

1.4.1.3.3 AAV Gene Therapy for Lysosomal Storage Diseases

Lysosomal storage diseases encompass over 50 different diseases that arise from defective catabolism of some molecules leading to their accumulation within lysosomes and cell toxicity. The standard treatment for these diseases is trough enzyme replacement that leads to the degradation of the accumulated macromolecules. However, some of these diseases such as metachromic leukodystrophy (MLD) and mucopolysaccharidosis type III A (MPSIIIA) encompass a neurological component that cannot be treated by enzyme replacement due to the inability of the enzymes to cross the BBB (Bradbury et al. 2015; Pastores & Hughes 2015).

Metachromic leukodystrophy (MLD) is a disease that is still untreatable and it is caused by an inherited mutation in the arylsulfatase A (*ARSA*) gene resulting in the accumulation of sulphatide in Schwann cells, oligodendrocytes and brain neurons. The first Phase I gene therapy clinical trial is underway using AAVrh10 to deliver ARSA intracerebrally to early-stage or presymptomatic MLD patients. Preclinical studies in animal models of the disease showed phenotype correction but results from the human trial have not been published yet (Piguet et al. 2012).

Another lysosomal storage disease with a neurological component currently being tested in Phase I/II trials is MPSIIIA, also known as Sanfilippo type A. This disorder is caused by a mutation in the lysosomal heparan-N-sulfamidase gene (SGSH), which leads to cognitive delay, abnormal behaviour, and seizures (Valstar et al. 2010). Both trials are testing the efficacy of AAVrh10 intracranial transgene delivery and reports have shown no safety issues associated with the vector. Preliminary efficacy data with regard to brain atrophy for some patients and possible improvements in behaviour and sleep have been reported (Tardieu et al. 2014).

1.4.1.4 AAV-Mediated Gene Transfer to Skeletal Muscle

The muscle is an attractive target tissue for gene transfer strategies aimed at correcting neuromuscular and metabolic diseases (Mendell et al. 2009; Manno et al. 2003). In fact, the only gene therapy currently approved for

commercialisation is based on the intramuscular delivery of AAV1 to treat lipoprotein lipase (LPL) deficiency (Morrison 2015).

Intramuscular AAV administration is the preferred route for muscle targeting. Ease of delivery and local retention of the vector are among the advantages of intramuscular delivery. However, this route of administration has been associated with a higher risk of triggering an immune response against the transgene compared to systemic delivery (Mendell et al. 2010). Although evidence suggests that intravascular AAV vector delivery is less prone than intramuscular administration to trigger immune responses directed against the transgene product, it increases the exposure of the vector to neutralisation by pre-existing antibodies.

1.5 Future Perspectives of AAV Gene Therapy

To date, one rAAV product has reached the market in Europe and following the many preclinical studies reporting promising results with AAV gene therapy, numerous rAAV vectors have entered clinical trials (Morrison 2015). As of July 2015, 137 clinical trials were conducted using AAV (Anon 2015). Although representing only 6.2% of the gene therapy trials conducted to this date, this number is expected to grow as protocols of AAV production are improved, more potent and optimised vectors are developed and investment from the private sector and the pharmaceutical industry increases.

1.6 Parkinson's Disease

In 1817 the English physician James Parkinson described the symptoms of the "shaky palsy", a condition that was later described in greater detail and named after him (Parkinson 2002). Parkinson's disease (PD) symptoms might be first noticed as a twitching in the fingers that instead of going away turns into a tremor of the hand and eventually of the entire arm. Affected people typically assume a bent posture, have a short gait, slow speech and a face lacking expressions or emotions. With time, these symptoms worsen and spread out and essential routine activities such as standing, walking and swallowing become hugely cumbersome. These difficulties are a consequence of resting tremor,

cogwheel rigidity, akinesia (loss or impairment of the power of voluntary movement), bradykinesia (slowness) and postural instability, the motor hallmarks of PD. Although motor symptoms are typically associated with PD, affected people also suffer from wide a range of non-motor symptoms such as depression, apathy, pain, sexual difficulties, bowel incontinence, visual impairment, hallucinations and insomnia, all of which still remain under-recognised and, consequently, under-treated (Chaudhuri & Schapira 2009). PD affects around 1-2% of the population above the age of 55. It is the most common movement disorder and the second most common neurodegenerative disease of the human brain after Alzheimer's disease with a higher incidence expected to follow the increase in life expectancy (de Lau & Breteler 2006).

Nearly 200 years after it was first described, the ultimate cause of the disease development still remains unknown. PD seems to be a complex multifactorial disorder with variable contributions of environmental factors and genetic susceptibility. Genetic predisposition accounts for 10% of the cases but the other 90% remain described as idiopathic (also known as sporadic), with age being one of the main risk factors. Most of the progress in PD research pathogenesis has been made in understanding the neuronal death that leads to the typical motor complications of the disease. Cellular death occurs in a group of dopamine-synthetic neurons that populate the area near the brainstem known as substantia nigra pars compacta (SNc) and innervate the subcortical nucleus of the basal ganglia known as striatum supplying it with the neurotransmitter dopamine for the fine-tuning of movement. It is not until 70% of the nigral cells are lost that dopamine levels reach a clinically significant threshold and a cascade of motor complications start to manifest. Neuronal death in the SNc has been associated with the presence of protein aggregates known as Lewy bodies and Lewy neurites. Although these neurons are the most vulnerable, PD pathology seems to start at the olfactory system and the gut-connected dorsal motor nucleus of the vagus.

1.6.1 α-synuclein Aggregation and Parkinson's Disease

α-synuclein, a hydrophilic protein abundant in presynaptic terminals, is a major component of the Lewy bodies and Lewy neurites. For reasons still unknown, it can leave its binding site within the synaptic terminals and start forming toxic insoluble aggregates that spread to different regions of the nervous system. Studies have shown that sporadic PD, the most common form of the disease, is an α-synucleinopathy that can be classified into six different stages according to its degree of spread in the central nervous system. The abnormal deposition of α-synuclein starts at lower regions of the brain and spreads gradually towards the cortex in a predictable pattern. After its occurrence in the olfactory system and the gut-connected dorsal motor nucleus of the vagus, which characterises stage 1, α-synuclein aggregates spread to the medulla oblongata and the pontine tegumentum (stage 2). It is only at stage three, when the pathology reaches the amygdala and the substantia nigra that the motor symptoms of PD begin to appear. The pathology worsens when the aggregates reach the temporal cortex (stage 4) but it is at stages 5 and 6, when the neocortex is affected, that many of the cognitive impairment symptoms appear (Braak et al.). It is important to note that this rating scale is based on the progression of the α-synucleinopathy and that other scales based on the severity of PD symptoms (most commonly the motor ones) are more practical in the management of the disease and are therefore used by physicians to rate disease progression and to decide upon a treatment. Furthermore, post-mortem analysis of brains from people who had suffered from genetic and sporadic forms of PD showed distinct patterns of α-synucleinopathy, bringing into question whether all forms of PD are the same (Doherty et al. 2013). Nonetheless, the clear abnormal deposition of α-synuclein in most people suffering from PD suggests that it might fall under the category of the so-called amyloid diseases. The common feature of these diseases is the presence of proteins that assume a β-sheet conformation and aggregate into insoluble forms. Despite affecting different kinds of proteins, these aggregates exhibit the same subatomic pattern in different amyloid diseases: α-synuclein in Parkinson's disease, Lewy body dementia and multiple system atrophy; amyloid-β and tau protein in Alzheimer's disease; polyglutamine protein in Huntington's disease; and amylin protein in

type 2 diabetes (Chiti & Dobson 2006). Strengthening the notion that PD is an amyloid disease is the observation from a trial in which people with PD received a transplantation of dopamine-producing neurons in the striatum. Some patients showed only a temporary improvement of the motor symptoms and post-mortem autopsy revealed that the disease had spread from the patients' brain to many of the transplanted neurons in a prion-like fashion (Li et al. 2008). Overall, there is strong evidence that suggest that the aberrant α-synuclein deposition is the driving force in PD pathogenesis (Stefanis 2012).

1.6.2 Mitochondrial Dysfunction and Parkinson's Disease

Aberrant mitochondrial function and increased oxidative stress have also been implicated in the pathogenesis of PD. The first evidence for this link appeared when, in the late 70's, heroin users developed PD symptoms a few days after injecting an impure batch of the drug. It was soon discovered that the drug contained the contaminant MPTP, which is preferentially taken up by the dopaminergic neurons in the SNc. Once inside the dopaminergic neurons, MPTP is catalysed into a toxic molecule that functions as an inhibitor of the mitochondrial complex I leading to oxidative stress followed by cell death (Bajpai et al. 2013). Further evidence providing a link between abnormal mitochondrial function and PD pathology came from brain autopsies from PD affected people, which revealed a deficiency in mitochondrial complex I activity. In addition, ground breaking advances in PD research led to the identification of genes that are responsible for the less common genetic forms of the disease. It is now known that mutations in the genes encoding α-synuclein and LRRK2 (leucine-rich repeat kinase 2) are responsible for the autosomal dominant forms of PD, whilst mutations in the genes encoding parkin, PINK1 (PTEN-induced putative kinase 1), HTRA2 (high temperature requirement protein A2) and DJ-1 mediate autosomal recessive forms of PD. These genes have been shown to directly or indirectly affect mitochondrial integrity, thereby providing a link to further pathophysiological alterations observed in sporadic PD.

Because sporadic and genetic forms of PD share important clinical, pathological and biochemical features, in particular the progressive loss of

dopaminergic neurons in the SNc, insight into the function of PD-associated gene products can help to elucidate the primary mechanisms leading to neuronal cell death.

1.6.3 Dopamine Metabolism in the Central Nervous System

Dopamine is a catecholamine neurotransmitter found predominantly in the central nervous system (CNS); it is involved in different pathways related to reward-motivated behaviour, memory, attention, mood, circadian rhythm and motor control. Dopamine also functions in the peripheral nervous system and in organs such as the kidneys, pancreas and the upper gastrointestinal tract, where it is synthesised and acts in a paracrine manner (Ustione et al. 2013). Dopamine is also synthesised in the adrenal medulla, where it is used as precursor for the synthesis of the hormones and neurotransmitter epinephrine and norepinephrine (Daubner et al. 2011).

In the CNS, the four major neural pathways that use dopamine as a neurotransmitter are the mesolimbic, mesocortical, tuberoinfundibular and nigrostriatal (Figure 6). The mesolimbic and mesocortical pathways contain neuronal projections that connect a structure located in the midbrain, called ventral tegmental area (VTA), to the limbic system and the frontal cortex, respectively. Both pathways are essential for reward-motivated behaviour, cognitive control, motivation and emotional response and disorders in these pathways are associated with schizophrenia and addiction. The tuberoinfundibular pathway transmits dopamine from the hypothalamus to the pituitary gland and it regulates the secretion of the hormone prolactin. The nigrostriatal pathway connects the SNc with the dorsal striatum and is involved in motor control. The selective degeneration of the nigrostriatal dopaminergic neurons is responsible for the motor complications of PD.

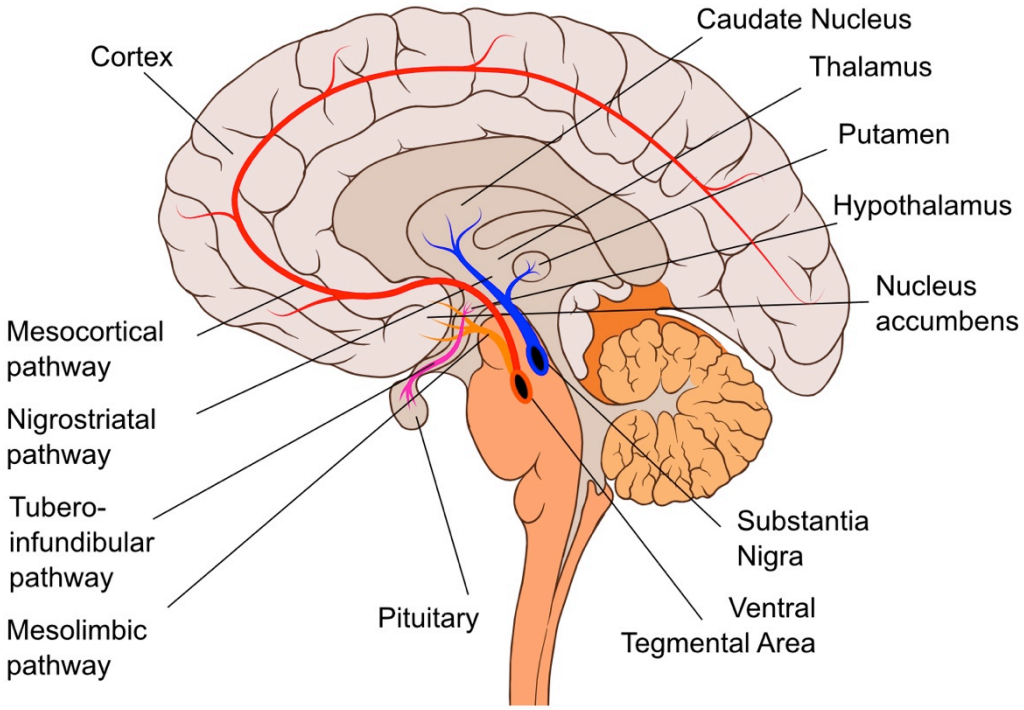

Figure 6: The four major dopaminergic pathways in the CNS.
The pathways that use dopamine as a neurotransmitter are the mesolimbic pathway (orange); the mesocortical pathway (red); the tuberoinfundibular pathway (pink) and the nigrostriatal pathway (blue). Together, the caudate nucleus and the putamen form the dorsal striatum, which is involved with motor control. The selective degeneration of the nigrostriatal dopaminergic neurons is the responsible for the motor complications of PD. (Adapted from: https://www.wikimedia.org).

Dopamine is synthesised from the amino acid tyrosine through a tightly regulated pathway (Figure 7). The first step in its biosynthesis is the hydroxylation of the amino acid tyrosine to L-DOPA by the rate-limiting enzyme tyrosine hydroxylase (TH), which uses tetrahydrobiopterin (BH4) as cofactor. The second reaction is the removal of the carboxyl group from L-DOPA by the enzyme aromatic amino acid decarboxylase (AADC) to form dopamine. Immediately after it is synthesised, dopamine is relocated from the cytoplasm into synaptic vesicles by the protein vesicular monoamine transporter 2 (VMAT2), where it is up to 1000 times more concentrated than in the cytosol (Elsworth & Roth 1997; Eiden et al. 2004). Upon arrival of an action potential, calcium influx leads to the fusion of the synaptic vesicles with the neuronal membrane and release of dopamine into the synaptic cleft by exocytosis. The extent of dopamine release is dependent on the neuron's firing rate and pattern and once released, dopamine exerts its effect through interaction with dopamine D1–5 receptors. Dopamine can be taken up by the membrane protein dopamine

transporter (DAT) of the presynaptic neuron where it can either be recycled into the vesicles via VMAT2 or degraded. DAT is the primary mechanism by which dopamine is cleared from the synaptic cleft and it controls the spatial and temporal dynamics of dopamine neurotransmission (Vaughan & Foster 2013). Degradation of dopamine can occur via the monoamine oxidase (MAO) and the catechol-*O*-methyl transferase (COMT) enzymes into its main end-product homovanillic acid (HVA). MAO exists in two isoforms (A and B), which catalyse the oxidative deamination of dopamine into 3,4-dihydroxyphenylacetic acid (DOPAC), which is then further converted into HVA. This is the main pathway of dopamine inactivation in the striatum. In other regions of the brain, dopamine is preferentially methylated by COMT to form 3-methoxytyramine (3-MT), which is in turn converted into HVA by MAO. The end product HVA has no known biological activity and is excreted (Leonard 1993).

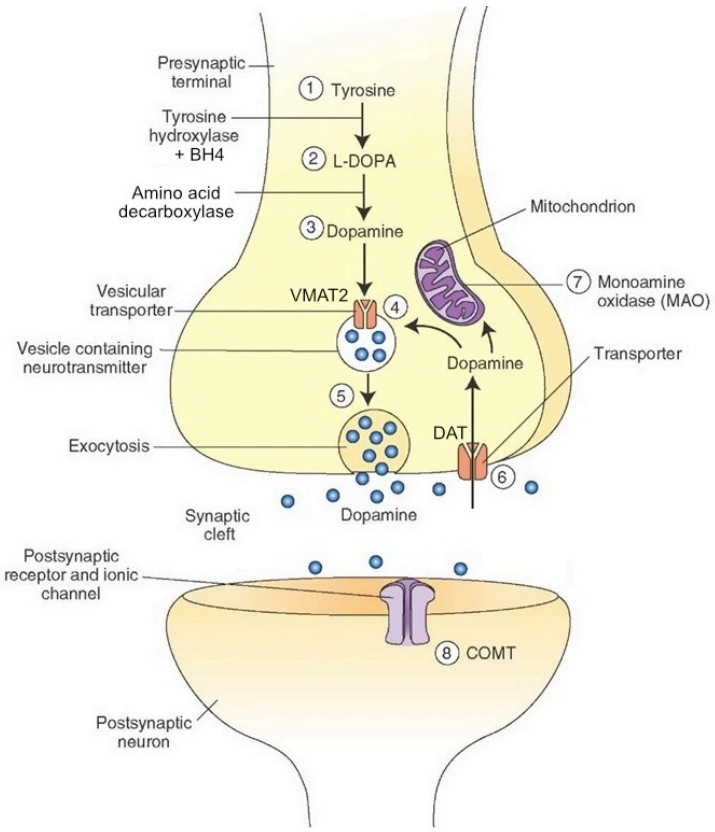

Figure 7: Schematic of dopamine synthesis and regulation in the CNS. (Modified from http://what-when-how.com/neuroscience/neurotransmitters-the-neuron-part-3).

1.6.4 L-DOPA Pharmacotherapy in Parkinson's Disease

Although extensive research has brought a deeper understanding of the genetic and environmental factors affecting the susceptibility for PD and the molecular processes that lead to neuronal loss, the ultimate cause of the disease remains unknown. The severity of the disease seems to be proportional to the loss of dopamine input in the striatum and existing therapies focus on the restoration and preservation of the brain's dysfunctional dopaminergic system (Hohen & Yahr 1967; Kish et al. 1988; Feng & Maguire-Zeiss 2011).

The discovery in 1958 that dopamine acts as a neurotransmitter that controls movement led to the development of treatments that aim for the restoration of dopamine neurotransmission. L-DOPA, the precursor of dopamine, entered the clinical scene as a direct consequence of this discovery and, because of its ability to provide powerful symptomatic relief in PD patients, it was regarded as a miracle drug (Degkwitz et al. 1960; Birkmayer & Hornykiewicz 1961). In the first years after its discovery as an antiparkinsonian agent, L-DOPA was administered without a peripherally acting AADC inhibitor (e.g. benserazide) and the peripheral conversion of L-DOPA to dopamine caused problems such as hypotension, nausea, vomiting, and anorexia. The administration of AADC inhibitors together with L-DOPA allowed for a reduction in the dose by as much as 60–80% and a faster onset of L-DOPA's antiparkinsonian effects without any loss in therapeutic efficacy (Birkmayer et al. 1974; Nutt et al. 1985). In addition to benserazide, COMT inhibitors, such as tolcapone and entacapone, are commonly used in the clinic to avoid peripheral degradation of L-DOPA and extend the duration of its antiparkinsonian effects (Ruottinen & Rinne 1996; Napolitano et al. 1999). The absorption of L-DOPA happens in the duodenum and proximal jejunum by active transport via the large neutral amino acid (LNAA) system. This same system is responsible for its transport across the blood-brain-barrier and is present in endothelial cells and astrocytes (Wade et al. 1973; Kageyama et al. 2000). Because L-DOPA relies on active transport to enter the gut and the brain, meals rich in protein interfere with its absorption and affect peak plasma levels after oral medication (Nutt et al. 1984).

L-DOPA is an amino acid that has proven to be very difficult to manage clinically. Its half-life is very short (60 minutes) and its pharmacodynamics

interaction with the disease progression is poorly understood. Despite an increased half-life and bioavailability achieved with AADC and COMT inhibitors, prolonged treatment with L-DOPA will inevitably lead to side effects in over 80% of the patients within the first 5-10 years of treatment. L-DOPA induced side effects are disabling and include severe involuntary movements known as dyskinesias and swings between mobility and immobility known as ON–OFF phenomena, which are characterised by improved mobility (ON) due to L-DOPA followed by sudden unpredictable impaired mobility (OFF). Other L-DOPA induced side effects may include hypotension, sexual dysfunction, and psychiatric disorders.

The introduction of L-DOPA as a medicine to treat the symptoms of PD more than 50 years ago was so revolutionary that better drugs have yet to be developed and most of the research focus has revolved around ways to maximise L-DOPA's therapeutic benefit without triggering side effects (Abbott 2010).

1.7 L-DOPA Induced Dyskinesia

Oral medication with L-DOPA is the gold-standard treatment for PD. During the early years of PD, when motor complications are the predominant symptoms, L-DOPA provides enormous symptomatic relief and substantially improves quality of life of patients (Kordower & Goetz 1999). However, chronic treatment with L-DOPA to manage parkinsonian symptoms leads to the development of side effects, most remarkably the so-called L-DOPA induced dyskinesia (LID). Dyskinesia is the medical term for any involuntary movement other than tremor and the spectrum of LID includes a variety of movements, such as chorea, dystonia, athetosis, and ballism.

Choreic movements are non-rhythmic, irregular, spasmodic, and involuntary movements that appear to flow from one muscle to the next. It occurs more commonly in distal muscles and is best seen in the fingers, toes, wrists, and/or the ankles. Chorea can also affect the craniofacial muscles and the neck but its prevalence in these muscles is less common in PD patients.

Dystonia means "bad tone" and is medically defined as sustained or intermittent involuntary, patterned, and often repetitive contractions of

opposing muscles. Dystonia is often initiated or worsened by voluntary actions and it causes twisting movements or abnormal postures, or both. In PD patients that developed LID, dystonia is caused either by the wearing "OFF" of L-DOPA or during the "ON" phase. Dystonic symptoms can be disabling and result in significant pain (Fabbrini et al. 2007).

Athetoid movements are slow, involuntary, writhing movements of the fingers, hands, toes, and feet and in some cases can affect the arms, the legs, the neck, and the tongue.

Ballistic movements manifest through muscle contractions that exhibit maximum speed and acceleration over a short period of time. Clinically the movements affect mainly proximal muscles, i.e., sudden abrupt violent movement of the whole arm or leg.

Phenotypically, LID manifests as any of the involuntary movements described above but most often it is characterised by mixtures of dystonia and chorea. Once established, dyskinesia tends to remain persistent and with the progression of the disease it becomes increasingly more difficult to deliver L-DOPA doses that control the parkinsonian features without triggering dyskinesia (Moskovitz et al. 1978; Olanow et al. 2000). Although it can be reduced by some pharmacological manipulations and surgical procedures, LID is a significant source of disability and is difficult to treat, therefore efforts are made to minimise or prevent its appearance.

Among the factors that affect the induction of LID is the pulsatile stimulation of dopamine receptors by oral administration of L-DOPA. Supporting this notion is the observation that intravenous administration of L-DOPA shows a more prolonged and stable clinical response with minimal side effects, including improvement in dyskinesia (Schuh & Bennett 1993). However, practical considerations hinder its clinical use and intravenously administered L-DOPA is only used in research studies. More recently, a new therapy for continuous stimulation of dopamine receptors by continuous duodenal L-DOPA delivery was developed. Continuous duodenal infusion by a surgically implanted pump circumvents the problem of supra-physiological dopamine swings associated with intermittent oral medication with L-DOPA; this continuous mode of delivery has been shown to improve not only motor fluctuations in PD but also to reduce

the severity and duration of dyskinesias (Olanow et al. 2000; Nutt et al. 2000; Nyholm et al. 2005). As continuous duodenal L-DOPA infusion is not employed in early stages of PD, it is not known whether its early use could prevent the development of dyskinesia. Because L-DOPA is still the best known antiparkinsonian drug, the development of LID is still an major issue in the management of PD. Therefore, research on PD has focused in developing strategies to avoid LID.

1.7.1 Basal Ganglia Circuitry and L-DOPA Induced Dyskinesia

The basal ganglia are a group of subcortical nuclei that comprise the substantia nigra, the striatum, the internal and external segments of the globus pallidus (GPi and GPe, respectively) and the subthalamic nucleus (STN) (Obeso et al. 2000). The striatum is divided into a ventral and a dorsal sub-region. The ventral striatum functions as a part of the reward system and is comprised by the nucleus accumbens and the olfactory tubercle, whilst the dorsal striatum plays a major role in movement control and is composed of the caudate nucleus and the putamen. In rodents there is no clear separation between the caudate nucleus and the putamen and both structures are collectively called striatum. Among the functions of the basal ganglia is the control of movement, which is accomplished through a complex intercommunication between the different nuclei that ultimately leads to the inhibition of the thalamus. The thalamus is normally kept under inhibition and only upon release it stimulates the motor and premotor cortices leading to body movement.

The major inputs into the basal ganglia are dopaminergic, from the nigrostriatal pathway, and glutamatergic, acetylcholinergic, serotonergic and to a lesser extent noradrenergic from other pathways. The output from the basal ganglia is mainly gamma-aminobutyric acid (GABA)-ergic (which is inhibitory) and projects from the GPi to the thalamus.

In the classical model of basal ganglia circuitry, the striatum projects neurons to the other nuclei through a direct and an indirect pathway, which are named according to how they synapse with the GPi. As the name suggests, in the direct pathway neuronal projections synapse directly with the GPi, which sends

inhibitory projections to the thalamus. The neurons of the direct output pathway have D1 dopamine receptors on their cell bodies. The striatal projections in the indirect pathway reach the GPi through synapses with the GPe, from where they send inhibitory projections to the STN, which in turn makes excitatory synapses with the GPi (Figure 8A). The output neurons of the indirect pathway have D2 dopamine receptors in their cell bodies. While stimulation of D1 receptors leads to an increase in the intracellular levels of the secondary messenger cAMP, stimulation of D2 receptors leads to its decrease, therefore the direct pathway has excitatory receptors and its activation stimulates the inhibitory GABA-ergic output to the GPi. The GPi also sends inhibitory GABA-ergic projections to the thalamus, therefore inhibition of the GPi leads to a decreased inhibitory action on the thalamus, which becomes more active and stimulates the motor and premotor cortices. Therefore, dopamine stimulation of the direct pathway leads to decreased GPi activity, which leads to increased thalamic activity, culminating in increased activity of the motor cortex.

In the striatal indirect pathway, stimulation of the D2 receptors leads to a decreased activity of the inhibitory GABA-ergic neurons that synapse with the GPe. Because the GPe also sends inhibitory GABA-ergic projections to the STN, inhibition of the GPe leads to increased activity of the STN. The STN sends excitatory projections to the GPi, which in turn increases its inhibition of the thalamus. Thus, dopamine stimulation of the indirect pathway leads to increased GPi activity, which inhibits the thalamus leading to decreased stimulation of the motor and premotor cortices. Although already quite complex, the classical model of the basal ganglia circuitry is even more complicated than presented here. Reciprocal pathways between the basal ganglia nuclei add further layers of complexity to their structure and organisation.

The degeneration of the nigral dopaminergic neurons that innervate the striatum leads to an imbalance in the activity of the direct and indirect pathways resulting in voluntary movement decline and the motor features that characterise PD (Figure 8B). However, the mechanisms through which L-DOPA treatment leads to the development of dyskinesia are not completely understood. According to the classical model presented here, L-DOPA treatment overstimulates D1 and D2 receptors leading to underactivity of the indirect

pathway and overactivity of the direct pathway. As a consequence, the GABA-ergic repression of the thalamus is released and its increased firing rates lead to involuntary movements (Figure 8C).

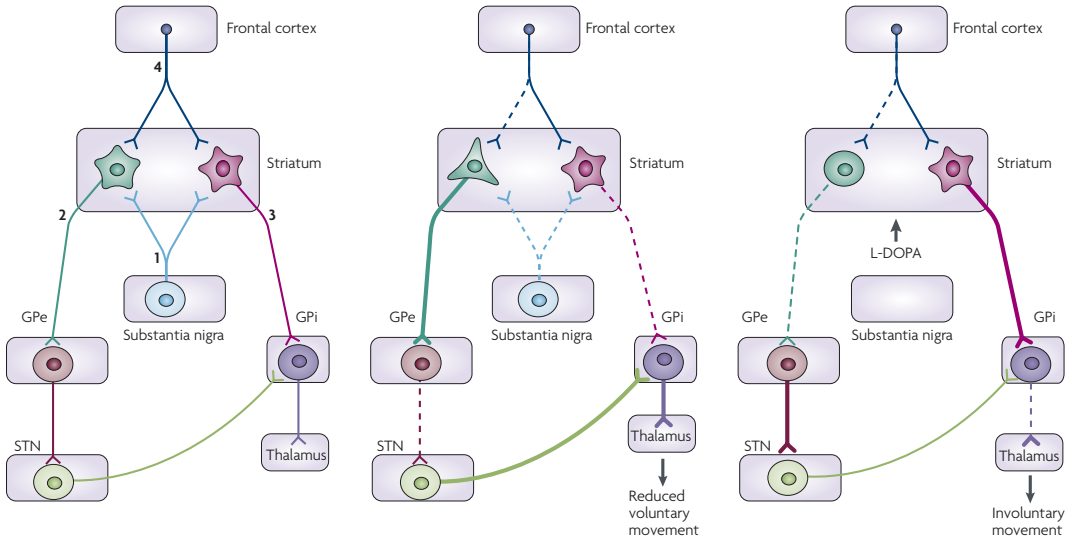

Figure 8: Classical model of the basal ganglia circuitry and LID in PD.
A. Basal ganglia circuitry in the healthy brain. Dopaminergic input from the nigrostriatal pathway (1) synapses with the striatal output neurons that make up the indirect and direct GABA-output pathways. In the striatal indirect pathway (2), stimulation of the D2 receptors leads to a decreased activity of the inhibitory GABA-ergic neurons that synapse with the GPe. The GPe also sends inhibitory GABA-ergic projections to the STN and inhibition of the GPe leads to increased activity of the STN. The STN sends excitatory projections to the GPi, thereby increasing the inhibition of the thalamus. The direct output pathway (3) has excitatory D1 dopaminergic receptors on its surface and dopamine stimulation from the SNc (1) leads to excitation of the inhibitory GABA-ergic neurons that synapse with the GPi. The inhibited GPi in turn releases is repression of the thalamus. Another major input to the striatum comes from the frontal cortex (4). B. According to classical thinking about PD, loss of dopaminergic input from the SNc leads to reduced voluntary movement through the overactivity of the indirect output pathway and underactivity of the direct output pathway. C. Treatment with oral L-DOPA was thought to bring about changes in the opposite directions, with underactivity of the indirect pathway and overactivity of the direct pathway. However this view has been challenged and the precise mechanism through which LID occurs is not fully understood. (From: Jenner, P; Nat Rev Neurosci. 2008 Sep;9(9):665-77).

Over the years, however, this classical model of basal ganglia circuitry and its role in LID has been challenged. For example, additional layers of connections between the nuclei were added after the observation that activity of the indirect pathway does not decrease in dyskinetic MPTP-lesioned NHP (Vila et al. 1996; Vila et al. 1997). Furthermore, according to the classical model, disrupted GPi repression of the thalamus must lead to increased involuntary movement. However, a trial in which 115 patients received a lesion on their GPi led to

reduction of dyskinesia in 40% of the participants. These observations suggest that alternative views need to be considered when looking at the connection between basal ganglia function, PD and dyskinesia (Leblois et al. 2006; Jenner 2008). Despite our poor understanding of the mechanisms underlying the development of LID, clinical observations suggest that the extent of nigral denervation and the mode of L-DOPA administration play central roles in the manifestation of dyskinesia.

1.8 Gene Therapy Strategies for the Treatment of Parkinson's Disease

PD is a well-suited candidate for gene therapy and different strategies have been explored as a treatment. One factor that makes PD a well-suited candidate for gene therapy is that viral vectors enable the targeting and the expression of complex molecules or enzymes in specific areas of the brain affected by the disease. Furthermore, while improvement in the treatment of the motor symptoms of PD has been achieved trough the introduction of compounds such as long lasting dopamine agonists and enzyme inhibitors that increase the half-life and the bioavailability of oral L-DOPA, the cost of these treatments represents a significant financial burden on patients. Gene therapy, on the other hand, has the potential to alleviate this burden by reducing or even abolishing the necessity for some medicines because it is based on a single intervention principle with life-long effects. In total, nine gene therapy trials have been initiated to treat PD. Their therapeutic strategies are based on a number of preclinical and clinical observations and can be divided in three categories: (1) modification of disease progression by neuroprotection; (2) modulation of the activity in the basal ganglia downstream of the striatum; and (3) restoration of dopamine synthesis in the striatum.

1.8.1 Modification of Disease Progression by Neuroprotection

Because PD is a progressive neurodegenerative disorder, attempts to delay and even halt disease progression have been extensively pursued. In the 90's molecules known as neurotrophic factors were identified that showed promising

neuroprotective potential. Two of them, glial derived neurotropic factor (GDNF) and neurturin (NTN) were shown to promote the survival of dopaminergic neurons in the midbrain both *in vitro* and *in vivo* and the promising preclinical data prompted rapid clinical testing soon after their discovery (Lin et al. 1993; Björklund et al. 1997; Horger et al. 1998; Tseng et al. 1998). AAV-mediated gene transfer of NTN into the putamen and the substantia nigra of patients met the safety endpoints of Phase I clinical trials but subsequent Phase II trials showed no efficacy over control groups (Marks et al. 2016). The project leaders hypothesised that possible reasons for the trial failures is that benefits in animal models might not translate into benefits in patients because they do not recapitulate the pathology, more specifically the accumulation of α-synuclein found in PD. Another factor is that the trials were performed in advanced PD patients, which could have had an impact on the probability of the study to meet its endpoints. Since the strategy is based on the assumption of a neuroprotective action, efficacy might only be seen if patients with a less advanced form of the disease, and therefore with a greater residual dopaminergic system still present, are enrolled (Warren Olanow et al. 2015). A Phase I clinical trial to test the safety and tolerability of AAV2-mediated GDNF delivery to the putamen is currently recruiting patients, however its protocol has been criticised for not addressing some of the issues raised by the AAV2-NTN trials (Bartus et al. 2014). Overall, no neuroprotection study has yet been able to demonstrate positive results in a double blind trial to support advancing to a Phase III trial.

1.8.2 Modulation of the Activity in the Basal Ganglia Downstream of the Striatum

Neurosurgical intervention to reduce motor complications in PD has been successfully accomplished by a technique called deep brain stimulation (DBS). It consists of the implantation of intracranial electrodes in the internal segment of the globus pallidus (Gpi) and the subthalamic nucleus (STN), which send electrical impulses to the brain in an attempt to better control dyskinesia. DBS works as a “brain pacemaker” and although its mechanism of action is not completely understood, it is thought to act by inhibiting hyperactive regions in

the basal ganglia. DBS can mitigate motor symptoms of PD and/or directly diminish the side effects induced by L-DOPA pharmacotherapy, thereby allowing a decrease in medication dose allowing for a better management of motor symptoms.

The success of DBS has driven the gene therapy strategy of AAV-mediated expression of glutamic acid decarboxylase (GAD) in the STN, which is based on the assumption that ectopic GAD will catalyse the synthesis of gamma-aminobutyric acid (GABA), the major inhibitory neurotransmitter in the CNS, thereby providing lost inhibitory control in the STN and restoring appropriate synaptic balance. A Phase I clinical trial showed safety and tolerability to AAV2-mediated GAD gene transfer to the STN but after a Phase II randomised, multi-center, double blind, placebo control study, the programme was suspended because the results, although encouraging, did not surpass the current standard of care (Kaplitt et al. 2007; Bartus et al. 2014).

1.8.3 Restoration of Dopamine Synthesis in the Striatum

Since the discovery of dopamine as a neurotransmitter involved in the manifestation of PD pathology, the focus of pharmacological therapies has been on restoring the dopaminergic tone in the brain. Therapeutic strategies pursuing this goal follow one of three approaches, which are distinct in their interpretation as to which enzymes must be ectopically expressed to restore the imbalanced dopaminergic tone in the brain (Figure 9).

A. Pro-drug approach for enhanced DA synthesis

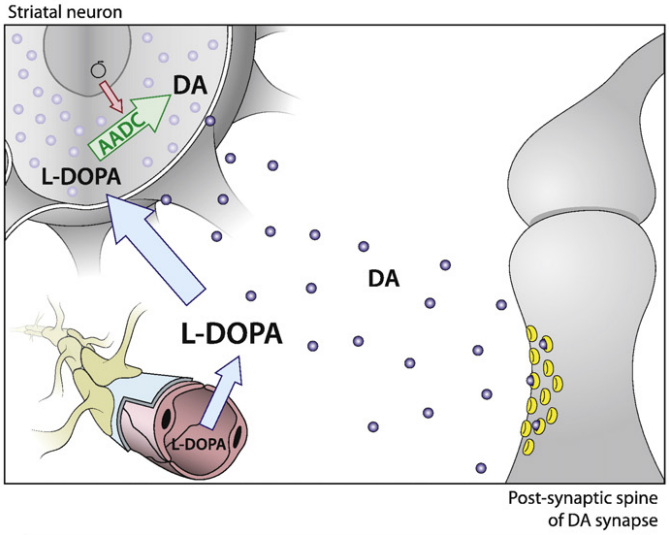

B. Dopamine replacement

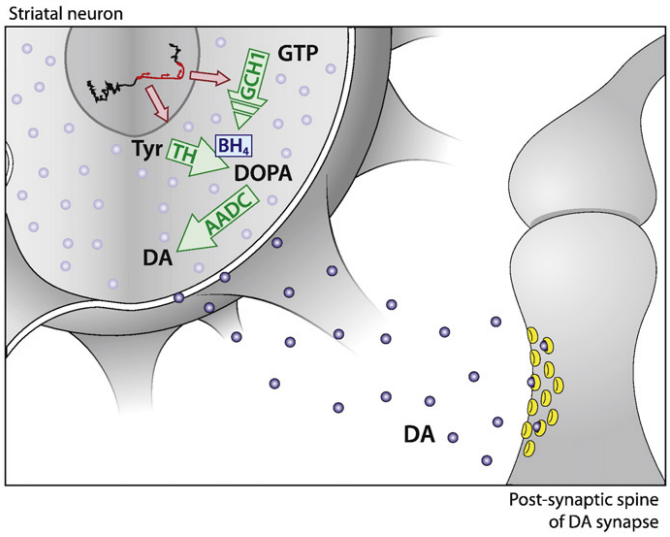

C. Continuous DOPA delivery strategy

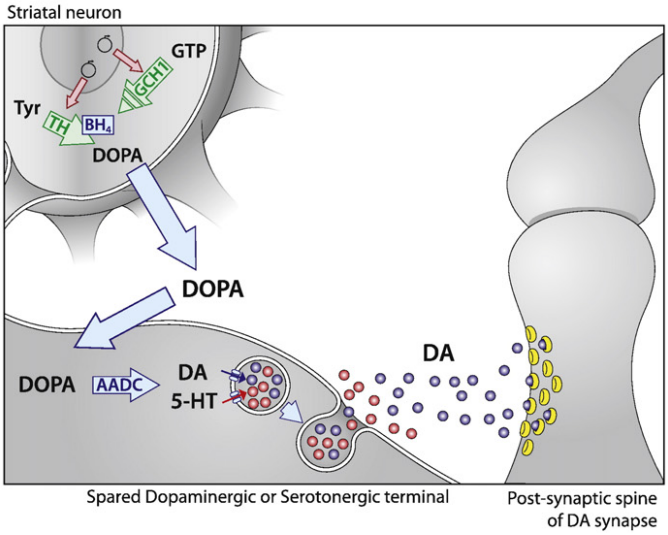

Figure 9: Schematic representation of viral vector-mediated enzyme replacement strategies for the restoration of the dopaminergic tone in the brain.
(A) Pro-drug approach for enhanced dopamine synthesis. L-DOPA from oral pharmacotherapy enters the brain over the BBB, is taken up by the transduced striatal neuron and is converted by the ectopic AADC to dopamine. The newly synthesised dopamine probably accumulates in the cytoplasm and diffuses towards the post-synaptic dopamine receptors providing symptomatic relief. (B) Dopamine replacement. Lentiviral-based expression of TH, GCH1 and AADC for dopamine synthesis. (C) Continuous DOPA delivery strategy. rAAV mediated gene transfer of TH and GCH1 results in transduced striatal neurons that can synthesise DOPA form dietary tyrosine at a constant rate. However, as the cells do not express AADC, L-DOPA exits the cell and ends up in spared dopaminergic fibres or serotonergic terminals, where it is converted by endogenous AADC into dopamine and stored in vesicles by the VMAT2 transporter. DA: dopamine; 5-HT: serotonin; TH: tyrosine hydroxylase; GCH: GTP-cyclohydrolase; AADC: aromatic amino acid decarboxylase; BH4: tetrahydrobiopterin; Tyr: tyrosine. (From: Björklund T. and Kirik D. Biochim Biophys Acta. 2009 Jul;1792(7):703-13).

The first approach, which proposes enhanced dopamine synthesis by the ectopic expression of AADC is known as the pro-drug approach. This approach is based on the clinical observation that PD patients have decreased AADC levels in their striatum and predicts that ectopic expression of AADC at high levels in the striatal neurons can restore the dopaminergic tone in the brain when the pro-drug (L-DOPA) is provided orally. This strategy has shown long-lasting therapeutic benefit in MPTP-lesioned NHP for up to 6 years after injection of an AAV2 vector expressing AADC in the putamen and is regarded a safe strategy because it allows for peripheral regulation of L-DOPA (Bankiewicz et al. 2006). So far, this approach has been successfully tested in two Phase I clinical trials (Christine et al. 2009; Muramatsu et al. 2010). However, a long-term follow-up study of the subjects enrolled in one of the trials demonstrated that following an improvement in the Unified Parkinson's Disease Rating Scale (UPDRS) in the first year, rating scores slowly deteriorated over the subsequent years (Mittermeyer et al. 2012). In response to this observation, delivery techniques were improved in order to achieve increased vector coverage in the putamen (San Sebastian et al. 2012). At the moment a Phase II AAV2-AADC trial is in progress but no data have been released yet.

The second approach to restore the dopaminergic tone in the brain is the dopamine replacement approach, which is based on the intrastriatal delivery of the three enzymes required for dopamine synthesis: TH, GCH1 and AADC. Ectopic dopamine production in the striatum, however, raises some concerns. Since the complete dopamine-synthetic machinery will be expressed in striatal

neurons that lack a dopamine vesicular storage system, dietary tyrosine reaching transduced neurons will be readily converted into free cytosolic dopamine. This has two potential undesired effects: firstly, the TH enzyme in the cytoplasm can be strongly inhibited by dopamine through its end-product negative feedback mechanism, thus compromising the therapeutic efficacy (Zigmond et al. 1989; Daubner et al. 2011). Secondly, cytosolic dopamine can cause severe oxidative stress and lead to cell death. This approach was tested in rodents and NHP using an integrating lentiviral vector to deliver the three enzymes to the striatum. The feedback inhibition issue was addressed by using a truncated form of the TH enzyme lacking its N-terminal regulatory domain, which abolishes its end-product inhibition mechanism. The NHP study showed efficacy of the lenti-TH-AADC-GCH1 gene transfer without triggering OFF drug dyskinesias as had been seen in previous studies with foetal grafting to treat PD (Freed et al. 2001; Olanow et al. 2003; Rylander Ottosson & Lane 2016). However, in an uncontrolled, open label Phase I/II clinical trial, this lentiviral gene transfer approach showed only modest efficacy, which was within the placebo range observed in the AAV2-NTN and AAV2-AADC trials (Marks et al. 2008; Christine et al. 2009). Nevertheless, the strategy was deemed as safe, with no adverse effects reported related to the gene therapy intervention. This observation is of paramount importance given that this was the first report of a lentiviral-based vector used to treat a condition affecting the CNS. Because of the modest efficacy seen in the trial and the failure of other gene therapies to meet the primary endpoints for efficacy in double-blind placebo controlled trials, the study leaders decided to continue only once their delivery strategy and vector have been optimised.

The third approach is an alternative to the dopamine delivery strategy and consists of continuous L-DOPA delivery to the striatum. At first, both strategies might look similar but in fact they differ in a number of key points. A first difference is in regard to the enzymes that are delivered by the viral vectors. Instead of providing the whole dopamine-synthetic machinery, the continuous L-DOPA synthesis approach delivers TH and GCH1, the two rate-limiting enzymes in L-DOPA synthesis and relies on endogenous AADC dopamine synthesis. This strategy addresses the potential issues raised for the dopamine replacement

approach by separating the compartment in which L-DOPA is synthesised (the transduced striatal neurons) and the compartment where it is converted into dopamine (the spared dopaminergic and serotonergic neurons expressing AADC). Through this separation, dopamine synthesis is restricted to neurons that naturally express AADC and are able to store the neurotransmitter in vesicles for controlled release. Although it might sound counter-intuitive to rely on the endogenous expression of AADC in a cell population that is affected by the progressive character of the disease, the gold-standard treatment with oral L-DOPA pharmacotherapy suggests that the endogenous levels of AADC expressed in spared neurons are sufficient to convert L-DOPA into dopamine. In addition, the progression of PD affects the serotonergic neurons (another source of AADC in the striatum) to a much lesser extent than the dopaminergic neurons and can therefore be regarded as a long-term source of AADC (Kish et al. 2008). Preclinical studies using AAV-mediated TH and GCH1 continuous L-DOPA synthesis in the striatum have shown improvement in motor tests as well as decrease in dyskinesia (Carlsson et al. 2005). Furthermore, dopamine synthesised after this gene therapy approach reaches post-synaptic receptors on striatal neurons in a physiological manner (Leriche et al. 2009).

The potential advantages of AAV-mediated continuous L-DOPA synthesis over direct dopamine synthesis lay the scientific rationale for studies done in this thesis: the expansion of this approach from the CNS to the periphery and the safety and efficacy studies in NHP following promising preclinical results in a rat model of PD.

1.9 Aims of the Thesis

Chronic intermittent oral L-DOPA pharmacotherapy leads to the development of side effects such as motor fluctuations and LID. Although the underlying pathophysiology of LID development remains elusive, the relationship between swings in the levels of circulating L-DOPA and LID is indisputable and patients under continuous dopamine receptor stimulation present significantly reduced dyskinesia compared with the standard intermittent oral L-DOPA therapy. Continuous L-DOPA synthesis can be achieved by gene transfer of the L-DOPA-

synthetic genes *TH* and *GCH1* to the CNS, as shown in a rodent model of PD, resulting in decreased parkinsonism and L-DOPA induced side effects.

This thesis evaluates two novel gene therapy strategies that propose a combination treatment of oral L-DOPA and a one-time AAV injection to deliver TH and GCH1 in order to achieve a continuous and basal L-DOPA supply, thereby diminishing the fluctuations inherent to oral treatment alone and improving management of L-DOPA induced side effects. The main aims of the proposed study are to:

1) Test whether elevated L-DOPA levels can be detected in the periphery of healty mice upon AAV-mediated delivery of the *GCH1* and *TH* genes to the liver.
2) Test the preclinical efficacy and safety of a candidate AAV vector in a NHP model of PD as well as develop and test improved versions thereof.

Chapter 2 Materials and Methods

2.1 Standard Molecular Biology Techniques

2.1.1 Molecular Cloning

2.1.1.1 Standard Polymerase Chain Reaction (PCR)

This is the basic PCR reaction that was used for colony screening and other tests. The polymerase kit used is the standard GoTaq® DNA polymerase (Promega). PCR reactions were carried out in a total volume of 25µl containing (final concentrations): 200µM dNTPs (NEB), 1X Colourless GoTaq Reaction Buffer, 1.25U GoTaq DNA polymerase, 1µM each of the primers, ~50ng DNA, and ddH_2O to a final 25µl volume. 0.01µmol of unmodified oligonucleotide primers for PCR amplification were obtained from Eurofins MWG Operon and resuspended with ddH_2O to make stock solutions at 100µM. Forward (sense) and reverse (anti-sense, reverse complement) oligonucleotide primers were designed following the manufacturer's instructions: 15-30 nucleotides in length, 40-60% GC content, and terminating in at least one G/C base. For information on the primers used in this thesis see table (Appendix A p. 217). PCRs were performed using an Eppendorf Mastercycler ep gradient thermocycler. A typical PCR reaction initiated with a 2 minute denaturing step at 95˚C followed by 25-35 cycles including a denaturing step of 20 seconds at 95˚C, an annealing step of 45 seconds at the optimal temperature for each primer pair and an extension step of 1 minute per kb at 72°C. A final 5 minutes extension at 72°C followed the cycles. Reactions were kept at 4°C until use.

2.1.1.2 High Fidelity PCR

For all PCR reactions performed to amplify DNA fragments for cloning, the Phusion High Fidelity polymerase kit (Thermo Scientific) was used to ensure high fidelity amplification of target sequences. PCR reactions were carried out in a total volume of 25µl, in a mixture containing (final concentrations) 10-50ng of DNA template, 0.5µM of forward and reverse primers, 10mM of dNTPs (NEB), 0.02u/µl Phusion® High-Fidelity DNA polymerase (Thermo Scientific), 1X

Phusion® HF or GC Buffer and brought to the final volume with ddH_2O. PCRs were performed using an Eppendorf Mastercycler ep gradient thermocycler. Phusion GC buffer was used in reactions that initially did not work with HF buffer, as it is indicated for GC-rich templates or those that form secondary structures. Reaction conditions varied depending on the size and GC content of the fragment to be amplified. A typical PCR reaction initiated with a 30s denaturing step at 98°C followed by 25-35 cycles including a denaturing step of 10s at 98°C, an annealing step of 20s at the optimal temperature for the primer pair and an extension step of 30s/kb at 72°C. A final 5 min extension at 72°C followed the cycles. Reactions were kept at 4°C until use. The annealing step temperature was adjusted to the melting temperature of the primers. Primers were designed and obtained from Eurofins MWG Operon. For some cloning strategies, primers were designed with external overhangs containing restriction endonuclease sites matching those in the destination construct. For information on the primers used in this thesis see table (Appendix A, p. 217).

2.1.1.3 Site-directed Mutagenesis for the Generation of LP1-mutated Constructs

Side-directed mutagenesis was used to insert point mutations in the LP1 promoter sequence. Mutagenesis primers were ~40nt long and included a central mismatched nt flanked by ~20nt homologous to the parental plasmid. Reactions were done in a total volume of 50µl using 30ng of template DNA, 200µM dNTPs (NEB), 8µl 5M betaine solution (Sigma), 125ng of each primer and 1.25µl Phusion High Fidelity Polymerase (Fischer Scientific) in appropriate buffer. Conditions of the PCR amplification were as follows: 98°C (30s), followed by 12 cycles of 98°C (10s)/ 55°C (60s)/ 72°C (3min), and a final extension at 72°C for 10min. For information on the primers used in this thesis see table (Appendix A, p. 217).

2.1.1.4 Agarose Gel Electrophoresis

Amplified DNA PCR products or DNA fragments from restriction endonuclease digestions were diluted with 5X DNA loading dye (NEB). Agarose gels were

prepared by dissolving agarose powder (UltraPure™ Agarose, Life Technologies) in 1X TAE buffer (10X: Tris-Base 48.4g/L, Acetic acid 11.4ml/L, EDTA 3.7g/L) and heating until dissolved. The agarose percentage was varied between 0.8% and 1.5% depending on the size of the fragment to be observed/isolated, with higher percentages used to achieve better separation of smaller fragments. After allowing the dissolved agarose to cool down, 1µg/ml of Ethidium bromide solution (Sigma) was added and the mixture was poured into an electrophoresis tank (BioRad). Once solidified, the gel was immersed in 1X TAE buffer and DNA samples were loaded in the wells of the gel. Gels were run at 120V for about 30-90 minutes, depending on the separation required between bands. Band sizes were monitored with the 100bp or the 1kb DNA ladder (NEB), which was run in parallel to the samples. Ethidium bromide-stained DNA fragments were visualised under a ultra-violet trans-illuminator using a ChemiDocTM XRS+ System (BioRad).

2.1.1.5 Extraction and Purification od DNA Fragments from Agarose Gels

DNA fragments of interest were excised from agarose gels and purified using the Qiagen Gel Extraction Kit. Three volumes of solubilisation and binding QG buffer were added to the agarose gel slice, the mixture was heated to 50°C for 10 minutes and mixed to dissolve the slice. One volume of isopropanol was added to the mixture, which was subsequently loaded onto a QIAquick spin-column. DNA was bound to the column by centrifugation at 13000 rpm for 1 min, after which flow-through was discarded and the column was washed with 750µl of ethanol-containing PE buffer and centrifuged twice to completely remove ethanol. The DNA was finally eluted into a sterile eppendorf tube with 30µl of ddH_2O.

A similar procedure was used to purify restriction endonuclease digestion products that were not run on agarose gels. The same kit and protocol were used, with the exception that the restriction endonuclease digestion mixture was directly mixed with the QG buffer and isopropanol.

2.1.1.6 DNA Digestion with Restriction Endonucleases

For analytical restriction endonuclease (RE) digestions, 0.5µl of RE (NEB) were used to digest 500ng of plasmid DNA in a 1X solution of the manufacturer's supplied buffer, and total reaction volume was adjusted to 50µl with ddH2O. For RE digestions to generate fragments for cloning, 1µl of RE was used to digest 2-5µg of DNA. All reactions were performed at the indicated temperature for the used RE (generally at 37˚C) for 2 hours. When double digestions with two different restriction enzymes were performed, a compatible reaction buffer was used as indicated by manufacturer. After single-enzyme digestions to generate plasmid fragments for cloning, vector DNA was treated with calf intestinal phosphatase (CIP, NEB) to remove the 5' phosphate group from the digested vector and to prevent re-circularisation between compatible ends. 0.5µl of CIP were added directly to the RE digestion mixture and incubated at 37˚C for 30 minutes and further purified as described above.

2.1.1.7 DNA Ligations

The purified DNA insert and vector were mixed at a 3:1 ratio with 1µl of 10X T4 ligase buffer (NEB) and 0.5µl of T4 ligase enzyme (NEB), in a total reaction volume adjusted to 10µl with ddH_2O. Reactions were incubated at room temperature for 2 hours or overnight at 16˚C.

2.1.1.8 Competent Bacterial Cells: Media and Maintenance

For DNA transformations and plasmid DNA amplification two strains of chemically competent bacteria were used. The *Escherichia coli* SURE supercompetent cells (Stratagene), that have reduced recombination potential, were used for transformation and amplification of plasmids containing AAV ITRs and grown at 30˚C. The *Escherichia coli* DH10B competent cells (Thermo Fisher) were used for all other plasmids and cultured at 37˚C. Competent cells were stored at -80˚. Autoclaved LB (Fisher Scientific, 20g/L ddH_20) was used for liquid cultures. Autoclaved LB agar (37g/L ddH_20) set in Sterilin 10cm Petri dishes was used for solid phase growth cultures. Antibiotics were added to room temperature autoclaved broth or autoclaved agar cooled to 50°C. Ampicillin

(Sigma, 100µg/ml in dH_2O) or Kanamycin Sulphate (Fisher Scientific, 50µg/ml in ddH_2O) were used for selection. Stock preparations of transformed bacteria were kept as glycerol stocks (bacterial pellet resuspended in LB containing 10% glycerol) at -80˚C.

2.1.1.9 Transformation of Competent Bacteria

5µl of the DNA insert-vector ligation reaction or 10-50ng of plasmid DNA was used for transformation into competent cells following the manufacturer's protocol. For SURE competent cells, 50µl of competent bacteria cells were initially incubated with 1µl of β-mercaptoethanol for 10 minutes on ice. DNA was then added and incubated for 30 minutes on ice, followed by a heat shock at 42°C for 45 seconds and further 2 minutes on ice. For DH10B competent cells, 50µl of cells were mixed with DNA and incubated for 30 minutes on ice, followed by a 30 second heat shock at 42˚C and a final 2 minutes incubation on ice. In both cases, reactions were then incubated with 250µl of LB at 30˚C for 1 hour and plated on LB agar plates containing the appropriate antibiotic. Plates were incubated upside down at 30˚C or 37°C overnight.

2.1.1.10 Plasmid DNA Amplification and Purification – Mini Preps

Single colonies from transformed or re-streaked bacteria were inoculated in 3ml of LB containing antibiotic and incubated at the appropriate temperature overnight in a shaking incubator. On the following day, 2ml of the culture were transferred to an eppendorf tube and cells were pelleted in a bench-top centrifuge at 8000rpm for 4 minutes. DNA was extracted using the Qiagen mini prep kit. Briefly, cells were re-suspended Qiagen P1 buffer and then lysed in 250µl of P2 lysis buffer and mixed by inverting the tube. After a 3-minutes incubation at room temperature, P3 neutralisation buffer was added to the mixture and DNA was separated from bacterial debris by centrifugation at 14000 rpm for 10 minutes in a bench-top centrifuge. Supernatant containing DNA was then transferred to a QIAprep spin column to bind DNA followed by washing with ethanol containing PE buffer and elution in 30µl of ddH_2O. DNA was kept at 4˚C for short term storage or at -20˚C for longer storage.

2.1.1.11 Plasmid DNA Amplification and Purification – Midi/Maxi Preps

One ml of transformed bacteria culture or a 10µl from a glycerol stock were inoculated overnight in 100ml (400-600ml for maxi preps) of LB with antibiotic selection. Cells were harvested by centrifugation at 6000 g for 15 min at 4°C and DNA extraction was performed using the NucleoBond® Xtra Midi/Maxi kit (Macherey-Nagel), following the manufacturer's protocol. The general principle behind this plasmid purification protocols is based on a modified alkaline lysis procedure, followed by plasmid DNA binding to a NucleoBond resin under appropriate low salt and pH conditions. RNA, proteins, dyes and low molecular–weight impurities are removed by several washing steps, and the plasmid DNA is finally eluted in a high-salt buffer, concentrated and desalted by isopropanol precipitation and washed in ethanol. Finally, the clean DNA pellet was allowed to air dry before re-suspension in 100-1000µl ddH_2O depending on the amount of purified DNA and the desired final concentration. DNA concentration was subsequently measured (see below). Preparations obtained by this method were typically at a concentration of 0.5-1µg/µl and stored short-term at 4˚C or for long-term at -20˚C.

2.1.1.12 Determining DNA Concentration

DNA concentration was determined using a Nanodrop ND-100 Spectrophotometer (Labtech International). Following a blank measurement with the solvent solution, 1µl of undiluted DNA preparation was loaded onto the measuring pedestal. The Nanodrop calculates the DNA concentration measuring the sample absorbance at 260nm (OD_{260}) and assuming that 1 OD_{260} unit corresponds to 50µg/ml of double-stranded DNA. The purity of the DNA sample can be assessed by the OD_{260}/OD_{280} ratio, which at ~1.8 is considered free from protein contamination.

2.1.1.13 DNA Sequencing

DNA sequencing was performed by Eurofins MWG Operon from 1.5µg of plasmid DNA in 15µl ddH_2O pre-mixed with 2µl of the appropriate primer at 10pmol/µl. Sequencing was performed using the Value Read service in tube format, results were returned online and subsequently analysed using the APE DNA analysis software and the NCBI Blast tool.

2.1.2 Total DNA Extraction

For total/genomic DNA extraction the Qiagen DNeasy Blood & Tissue Kit was used as per manufacturer's instructions. Cells are first washed in PBS and pelleted (~30mg frozen tissue was cut and weighed), followed by lysis and proteinase K digestion to remove all proteins. The DNA isolation/purification is performed using a silica-based DNA purification in spin-columns using the kit buffers.

2.1.3 Total RNA Extraction

RNA extraction was performed using the RNeasy mini Kit (Qiagen), following the manufacturer's instructions. Cells were first washed in PBS and pelleted, followed by lysis in the supplied buffer, homogenization using a syringe and a 21 gauge needle, and column purification. RNA was eluted using 50µl RNAse-free water (supplied) and the concentration determined using the Nanodrop spectrophotometer in a procedure analogous to that used for DNA. The RNA was diluted in a total volume of 85µl RNAse-free water and mixed with 10 µl Buffer RDD and 5µl of DNase I stock solution and incubated for 20 min at room temperature. The DNAse I-treated RNA was then re-cleaned using the RNeasy kit (following the RNA clean-up protocol). The DNase I stock solution was prepared by dissolving the lyophilised DNase I (1500 Kunitz units, QIAGEN) in 550µl of the RNase-free water provided. RNA was stored at -80˚C.

2.1.4 Total Protein Extraction

Volumes indicated are for a well of a 24 well plate. Cells were harvested and washed in PBS and pelleted. The cell pellet was then dissolved in 50µl NP-40 lysis buffer (150mM NaCl, 1% NP-40, 50mM Tris HCl pH 8) containing 2µl of 25X protease inhibitor cocktail (Complete, Roche), and incubated on ice for 10 min. For tissues, ~30mg were mixed with 450 µl NP-40 lysis buffer, sonicated 4x 10s and mixed for 2h at 4˚C. Lysates were then spun at 13000 rpm for 10 min at 4˚C and the supernatant transferred to a clean 1.5ml tube. Proteins were stored at -80˚C.

2.1.5 DNA and RNA Detection and Analysis

2.1.5.1 Reverse Transcription

For gene expression analysis, RNA was reverse-transcribed using the High-Capacity cDNA Reverse Transcription Kit (Applied Biosystems) following the manufacturer's instructions. First, a 2X RT master mix was prepared by mixing (volumes for one reaction) the following provided reagents: 2µl 10X RT buffer, 0.8µl dNTP mix (100mM), 2µl 10X RT random primers, 1µl MultiScribe™ Reverse Transcriptase, 4.2µl nuclease-free ddH_2O. 10µl of 2X RT master mix were then mixed with 10µl RNA at the desired concentration. Reverse transcription was performed using a thermal cycler with the following program: 10 min at 25˚C, 2h at 37˚C, 5 min at 85˚C. The obtained cDNA was stored at 4˚C for short-term storage or at -20˚C for long-term storage, and was used for relative quantification by qPCR (see below).

2.1.5.2 Real-time quantitative PCR: relative quantification

3'FAM-5'MGB-conjugated qPCR probes and qPCR primers designed to bind to the *TH*, *GCH1* or the *β-actin* genes were obtained from Thermo Fischer. qPCR was performed on cDNA using the TaqMan Universal PCR master mix (Life Technologies) and the custom primer-probe mix of choice; primers were used at a final concentration of 900nM, and probes at 250mM. Relative expression levels

were determined by the comparative threshold cycle (Ct) method (Schmittgen & Livak 2008).

2.1.6 Protein Detection and Analysis

2.1.6.1 SDS-PAGE

10µl of protein extracts in NP-40 lysis buffer were mixed with 2µl of loading buffer (0.8g SDS, 5ml Tris pH 6.8, 5ml glycerol, 4mg bromophenol blue, 5% beta-mercaptoethanol) and denatured by boiling for 15 min. Subsequently, proteins were separated in 10% or 12% polyacrylamide gels. The percentage was determined by altering the volume of 40% Acrylamide solution (Acrylamide:Bis-Acrylamide 29:1, Fisher Scientific) and ddH_2O to a reaction mixture of 1.5M Tris-HCl pH 8.8, 0.4% SDS, 3.3µl/ml 10% ammonium persulphate (APS, Sigma) and 0.6µl/ml of N,N,N'N'- Tetramethylethylenediamine (TEMED, Sigma). The stacking gels were made using 0.5M Tris-Cl pH 6.8, 0.4% SDS, 5µl/ml 10% APS, 1µl/ml TEMED and ddH_2O. Polymerised gels were transferred to the running tank and immersed in running buffer (100ml 10X Tris-glycine and 10ml 10% SDS and ddH_2O to 1L). 10X Tris-glycine was prepared by mixing 61g Tris base and 288g glycine in 2L ddH_2O. Gels were typically run at 120V until the blue dye front had migrated to the bottom of the gel, using the Protean II mini gel electrophoresis kit (BioRad). 2µl of Precision Plus Protein Dual Colour Standards (Bio-Rad) was used as a guide for molecular weights in all gels.

2.1.6.2 Western Blot

Proteins resolved in SDS-PAGE were transferred onto pure nitrocellulose 0.45µm membrane (VWR International). Gel to membrane transfer was achieved using a BioRad Mini Trans-Blot® transfer system with transfer buffer (100ml 10X Tris-glycine, 200ml methanol, 700 ml ddH_2O) at 16V overnight or at 100V on ice for 60 min. After transfer, membranes were removed from the transfer tank and blocked with 5% (w/v) skimmed dried milk in PBS-Tween (1X PBS, 0.1% Tween 20, Sigma) for 1h. Membranes were then incubated with the

indicated primary antibody in 5% milk in PBS-Tween for 3h at room temperature or overnight at 4˚C. Next, membranes were washed 3 times for 15 min in PBS-Tween and subsequently incubated with the corresponding horseradish peroxidase (HRP)-conjugated secondary antibody for 1h. Finally, membranes were washed three times for 15 min in PBS-Tween and developed. The signal of membranes incubated with HRP-conjugated secondary antibodies was detected using the SuperSignal West Pico chemiluminescene substrate (Thermo Scientific), prepared according to the manufacturers' instructions and applied on the membrane for 5 min. The membrane was then placed between two clear plastic sheets and imaged using a Image Quant LAS4000 (GE Healthcare) chemiluminescence imaging technology.

2.1.7 Engineering of Recombinant AAV Producer Plasmids

2.1.7.1 AAV Plasmids for Brain Targeting Vectors

2.1.7.1.1 pAAV-SYN-GCH1-SYN-TH (pGPT002)

The AAV producer plasmid pAAV-SYN-GCH1-SYN-TH-WPRE (pGPT002) expresses both enzymes, GCH1 and TH, from a single-vector genome with two identical and independent promoters. The organisation of the expression cassettes is identical to the one used by Cederfjäll et al (Cederfjäll et al. 2012). Expression of GCH1 and TH genes is under the control of the human synapsin promoter (SYN) and a modified posttranscriptional regulatory element of the woodchuck hepatitis virus (WPRE), in which expression of the putative oncogenic woodchuck hepatitis virus X protein (WHX) was silenced, is present between the TH coding sequence and the SV40 polyA. The expression cassettes were synthesised with flanking BglII restriction endonuclease sites (p65050), which were then used to subclone them into the AAV2 ITR-containing plasmid pTRUF11.

2.1.7.1.2 pAAV-SYN-GCH1-SYN-tTH (pLA109)

The AAV producer plasmid pAAV-SYN-GCH1-SYN-tTH-WPRE (pLA109) is almost identical to GPT002, with the difference being the absence of the first 465nt of the TH gene (correspondent to the first 155 N-terminus amino acids). This truncation, that renders a constitutively active TH, was generated by isothermal assembly followed by PCR and replacement of the full length TH in GPT002 by the truncated PCR product. In brief, a first PCR was carried out to generate a ~2050bp fragment of the SYN-GCH1-SYN sequence containing a BglII restriction endonuclease site on the 5' end and a 3' overhang with a start codon followed by a sequence overlapping the 18nt correspondent to amino acids 157 to 163 in the TH protein. Fragment one was amplified using Phusion High Fidelity Polymerase (Fischer Scientific) in appropriate buffer, 200µM dNTPs (NEB), p65050 as a DNA template and primer pair LA43/LA44. The cycling conditions were: 98°C (30s), followed by 30 cycles of 98°C (10s)/ 63°C (30s)/ 72°C (60s), and a final extension at 72°C for 10 min. A second PCR was done on p65050 to amplify the TH gene without the 465nt immediately after the start codon using the same cycling conditions as above and primer pair LA45/LA46. This generated a product of ~1850bp in which the first 18bp of the 5' end were complementary to the last 18bp at the 3' end of fragment one, allowing their combination by isothermal assembly (Gibson et al. 2009). The isothermal assembly was done by mixing equimolar amounts (~100ng) of fragments one and two, isothermal assembly buffer and 1M betaine solution (Sigma) in a total volume of 20µl. The mix was incubated for 1h at 50°C, after which 5µl were used as a template for a PCR reaction. Because the length of the assembled fragment obtained in the reaction (~4kb) could be difficult to amplify, a new primer pair was designed (LA47/LA48), which led to the amplification of a ~1.5kb fragment comprised of the GCH1 polyA followed by the SYN and approximately half of the newly truncated TH gene. The PCR was done using Phusion High Fidelity Polymerase (Fischer Scientific) in appropriate buffer and 200µM dNTPs (NEB). The cycling conditions were: 98°C (30s), followed by 30 cycles of 98°C (10s)/ 63°C (30s)/ 72°C (60s), and a final extension at 72°C for 10 min. The resulting fragment was cloned into pGPT002 digested with the restriction endonucleases NsiI and EcoNI (NEB), thereby creating pLA109.

2.1.7.1.3 pAAV-SYN-GCH1-CMV-TH (pGPT004)

The AAV producer plasmid pAAV-SYN-GCH1-CMV-TH-WPRE (pGPT004) was created by amplifying the CMV-TH cassette from the vector pAAV-TH (Muramatsu et al. 2002) and cloning it in pGPT002 in place of the SYN-TH sequence . The CMV-TH fragment was amplified in a 20µl reaction using 50ng pAAV-TH as a template, 200µM dNTPs (NEB), Phusion High Fidelity Polymerase (Fischer Scientific) in appropriate buffer and primer pair AA133/AA134. Conditions of the PCR amplification were as follows: 98°C (30s), followed by 30 cycles of 98°C (10s)/ 59°C (15s)/ 72°C (80s), and a final extension at 72°C for 10 min. The ~3.2 kb fragment was digested and ligated into pGPT002 digested with the restriction endonucleases MfeI and partially digested with BglII (NEB), so that only the SYN-TH sequence was removed. The partial digestion was necessary due to the presence of a second BglII endonuclease restriction site present immediately downstream of the L-ITR in pGPT002. This bicistronic construct was named pGPT004.

2.1.7.2 AAV plasmid for Liver Targeting Vectors

2.1.7.2.1 pdsAAV-LP1-GCH1 and pdsAAV-LP1-tTH (pAA009 and pAA010)

The AAV producer plasmids pdsAAV-LP1-GCH1 (pAA009) and pdsAAV-LP1-tTH (pAA010) were used to produce the double-stranded rAAV2/8-LP1-GCH1 and rAAV2/8-LP1-tTH, respectively. Briefly, pAA009 and pAA010 were constructed by digesting scAAV-LP1-hFIXco with XbaI and SpeI and ligating it after NheI digestion with either the GCH1 or tTH PCR fragment isolated from pLA100 (ssAAV-SYN-GCH1-SYN-TH-WPRE) and pLA109 (ssAAV-SYN-GCH1-SYN-tTH), respectively. The scAAV-LP1-GCH1 (pAA009) and scAAV-LP1-tTH (pAA010) vectors were constructed as follows: The 992bp GCH1 fragment of pLA100 (AAV-SYN-GCH1-SYN-TH) was amplified using primer pair AA16/AA17 at a concentration of 0.75pmol/µl with 25ng template pLA100, 200µM dNTPs (NEB) and GoTaq Polymerase (Promega) in appropriate buffer. Conditions of the PCR amplifications were as follows: 95°C (2min), followed by 30 cycles of 95°C (30s)/ 65°C (30s)/ 72°C (30s), and a final extension at 72°C for 5 min. The

1858bp tTH-WPRE fragment of pLA109 (AAV-SYN-GCH1-SYN-tTH) was amplified using primer pair AA33/AA34 0.4pmol/µl, 25ng template pLA109, 200µM dNTPs (NEB) and Phusion Polymerase (Thermo Scientific) in appropriate buffer. Conditions of the PCR amplifications were as follows: 98°C (30s), followed by 30 cycles of 98°C (10s)/ 63°C (30s)/ 72°C (1min), and a final extension at 72°C for 10 min.

The final transgene constructs are two plasmids for dsAAV production containing either the human GCH1 or the tTH gene under the control of the liver-specific LP1 enhancer/promoter, all flanked by AAV2 ITRs.

2.1.7.2.2 pAAV-LP1-GCH1-LP1-tTH (pAA019)

AAV producer plasmid pAAV-LP1-GCH1-LP1-tTH-WPRE (pAA019) was used to generate the single-stranded rAAV2/8-LP1-GCH1-LP1-tTH-WPRE and its recombination by-product rAAV2/8-LP1-tTH. Briefly, the expression cassettes LP1-GCH1-LP1-tTH-WPRE were subcloned into pBluescript II SK(+) to make pAA018 prior to cloning into the AAV ITR containing backbone pSUB201 (pAA019).

The first LP1 promoter was amplified using scAAV-LP1-hFIXco (Nathwani et al. 2006) as a template and cloned into pTRUF11 (ATCC® MBA-331™) between the BlpI and SbfI restriction sites, thereby generating pAA001. Next, the GCH1 gene was amplified from pLA100 (pAAV-SYN-GCH1-SYN-TH-WPRE) as a template and subsequently cloned into pAA001 using the SbfI and Tth111I sites, thereby forming pAA002. Next, the LP1-GCH1 fragment was amplified from pAA002 using the primer pair AA37/AA38, which contained 5' XbaI/BlpI and 3' XbaI/SphI/BstBI/Tth111I multiple cloning site overhangs to allow the construction of a modular vector. The LP1-GCH1 fragment was ligated into the AAV backbone pSUB201 (Samulski et al. 1987) through XbaI restriction sites, thereby forming pAA003. To avoid cloning difficulties due to the presence of ITRs in psub201, the LP1-GCH1 cassette was transferred to the cloning vector pUC18 (Thermo Scientific) through the XbaI sites, thereby generating pAA004. The second LP1 promoter was amplified from pAA010 with the primer pair AA006/AA07 and cloned into pAA004 using BstBI and Tth111I restriction sites,

thereby generating pAA005. In order to add the tTH gene to the construct, the LP1-GCH1-LP1 fragment had to be transferred to the pBluescript II SK(+) vector due to the presence of an extra SphI site in the pUC18 backbone. The backbone transfer was done by cutting LP1-GCH1-LP1 out of pAA005 using the XbaI sites and ligating it into pBluescript II SK(+). The new construct was named pAA006. Next, the tTH-WPRE fragment was amplified from pLA109 (pAAV-SYN-GCH1-SYN-tTH-WPRE) using primer pair AA53/AA65. The tTH-WPRE sequence was inserted into pAA006 through the restriction sites SphI and BstBI, thereby forming pAA017. After sequencing of pAA018, a mutation on the Tth111I site was found and fixed by recloning the GCH1-LP1 sequence. At this point, a new primer set was designed to add a BglII restriction site immediately downstream of the Ttth111I site and, additionally, to allow the incorporation of the GCH1 Kozak sequence as in pLA100 and pLA109. Primer pairs AA73/AA84 and AA85/AAA07 were used to amplify the new GCH1 sequence and the second LP1 promoter, respectively. An overlapping PCR was done to fuse GCH1-LP1 using primer pair AA73/AA07, which was subsequently cloned into pAA017 using restriction sites SbfI and BstBI, thereby forming pAA018. Finally, the bicistronic LP1-GCH1-LP1-tTH expression cassette was transferred back to the AAV backbone psub201. This final plasmid was called pAA019 and was used for the production of a rAAV containing both human GCH1 and tTH genes under the control of the liver-specific LP1 enhancer/promoter, all flanked by AAV2 ITRs.

The 568bp LP1 fragment of the first LP1 promoter for pAA001 generation was amplified in a 20µl PCR reaction using 12.5ng scAAV-LP1-hFIXco template DNA, 200µM dNTPs (NEB), 0.5µM of primer pair AA01/AA02 and GoTaq Polymerase (Promega) in appropriate buffer. Conditions of the PCR amplification were as follows: 95°C (2min), followed by 30 cycles of 95°C (30s)/ 65°C (30s)/ 72°C (35s), and a final extension at 72°C for 5 min.

The ~1kb GCH1 fragment for pAA002 generation was amplified in 3x 25µl PCR reactions using 27ng pLA100 template DNA, 200µM dNTPs (NEB), 0.5µM of primer pair AA03/AA004 and GoTaq Polymerase (Promega) in appropriate buffer. Conditions of the PCR amplification were as follows: 95°C (2min), followed by 30 cycles of 95°C (30s)/ 68°C (30s)/ 72°C (35s), and a final extension at 72°C for 5 min.

The ~1.5kb LP1-GCH1 fragment for pAA003 generation was amplified in 5x 20µl PCR reactions using 20ng pAA002 template DNA, 200µM dNTPs (NEB), 0.5µM of primer pair AA37/AA38, 4µl/reaction of 5M betaine solution (Sigma) and Phusion High Fidelity Polymerase (Fischer Scientific) in appropriate buffer. Conditions of the PCR amplification were as follows: 98°C (30s), followed by 30 cycles of 98°C (10s)/ 56°C (30s)/ 72°C (45s), and a final extension at 72°C for 10 min.

The ~550bp LP1 fragment of the second LP1 promoter for pAA005 generation was amplified in a 20µl PCR reaction using 50ng pAA010 template DNA, 200 µM dNTPs (NEB), 0.5µM of primer pair AA006/AA07 and Phusion High Fidelity Polymerase (Fischer Scientific) in appropriate buffer. Conditions of the PCR amplification were as follows: 98°C (30s), followed by 30 cycles of 98°C (10s)/ 65°C (15s)/ 72°C (9s), and a final extension at 72°C for 10 min.

The ~1.8kb tTH-WPRE fragment for pAA017 generation was amplified in a 20µl PCR reaction using 50ng pLA109 template DNA, 200µM dNTPs (NEB), 0.5µM of primer pair AA53/AA65 and Phusion High Fidelity Polymerase (Fischer Scientific) in appropriate buffer. Conditions of the PCR amplification were as follows: 98°C (30s), followed by 30 cycles of 98°C (10s)/ 60°C (15s)/ 72°C (60s), and a final extension at 72°C for 10 min.

The ~1 kb GCH1 sequence to be used as a template for the overlapping PCR with the second LP1 was amplified in a 20µl PCR reactions using 25ng pLA109 template DNA, 200µM dNTPs (NEB), 0.5µM of primer pair AA73/AA84 and GoTaq Polymerase (Promega) in appropriate buffer. Conditions of the PCR amplification were as follows: 95°C (2min), followed by 30 cycles of 95°C (30s)/ 65°C (30s)/ 72°C (35s), and a final extension at 72°C for 5 min. The ~550 bp LP1 sequence to be used as a template for the overlapping PCR with GCH1 was amplified in a 20µl PCR reaction using 25ng pAA010 template DNA, 200µM dNTPs (NEB), 0.5µM of primer pair AA85/AA07 and Phusion High Fidelity Polymerase (Fischer Scientific) in appropriate buffer. Conditions of the PCR amplification were as follows: 98°C (30s), followed by 30 cycles of 98°C (10s)/ 65°C (15s)/ 72°C (20s), and a final extension at 72°C for 10 min. The overlapping PCR to fuse the GCH1 to the second LP1 was done in a 20µl reaction using 100ng and 50ng of GCH1 and LP1, respectively as template DNA, 200µM dNTPs (NEB),

0.5µM of primer pair AA73/AA07 and Phusion High Fidelity Polymerase (Fischer Scientific) in appropriate buffer. Conditions of the PCR amplification were as follows: 98°C (30s), followed by 30 cycles of 98°C (10s)/ 65°C (15s)/ 72°C (45s), and a final extension at 72°C for 10 min.

2.1.7.3 AAV Plasmids for Systemic Vectors

2.1.7.3.1 pAAV-EF1α-tTH-IRES-PTPS-2A-GCH1-WPRE-miR208aT (pAA062)

AAV producer plasmid pAAV-EF1α-tTH-IRES-PTPS-2A-GCH1-WPRE-miR208aT (pAA062) was constructed as follows. The short EF1α promoter was amplified using pMB13 as a template and cloned in place of the first LP1 promoter in pAA018 between the BlpI and SbfI restriction sites, thereby generating pAA057. Next, the tTH gene without the WPRE was amplified from pAA016 (pscAAV-HLP-tTH-WPRE) and subsequently cloned in place of the of the GCH1 gene in pAA057 using the SbfI and BglII sites, generating pAA058. Next, the encephalomyocarditis virus (EMCV) internal ribosome entry site (IRES) sequence was amplified from pCSIG (Matheson et al. 2015) and cloned into pAA058 using BglII and BstBI sites in place of the LP1 promoter, generating pAA059. Next, the EF1α-tTH-IRES-tTH-WPRE sequence was removed from the pBluescript II SK(+) backbone using XbaI (NEB) and ligated into the AAV backbone pSUB201, forming pAA060. The 6-Pyruvoyl-tetrahydropterin synthase (PTPS) and GCH1 genes were amplified from pAA020 and cloned into pAA060 using BstBI and SpeI restriction endonuclease sites in place of the second tTH, thereby generating pAA061. In a final step, two in tandem copies of the target sequence of the cardiac-specific microRNA-208a (Roudaut et al. 2013) were added to the cassette. The 42nt tandem sequence, that was originally synthesised and cloned into pAA056, was amplified and subsequently inserted into pAA061 through the restriction sites SalI and SpeI. This final plasmid was called pAA062 and it supports the production of a rAAV containing a truncated form of the human TH, the human PTPS and GCH1 under the control of the short EF1α promoter. The IRES sequence allows for the expression of the three genes from the same mRNA. The PTPS and GCH1 genes are linked in frame through the foot-

and-mouth disease virus (FMDV) 2A sequence, which, though a ribosomal skipping mechanism (Donnelly et al. 2001), leads to equimolar translation of both proteins.

The 268bp EF1α promoter sequence for pAA057 generation was amplified in a 20µl PCR reaction using 75ng pMB13 template DNA, 200µM dNTPs (NEB), 0.5µM of primer pair AA150/AA151 and Phusion High Fidelity Polymerase (Fischer Scientific) in appropriate buffer. Conditions of the PCR amplification were as follows: 98°C (30s), followed by 30 cycles of 98°C (10s)/ 59°C (15s)/ 72°C (10s), and a final extension at 72°C for 10 min.

The ~2.5kb tTH fragment for pAA058 generation was amplified in a 50µl PCR reactions using 25ng pAA016 template DNA, 200µM dNTPs (NEB), 0.4µM of primer pair AA152/AA153 and Phusion High Fidelity Polymerase (Fischer Scientific) in appropriate buffer. Conditions of the PCR amplification were as follows: 98°C (30s), followed by 30 cycles of 98°C (10s)/ 59°C (15s)/ 72°C (30s), and a final extension at 72°C for 10 min.

The ~600bp IRES sequence for pAA059 generation was amplified in a 20µl PCR reaction using 30ng pCSIG template DNA, 200µM dNTPs (NEB), 0.25µM of primer pair AA154/AA155 and Phusion High Fidelity Polymerase (Fischer Scientific) in appropriate buffer. Conditions of the PCR amplification were as follows: 98°C (3 s), followed by 30 cycles of 98°C (10s)/ 53°C (30s)/ 72°C (9s), and a final extension at 72°C for 10 min.

The ~1.3kb PTPS-2A-GCH1 fragment for pAA061 generation was amplified in a 20µl PCR reaction using 30ng pAA020 template DNA, 200µM dNTPs (NEB), 0.125µM of primer pair AA156/AA157 and Phusion High Fidelity Polymerase (Fischer Scientific) in GC buffer. Conditions of the PCR amplification were as follows: 98°C (30s), followed by 30 cycles of 98°C (10s)/ 53°C (30s)/ 72°C (10s), and a final extension at 72°C for 10 min.

The 42nt tandem copy of microRNA-208a sequence was amplified together with the WPRE sequence in a 20µl PCR reaction using 40ng pAA056 template DNA, 200µM dNTPs (NEB), 0.25µM of primer pair AA60/AA158 and Phusion High Fidelity Polymerase (Fischer Scientific) in appropriate buffer. The PCR cycling conditions were as follows: 98°C (30s), followed by 30 cycles of 98°C (10s)/ 55°C (30s)/ 72°C (14s), and a final extension at 72°C for 10 min.

2.1.7.3.2 pAAV-EF1α-TH-IRES-PTPS-2A-GCH1-WPRE-miR208aT (pAA063)

AAV producer plasmid pAAV-EF1α-TH-IRES-PTPS-2A-GCH1-WPRE-miR208aT (pAA063) was constructed as follows. The 543bp fragment that corresponds to the regulatory N-terminus portion of TH was removed from pGPT002 using the restriction endonuclease sites BstEII and ligated with the 7919bp fragment of pAA062 digested with the same enzyme.

2.2 Cell Culture and Transfections

2.2.1 Maintenance of Cell Cultures

All cell culture work was performed in assigned mycoplasma-free tissue culture hoods. Human embryonic kidney 293T cells (HEK293T) and human neuroblastoma cells (SH-SY5Y), obtained from the American Tissue Culture Collection (ATCC), were grown in Dulbecco's modified Eagle medium (DMEM) +4.5g/L Glucose, +L- Glutamine, +Pyruvate (GIBCO 41966, Invitrogen), and 10% heat inactivated (56°C for 30 min) foetal bovine serum (FBS, Invitrogen). Human hepatocellular carcinoma cells (Huh7.5) were obtained from ATCC and maintained in DMEM with 10% FCS and supplemented with non-essential amino acids (100X NEAA; Life Technologies) to a final concentration of 1X. All Cells were cultured at 37°C and 5% CO2 in 10cm dishes (Corning). Unless otherwise required, cells were regularly passaged using 1ml TrypLE™ Express (GIBCO 12605, Invitrogen). To passage them, cells were incubated with trypsin for 1-3 min at 37°C, re-suspended by repeated pipetting and the required proportion was transferred to a new 10cm dish containing pre-warmed fresh complete DMEM.

2.2.2 Freezing and Thawing of Cell Lines

Stocks of frozen cells were long-term stored in liquid nitrogen. To freeze cells, at least 2-3 confluent 10cm dishes of each cell line were prepared. Cells were detached using 1ml of trypsin and washed in 5-10ml fresh culture medium. After

harvesting the cells by centrifugation at 1200 rpm for 5 min, cells were re-suspended in 1ml of freezing medium containing 10% DMSO (Sigma), 50% FBS (Invitrogen) and 40% culture medium and immediately transferred to a 1.8ml labelled cryovial. Cryovials were initially stored at -80˚C and after 24-48 hours moved to a liquid nitrogen tank. To later recover the cryo-preserved cells, vials were thawed rapidly at 37°C, cells were pelleted at 1200 rpm for 5 min and rapidly resuspended into 10ml of pre-warmed DMEM with 10% FBS. Cells were left to recover in 10cm dish for at least 24-48h.

2.2.3 Mycoplasma Testing

Standard mycoplasma testing was performed regularly on all cells cultured in the mycoplasma-free tissue culture room using the MycoAlert™ Mycoplasma Detection Kit (Lonza) and the controls from the MycoAlert™ Assay Control Set (Lonza) following the manufacturer's protocol. This test is based on the activity of mycoplasmal enzymes that are found in all six of the main mycoplasma cell culture contaminants but are not present in eukaryotic cells, which convert ADP present in the Mycoalert substrate to ATP. The ATP is then transferred into a light signal via the luciferase enzyme in the MycoAlert Reagent. By measuring the level of ATP in a sample both before (read A) and after the addition of the MycoAlert Substrate (read B), a ratio can be obtained which is indicative of the presence or the absence of mycoplasma.

2.2.4 Transient Transfection of DNA Plasmids

For regular plasmid DNA transfection, HEK 293T cells were seeded and transfected 24 h later using polyethylinimine (PEI, Polysciences). On the day of transfection, DNA and PEI (3.5µl/µg DNA, pH 7) were separately diluted in serum-free DMEM before being mixed together and incubated for 20 min at room temperature before being added to the cells. The final volume of the transfection mix was 1/10 the volume of the final culture vessel cells were grown in.

2.2.5 Recombinant AAV Production and Titration

2.2.5.1 Transfection with Producer Plasmids and Harvesting

To prepare rAAV vector stocks, HEK 293T cells were seeded in 10-stack cell chambers (6360 cm^2/chamber) (Corning) in a density of $5x10^8$ cells/chamber. Twenty-four hours later, the cells were 60-70% confluent and ready to be transfected. Transfection mixes were set up as shown in Table 1:

Reagent/Plasmid	Amount/chamber
Transgene plasmid	160 µg
pLT2-AAV8 (Rep and Cap)	160 µg
HGTI helper plasmid	480 µg
DMEM Serum Free	120 ml
PEI Max, pH 7	2.8 ml

Table 1: Reagents and plasmids used in triple transfection schemes for rAAV2/8 production.

pLT2-AAV8 codes for serotype 2 Rep78 and serotype 8 VP1, VP2 and VP3 capsid proteins; HGTI codes for the adenoviral proteins E2a and E4orf6 and the VA RNAs (Matsushita et al. 2004; McIntosh et al. 2013), which together provide the helper functions. HEK293T cells express the additional adenoviral helper proteins required for rAAV production. rAAV produced following this triple transfection scheme was a pseudotyped AAV8 vector containing AAV2 ITRs and AAV8 capsid proteins (AAV2/8). AAV8 has a tropism for the liver and was therefore used in this study (Nakai et al. 2005). After 20 min incubation at room temperature, the transfection mix was added to 1L pre-warmed DMEM (Gibco) supplemented with 10% FBS. This transfection media was subsequently added to the 10-stack cell chamber in replacement of the old media. After 72h incubation, media from the chamber was collected; attached cells were washed with PBS and harvested with trypsin. The cells were subsequently spun at 2000g for 10 min, the pellets washed with PBS, spun again at 2000g for 10 min, and resuspended in 15ml of lysis buffer (150mM NaCl, 50mM Tris pH 8.5). Cell lysis was done by three freeze/thaw cycles (alternating - 80˚C to 37˚C water bath). The virus present in the media was precipitated with ammonium sulphate

(31.3g/100ml media) and the pellet resuspended in 15 ml lysis buffer. The crude lysate and supernatant precipitate were then treated with 5000 units/chamber of benzonase (Sigma) in the presence of 1mM $MgCl_2$, and incubated in a 37°C water bath for 30 min before further purification either by AVB sepharose affinity column or iodixanol density gradient.

2.2.5.2 Recombinant AAV Purification on AVB Sepharose Column

AVB Sepharose is an affinity medium with affinity for several AAV serotypes and enables its purification in one step with high purity.

Crude lysate was filtered through a 0.2µm filter before loading into the AVB sepharose column equilibrated with PBS at pH 7.0. In a second step, the column was washed with PBS to eliminate unbound particles. AAV was eluted in 50mM glycine solution pH 2.7 and collected in 1ml fractions into tubes containing 30µl Tris buffer pH 8.8 to neutralise the glycine elution buffer. Tubes corresponding to the 260mm and 280mm graph peaks are the ones containing the virus. They were pooled together (~2.5ml) and injected into 10000 MWCO dialysis cassettes (Thermo Scientific). Dialysis cassettes containing the purified virus were stirred overnight in 1L PBS at 4°C. Finally, the dialysed virus was removed from the cassette and stored at 4°C until titration.

2.2.5.3 Recombinant AAV Purification by Iodixanol Density Gradient

Following benzonase treatment, the lysis buffer containing the lysed cells and the respuspended proteins from the supernatant were spun at 4200 rpm for 30 min. The supernatant was loaded onto ULTRA-Clear 14 x 89mm ultracentrifuge tubes (Beckman Coulter) containing 1.55ml, 1.55 ml, 1.88 ml and 2.8ml of 60%, 40%, 25%, 15% iodixanol solution layers, respectively. This gradient was spun at 40000 rpm for 3h at 18°C in a Sorvall Discovery 90SE ultracentrifuge using a TH-641 rotor. The virus fraction was collected by piercing the gradient tube between the 60% and the 40% fractions with a 19G 11/2 needle. Approximately 1ml of virus was collected per tube and pooled together for buffer exchange.

2.2.5.4 Recombinant AAV Buffer Exchange/Concentration

After purification, viruses were buffered/concentrated using a Vivaspin 20, 100KDa cut off concentrator (Vivascience). First, 5ml of PBS were added to the concentrator, which was shaken well to remove any debris. The PBS was discarded and another 10ml PBS were added to the concentrator and spun 5 min at 2000 rpm to clean the membrane from any trace of glycerine and sodium azide, after which the bucket was emptied and the remaining PBS in the concentrator was discarded. Iodixanol samples were diluted at least 3 times into PBS and spun at 1000g until the volume in the concentrators reduced to 1ml. Next, the concentrator was filled up to 20ml with PBS and spun at 1000g until the volume in the concentrators reduced to 1ml. This process was repeated once again and spun to a final volume of 500 to 800µL. Finally, the virus prep was transferred from the concentrator to a new eppendorf tube.

2.2.5.5 Determination of Recombinant AAV Genome Titre by Real-Time Quantitative PCR

Real-time quantitative PCR (qPCR) was used to determine the genome-containing particle (gcp) titre of rAAV preparations. The SYBR Green Jump Start Taq ready mix without $MgCl_2$ (Sigma) was used according to the manufacturer's instructions on an ABI Prism cycler (AB Applied Biosystems) for absolute gcp titre quantification. The $MgCl_2$ and primer concentrations were optimised previously to 4mM and 0.25µM, respectively. Linearised transgene plasmids were used to prepare standard curves, using concentrations ranging from 10^8 to 10^3 genome copies. One µl of the viral stock prep and dilutions thereof were used as sample. The following specific primer pairs were used for the titrations: AA39/AA40 for viruses containing the GCH gene and AA41/AA42 for viruses containing the TH gene. The cycling parameters were as follows: 2 min at 94˚C followed by 40 times 15s at 94˚C, 15s at 58˚C and 1 min at 72˚C. The amount of genome containing particles (gcp) in the viral samples was calculated from the amount of DNA detected relative to the standard curve. Each standard, negative control and virus sample was loaded in duplicate.

2.2.5.6 Alkaline Gel Electrophoresis for Recombinant AAV Genome Titration and Quality Control

AAV samples were loaded on an alkaline agarose gel made of 0.8% agarose, 2ml 50x alkaline running buffer (2.5M NaOH, 50mM EDTA) were added to 98ml of dissolved agarose (0.8% w/v) and allowed to set. The alkaline agarose gel was run at 18V overnight in a cold room. Prior to loading, 25µl AAV were mixed with 8.5µl alkaline loading buffer (20% glycerol, 4x alkaline running buffer, 1.2% SDS and xylene cyanol). On the following day, the gel was gently rocked in 3 gel volumes of 0.1M Tris pH 8.0 for 1h and subsequently transferred to a 1 gel volume solution of 4X Gelred (Cambridge Bioscience) in 0.1M NaCl and rocked gently for 2h. Finally, the gel was rinsed briefly 2X in tap water and was imaged using a UV transilluminator. Hyperladder I (Bioline) was used as a size reference and for quantification of the AAV titre by relative quantification of the intensities of the DNA bands.

2.2.5.7 Determination of rAAV Capsid Titre by Sodium Dodecyl Sulphate Polyacrylamide Gel Electrophoresis (SDS-PAGE) Protein Gel

12% SDS-PAGE protein gels were used to determine the rAAV capsid titre. The viral protein concentrations were determined using a Bovine Serum Albumin (BSA) standard curve. To prepare the BSA curve, 10µl of appropriate BSA dilution was mixed with 5µl of water and 3µl of 6X loading buffer (0.8g SDS, 5% β-mercaptoethanol, 5ml Tris pH 6.8, 5ml glycerol, 4mg bromophenol blue). For viral samples, 15µl of purified virus were mixed with 3µl of 6X loading buffer. All samples were boiled at 95°C for 5 min before loading. 5µl of Precision Plus Protein Dual Colour Standards (Bio-Rad) was used as ladder.

The gel was run in 1X Tris-Glycine running buffer (1 in 5 dilution from a 5X stock solution containing 15.1g Tris base, 94g glycine, 50ml SDS 10% and add ddH_2O to a total volume of 1L) at 80V until the samples had reached the separating gel, then the voltage was increased to 120V and the gel run until the blue dye front ran out of the gel. The gel was removed from the glass plates and fixed in a solution of 50% ethanol and 15% acetic acid in water, washed with water, and stained with the KryptonTM Infrared Protein Stain (Thermo

Scientific) for at least 2h in a shaking tray. The gel was distained in a solution made of 5% acetic acid and 0.1% Tween®20 (Sigma-Aldrich) in water. The gel was finally scanned using a LI-COR Odyssey® Infrared Imaging system, and the band showing the viral VP3 protein quantified using the Odyssey software. The protein content of the VP3 band (in ng) was deduced from the BSA standard curve and the viral particle titre was calculated based on the known amount of VP3 proteins per capsid (4.986868 x 10-9ng/capsid) and the volume of virus loaded.

2.2.6 Recombinant AAV Infection and Transduction

The cells to be infected were grown to 70% confluency, incubated with rAAV in a low volume (200µl for a well of 24-well plate, volumes adjusted proportionally to the size of the culture vessel) and incubated for 1h at 37˚C. This adsorption step ensures maximal infection/transduction efficiency. After 1h, the medium was replenished to the normal culture volume (i.e. 500µl for a well of 24-well plate). Cells were harvested after 48 h for further analysis (RNA and protein expression).

2.3 Animal Studies

2.3.1 Mouse Experiments

2.3.1.1 Study Design

Mouse work was carried out at the Biological Services Unit from King's College London in the United Kingdom and performed under the authority of the UK Home Office Project and Personal Licences regulations and was compliant with the guidelines of King's College London ethical review committee. CD1® mice were obtained from Charles River Laboratories Inc. (Wilmington, MA, USA). This is a suitable rodent model for toxicity testing, for which extensive background data are available and is acceptable as a model for toxicity testing by regulatory authorities.

AAV vector genomes diluted in phosphate-buffered saline were slowly administered by tail vein injection at doses indicated in table 2. Animals were also dosed with benserazide hydrochloride and either tolcapone or entacapone.

Benserazide is a DOPA decarboxylase inhibitor that is frequently used in combination with other treatments for PD, to inhibit the carboxylation of L-DOPA, which diminishes its therapeutic efficacy.

Tolcapone and entacapone are catechol-O-methyl transferase (COMT) inhibitors that are co-administered with decarboxylase inhibitors and L-DOPA to minimise peripheral L-DOPA catabolism and to increase its bioavailability to the brain.

In studies one and two, test animals were given a single dose of the AAV vectors on day 1 (Table 2). The animals were then maintained until day 28 when three intraperitoneal benserazide hydrochloride injections (sub-doses of 2.4 mg/kg) and oral doses of tolcapone (sub-doses of 10 mg/kg) were administered at approximately 4 hour intervals to all test groups. In studies one and two, control animals received the same dosing regimen of benserazide hydrochloride and tolcapone as described above on day 15 to ensure its suitability for administration to the test groups and sacrificed 4 hours after the last sub-dose. In study three, test and control animals received a single intraperitoneal injection of benserazide and entacapone on day 28 one hour prior to sacrifice.

From each animal, 750µl blood samples were obtained 4 hours (studies 1 and 2) or 1 hour (study 3) after the final dose administration of benserazide and the COMT inhibitor. Animals were then sacrificed and a section from the liver was taken, washed with saline and either snap-frozen and stored in liquid nitrogen or fixed in 4% paraformaldehyde for further analysis (studies 1 and 2) or perfused first with PBS to wash out the blood and then with 4% paraformaldehyde (study 3). A schematic time course of all three studies is shown in Figure 10.

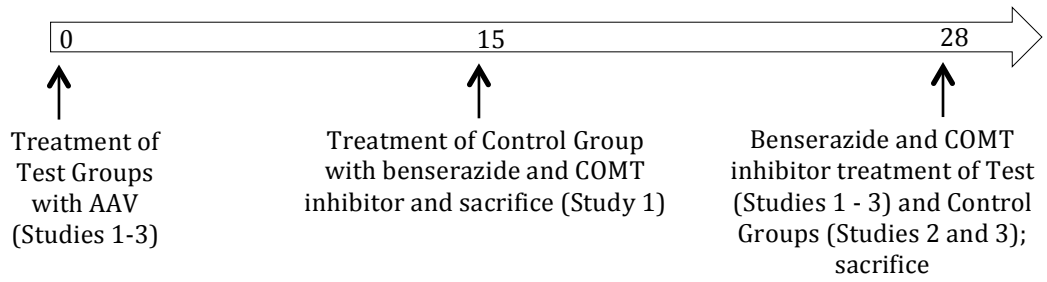

Figure 10: Time course scheme of the three mouse studies.
Animals were dosed with AAV vectors at day 0. In study 1, control animals received three intraperitoneal benserazide injections and oral doses of tolcapone at 4 hours intervals in a total dose of 12 and 30 mg/kg, respectively, at day 15 to ensure the suitability of this regimen for administration to the test groups. At day 28 the same dosing regimen of benserazide and tolcapone was administered to the test groups. Animals were sacrificed 4 hours after the final sub-dose. In study 2, all animals received a single dose of benserazide and COMT inhibitor at the day of sacrifice, while in study 3, three sub-doses were administered 4 hours apart. Total dose was 10 mg/kg for benserazide and 30 mg/kg COMT inhibitor in all studies.

Study	n	Sex	AAV2/8 Injected	Dose (vg/mouse)	Benserazide (mg/kg)	COMT Inhibitor (mg/kg)	Number of Doses of Inhibitors	Time of Sacrifice After Last Inhibitor Injection
1	6	M	PBS	-	4	10	3	4
1	6	M	scLP1-tTH	$3.51x10^{10}$	4	10	3	4
			scLP1-GCH1	$3.51x10^{10}$				
1	6	M	scLP1-tTH	$7.02x10^{10}$	4	10	3	4
2	3	F	PBS	-	12	30	1	1
2	3	F	ssLP1-GCH1-LP1-tTH	$3.6x10^{12}$	12	30	1	1
2	3	F	ssLP1-GCH1-LP1-tTH	$1.3x10^{12}$	12	30	1	1
3	3	M	PBS	-	4	10	3	1
3	5	M	ssLP1-GCH1-LP1-tTH	$1.3x10^{12}$	4	10	3	1
3	3	M	Oral L-DOPA	10 mg/kg	4	10	3	1

Table 2: Treatment scheme in all three mouse studies.
Mice dosed with two self-complementary (sc) vectors received a 50/50 mix of each. In study 1, untreated control animals were maintained untreated throughout the study until day 15, when they were dosed with benserazide and tolcapone 4 hours prior to sacrifice.

2.3.1.2 Mouse Liver Analysis

For immunostaining analysis, 6µm thick sections of paraffin embedded liver were cut and blocked in PBS containing 10% BSA. Before incubation with the primary antibody, tissue sections were blocked for endogenous biotin in 100µl avidin (0.1mg/ml) for 1 min, washed three times for 5 min, then incubated with 100µl biotin (0.5mg/ml) and washed three times for 5 min with PBS.

Biotin is particularly enriched in the liver and the immunodetection system used here is based upon avidin-biotin coupling. Thus, the endogenous biotin needs to be blocked prior to immunostaining to prevent the avidin-peroxidase conjugate binding to it. Biotin can bind to only one molecule of avidin, whereas avidin can bind four molecules of biotin. Avidin is applied to the section in excess, so that all endogenous biotin molecules are bound to one of each of the avidin biotin-binding sites. Excess Biotin is then applied and this will bind to the remaining three biotin – binding sites of the bound avidin. All avidin-biotin binding sites are thus saturated.

After blocking endogenous biotin, primary antibodies were used as follows: 2h goat monoclonal anti-human GCH1 (1:350, Sigma; 2h rabbit polyclonal anti-human TH (1:1000, Abcam #ab137869). Samples were washed 3x with PBS and then incubated with biotinylated species-specific secondary antibody at room temperature for 30 min. Finally, samples were developed in ABC-Peroxidase solution for 30 min at room temperature.

The haematoxylin and eosin staining (H&E) was performed on 6µm thick sections of paraffin embedded liver sections. Haematoxylin stains the nucleus, while eosin stains the cytoplasm of the cells. Sections were cut, mounted and dried in an oven at 60°C overnight. Next, they were de-waxed in 100% xylene for 3 min 3x and washed in 100% industrial methylated spirit (IMS). Slides were then incubated in haematoxylin for 5 min, washed under running tap water to remove excesses and differentiated in 0.5 HCl/70% IMS and washed under running tap water. Next, sections were incubated for 10s in eosin and washed under running tap water to remove excesses. Sections were then dehydrated 4x for 30s in 100% IMS and 2x for 30s in 100% xylene. Finally, slides were cover slipped with DePeX mounting medium and dried overnight at room temperature before imaging using a fluorescence phase contrast microscope (Zeiss Axioskop).

2.3.1.3 Cell Count in Histological Liver Sections

To evaluate the number of transduced cells in the liver, 10 random sections per animal stained for GCH1 and TH were manually counted at 20x magnification with a fluorescence phase contrast microscope (Zeiss Axioskop).

2.3.2 HPLC System and Determination of L-DOPA and its Metabolites in the Plasma and Liver

2.3.2.1 HPLC System

The HPLC system consisted of a pump, an autosampler, a column compartment (UltiMate 3000 series; all from Dionex, UK), a Spherisorb ODS(2) 3μm particle size HPLC column (SpheriClone 0.46cm x 13cm; Phenomenex, UK) and the INTRO electrochemical detector with a VT-03 flow cell potassium chloride reference electrode (Antec, UK). The electrode contained a 50μm thick spacer (Aquilant Scientific (Presearch), UK). The mobile phase consisted of 0.1M NaH_2PO_4 buffer containing 1mM EDTA disodium, 0.01-0.02% OSA and 12% methanol at pH2.9-3.2 (pH adjusted with 3.0M orthophosphoric acid), as appropriate (Table 3). The mobile phase was filtered (polyamide membrane filters, 0.2μm pore size; Sartorius, Germany) and degassed during HPLC analysis. Isocratic elution was performed with a flow rate of 0.8ml/min. The samples and standard solutions were maintained at 9ºC in the autosampler. The column was maintained at 30ºC in the column compartment. A potential of 0.72V was maintained across the glassy carbon working electrode. A volume of 10μl sample or standards was injected into the system. A range of sensitivity (2 – 50nA/V) was set to obtain optimum peak height as appropriate (Table 3). The system was calibrated using a standard solution at a concentration of either 200ng/mL, 10μg/mL or 5μM as appropriate (Table 3). The samples and standards were analysed for 15 min each.

A range of standards containing L-DOPA and 3-OMD were prepared in homogenising acid (0.4M perchloric acid (PCA) containing 0.01% sodium metabisulfite and 1mM Na_2-EDTA. This homogenising acid is referred as PC

solution), as appropriated (Table 4). An internal standard (either AMD or DHBA) was also prepared separately.

Peak height of the analytes and internal standards were measured using the Chromeleon 6.8 Chromatographic Data System (Dionex, UK). Sample concentrations were determined by the comparison of peak height ratio (PHR) between the internal standard peak and analytes using the following equation:

$$Amount\ in\ sample\ = \frac{PH\ (sample\ L{-}DOPA) x\ [STD] x\ PH\ (internal\ STD\ in\ STD)}{PH\ (internal\ STD\ in\ sample) x\ PH\ (STD\ L{-}DOPA)},$$

where PH = peak height and STD = standard.

Calibration curves were calculated using PHR to the internal standard.

2.3.2.2 Determination of Plasma L-DOPA Concentrations

Blood plasma samples were analysed by HPLC with electrochemical detection (ED). The first set of plasma samples was analysed by ABS Laboratories, while the second set of plasma samples was analysed at King's College London. In this section, the protocol for the outsourced samples is described. The protocol used at King's College London is described in the following section.

For each sample, 20µl were injected by a cooled autosampler (Spark Holland Midas) into an electrochemical detector (ESA Coulochem III) coupled to a guard cell (ESA 5020) and a glass-carbon electrode analytical cell (ESA 5011). For DOPA detection, a reverse-phase C18 column (3µm ReproSil-pur, 4.6mm Ø, 150mm length, Chrompack) was used for compound separation.

The mobile phase for DOPA detection contained 100mM NaH_2PO_4 adjusted to pH 3.0 with H_3PO_4, 90µM Na_2-EDTA and 2.8mM 1-octanesulfonic acid (OSA) in 10% methanol. The mobile phases were delivered at a flow rate of 500µl/min. Peak identification and quantification were conducted using the Clarity Chromatographic software package (DataApex, Prague, Czech Republic).

2.3.2.3 Determination of L-DOPA and 3-OMD Concentrations in the Liver

A range of standards containing L-DOPA and 3-OMD (25 – 1000ng/mL) were prepared in the 0.4M PCA solution. AMD or DHBA was also added to the standards at a final concentration of 200ng/mL or 10µg/mL, respectively.

In order to determine plasma and hepatic concentrations of L-DOPA and 3-OMD, blood plasma and liver samples were thawed at 4ºC on ice. The blood plasma samples were homogenised (9:1 volume/volume ratio) in the 0.4M PCA solution containing AMD as an internal standard at a final concentration of 200ng/ml. PCA (70%; 3:10 volume/volume ration) was further added to the plasma samples to deproteinise. The liver samples were homogenised (1:8 weight/volume ratio) in the 0.4M PCA solution containing DHBA as an internal standard at a final concentration of 10μg/ml. The liver samples were filtered using Vivaspin 500 tubes (10000 MWCO; GE Healthcare, UK) by centrifuge, 30 min at 4ºC at 13000 rpm. Both plasma and liver samples were sonicated using a Microson ultrasonic tissue disruptor to further progress acidification of proteins. The samples were then centrifuged at 14000rpm for 10 min at 4ºC and the supernatant was collected and analysed by HPLC-ED as described above. Data were expressed as μg/mL/10μL sample.

2.3.2.4 Hepatic TH Activity

Alumina was prepared before the start of the assays. Aluminum oxide was added to HCl (2N; 1:5 weight/volume ratio) and heated at 90ºC for 45 min with continuous and rapid stirring. The supernatant was removed and the precipitate was washed twice with HCl (2N) at 70ºC for 10 min and twice with HCl (2N) at 50ºC for 10 min. Alumina was further washed with distilled water to increase its pH to 3.4. Alumina was then dried in an oven at 120ºC for 1h and at 200ºC for 2h. The dried alumina was stored in an aluminum foil-covered tube with desiccants until use.

Mouse liver tissue was homogenised in 0.32M sucrose (1:9 weight/volume ratio) using the Microson ultrasonic tissue disruptor. This homogenate was used as a source for the enzyme. The reaction medium contained hepatic homogenate (equivalent to approximately 3mg of tissue), 6,7-dimethyl-5,6,7,8-tetrahydropterine (DMPH4, enzymatic cofactor, final concentration 1mM; dissolved in 1M 2-mercaptoethanol), ferrous ammonium sulphate (final concentration 1mM) and acetate buffer (final concentration 100mM) (Table, see below). The reaction was initiated by the addition of 2mM L-tyrosine (final

concentration of 0.4mM), followed by 30 min incubation at 37 °C. The reaction was terminated by the addition of 100µl 0.4M PCA solution containing 10µM AMD as an internal standard and the mixture was centrifuged for 10 min. L-DOPA and AMD were extracted onto acid washed alumina (140–150mg) from 150µl of the resultant supernatant. Tris buffer (pH8.6, 1ml) was added and the mixture was vigorously shaken for 10 min at room temperature. The supernatant was aspirated and the alumina residue washed twice with water. After the second wash, 200µl of 0.4M PCA solution were added and shaken vigorously for 10 min to elute the L-DOPA and AMD from the alumina. Following centrifugation at 14000 rpm for 10 min at 4ºC, the resultant supernatant was used for HPLC–ECD analysis to determine the concentration of L-DOPA. The assay was performed in triplicate. Non–enzymatic formation of L-DOPA was determined by the addition of D-tyrosine and 3-iodotyrosine (tyrosine hydroxylase inhibitor) instead of L-tyrosine (a blank; Table 4, see below). The concentration of L-DOPA was calculated as described above. The concentration of L-DOPA in the blank was subtracted from the sample. This difference corresponded to the final concentration of L-DOPA in the samples. Data were expressed as L-DOPA formed/30min/3mg tissue. The rates of alumina extraction for L-DOPA and AMD were 38% and 40%, respectively.

	Experiment	**Determination of L-DOPA and 3-OMD Concentrations**		**TH Activity**
	Types of samples	Blood plasma	Liver tissue	Liver tissue
Mobile Phase	1-octanesulfonic acid	0.01%	0.012%	0.02%
	pH	2.9	3.2	3.2
HPLC settings	Flow rate	0.8mL/min	0.8mL/min	0.8mL/min
	Sample temperature	9ºC	9ºC	9ºC
	Column temperature	30ºC	30ºC	30ºC
	Potential	0.72V	0.72V	0.72V
	Sensitivity	2nA/V	50nA/V	2 – 10nA/V
Standards	Internal standard used	AMD (200ng/mL)	DHBA (10µg/mL)	AMD (10µM)
	A range of standard concentrations used for calibrations	25–1000ng/mL	0.01–100µg/mL	0.1-50 µM

Table 3: List of HPLC settings used in the mouse studies.

TH reactions	Blank
30µl tissue homogenate	30µl tissue homogenate
10µl $DMPH_4$ (10mM) in mercaptoethanol	10µl $DMPH_4$ (10mM) in mercaptoethanol
20µl distilled water	20µl distilled water
10µl Ferrous ammonium sulphate (10mM)	10µl distilled water
10µl Acetate buffer (1M)	10µl Acetate buffer (1M)
20µl L-tyrosine (1M)	20µl D-tyrosine (2mM)/ 3-iodotyroine (2mM)

Table 4: Reaction mixtures used in the hepatic TH activity assay.

2.3.3 Rat Experiments

2.3.3.1 Animal Selection

Female Sprague-Dawley or Hodded rats weighing 225–250g were purchased from Charles River (Schweinfurt, Germany) and were housed in groups of 2–3 animals per cage with free access to food (except during the corridor tests) and water under a 12h light/12h dark cycle. All experimental procedures performed in this study were approved by the Ethical Committee for use of Laboratory Animals in the Lund-Malmö region.

2.3.3.2 Surgical Procedures

All surgical procedures were conducted under anaesthesia induced by an intraperitoneal injection of a 20:1 mixture of Fentanyl and medetomidine (Dormitor; Apoteksbolaget, Sweden) in ~6ml/kg. The stereotactic injections were conducted with a Hamilton syringe with the animal mounted in a stereotactic frame (Stoelting, Wood Dale, US). The anteroposterior (AP) and mediolateral (ML) coordinates were calculated from bregma and the dorsoventral (DV) coordinates from the dural surface (Pinxos & Watson 1986).

2.3.3.3 6-OHDA Lesions

The neurotoxin 6-OHDA (Sigma-Aldrich AB, Stockholm, Sweden) was injected unilaterally into the left medial forebrain bundle to lesion the ascending dopamine (DA) projections (Ungerstedt & Arbuthnott 1970). Fourteen microgram free base 6-OHDA was administered in ascorbate-saline (0.02%) at a

concentration of 3.5µg/µl into one deposit along the fibre bundle to ensure a specific lesion of the dopamine fibres, sparing the serotonin projection system (Carta et al. 2007). The injection was conducted at the following coordinate: AP: –4.4mm; ML: –1.2mm and DV: –7.8mm with the tooth bar set to -2.4mm with a 26-gauge needle attached to the Hamilton syringe. The toxin was injected at a speed of 1µl/ min and the needle was kept in place for an additional 3 min before it was slowly retracted from the brain parenchyma.

2.3.3.4 AAV Vector Injections

The animals treated with vectors received intrastriatal injections of 5µl AAV vector in PBS. The injections were performed at two sites with two deposits each, 1.5µl in the more ventral site and 1µl in the more dorsal, delivered with a pulled glass capillary (outer diameter 60–80µm) mounted on a 22-gauge needle attached to the Hamilton syringe. The injection coordinates were: (i) AP: +1.0mm; ML: –2.8mm, and DV: –4.5, –3.5mm and (ii) AP: 0.0mm; ML: –4.0mm, and DV: –5.0, –4.0mm with the tooth bar set to –2.4mm. The injection rate was 0.4µl/minute and the needle was kept in place for 1 min after the first and 3 min after the second deposit, before it was slowly retracted.

2.3.3.5 Behavioural Tests

2.3.3.5.1 Drug-induced Rotation

Drug-induced rotation tests were performed by measuring full-body turns with automated rotometer bowls (AccuScan Instruments, Columbus, US), after an injection of d-amphetamine sulphate (2.5mg/kg, intraperitoneal; Apoteksbolaget, Sweden) and quantified continuously for 90 min. Rotational asymmetry scores are presented as net full body turns/minute. The drug-naïve spontaneous rotation test was performed with the same setup with the exception of the drug challenge.

2.3.3.5.2 Cylinder Test

Cylinder test assessing exploratory forelimb use asymmetry was performed as described by Kirik et al. (Kirik et al. 2001), with minor modifications. Each rat was placed in a 20cm in diameter glass cylinder and exploratory behaviour was recorded with a digital video camera. Two perpendicular mirrors were placed behind the glass cylinder, which allowed the complete surface of the cylinder to be clearly visible on the recording. The animal was left in the cylinder until at least 20 forelimb touches on the cylinder wall were observed. Forelimb placement and use on the cylinder wall was scored post-hoc with frame-by-frame analysis by an observer blinded to the group treatment. The paw used during each of the 20 contacts with the cylinder walls during rearing was scored and presented as right forepaw touches as a percentage of the total number of touches.

2.3.3.5.3 Stepping Test

The stepping test was initially described by Schallert et al.; its modified side-stepping version was performed in the this study (Schallert et al. 1979; Olsson et al. 1995). Forelimb akinesia was assessed by an investigator blinded to the animal's group identity by holding the rat with two hands only allowing one fore-paw to reach the table surface. The animal was then moved sideways over a defined distance of 90cm at a constant pace over 4–5s. The investigator scored the numbers of adjusting side steps in both forehand and backhand direction twice, and the average was calculated. The animals were trained for 6 days during the seventh week post-AAV injection and then scored by taking the average of their performance during days 7–9, when the daily variability had minimised. For the 12-week post-AAV injection time point, the animals only needed habituation for 1 or 2 days and were then scored during three consecutive days.

2.3.3.5.4 Corridor test

The corridor test was performed 8 and 12 weeks post-AAV injections, as previously described, to study lateralised sensorimotor response selection

(Dowd et al. 2005). Briefly, the rats were placed in the end of a corridor (1,500 × 70 × 230mm) with 10 adjacent pairs of lids, evenly distributed along the floor. Each lid was filled with approximately five sugar pellets. Retrieval was defined as each time the rat poked its nose into a unique cup, regardless of whether it ate any pellets. Revisits without interleaving other retrievals were not scored. Each rat was tested until 20 retrievals were made or a maximum time of 5 min elapsed. The rats were food restricted prior and throughout testing and habituated for 10 min for 2 days in the corridor, with sugar pellets scattered along the floor. To reduce exploratory behaviour the rats were placed in an empty corridor before scoring. The rats were then scored for 4 days and the results were presented as an average of the last 2 days of the number of contralateral retrievals (right) as a percentage of total retrievals.

2.3.4 Non-human Primate Experiments

2.3.4.1 Animal Selection

Male F2 captive bred *Macaca mulatta* or, whenever specified, *Macaca fascicularis*, were purchased by Motac from the contracted provider (Xierxin Laboratory Co. Ltd., Beijing, China). Animals underwent a period of quarantine (40 days) according to the test facility vendor management program. Animals were inspected daily for signs of illness and further clinical examinations were performed if necessary. Two parasitological treatments were given for internal and external parasites over the quarantine period prior to delivery. Animals were identified by a neck collar. Cage labels indicated the individual animal identification numbers.

2.3.4.2 Housing and Acclimatisation

Animals were housed in pairs in an air-conditioned animal room with non-recycled air that was changed at least eight times per hour. An artificial 12 hour (h) day/night cycle with lights on at 8.00 a.m. was provided. Animals were acclimatised for a minimum of 21 days in the facility where behavioural

assessments were conducted. During this period, daily inspections for illness were carried out for each animal and further clinical examinations were performed if necessary. Animals were reported to be free of enterobacteria. Animals underwent a serological test for viral herpes B. However, they were not required to be negative to be included in the study.

2.3.4.3 Diet and Drinking Water

Housing conditions: SAUE Ltd Old World Monkey pellets were available *ad libitum* and were distributed in the morning and afternoon. The batch used was not quality controlled and no certificate of analysis is available. The diet was supplemented daily with fresh fruit and vegetables. If, at any point, an animal's condition required supplemental feeding, nutritional milk (Heinz) was given by gavage (up to three times 100 ml per day). Drinking water was available *ad libitum.*

2.3.4.4 Preparation of the MPTP-lesioned Macaque Model of Parkinson's Disease

Forty macaques were injected once daily with a low dose (0.2 mg/kg, i.v.) of MPTP to induce parkinsonism (Bezard et al. 2001). MPTP treatment was carried out until the animal reached a parkinsonian disability score of 6 on the validated parkinsonian macaque clinical rating scale (Benazzouz et al. 1993). A score of 6 was chosen as this level of parkinsonism permitted forthcoming surgical procedures to commence under general anaesthesia, with a reduced risk in compromising animal recovery and post-surgical health.

The degree of parkinsonism was assessed daily from the beginning of MPTP administration using a parkinsonian macaque clinical rating scale, which has been validated for direct observational studies (Imbert et al. 2000).

2.3.4.5 Tailoring of L-DOPA Dose

Following stabilisation of parkinsonian motor symptoms, animals were primed with L-DOPA over 2 weeks. Each animal was treated twice daily, with a

tailored dose of Madopar (L-DOPA/benserazide, ratio 4:1, p.o.) based on the animal's weight. This dose was selected to maximally reverse parkinsonian motor symptoms and cause hyperactivity in animals, which has been associated with the development of dyskinesia. L-DOPA was administered until dyskinesia stabilised. After this L-DOPA priming treatment regimen, the so called 'treatment dose' (treatment dose = 100%; priming dose = 133% of 'treatment dose') was defined as the lowest dose that produced complete reversal of parkinsonian motor symptoms.

2.3.4.6 Pre-operative Procedures

On the day prior to surgery, each animal was given duphamox (15mg/kg; s.c.) for infection prophylaxis.

On the day of surgery, each animal was given atropine SO_4 (0.04mg/kg; i.m.) before surgery. The non-steroid anti-inflammatory drug ketophen was also administered (2mg/kg; s.c.). There was a minimum of 10 min before animals received general anaesthesia (ketamine HCl; 10mg/kg, i.m.) following ketophen administration.

Xylocaine cream was applied topically as a local anaesthetic lubricant. The animal was then intubated and maintained under anaesthesia with isoflurane, which was delivered through a volume-regulated respirator. The heart rate and oxygen saturation of the animal was monitored and recorded within 30 min intervals throughout the surgical procedure. Animals were placed on a heating pad during surgery. The core body temperature of the animal was also measured within 30 min intervals throughout the surgical procedure, with a temperature probe placed in the rectum. A second heat pad was used to maintain core body temperature when required.

Other drugs for appropriate anaesthetic and clinical management of the animal were used if required. Each drug, dose, route and site of administration was documented in the surgical records. All vital signs recorded were documented in the surgical records.

During surgery, ophthalmic ointment was applied to each eye (Liposic ophthalmic gel). The hair was clipped from the cranium and cranio-dorsal

portion of the neck and sides. Each animal was then positioned in a stereotactic apparatus. The surgical site was made aseptic by cleaning with 70% isopropyl alcohol scrub. A drape was placed on each animal to maintain strict aseptic surgery.

2.3.4.7 AAV Vector Injections

For the location of injection sites, intracerebral sites were identified for each individual macaque by using the standard Horsley Clarke stereotaxic technique. Sagittal and frontal ventriculography was used to locate the borders of the third ventricles, and also the edges of the anterior and posterior commissures to improve the accuracy of site location.

Firstly, a hole was drilled (Dremel) into the skull of each macaque without damaging the dura matter. A ventriculographic cannula mounted on a glass syringe was then placed into the anterior horn of the lateral ventricle, followed by injection of contrast medium (Omnipaque, Nycomed, Norway). The precise neuroanatomical location of the ventricles was identified with referral to a stereotaxic atlas (François et al. 1996). Coordinates were then adjusted before further insertions into the skull. Ventriculography was used to locate the anterior commissure. The defined position of anterior commissure was then combined with a stereotaxic population-based historical atlas of the basal ganglia to locate the position of the left and right putamen. An infusion cannula for delivery of the test item was then placed into position as described below.

The drilled area was cleaned with sterile saline. Stereotactic injections of the test item were made into the striatum (putamen). Theoretical targets were defined based upon the atlas of François and Percheron but were also determined practically in individual animals, based on the findings from stereotactic ventriculography. The delivery of the test item was made along three tracks in each hemisphere, with two to four deposits per track.

Deposit coordinates had been validated from a previous pilot study using an inactive AAV2/5 GFP vector.

Track	Anteroposterior (relative to AC)	Lateral (from midline)	Deposits (relative to AC-PC line)	
1	AC+1 mm	14 mm	0 mm	+3mm
2	AC-1 mm	14 mm	0 mm	+3mm
3	AC-4 mm	15 mm	0 mm	+3mm

Table 5: Theoretical deposit coordinates for the stereotactic injection of the AAV2/5 vectors in the putamen of MPTP-lesioned NHP.
Theoretical targets were defined based upon the atlas of François and Percheron and determined practically in individual animals. AC: anterior commissure; PC: posterior commissure.

The infusions were made at a rate of 2µl/min with a Hamilton syringe (needle gauge 28). Following completion of all stereotactic injections, skin wounds were closed in layers with a continuous suture using absorbable suturing material. Animals were then monitored until recovery from general anaesthesia.

2.3.4.8 Post-operative Care

Each animal was extubated and then closely monitored during post-operative care. Animals were kept warm until swallowing and righting reflexes were regained. Care was provided for the animals by experienced technicians and veterinary support was available at any time.

2.3.4.9 Post-operative Therapy

One day post-surgery, animals were given duphamox (15mg/kg; s.c.) for infection prophylaxis. Analgesia (ketophen, 2mg/kg; s.c.) was administered over the first three days post-surgery. If required, a stronger analgesic drug was provided following veterinary advice and documented in the surgical record sheets. Other drugs were administered for clinical management if required. Each drug, dose, route and site of administration was documented in the surgical records.

2.3.4.10 Behavioural tests

2.3.4.10.1 Locomotor activity

A quantitative assessment of the amount of movement for each animal was obtained in 5 min time bins for the duration of the experiment. Recordings were made using computer-based activity monitors.

2.3.4.10.2 Parkinsonian disability

Parkinsonian disability was assessed using non-parametric measurements of video recorded behaviour. Behaviour subtypes and rating scales were as follows:

a) *Motor (range of movement)*:

0 = no movement

1 = movement of head only

2 = movement of head, limbs and/or trunk, without locomotion, for >30% of the observation period

3 = walking on the floor and/or climbing on the walls of the cage for <30% of the observation period

4 = walking on the floor and /or climbing on the walls of the cage for >30% of the observation period

The score given was the maximum achieved in each 10 min observation period.

b) *Bradykinesia*:

0 = initiation of movement and normal speed of movement

1 = mild, slowing of movement

2 = moderate slowing, difficulty initiating and maintaining movement, marked freezing

3 = akinetic, unable to move, with prolonged freezing episodes

The score given was representative of behaviour over the observation period.

c) *Postural abnormality*:

0 = normal, upright, holds head up, normal balance

1 = hunched body, holds head up

2 = hunched body and neck, face down, may lose balance.

The score given was representative of behaviour over the observation period.

d) *Tremor*:

0 = absent

1 = present

The score given was representative of behaviour over the observation period.

e) *Parkinsonian disability*:

(4 - Range of movement) + bradykinesia + postural abnormality + tremor. This score was a maximum global parkinsonian disability score out of 10.

2.3.4.10.3 Dyskinesia

Non-parametric measurements of video recorded behaviour. Behaviour subtypes and rating scales were as follows:

a) *Chorea:*

0 = Absent

1 = Mild, fleeting, present <30% of the observation period

2 = Moderate, not interfering with normal activity, present >30% of the observation period

3 = Marked, at times interfering with normal activity; present <70% of the observation period

4 = Severe, continuous, replacing normal activity, present >70% of the observation period.

b) *Dystonia:*

0 = Absent

1 = Mild, fleeting, present <30% of the observation period

2 = Moderate, not interfering with normal activity, present >30% of the observation period

3 = Marked, at times interfering with normal activity, present <70% of the observation period

4 = Severe, continuous, replacing normal activity, present >70% of the observation period.

Following L-DOPA treatment with priming or treatment doses, behaviour was assessed for 4h post administration. In the OFF state, behaviour was assessed for 1h. For assessment of locomotor activity, scores were recorded in 5 min intervals. For assessment of parkinsonian disability and dyskinesia, video-recorded behaviour was scored over 10 min intervals by an observer blinded to treatment.

2.3.4.11 Analysis of Data

All statistical analyses were carried out using Graphpad Prism (versions 5.0 and later version 5.04c). The data were analysed with the non-parametric equivalent of the t-test Wilcoxon matched pairs test, Mann-Whitney test or the non-parametric equivalent of the one-way ANOVA Kruskal-Wallis or Friedman's test, followed by Dunn's multiple comparisons.

Chapter 3 AAV-mediated Continuous L-DOPA Synthesis in the Periphery

3.1 Introduction

The study described in this chapter is aimed to test a proof-of-principle therapeutic strategy to improve treatment of PD. It proposes a combination therapy of oral L-DOPA and a one-time intravenous AAV injection to deliver TH and GCH1 to the liver in order to achieve a continuous and basal hepatic L-DOPA synthesis, thereby potentially diminishing the fluctuations inherent to oral treatment alone and improving management of L-DOPA induced side effects (Figure 11). The question being tested here is whether elevated L-DOPA levels can be detected in the periphery of healty mice upon AAV-mediated delivery of the *GCH1* and *TH* genes to the liver.

Since the discovery of dopamine as a neurotransmitter and its role in PD, restoration of the dopaminergic tone in the brain has been the focus of pharmacological therapies for PD. The oral administration of L-DOPA together with an aromatic amino acid decarboxylase (AADC) inhibitor is one of the most effective therapies and is currently the gold standard treatment for the disease. During the early years of PD, when motor complications are the predominant symptoms, L-DOPA oral treatment provides enormous symptomatic relief and substantially improves life quality of patients (Kordower & Goetz 1999). However, over 80% of the patients develop side effects to L-DOPA treatment 5-10 years after initiation of the therapy. L-DOPA induced side effects can be disabling and include dyskinesias and motor fluctuations such as freezing episodes. Once established, dyskinesia tends to remain persistent and with the progression of the disease it becomes increasingly more difficult to deliver L-DOPA doses that control the parkinsonian features without triggering side effects. It is thought that L-DOPA induced dyskinesia (LID) develops as a consequence of the pulsatile stimulation of dopamine receptors by oral administration of L-DOPA. As a corollary, stabilising L-DOPA plasma levels by continuous duodenal infusion has been shown to delay the onset and diminish the severity of LID. The efficacy of continuous duodenal L-DOPA infusion has

been demonstrated in a 12-week Phase III double blind and a 52-week open-label trial. The results showed improvement in the ON-time without troublesome dyskinesia and reduced OFF-time. However, the need for an invasive intestinal surgical procedure and permanent tube maintenance poses limits to a wider application of this therapy. Furthermore, those eligible for duodenal L-DOPA infusion experience adverse effects related to the implanted device such as intestinal tube dislocation, intestinal tube occlusion, pump malfunction and stoma leakage in 89% of the cases (Olanow et al. 2000; Nyholm et al. 2005; Seeberger & Hauser 2015).

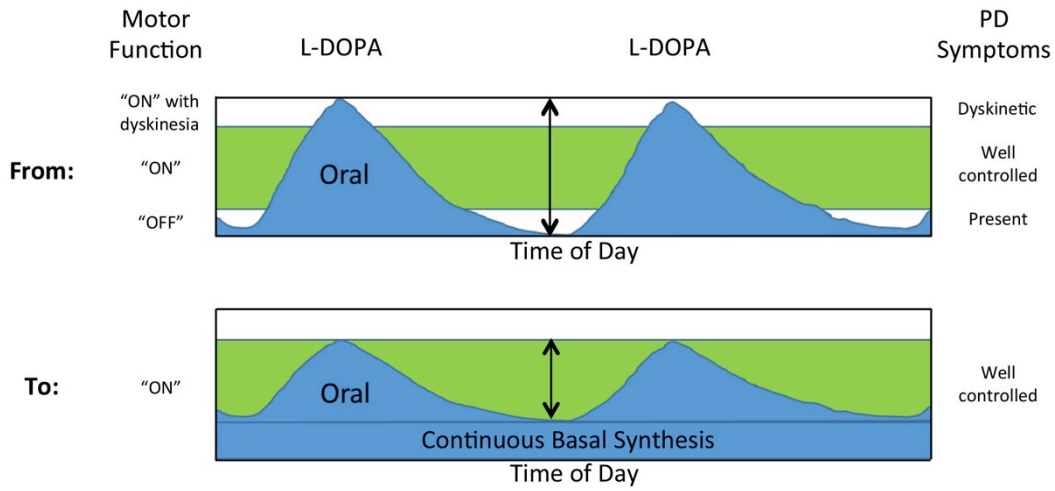

Figure 11: Rationale for continuous systemic L-DOPA delivery.
Providing a continuous basal supply of systemic L-DOPA has the potential to increase the efficacy of the standard oral medication treatment by facilitating the management of parkinsonian features without transcending the therapeutic window.

The liver is a suitable candidate organ for this gene therapy strategy because it provides the amino acid tyrosine, which is produced by the enzyme phenylalanine hydroxylase (PAH) and is the substrate for L-DOPA synthesis, as well as BH4, the cofactor required by PAH and TH for their catalytic activity (Figure 12). *GCH1* codes for the rate-limiting enzyme in the biosynthesis of BH4 and its expression together with TH was shown to be sufficient and necessary for L-DOPA synthesis *in vivo* (Mandel et al. 1998). Although the liver synthesises BH4, GCH1 was delivered through the vector to ensure robust TH activity without the risk of depleting it from the liver.

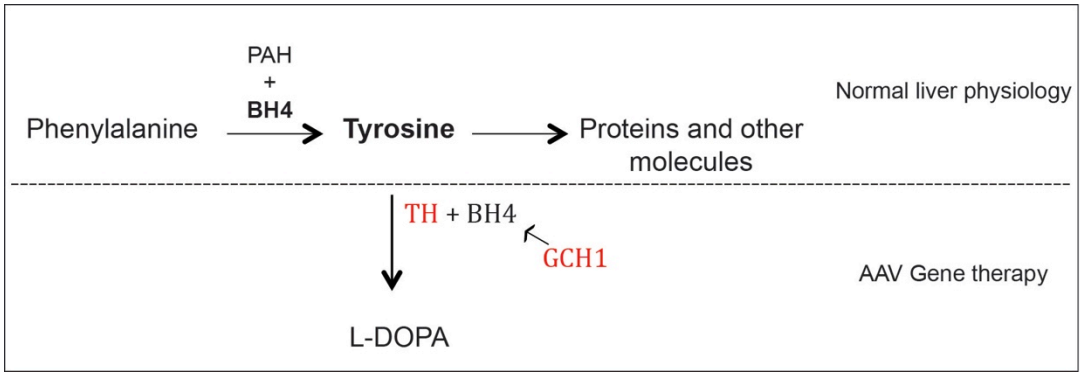

Figure 12: Therapeutic strategy for AAV-mediated L-DOPA synthesis in the liver.
This strategy can benefit from the presence of endogenous hepatic tyrosine and BH4. AAV-mediated gene addition of *TH* and *GCH1* will lead to hepatic synthesis of L-DOPA. PAH: phenylalanine hydroxylase; BH4: tetrahydrobiopterin; TH: tyrosine hydroxylase; GCH1: GTP-Cyclohydrolase-1.

The proposed gene therapy was tested following two different approaches. The first one attempted to achieve co-linear expression of the L-DOPA-synthetic enzymes GCH1 and TH from two separate vectors. In the second approach, expression of TH and GCH1 was achieved from a single AAV vector in order to guarantee equal transduction efficiencies of both genes in the liver.

3.2 Results

3.2.1 Generation and Titration of the Monocistronic Liver Vectors

In the first approach double-stranded AAV (dsAAV) was used to take advantage of its rapid onset of transgene expression (Wang et al. 2003). The double-stranded monocistronic vectors were designed to express the rate-limiting enzymes in L-DOPA synthesis, TH and GCH1, from separate vectors. Transgene expression in each vector was controlled by the liver-specific LP1 promoter, which was constructed by joining core liver-specific elements of the human apolipoprotein hepatic control region (HCR), the human alpha-1-antitrypsin (hAAT) gene promoter and a modified SV40 small T antigen intron (Nathwani et al. 2006). This synthetic promoter has been shown to achieve strong liver-specific transgene expression in animal models and has been used successfully in clinical trials using AAV for the treatment of haemophilia B (Nathwani et al. 2012).

The monocistronic TH vector expresses a truncated TH lacking the first 155 N-terminal amino acids. This truncation eliminates the regulatory domain thereby rendering the enzyme constitutively active and allowing L-DOPA synthesis to reach maximum levels *in vivo* (Daubner et al. 2011). Downstream of the *TH* coding sequence, the woodchuck hepatitis virus post-transcriptional regulatory element (WPRE) was introduced, a *cis*-acting sequence that functions by enhancing mRNA trafficking to the ribosome thereby increasing its translation (Zanta-Boussif et al. 2009). Enhanced expression of TH had been shown to be important for the achievement of the optimal 5:1 stoichiometric ratio of TH:GCH1 (Björklund et al. 2009). The monocistronic GCH1 vector contains the *GCH1* gene under the control of the liver-specific promoter LP1.

A schematic representation of both monocistronic liver vectors is shown in Figure 13.

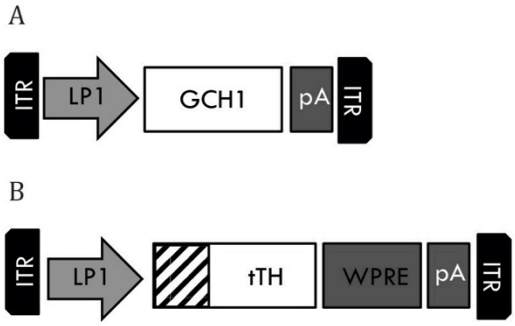

Figure 13: Schematic of monocistronic liver vectors.
The monocistronic liver vectors harbour the *GCH1* gene (A) and the truncated *TH* gene (tTH) (B) under the control of the liver-specific LP1 promoter. The WPRE sequence was introduced downstream of the *TH* coding sequence to enhance its expression. The shaded area in the TH gene indicates the truncated region (t).

Once the construction of each vector was finalised, they were verified by sequencing and the integrity of the ITRs was confirmed by restriction endonuclease analysis. The AAV ITRs are the viral *cis*-elements required for viral replication and their integrity is therefore extremely important for the production of rAAV. However, due to their palindromic nature, the AAV ITRs are very recombinogenic. Because each ITR contains two SmaI endonuclease sites, digestion of an ITR-containing plasmid with this enzyme is suitable to assess ITR integrity. ITR recombination leads to a partial deletion of one ITR with the consequent elimination of two SmaI sites from the AAV plasmid; this can be

easily diagnosed by endonuclease digestion followed agarose gel electrophoresis.

Production of the recombinant vectors AAV2/8-LP1-GCH1 and AAV2/8-LP1-tTH-WPRE was done by triple transfection of HEK293T cells; the vectors were purified by FPLC using an AVB sepharose affinity column (Grieger & Samulski 2012). The annotation AAV2/8 indicates that the transgene cassette was flanked by AAV2 ITRs and packaged into an AAV8 capsid. Serotype 8 was chosen for this study due to its strong tropism for the mouse liver (Nakai et al. 2005). Since AAV8 is also able to efficiently transduce muscle tissue, the liver-specific LP1 promoter was used in the vector to ensure liver-specific transduction (Nathwani et al. 2006).

Titration of the AAV vectors was done by total particle and genome containing particles (gcp) quantification. The particle titration combined with real time PCR and/or alkaline agarose gel electrophoresis for genome titration provides a good estimate of vector production and packaging efficiency. The particle titre of both vectors was determined by SDS-PAGE quantification of the AAV capsid protein VP3 relative to a BSA standard curve (Kohlbrenner et al. 2012) (Figure 14); the genome titre was determined by the adapted real-time quantitative PCR method for genome quantification of double-stranded AAV vectors (Fagone et al. 2011). SDS-PAGE for the particle titration demonstrated that the purification of both dsAAV vectors led to high-purity preparations, with only AAV capsid proteins VP1, VP2 and VP3 being detected.

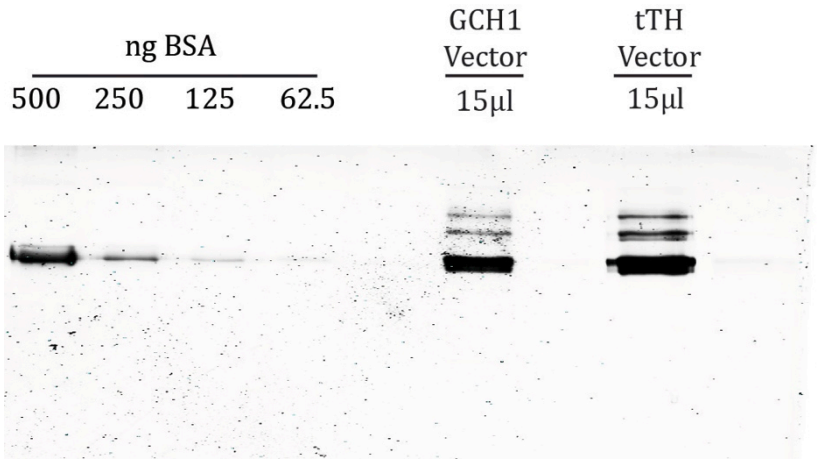

Figure 14: SDS-PAGE capsid titration of monocistronic liver vectors.

Viral proteins VP1, VP2, VP3 (top to bottom) were the absolute majority of proteins detected on the gel, indicating the purity of the preparation. Particle titres calculated from this gel are shown in Table 6.

Total particle titres were $8.25x10^{12}$ and $1.84x10^{13}$ particles/ml, while genome titres were $4.88x10^{12}$ and $3.97x10^{11}$ gcp/ml for GCH1 and TH vectors, respectively. In an efficient rAAV preparation, the ratio between particle and genome titres does not exceed 10. While the particle:genome ratio for the GCH1 vector was around 2, the ratio for the TH vector was approximately 46, indicating that packaging of the latter was very inefficient (Table 6). This issue most likely arose as a result of its oversized 2.6kb genome, which exceeded the optimal packaging capacity of dsAAV by 0.25kb. The optimal packaging size for dsAAV is 2.35kb – half of that of the single-stranded 4.7kb wild-type genome.

Vector (dsAAV2/8)	Genome Titre (gcp/ml)	Particle Titre (particles/ml)	Ratio particle:genome
LP1-GCH1	4.88×10^{12}	8.25×10^{12}	1.7
LP1-tTH	3.97×10^{11}	1.84×10^{13}	46.3

Table 6: Genome and particle titres of monocistronic liver vectors.
Titres were determined by real time PCR and SDS-PAGE. Packaging efficiency is indicated in the last column. A particle:genome ratio >10 is indicative of inefficient genome packaging.

3.2.2 *In vivo* Efficacy of the Monocistronic Liver Vectors

To evaluate the *in vivo* efficacy of both monocistronic liver vectors, a study was designed with the aim to assess their transduction efficiency in the mouse liver and to evaluate their ability to raise systemic levels of L-DOPA after a single systemic injection. Two different vector treated groups (TH vector +/- GCH1 vector) were used to investigate whether ectopic expression of both genes is necessary to support L-DOPA synthesis in the liver. Since BH4 is a co-factor for the naturally occurring liver enzyme PAH, the necessity for ectopic BH4 to support L-DOPA synthesis in the liver is not known. Male mice received a tail-vein injection of $7.02x10^{10}$ gcp total, with the group treated with both vectors receiving a 50/50 mix of each (n= 6/group) (Table 7).

Treatment Group	Dose (gcp/mouse)	n
Vehicle	-	6
dsAAV2/8-LP1-tTH	$7.02x10^{10}$	6
dsAAV2/8-LP1-tTH + **dsAAV2/8-LP1-GCH1**	$3.51x10^{10}$ $3.51x10^{10}$	6

Table 7: Treatment groups and doses of monocistronic dsAAV vectors injected into mice.

The total dose used in the study was limited by the genome titre of the TH vector due to its lower genome titre. Immediately prior to the termination of the study, plasma from each animal was collected after a three-dose regimen treatment with the AADC and COMT inhibitors benserazide and tolcapone, which were given to block peripheral conversion of L-DOPA to dopamine and inhibit COMT-mediated L-DOPA degradation (Figure 15).

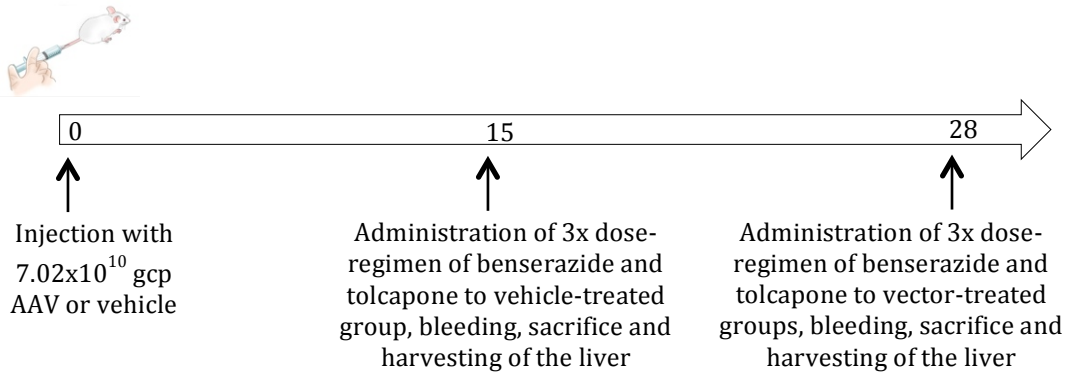

Figure 15: Timeline of the first mouse study.
Male mice (n=6/group) were dosed with AAV vectors at day 0. At day 15, vehicle-treated animals received three intraperitoneal injections of benserazide and three oral doses of tolcapone in approximately 4-hour intervals in a total dose of 12 and 30 mg/kg, respectively. Vehicle-treated animals were sacrificed at an earlier time-point in order to ensure benserazide and tolcapone's suitability for administration to the test groups. At day 28 the same dosing regimen of benserazide and tolcapone was administered to the vector-treated groups. Animals were sacrificed 4 hours after the final sub-dose.

Transduction of both monocistronic vectors was assessed by immunohistochemistry (IHC) of paraffin embedded liver sections. As shown in Figure 16, transgene expression of both GCH1 and TH vectors was detected in <1% of hepatocytes. In the liver sections of animals treated with the TH vector only, an average of 2.8±2.4 cells/field were positive. The average number of cells per field was 857.

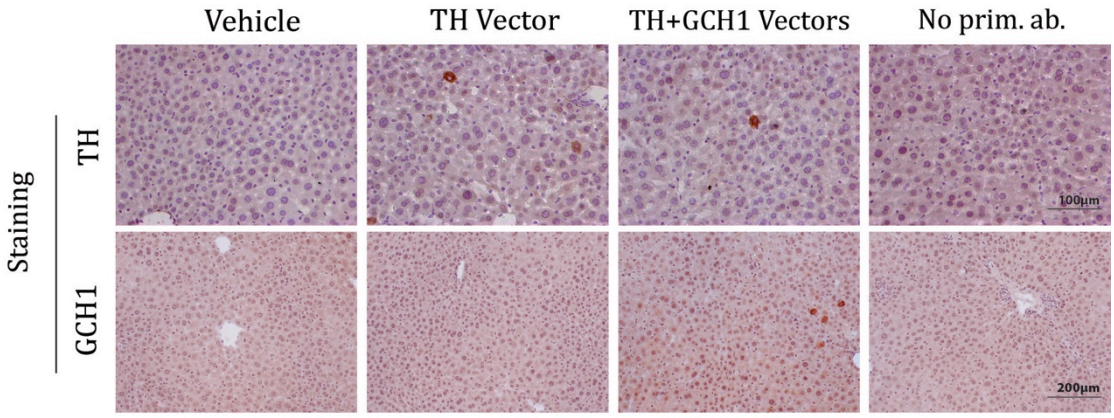

Figure 16: Transduction efficiency of the TH and GCH1 vectors in the mouse liver. Transduction levels 15 days (Vehicle) or 28 days (TH Vector and TH+GCH1 Vectors) post-injection. No transgene expression was observed in the vehicle-treated animals. Transgene expression was detected in a very low number of hepatocytes in vector-treated animals (brown cells). Liver sections stained without primary antibody incubation were used as a control for unspecific staining.

The plasma levels of L-DOPA after treatment with the monocistronic AAV vectors were quantified by HPLC coupled with electrochemical detection. At the time this first animal study was performed, a protocol for in-house L-DOPA detection had not been established yet and the assay was therefore outsourced to ABS Laboratories (London, UK). No significant difference in L-DOPA plasma levels between vehicle- and vector-treated animals was observed: vehicle treated animals had 0.75±0.2nmol/ml, whereas animals treated with the TH vector only and both vectors together showed 0.8±0.11nmol/ml and 0.86±0.13µg/ml of circulating L-DOPA, respectively (Table 8).

Group	Day of Sacrifice	L-DOPA plasma (nmol/ml)
Vehicle	15	0.75±0.2
TH Vector	28	0.80±0.11
TH+GCH1 Vectors	28	0.86±0.13

Table 8: L-DOPA plasma levels of animals treated with the monocistronic liver vectors. L-DOPA plasma levels 28 days post-injection measured by HPLC with electrochemical detection.

The results of this first animal study indicate that transduction efficiency of both vectors has to be greatly optimised in order to increase the potential for a therapeutic benefit from this gene therapy strategy. It is particularly important to ensure that both vectors transduce with equal efficiency in case TH alone is not sufficient to sustain L-DOPA synthesis in the liver. In order to achieve a higher transduction with both vectors a much higher dose would be necessary. However, as seen from the capsid:genome titres ratio for the TH vector, its genome packaging was very inefficient due to its oversized genome. As a consequence, upscaling the production of this vector proved to be cumbersome and impractical. Thus, to address the scalability problem and to guarantee efficient and equal transduction levels for both genes, the dual-vector approach was abandoned and a bicistronic vector was designed, which combines both the *GCH1* and *TH* genes in a single AAV genome.

3.2.3 Generation and Titration of the Bicistronic Liver Vector

The bicistronic liver vector used in this study was designed to combine both the *GCH1* and *TH* genes in a single AAV vector, with each gene being expressed from an independent cassette controlled by the liver-specific LP1 promoter. The rationale for using two identical promoters in a single vector stems from successful preclinical studies carried out in a rodent model of PD. Cederfjäll et al. showed that injection of a vector expressing both *GCH1* and *TH* genes from a single AAV genome into the rat's striatum resulted in widespread transduction and continuous L-DOPA synthesis in the CNS (Cederfjäll et al. 2012; Cederfjäll et al. 2013). Similarly to the monocistronic TH vector, the *TH* gene in the bicistronic vector was truncated (lacking the nucleotides correspondent to the first 155 N-terminal amino acids) and cloned immediately upstream of the WPRE sequence. This genome configuration had been shown to lead to an optimal TH:GCH1 ratio for *in vivo* L-DOPA synthesis (Cederfjäll et al. 2012). A schematic representation of the singe-stranded bicistronic vector is shown in Figure 17.

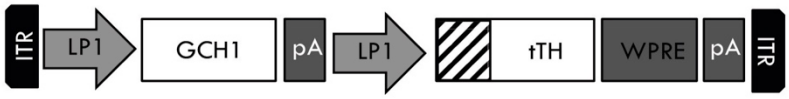

Figure 17: Schematic of the single-stranded bicistronic liver vector
The vector harbours the *GCH1* and the truncated *TH (tTH)* gene. Each expression cassette is independently controlled by the liver-specific LP1 promoter. The WPRE sequence was introduced downstream of the t*TH* coding sequence to enhance its expression. The shaded area in the *TH* gene indicates the truncated region.

The cloning strategy for the generation of the bicistronic liver vector was designed in a way to result in a modular construct in which each gene and regulatory element was flanked by a unique restriction endonuclease site to allow for future modifications if necessary. Therefore, both LP1 promoters, both transgenes and the WPRE were cloned individually one after another into the AAV ITR-containing backbone pSub201 (Samulski et al. 1987). The plasmid was quality controlled by restriction endonuclease analysis followed by sequencing after the completion of each cloning step. Once the construction of the modular vector was finalised, the integrity of the ITRs was confirmed by SmaI restriction endonuclease analysis.

Production of the recombinant vector AAV2/8-LP1-GCH1-LP1-tTH-WPRE was done by triple transfection of HEK293T cells; purification was done by iodixanol density gradient centrifugation (Grieger & Samulski 2012). This purification method was chosen after it was noticed that iodixanol density gradient purification delivered greater yields and better purity for AAV8 preparations compared to AVB sepharose chromatography purification.

Titration and purity assessment of AAV vectors was done by total particle and genome containing particle titration. The genome titre was determined by alkaline agarose gel electrophoresis. While real time PCR can be a more precise method for AAV genome titration, alkaline gel electrophoresis allows for a visual quality control of the vector's genome purity and integrity. Total particle and alkaline agarose gel genome titration showed titres of $5.2x10^{13}$ particles/ml and $1.69x10^{13}$ gcp/ml, respectively (Table 9), indicating that the viral genome was efficiently packaged upon production (i.e. capsid:genome ratio ≤ 10) (Figure 18).

Titration	AAV2/8-LP1-GCH1-LP1-tTH-WPRE
Particle titre (particles/ml)	$5.2x10^{13}$
Genome titre (gcp/ml)	$1.69x10^{13}$
Ratio particle:genome titre	3

Table 9: Particle and genome titres of AAV2/8-LP1-GCH1-LP1-tTH-WPRE.
Titres were determined by SDS-PAGE and agarose alkaline gel. A particle:genome ratio of <10 is indicative of efficient genome packaging.

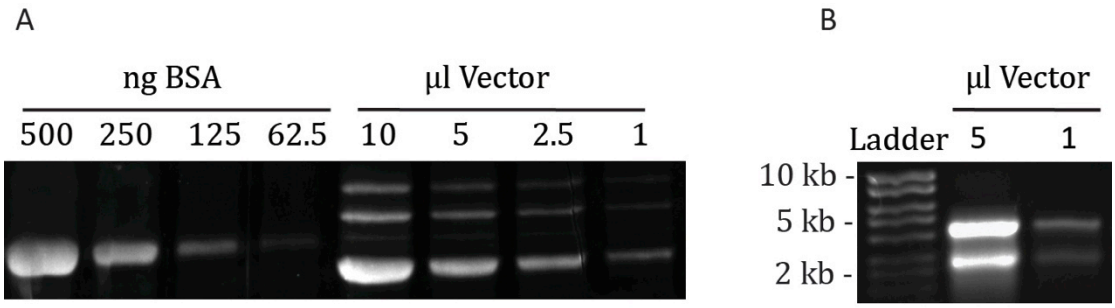

Figure 18: SDS-PAGE and alkaline agarose gel for AAV2/8-LP1-GCH1-LP1-tTH-WPRE titration
(A) SDS-PAGE for AAV capsid titration showing AAV capsid proteins VP1, VP2 and VP3 (top to bottom). (B) Alkaline gel electrophoresis showing the genome of AAV2/8-LP1-GCH1-LP1-tTH (4.4kb band) and a second band of 2.8kb formed upon vector production with the AAV production plasmid pAA019. Vector lanes represent dilutions of the same prep. Titres calculated from A and B are shown in Table 9.

When the vector AAV2/8-LP1-GCH1-LP1-tTH-WPRE was analysed by alkaline gel electrophoresis, the presence of a second band of approximately 2.8kb in length was consistently observed (Figure 18B – lower band). A similar band was also observed when different vectors with the same dual-promoter genome configuration were analysed by alkaline agarose gel electrophoresis. Therefore, I hypothesised that this secondary band was a by-product of homologous recombination (HR) triggered by the presence of two identical promoter sequences. If true, the predicted outcome of this process would be the excision of the LP1-GCH1 cassette followed by its degradation and packaging of the ITR-flanked LP1-tTH-WPRE cassette to form a functional virus. A schematic representation of the HR outcome is shown in Figure 19.

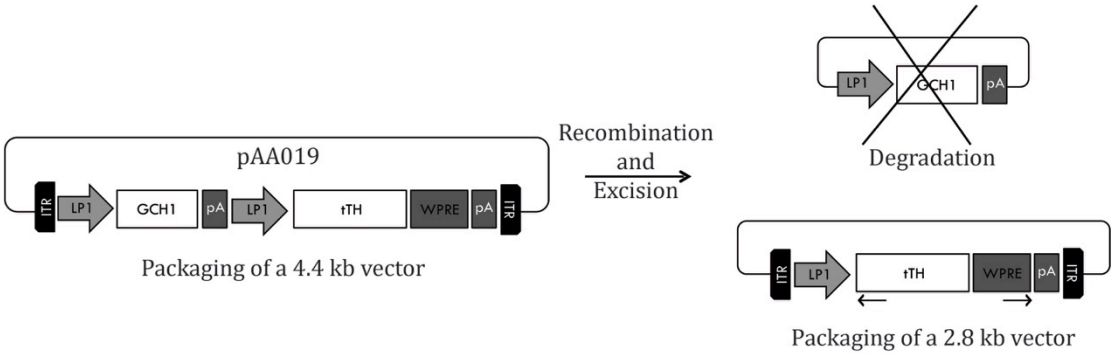

Figure 19: Schematic representation of by-product formation upon HR of the AAV vector. HR is triggered by the dual LP1 promoter, which leads to the excision and degradation of the GCH1 cassette. The remaining tTH cassette is packaged into an AAV capsid due to the presence of the flanking viral ITR sequences. Small arrows below the HR by-product vector indicate the annealing sites of the primers used in the sequencing reaction that confirmed the presence of both ITRs flanking the expression cassette.

To test the HR hypothesis, the 2.8kb DNA band was extracted from the alkaline gel and sequenced (primers used for sequencing are indicated by arrows in Figure 19). A reverse primer was designed that annealed at the 5' end of the *TH* gene and read through the LP1 promoter and part of the L-ITR. A second primer was designed to bind at the 3' end of the WPRE and to read into the beginning of the R-ITR. The sequencing results showed that the LP1-tTH cassette was indeed flanked by two AAV ITRs, thus confirming the occurrence of intramolecular HR during the production of the bicistronic liver vector. These findings show that the generation of the bicistronic liver vector will inevitably lead to the formation of a second vector harbouring the TH cassette only (AAV2/8-LP1-tTH-WPRE).

3.2.4 *In vitro* Validation of the Bicistronic Liver Vector

The *in vitro* validation of the bicistronic liver vector was performed in order to confirm the functionality of both transgene expression cassettes, more specifically promoter function and protein stability prior to *in vivo* testing. This was done by transducing the hepatocellular carcinoma cell line Huh7.5 with the recombinant bicistronic vector and verifying GCH1 and TH expression by western blot. Because this cell line is refractory to standard transfection techniques, validation of protein expression was performed by infection instead of transfection with the producer plasmid pAA019. Although AAV8 has the

ability to efficiently transduce liver tissue *in vivo*, efficient *in* vitro transduction is difficult to achieve in immortalised liver cell lines. Therefore, to ensure high transduction levels, cells were infected at a high MOI of 10^6 gcp/cell and viral-mediated protein expression was detected by western blot 48h post-infection. Figure 20 shows that the AAV2/8-LP1-GHC1-LP1-tTH-WPRE and its recombination by-product were able to express TH and GCH1. Uninfected Huh7.5 cells showed basal GCH1 expression as a result of the endogenous expression of this enzyme in the liver (Tatham et al. 2009).

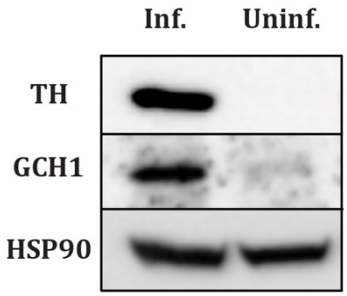

Figure 20: *In* vitro validation of AAV2/8-LP1-GCH1-LP1-tTH-WPRE.
Western blot was performed on cell extracts of the Huh7.5 cell line infected with the vector. 1x10^5 cells were infected at a MOI 10^6 gcp/cell. Protein expression from both transgenes was assessed 48h post-infection.

3.2.5 *In vivo* Efficacy of the Bicistronic Liver Vector

After it was confirmed that both transgene cassettes were able to express TH and GCH1 *in vitro*, a small-scale study was performed in female mice. This experiment aimed to assess: 1) whether a single systemic injection of the vector leads to broad hepatic transduction; 2) whether hepatic transduction was associated with tissue damage and leukocyte infiltration; and 3) whether hepatic transduction by the vector was associated with increased levels of circulating L-DOPA.

Hepatic transduction was assessed by IHC. Screening for histological signs of tissue damage and leucocyte infiltration was done by haematoxylin and eosin (H&E) staining. Finally, hepatic L-DOPA synthesis was assessed by HPLC analysis of plasma collected 28 days post-injection after animals were treated with the AADC and COMT inhibitors benserazide and entacapone.

The doses tested in this study ($3.6x10^{12}$ and $1.3x10^{12}$ gcp/mouse) represent a 50 and 19-fold increase relative to the study with the monocistronic vectors (Table 10).

Treatment Group	Dose (gcp/mouse)	n
Vehicle	-	3
AAV2/8-LP1-GCH1-LP1-tTH-WPRE	$3.6x10^{12}$	3
AAV2/8-LP1-GCH1-LP1-tTH-WPRE	$1.3x10^{12}$	3

Table 10: Treatment groups and doses of bicistronic AAV liver vector injected into mice.

The timeline of this study was slightly different from the one that tested the efficacy of the monocistronic vectors. Here, vehicle- and vector-treated mice were all sacrificed on the same day. In addition, a different treatment regimen of benserazide and COMT inhibitor (this time entacapone instead of tolcapone) was administered prior to sacrifice in one dose instead of three sub-doses (Figure 21). Entacapone and tolcapone are both inhibitors of COMT. The main difference between these inhibitors is the ability of tolcapone to cross the blood brain barrier. Since our interest is in peripheral L-DOPA synthesis, the choice of the COMT inhibitor used in this study is not of major importance.

Figure 21: Timeline of the second mouse study.
On day 0 animals were injected in the tail-vein with AAV vectors at two different doses. On day 28, mice received a single intraperitoneal injection of benserazide and an oral treatment with entacapone at a dose of 12 and 30 mg/kg, respectively. One hour after the benserazide and entacapone treatment, blood was collected, animals were sacrificed and their livers were harvested for fixation.

Hepatic transduction of the bicistronic liver vector for both doses tested was assessed by IHC in paraffin embedded liver sections. Both doses mediated broad hepatic expression of TH and GCH1. Variation in transduction efficiency was observed between animals (Figure 22 - TH staining in all three mice). However, on average, levels were similar to the 65.8 ± 9% transduction levels previously described for a dose of $1.8x10^{12}$ gcp/mouse of AAV8 (Nakai et al. 2005). It must be noticed that this extrapolation must be done with caution since the reference value from Nakai et al. was taken from mice injected via the portal vein, which was shown to lead to a higher transduction of the mouse liver than tail-vein injection. Furthermore, the stronger staining observed in the higher dose group suggests a stronger transgene expression per hepatocyte than in the lower dose group, most likely due to the presence of more viral genome copies per cell. The quantification of the vector genome copies per cell could not be performed because the whole liver was fixed after the animals were sacrificed. Of note, the broader liver transduction observed in this experiment supports the notion that animals in the first study were underdosed with the monocistronic vectors.

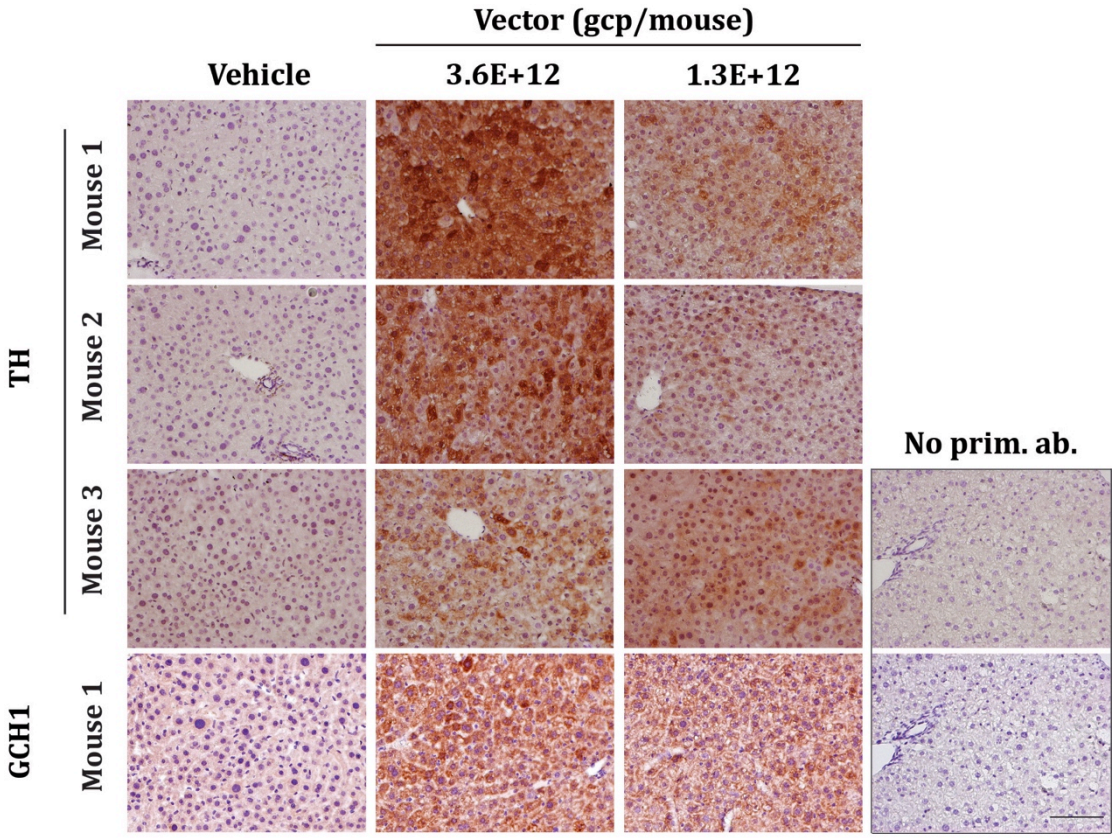

Figure 22: Transduction efficiency of the liver vector measured by IHC.
Stainings were performed against TH (three upper lanes) and GCH1 (bottom lane). Stained cells (brown) indicate vector-mediated expression of TH and GCH1. TH staining for all three mice is shown in order to highlight the variability in transduction between animals. Liver sections stained without primary antibody incubation were used to control for unspecific staining. The images for unspecific staining control are the same for TH and GCH1 but each one was subject to the same adjustments as the other images in the same lane. Scale bar 100 µm.

In addition to transduction efficiency, the integrity of the hepatic tissue 28 days post-injection was assessed by H&E staining (Figure 23). Hepatocytes of treated animals showed normal morphology similar to that of vehicle-treated animals. Furthermore, no hepatocyte necrosis or inflammatory cell infiltration was observed in any of the groups and no abnormal chromatin condensation (heterochromatin) was seen, indicating that the hepatocytes were transcriptionally active and functional (Wang et al. 2015; Maeda et al. 2016).

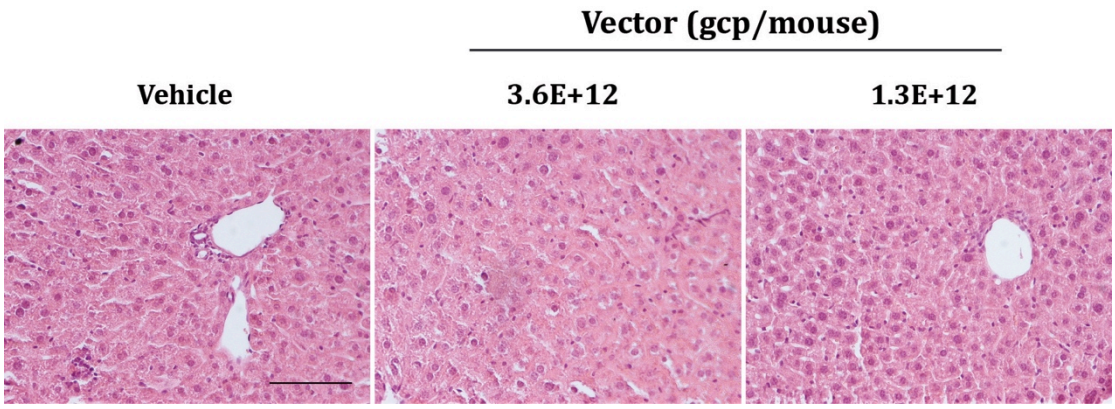

Figure 23: H&E staining on liver sections of animals treated with the bicistronic liver vector.
Staining were performed 28 days post-injection and no sign of tissue damage was detected in any of the groups. Scale bar 100 µm.

Following the IHC analysis of TH and GCH1 expression in the liver, plasma L-DOPA levels were measured by HPLC coupled with electrochemical detection. For this study, a protocol was established in collaboration with Dr. Sarah Salvage at King's College London.

As shown in Table 11, L-DOPA concentration in the plasma was 0.27±0.01nmol/ml in the vehicle-treated group, whereas vector-treated animals showed 0.47±0.16 and 0.47±0.12nmol/ml after treatment with the higher and lower doses, respectively. The rise in systemic L-DOPA corresponds to an average 1.8-fold increase relative to vehicle-treated animals (Figure 24). Plasma L-DOPA levels in vector-treated animals showed substantial intra-group variability.

Group	L-DOPA plasma (nmol/ml)
Vehicle	0.27±0.01
Vector 3.6x10^{12} gcp/ml	0.47±0.16
Vector 1.3x10^{12} gcp/ml	0.47±0.12

Table 11: L-DOPA plasma levels of animals injected with different doses of the bicistronic liver vectors.

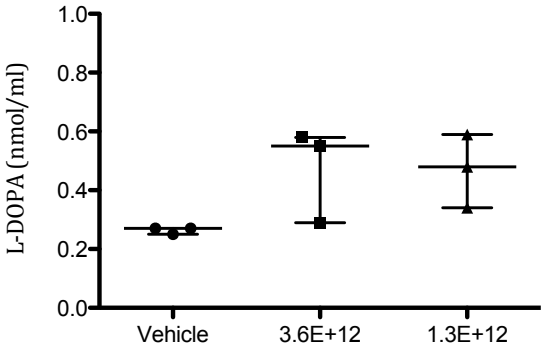

Figure 24: Scatter plot of L-DOPA plasma levels of animals injected with the bicistronic liver vector.
L-DOPA from individual animals was measured by HPLC coupled with electrochemical detection. An average 1.8-fold increase in systemic L-DOPA levels was observed for both doses tested. Bars represent median values ± range.

Interestingly, the fold-increase in plasma L-DOPA was similar for both doses tested. This could be an indication that either the dose difference between treated groups is not large enough to evoke a significant difference between them or that L-DOPA synthesis in the liver has reached a plateau. Although an increase of plasma L-DOPA was observed after vector treatment, the magnitude of the effect was limited considering the broad spread of the vector in the mouse liver. Of note, the lower levels of plasma L-DOPA measured in vehicle-treated mice in this study relative to vehicle-treated mice from the previous one are most likely a consequence of the different AADC and COMT inhibitors regimen adopted in each study – three sub-doses in study 1 vs. a single dose in study 2.

Since the liver is a metabolic organ, I hypothesised that perhaps no further increase in plasma L-DOPA was seen due to inadequate COMT inhibition, which led to the degradation of L-DOPA soon after its synthesis. Because the whole liver had been fixed at the termination of the experiment, the dissection of the L-DOPA pathway and detection of its metabolites in the animals' livers was not possible. Therefore, to test whether a different regimen of COMT inhibitor treatment could lead to a greater increase of systemic L-DOPA after injection with the liver bicistronic vector, new animals were injected with $1.3x10^{12}$ gcp, which corresponds to the lower-dose group. They were given a triple benserazide and tolcapone treatment regimen four hours apart on the day of sacrifice (instead of a single dose). In addition to the vehicle- and vector-treated groups, a group of mice was given oral L-DOPA to mimic the conventional dose and route of

medication in PD patients and to serve as a reference for comparison. Following plasma collection and sacrifice of the animals 28 days post-injection, the livers were divided for fixation and snap freezing in order to allow for a broader range of analysis.

3.2.6 Efficacy of the Bicistronic Liver Vector is not altered by Different AADC /COMT Inhibition Regimen and Sex

The data described in the previous section of this chapter show that despite broad and efficient hepatic transduction with the bicistronic liver vector, L-DOPA plasma levels increased only marginally 28 days post-injection. Studies have been published highlighting a gender-related effect in the mouse liver using AAV vectors (Pañeda et al. 2009). Therefore, to assess whether animal gender also affected hepatic transduction of the bicistronic vector, the *in vivo* experiment was repeated with male mice. Similarly to the one described in the previous section, this experiment aimed to assess: 1) whether a single systemic injection of the vector led to broad hepatic transduction in male mice and 2) whether hepatic transduction by the vector was associated with increased levels of circulating L-DOPA.

Here, hepatic transduction was assessed by IHC and western blot in individual mice. In addition, viral genome copy numbers per hepatocyte were quantified by qPCR. Hepatic L-DOPA synthesis was assessed by HPLC analysis of plasma collected 28 days post-injection after animals were treated with the AADC and COMT inhibitors benserazide and tolcapone.

In this study, animal groups and treatment doses were carried out as described in Table 12 and Figure 25. A group of male mice (n=3) was treated with vehicle, a second group (n=5) was treated with $1.3x10^{12}$ gcp/mouse and a third group (n=3) was given 10mg/kg L-DOPA orally. On the day of sacrifice, all animals were treated three times with 4mg/kg benserazide and 10mg/kg tolcapone and sacrificed 1h after the last dose. An exception was made with the oral L-DOPA group, which was given L-DOPA 1h after the last benserazide/tolcapone treatment and sacrificed 1h thereafter. The vector dose selected for this experiment was based on the observation from the previous

study in which a dose three times higher led to a similar raise in L-DOPA plasma levels. Furthermore, it was known from experience that the generation of a more concentrated AAV preparation would be cumbersome and impractical i.e. beyond the production limits of our laboratory. Scalability is of special relevance if vector production needs to be upscaled in the future for use in larger animal models.

Treatment Group	Dose (gcp/mouse)	n
Vehicle	-	3
AAV2/8-LP1-GCH1-LP1-tTH-WPRE	$1.3x10^{12}$	5
Oral L-DOPA	10 mg/kg	3

Table 12: Groups and doses of mice treated with bicistronic AAV liver vector and oral L-DOPA.

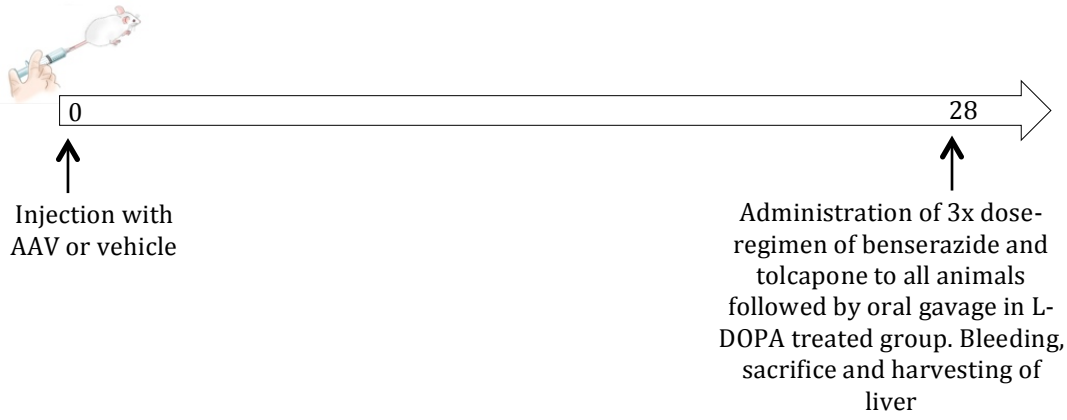

Figure 25: Timeline of the third mouse study.
On day 0 animals were dosed with vehicle or AAV vector. On day 28, all animals received three intraperitoneal injections of benserazide and oral doses of tolcapone at approximately 4 hours intervals in a total dose of 12 and 30 mg/kg, respectively. Animals were sacrificed one hour thereafter, with the exception of the oral L-DOPA treated group, which received an oral gavage of 10 mg/kg L-DOPA and sacrificed one hour later.

Unfortunately, two vector-treated animals were lost during the course of the experiment: one mouse (#4) had to be sacrificed at day 7 due to fight-related injuries and mouse #5 died on the final day immediately after the terminal isoflurane anaesthesia for reasons not clear to us. As soon as it was noticed that the mice were fighting, they were separated and kept in individual cages until

the termination of the experiment. The livers of both dead animals were harvested and frozen but blood could not be collected for future analysis.

Hepatic transduction of the bicistronic liver vector was assessed by IHC on paraffin embedded liver sections and quantitative assessment of transduction was performed for all mice except #4. This mouse was excluded from the analysis because its sacrifice at an early time-point (day 7) did not allow for a direct comparison with the other mice.

As in the previous animal study, IHC demonstrated variation in the transduction levels between animals: 53% and 52% in mice #2 and #3, respectively, and 22% and 15% for #1 and #5, respectively. Mice #2 and #3 had transduction levels comparable to those described by Nakai et al. However, this comparison must be done with caution due to the slightly different doses tested ($1.3x10^{12}$ vs. $1.8x10^{12}$ gcp/mouse) and the different administration routes (tail vein vs. portal vein). A similar transduction pattern was observed for GCH1 in vector-treated animals. Vehicle and oral L-DOPA treated animals showed no positive staining for either enzyme (Figure 26).

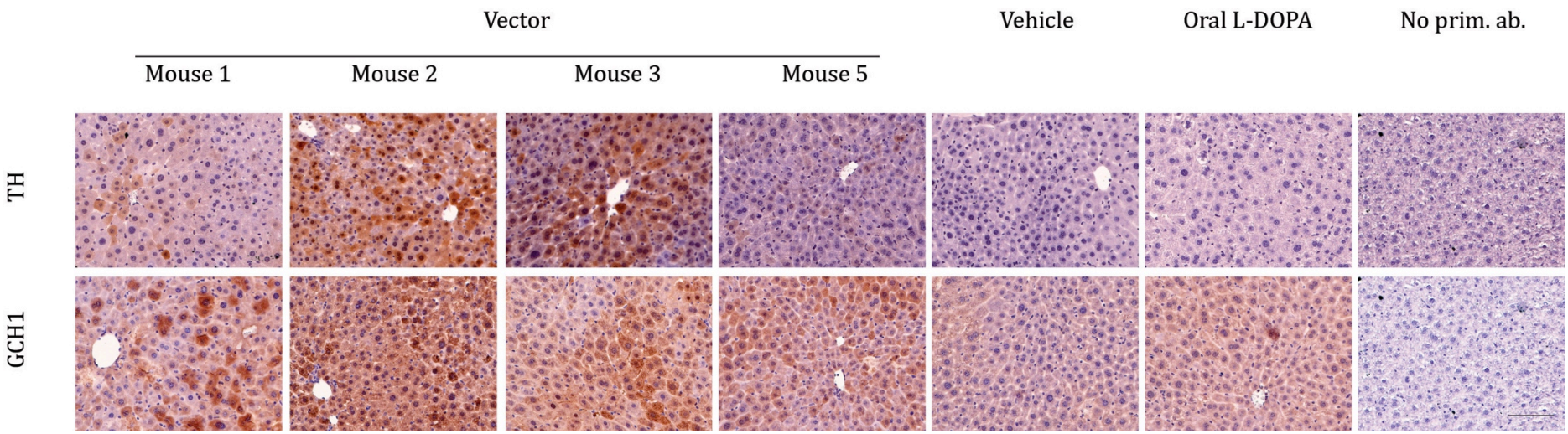

Figure 26: Transduction efficiency of the bicistronic liver vector measured by IHC against TH (upper lane) and GCH1 (bottom lane).
Images of all vector-treated mice are shown except mouse #4, which was sacrificed 7 days post-injection due to fight-related injuries. Brown staining indicates vector-mediated expression of TH and GCH1. TH positive cells were manually counted and compared to the total number of cells per field (244 in average). Liver sections stained without primary antibody incubation were used to control for unspecific staining. The images for unspecific staining control are the same for TH and GCH1 but each one was subject to the same adjustments as the other images in the same lane. Scale bar 100 µm.

In parallel to the IHC staining, transgene expression was assessed by western blot. Consistent with the IHC results, western blot on liver extracts showed varying levels of transgene expression among the vector-treated group. Mice #2 and #3 had the highest expression of TH and GCH1, followed by mice #1 and #5. Mouse #4, included in the western blot analysis, shows negligible TH expression and a more prominent GCH1 band (Figure 27).

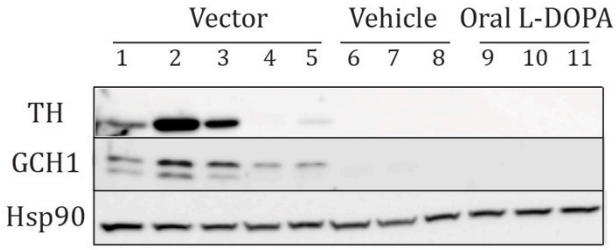

Figure 27: Western blot detection of TH and GCH1 expression in extracts from mouse liver. The organs were harvested 28 days post AAV injection and total protein was extracted from 30µg of liver tissue for the detection of vector-expressed proteins. All animals used in the study are shown.

In addition to the transgene expression levels, the number of viral genome copies per hepatocyte was quantified by real-time quantitative PCR. Figure 28 shows that mice #2 and #3 had the highest viral copy numbers with 794 vs. 409 *TH* copies and 480 vs. 202 *GCH1* copies per hepatocyte, respectively. Mice #1 and #5 presented 338 vs. 108 *TH* copies and 235 vs. 59 GCH1 copies per hepatocyte, respectively. The amount of genome copies per hepatocyte followed the same pattern seen for the IHC and the western blot analysis: #2>#3>#1>#5. Although mouse #4 presented high viral copy numbers, at the time of its sacrifice protein expression from the vector had not reached maximal levels yet. As expected, vehicle and L-DOPA treated mice had basal levels (<0.5) of *TH* and *GCH1*.

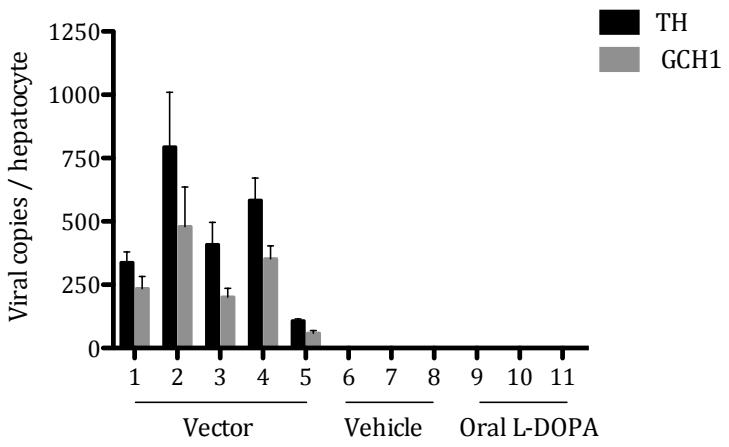

Figure 28: Quantification of viral genome copy numbers per hepatocyte.
The quantification was performed using independent primer pairs for each transgene. Cell numbers were estimated by quantifying the copy numbers of the mouse cyclophilin gene. Results are presented as viral genome copies per hepatocyte.

Taken together, these results indicate a difference in the amount of vector present in the liver of each mouse, which reflects the observed variation in transduction efficiency. Of note, the copy number/hepatocyte of *TH* was on average 1.7x times higher than that of *GCH1*. This can be explained by the homologous recombination of the vector, which leads to the formation of a by-product consisting of the *TH* cassette only. Thus, more *TH* than *GCH1* copies were present in the vector preparation injected in the mice.

Following the detection of viral genomes and expression in the mouse liver, the plasma L-DOPA concentration was measured by HPLC coupled with electrochemical detection. Plasma L-DOPA quantification revealed a 1.8-fold increase in vector-treated animals relative to the vehicle group. This increase was the same as observed in the previous experiment, which suggests that a saturation of the system and not inefficient COMT inhibition might be the reason why no further increase in plasma L-DOPA was observed despite efficient liver transduction. Mice treated orally showed a 9-fold increase in plasma L-DOPA levels, indicating that the potency of this gene therapy approach is still below what would be required to demonstrate a potential therapeutic benefit (Table 13). Of note, absolute numbers of plasma L-DOPA concentrations differ between this and the previous animal study likely due to the difference in the benserazide and COMT inhibitor treatment regimen adopted

Group	L-DOPA plasma (nmol/ml)
Vehicle	0.91±0.15
Vector 1.3x10^{12} gcp/ml	1.67±0.58
Oral L-DOPA	8.13±4.18

Table 13: L-DOPA plasma levels of animals injected with the bicistronic liver vector in the second mouse study.

Levels of plasma L-DOPA mirrored the viral genome copy numbers per cell and TH expression data, with mouse #2>#3>#1. Again, significant variability was seen between vector treated mice. Interestingly, L-DOPA plasma levels showed a big variability in the orally treated group as well (Figure 29).

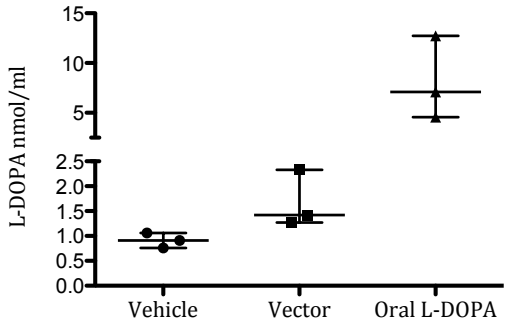

Figure 29: Scatter plot of L-DOPA plasma levels of mice injected with the bicistronic liver vector in study 2.
L-DOPA levels from individual animals were measured by HPLC with electrochemical detection. A 1.8-fold and 9-fold increase were seen in vector and oral L-DOPA treated mice, respectively, relative to the vehicle group. Bars represent median values ± range.

3.2.7 Dissection of Hepatic TH Activity and L-DOPA Synthesis Pathway

To better understand the reasons why plasma L-DOPA levels do not seem to increase further than 1.8-fold, three non-mutually exclusive hypotheses were proposed: (1) the amount of TH expressed in the liver is not sufficient to cause a more significant raise in plasma L-DOPA; (2) the liver does not release L-DOPA efficiently; and (3) the COMT present in the liver degrades the newly synthesised L-DOPA despite treatment with inhibitor (Figure 30).

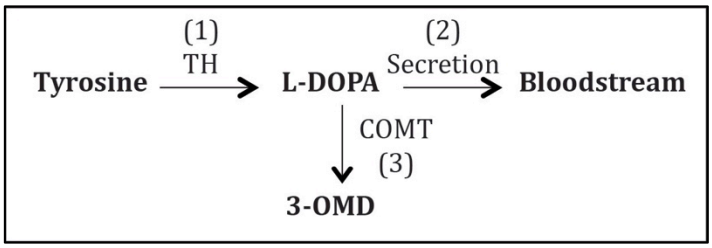

Figure 30: L-DOPA biosynthetic pathway in the liver and putative steps at which L-DOPA synthesis is being deterred.
(1) Insufficient TH to efficiently convert tyrosine into L-DOPA; (2) inefficient release of L-DOPA from hepatocytes into the bloodstream; (3) degradation of synthesised L-DOPA by liver COMT.

To test each of the hypotheses, the pathway of hepatic L-DOPA synthesis was dissected by measuring TH activity in the liver as well as hepatic L-DOPA and 3-OMD concentrations.

If enough TH is present in the liver of the vector-treated animals to sustain high levels of L-DOPA synthesis, a significant difference in the TH activity in liver extracts of vector-treated mice relative to untreated animals is expected. TH enzymatic activity was quantified by measuring the rate at which tyrosine was converted into L-DOPA after being incubated with homogenates equivalent to 3 mg of hepatic tissue. The conversion rate in vector-treated mice was 1.7-fold higher than that in vehicle and oral L-DOPA treated animals. However, when compared to the activity levels in naïve striatal tissue, vector-treated animals demonstrated a 15-fold lower TH activity (Figure 31).

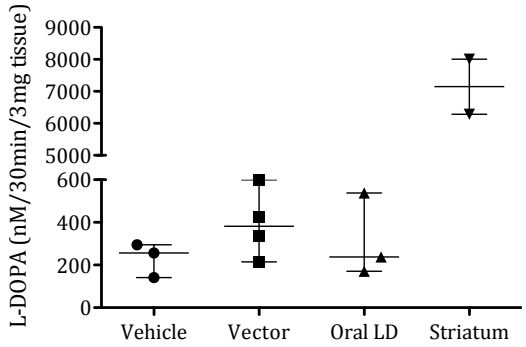

Figure 31: Scatter plot of hepatic TH activity of mice from study 2.
TH activity was measured from liver extracts by HPLC with electrochemical detection. Bars represent median values ± range.

Given that an increase in L-DOPA plasma levels was consistently observed after vector treatment, it is unlikely that the TH expressed by the vector is not

functional. Rather, the amount of TH expressed by the vector is insufficient to further raise L-DOPA plasma levels. To test this hypothesis the amount of TH present in the liver of the two mice expressing the highest levels was compared with the striatum of a naïve mouse. Figure 32 shows that mice #2 and #3 express respectively 2.5 and 17-fold less TH than normally present in striatal tissue. While the difference in TH expression levels and TH activity between the liver of mouse #3 and naïve striatal tissue was similar (~15-fold), mouse #2 presented low hepatic TH activity despite expressing half the amount of TH found in striatal tissue (Figure 32).

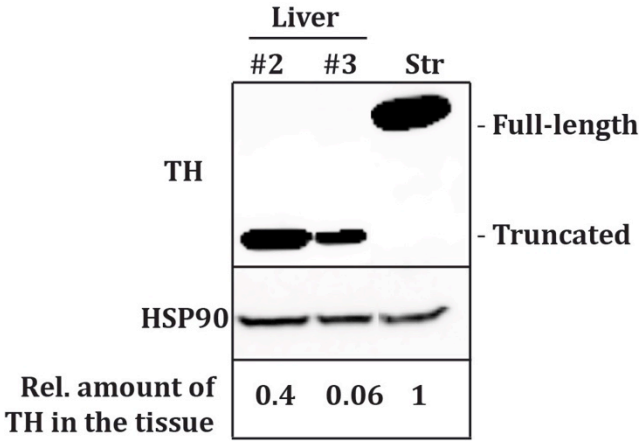

Figure 32: Relative amount of TH present in transduced liver normalised to naïve striatum.
Total protein was extracted from 30µg of liver of mice #2 and #3 and striatal tissue of a naïve mouse. TH levels were assessed by western blot, quantified and normalised to the amount of HSP90.

These results allow two possible interpretations: (1) the truncated TH expressed by the vector is less active than the wild-type striatal TH or (2) TH is not being expressed in sufficient amounts to raise L-DOPA plasma levels more than 1.8-fold. If hypothesis (1) is correct, the truncated form must be replaced by the full-length TH and re-tested *in vivo*. However, if hypothesis (2) is true, TH delivery must be significantly improved by enhancing expression from the vector or by broadening the range of tissues that can be targeted by the vector. Alternatively, increasing the AAV dose would lead to more vector genome copies per hepatocyte. However, further upscaling vector production is impractical.

Next, L-DOPA release from the liver was assessed by measuring its accumulation in the hepatocytes. Accumulation of hepatic L-DOPA to

concentrations higher than those observed in the plasma would be indicative of inefficient release into the bloodstream. There was a 2.3-fold accumulation of L-DOPA in the liver of vector treated animals relative to the vehicle treated group (Figure 33). This mirrors the difference in plasma levels seen between vector- and vehicle-treated animals (Table 13) suggesting that the L-DOPA synthesised in the liver is readily released into the bloodstream. The concentration of hepatic L-DOPA matched the pattern observed for transgene expression and L-DOPA plasma levels, with mouse #2 having the highest concentration, followed by mouse #3 and finally mouse #1. Mouse #5 had similar hepatic L-DOPA levels as vehicle-treated animals. This animal also had the lowest vector genome copy numbers per cell (Figure 28) and showed the weakest expression of TH and GCH1 by IHC and western blot (Figure 26 and Figure 27). Mouse #2 was the only animal that could suggest hepatic accumulation of L-DOPA as it had a 5-fold L-DOPA enrichment relative to control animals. Mice treated with oral L-DOPA showed no difference in intrahepatic L-DOPA compared to vehicle-treated animals (3.35±0.25 vs. 2.99±0.21 ng/mg liver). Mouse #4 was not considered in this assay due to its early death.

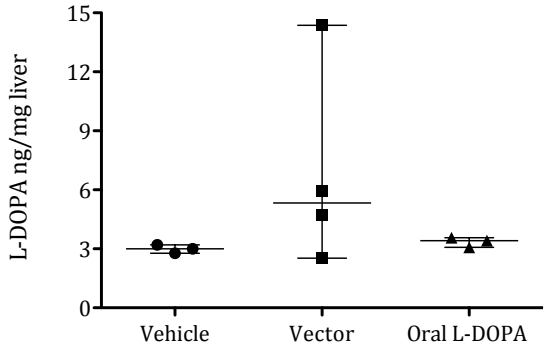

Figure 33: Scatter plot of hepatic L-DOPA levels from mice from study 2.
Hepatic L-DOPA was measured from individual animals by HPLC with electrochemical detection. Bars represent median values ± range.

Next, the L-DOPA catabolism hypothesis was tested by measuring the hepatic levels of 3-OMD. The catecholamine-degrading enzyme COMT, which L-DOPA is a substrate of, is present in the liver and the product of L-DOPA degradation by COMT is 3-OMD, a stable metabolite with a half-life of ~15h. Since the long half-life of 3-OMD allows the detection of any L-DOPA formed and subsequently

degraded, it is a good predictor of the stability of L-DOPA synthesised in the liver and the efficacy of the COMT inhibition regimen adopted in the study. Therefore, detection of high levels of 3-OMD in the liver would be indicative of L-DOPA degradation and insufficient COMT inhibition.

As Figure 34 shows, there was no hepatic enrichment of 3-OMD in vector-treated animals. Mice #2 and #3, which showed the highest plasma and hepatic L-DOPA levels, had 0.21 and 0.56 ng of 3-OMD per mg of liver tissue, respectively. 3-OMD levels in vector-treated mice #1 and #5 as well as in all vehicle-treated animals were below the assay's detection limit. Big variation was observed in mice treated with oral L-DOPA, with one mouse showing a low concentration (0.36ng/mg liver) and the other two showing much higher levels (1.23 and 3.05ng/mg liver).

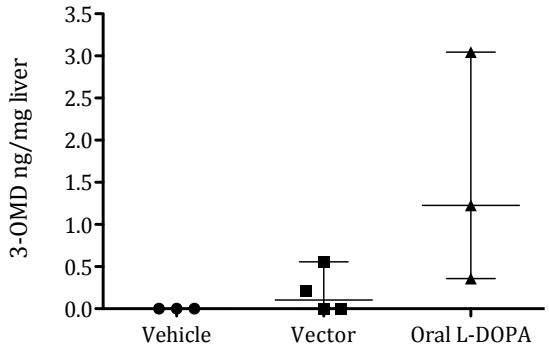

Figure 34: Scatter plot of hepatic 3-OMD concentrations.
Hepatic levels of 3-OMD in individual animals 28 days post-injection measured by HPLC with electrochemical detection. Bars represent median values ± range.

Taken together, these data indicate that AAV-mediated delivery of TH and GCH1 to the liver of healthy mice leads to a 1.8-fold increase in plasma levels of L-DOPA. Although this increase was caused by the AAV vector, its magnitude is not likely to have a potential therapeutic benefit in the prevention of LID. Analysis of vector transduction, hepatic TH activity and L-DOPA metabolism in the liver suggest that there is possibly insufficient TH expression in the liver. However, the possibility that the truncated TH form expressed by the AAV vector is less active than the full-length wild-type form cannot be disregarded. Both alternatives are being addressed by (1) testing a new vector that allows for

peripheral L-DOPA synthesis in other organs in addition to the liver and (2) comparing the activity of the tTH vs. full-length TH *in vitro*.

3.2.8 Peripheral L-DOPA Synthesis in Additional Tissues

The aim of the proposed gene therapy for L-DOPA synthesis in the periphery is to deliver L-DOPA in a continuous manner. By targeting the liver with the bicistronic vector, a rise in plasma levels from 0.91 to 1.67nmol/ml was observed, which corresponds to a 1.8-fold increase. In humans, the threshold for minimal clinical effect is estimated to be around 7nmol/ml, about the same plasma L-DOPA concentration reached in mice treated with the oral L-DOPA regimen (Dethy et al. 1997; Nutt & Woodward 1986). Therefore, although this gene therapy strategy does not aim to match the L-DOPA plasma levels reached by the oral L-DOPA therapy, but rather to provide a continuous basal supply, an AAV-mediated increase in L-DOPA levels to at least half of that achieved with oral L-DOPA medication is desired. Such a rise would be sufficient to allow for a significant decrease in oral L-DOPA intake and potentially improve LID by diminishing plasma peaks and troughs. The results presented so far show that further optimisation is necessary in order to reach a basal L-DOPA supply with a therapeutic potential when combined with the standard oral L-DOPA pharmacotherapy. The first step towards achieving this goal is testing if the truncated TH presents diminished catalytic activity relative to the full-length form. Allowing L-DOPA synthesis to occur at additional peripheral sites like skeletal muscle could potentially further increase plasma L-DOPA levels. Therefore, the vector was redesigned to allow for transgene expression in skeletal muscle in addition to the liver. It is known from several gene therapy trials that different tissues, including muscle, can be used as a system for synthesis and delivery of biologically active molecules (Ding et al. 2008; Nathwani et al. 2011; Balazs et al. 2012). Thus, allowing additional tissues to participate in the peripheral synthesis of L-DOPA has the potential to bridge the gap needed to achieve increased levels of systemic L-DOPA.

3.2.9 Design of an AAV Vector for L-DOPA Synthesis in Additional Tissues

Using AAV8 as a vector for gene therapy leads mainly to the transduction of liver, skeletal and cardiac muscle. However, gene addition of GCH1 and TH will not lead to L-DOPA synthesis in the muscle due to the lack of the TH cofactor BH4 in this tissue. In this scenario, the second enzyme in the BH4 biosynthetic pathway - 6-pyruvoyl tetrahydropterin synthase (PTPS) - must be present in order for BH4 synthesis to occur and consequently for TH to function normally (Ding et al. 2008). Therefore, two AAV vectors were constructed that harbour the *TH*, *PTPS* and *GCH1* genes in one single genome. Both vectors are almost identical with the only difference being in the *TH* gene. One vector contains a truncated *TH* gene, while the other has the 465bp that comprise the regulatory domain at the N-terminus portion of TH, allowing us to assess whether the tTH is less active then the full-length TH (Figure 25).

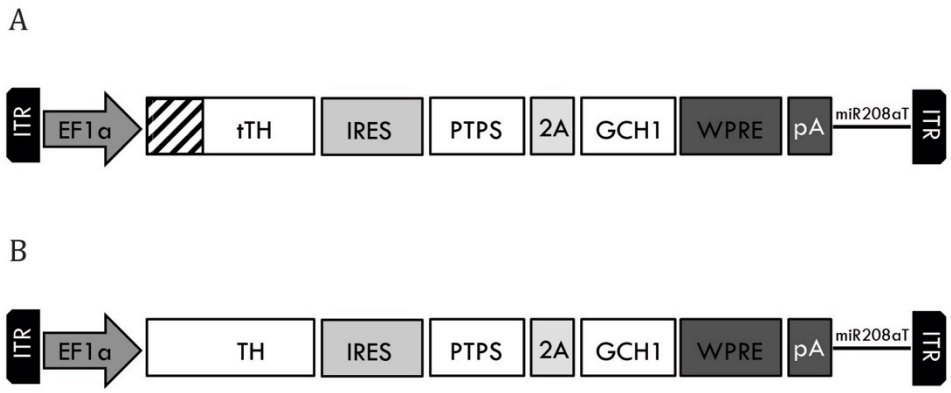

Figure 35: Schematic of systemic tricistronic vectors.
Vectors express the truncated TH (tTH) (A) or the full-length TH (B). Three genes necessary for L-DOPA synthesis in the periphery are expressed from a single constitutive human promoter. The *TH* gene is separated by an IRES from the PTPS, which is followed by the FMDV 2A sequence and then the *GCH1* gene. The miRNA208 target sequence will prevent expression of this vector in cardiac cells.

To achieve expression of the three proteins from a single mRNA, the design of the vector was modified relative to the bicistronic construct. The truncated or full-length forms of the TH coding sequence are immediately downstream of the EF1α promoter, a constitutive promoter of human origin. This is in turn followed by the encephalomyocarditis virus (EMCV) IRES that will allow translation of the *PTPS* and *GCH1* genes, which are linked by the foot-and-mouth disease virus (FMDV) 2A sequence. Because the PTPS stop codon is absent in this construct,

once the ribosome reaches the 2A sequence, it will read through and skip to the *GCH1* coding sequence, leading to the expression of two independent proteins. The resulting independent proteins will be slightly different to the wild-type forms due to the presence of the 2A sequence: the PTPS enzyme will have a 27 amino acid overhang at the C-terminus and the GCH1 will have a proline upstream of the start methionine. Between the GCH1 and the polyA, the WPRE sequence was added to enhance expression from this mRNA. Finally, immediately downstream of the polyA sequence, two copies of the microRNA-208a target sequence (miR208aT) were added in tandem. Cardicac muscle cells express the 22nt long non-protein-coding microRNA208a which, upon interaction with the 3' untranslated region of its target sequence miR208aT, will inhibit its translation, leading to the silencing of the vector (Roudaut et al. 2013; Wang et al. 2014). Thus, microRNA-mediated gene silencing of the vector in the heart will avoid off-target effects such as L-DOPA-induced cardiac arrhythmia (Landsberg 1972). The tricistronic vector was constructed by replacing individual elements in pAA019 to make pAA062 - expressing truncated TH – or pAA063 – expressing full-length TH. Once the cloning was finalised, plasmids were verified by sequencing and the integrity of the ITRs was confirmed by SmaI restriction endonuclease analysis.

3.2.10 In vitro validation of the systemic vectors

The *in vitro* validation of the systemic vectors was done by verifying the expression of the three enzymes in HEK293T cells. Cells were transfected with increasing amounts of DNA and protein expression was assessed by western blot 48 post-transfection. Figure 36 shows that the construct harbouring the truncated TH successfully expresses the three transgenes from a single mRNA *in vitro*. A dose-response effect is observed relative to the amount of transfected DNA. Moreover, the FMDV 2A sequence leads to the efficient translation of independent PTPS and GCH1 proteins. Because the construct expressing the full-length TH was generated at a later point, its expression could not be validated before this thesis was written. Although the data are missing at this point, a similar expression pattern as seen in Figure 36 is expected.

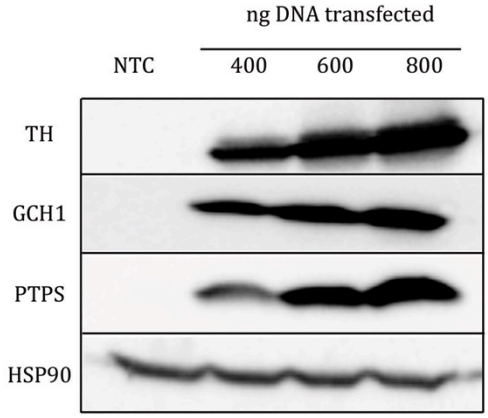

Figure 36: *In vitro* validation of the tricistronic vector construct.
Western blot was performed on cell extracts of the HEK293T cell line transfected with the tricistronic AAV producer plasmid harbouring the truncated *TH* gene. $4x10^5$ cells were infected in a 12 well plate with different amounts of plasmid. Protein expression from the three transgenes was assessed 48h post-transfection. NTC: non-transfected cells.

The strategy adopted to allow the expression of the three genes from a single mRNA was possible due to the inclusion of the FMDV 2A sequence. However, after the "cleavage" that will separate the PTPS from the GCH1 peptide, PTPS will contain 27 additional C-terminal amino acids. Given that this enzyme forms a homohexamer for its catalytic activity, the effect of these extra amino acids on the formation of higher-order structures is unknown. Thus, to validate the catalytic activity of the PTPS expressed by the new construct, COS-7 cells were transfected and the catalytic activity of PTPS is currently being measured using a protocol adapted from Heintz et al. (Heintz et al. 2012).

3.3 Discussion

In this chapter I tested the feasibility of AAV-mediated continuous L-DOPA synthesis in the periphery as a potential therapy to reduce the side effects currently associated with chronic oral L-DOPA uptake. To this end, I used rAAV8 vectors to achieve extrachromosomal gene addition of *TH* and *GCH1* in the liver of healthy mice in order to induce L-DOPA synthesis in this organ. I was able to show that the bicistronic vector is able to efficiently transduce the liver in both female and male mice and is well tolerated. A single systemic injection led to a 1.8-fold increase in the levels of circulating L-DOPA, however, this rise is not

likely to translate into therapeutic benefit and the gene therapy strategy must still be further optimised.

I explored two approaches to achieve peripheral L-DOPA production. In the first one, the *TH* and *GCH1* genes were delivered by separate vectors. The rationale was that this strategy would allow the investigation of whether vector-induced BH4 synthesis is necessary to support TH activity. BH4 occurs naturally in the liver and it functions as a cofactor for the enzyme PAH. In this experiment, dsAAV vectors were used to take advantage of their rapid onset of transgene expression; the target vector dose was in the range of $1x10^{11}$ gcp/mouse (Wang et al. 2003). Sufficient vector could be generated to treat mice with a total dose of $7x10^{10}$ gcp/mouse, which is close to the dose of $1x10^{11}$ gcp/mouse shown to lead to broad liver transduction with a dsAAV8 vector expressing its transgene from the same liver-specific LP1 promoter (Nathwani et al. 2006). Surprisingly, hepatic transduction achieved with this dose was below 1%, which was not sufficient to increase L-DOPA plasma levels 28 days post-AAV injection (Figure 16 and Table 3). The reasons for the low transduction efficiency observed with these vectors are not yet entirely clear. DNA sequencing and endonuclease quality control digestion demonstrated correct DNA sequences and ITR integrity in both vector producer plasmids. Likewise, SDS-PAGE analysis of both vectors showed preparations of high purity (Figure 14). In addition, given that both AAV producer plasmids were generated by a single cloning step to replace the transgene from the already validated dsAAV2/8-LP1-hFIXco, which harboured a codon optimised version of the human factor IX cDNA, protein expression from both vectors was not verified *in vitro* prior to injection. However, the low transduction efficiency observed with the monocistronic vectors urges for the verification of TH and GCH1 expression from both vectors in order to confirm transgene cassette integrity.

The findings of this experiment indicated that most likely transduction efficiency had to be significantly improved by increasing the injection dose. The optimal dose could be determined by preforming a dose escalation study, however, packaging efficiency of the dsAAV8-LP1-tTH vector was very low - total particle:gcp titre ratio > 10 (Table 6) – and significantly upscaling the production of this vector would not yield sufficient vector for the injection of

higher doses. Therefore, the dual vector approach was abandoned and a new vector was generated that combines the *TH* and *GCH1* genes into a single AAV genome. A similar vector had previously been shown to express both enzymes in the optimal 5:1 ratio and to lead to continuous L-DOPA synthesis in the striatum of a rat model of PD (Cederfjäll et al. 2012).

With the experiments using the bicistronic vector, I was able to demonstrate that it expressed both proteins *in vitro* and that *in vivo* doses of $1x10^{12}$ and $3.6x10^{12}$ gcp/mouse are well tolerated and lead to a broad vector spread in the liver (Figure 22 and Figure 13). The IHC results showed a strong TH and GCH1 staining, however, the broad viral transduction did not reflect in a significant increase of plasma L-DOPA, where only a modest 1.8-fold increase was observed (Figure 24). Interestingly, the magnitude of the effect on plasma L-DOPA levels was similar for both doses tested, suggesting a possible saturation of the system. Alternatively, it is possible that the difference between both doses was not big enough to evoke distinct effects detectable at the plasma level. The IHC staining was on average more intense in animals that received the higher dose, suggesting the presence of more vector copies/cell. This is the most plausible interpretation for this result given that there is a positive correlation between vector copy numbers and transgene expression (McIntosh et al. 2013). Unfortunately, quantification of vector genome copy numbers per hepatocyte was not possible in these mice because their livers were fixed with PFA after the termination of the experiment. The efficiency of the AADC and COMT inhibition given to the animals prior to blood collection and sacrifice was also questioned. Firstly, the dosing regimen used differed from that in our previous experiment – here mice were treated with one single dose instead of three sub-doses – and secondly because the COMT inhibitor may not have been sufficiently fresh to guarantee optimal activity. Because of the surprisingly low transduction seen with the monocistronic dsAAV vectors, the *in vivo* assessment of the bicistronic vector was at first conceptualised as a preliminary study with the aim to determine hepatic transduction efficiency by IHC on paraffin embedded tissue. However, on the day of sacrifice plasma collection from the animals for L-DOPA measurement was added to the study protocol. This change in protocol was responsible for the modified AADC and COMT inhibitor regimen as well as for the

use of an old reagent for the COMT inhibition. The fact that good transduction was seen after increasing the dose 19-fold suggests that animals injected with the dsAAV vectors in the previous experiment had been underdosed. The hepatic transduction observed for both doses of the bicistronic vector agrees with the 65% hepatic transduction published for single-stranded AAV8 (Nakai et al. 2005). In addition, the lack of evidence of tissue injury or inflammation is in agreement with the low toxicity and high tolerability of humans and animals to AAV vectors (Kaplitt et al. 2007; Muramatsu et al. 2010). Finally, the vector was able to increase the levels of circulating L-DOPA in female mice.

Because good transduction was observed with the bicistronic vector, which led to a 1.8-fold increase in plasma L-DOPA at both doses tested (3.6- and $1x10^{12}$ gcp/mouse), the lower dose was selected for the experiment in male mice. For this experiment, the number of animals in the vector-treated group was increased from 3 to 5. Furthermore, the original AADC and COMT inhibitor regimen from the first study was adopted and a group of mice receiving oral L-DOPA treatment was included to mimic the typical route and dose taken by PD patients to treat their motor symptoms (Table 12 and Figure 25). As seen in the female mice, male mice showed a 1.8-fold increase in plasma L-DOPA 28 days post-injection, a contrasting result to studies that show a gender effect in murine hepatic transduction with AAV vectors (Davidoff et al. 2003). Variability in vector transduction was observed between mice, which was confirmed by the vector genome copy numbers per cell, IHC and western blot data. Although IHC assessment of transduction indicated similar AAV expression levels between mice #2 and #3 and mice #1 and #5, the western blot data showed that the variation in the amount of TH expressed in the liver of the animals was more pronounced. The western blot data is supported by the quantification of the vector genome copy numbers per hepatocyte. The close correlation between the vector genome copies quantification and the western blot data can be explained by the higher sensitivity of both methods compared to IHC.

Possible reasons for the observed variability were: the use of CD-1 mice, an outbred strain, can have contributed to the variability in transduction levels. For example, the use of CD-1 mice has been shown to mask effects in toxicity screenings otherwise detected when inbred mouse strains are used (Festing

2010). Genetic variation could also explain the variability in plasma L-DOPA levels in the group treated with oral L-DOPA. However, inaccuracy during the injection of the vector cannot be excluded as the source of variability. On the day of injection it was observed that the mice had been fighting and most of them had body injuries including the tail. This made the localisation of the tail-vein and the injection procedure more difficult and possibly more variable between mice. The variability in the L-DOPA levels seen in the orally treated animals could be explained by factors that also affect L-DOPA peak doses in humans after oral medication: erratic gastric emptying and competition with other amino acids for absorption in the intestine (Kurlan et al. 1988; Camargo et al. 2014).

Despite the variation in vector transduction, mice showed on average a 1.8-fold increase in plasma L-DOPA levels. The highest levels were seen in mouse #2, which was the most aggressive one and did not show clear signs of fight-related injuries on its tail on the day of injection. Even if analysed alone, the fold-increase in plasma L-DOPA in mouse #2 relative to untreated mice was 2.5. When compared to the levels after L-DOPA oral treatment, vector-mediated L-DOPA production is modest and not likely to provide a basal L-DOPA supply with a potential therapeutic benefit. In an attempt to further understand the reasons for the modest L-DOPA rise, three possible roadblocks for AAV-mediated hepatic L-DOPA synthesis were investigated: (1) insufficient amount of TH expressed by the vector; (2) inefficient L-DOPA secretion form the hepatocyte; and (3) inadequate hepatic COMT inhibition.

These findings suggest that the amount of TH expressed in the mouse livers was lower than that found in the naïve striatum. Although only the livers of two mice were compared with the striatum, mouse #2 expressed half the amount of TH present in the naïve striatum, while mouse #3 expressed 16-fold less (Figure 32). Although the livers of mice #1 and #5 were not quantified by western blot, they had even less TH than mouse #3 as seen from the IHC and western blot data (Figure 16 and Figure 27). In general, the hepatic TH activity data does not correlate directly with the levels of transgene expression seen by IHC and western blot or with the genome copy numbers per cell. Taken together, the TH activity data suggest that the truncated form of the TH expressed by the vector is less active than the full-length wild-type form present in the striatum. There is

no evidence in the literature to support a decreased catalytic activity of TH after the removal of its regulatory domain. In fact, the opposite seems to be true: truncations of the first 40-165 amino acids (the truncated form used in the vector described here lacks the first 155 amino acids), which comprise the enzyme's regulatory domain, have been reported to increase enzymatic activity by up to 200% (Walker et al. 1994). Nevertheless, the data presented here might suggest the contrary and the means by which this question will be addressed is discussed later in this section.

After comparing the levels of TH expressed in the liver and the striatum, analysis of intrahepatic accumulation and the degradation of newly formed L-DOPA was performed. The data showed 2.3-fold increased hepatic L-DOPA levels in vector-treated animals relative to vehicle-treated ones. This is similar to the fold-increase observed in plasma L-DOPA and indicates that newly synthesised L-DOPA is readily released from the liver. However, it must be noticed that mouse #2 had a 5-fold hepatic L-DOPA accumulation.

Measurement of hepatic 3-OMD, the metabolite formed upon L-DOPA degradation by COMT, indicate that the inhibitor regimen adopted in this study was adequate and efficiently blocked the COMT-mediated degradation of L-DOPA. Due to its half-life of ~15h, degradation of L-DOPA would lead to the accumulation of this metabolite in the liver, however this was not observed.

A fourth alternative that could explain why plasma L-DOPA levels do not seem to increase any further than 1.8-fold is that the amount of tyrosine and BH4 present in the liver are not sufficient to sustain TH activity and L-DOPA synthesis. Although hepatic levels of both molecules were not measured before the completion of this thesis, it seems unlikely that BH4 could be a limiting factor given its natural occurrence in the liver and the additional synthesis supported by vector-mediated GCH1 expression. The measurement of hepatic tyrosine levels is planned for the future.

Taken together, the data presented in this chapter indicate that L-DOPA synthesis is hampered at some level following AAV-mediated expression of TH and GCH1 in the liver.

As discussed above, despite successful hepatic transduction and TH expression in two independent experiments, L-DOPA plasma levels do not

increase more than 1.8-fold. Possible reasons could be: (1) lack of tyrosine in the liver, (2) insufficient amount of TH in the liver or (3) sub-optimal catalytic activity of the truncated TH expressed by the vector. Possible ways to address hypotheses (1) and (2) would be to generate a vector that can transduce not only the liver but additional tissues, thereby allowing more cells to synthesise L-DOPA. Because not all AAV8 particles end up in the liver after systemic administration, cells from other tissues efficiently targeted by this serotype, e.g. skeletal muscle, could bridge the gap needed to achieve systemic levels of L-DOPA that have therapeutic potential. In line with this hypothesis, I have generated and validated the expression of a vector that has the potential to lead to L-DOPA synthesis in both liver and skeletal muscle (Figure 35). Although expression of the three enzymes has been confirmed by western blot, the *in vitro* validation of their enzymatic activity has not been performed yet. Validation of enzymatic activity is particularly important for the PTPS enzyme, which is linked at the DNA level to the *GCH1* gene by the FMDV 2A cleavage sequence. Once "cleaved", the 2A sequence will leave 27 extra amino acids at the C-terminus of PTPS, which can potentially affect its ability to form the higher-order oligomeric forms required for its catalytic activity. For this purpose, a collaboration was established with Prof. Beat Thöny at the University of Zürich who is testing the enzymatic activity of the PTPS expressed from this new vector. In parallel, a similar vector was generated, which harbours the full-length *TH* gene. These two almost identical constructs allow for the *in vitro* comparison of the catalytic activity in both truncated and full-length, thereby addressing alternative (3) mentioned above. Once validated, this vector will be tested at doses of $1x10^{12}$, $5x10^{11}$ and $1x10^{11}$ gcp/mouse in groups of six mice. As in the previous study, a group of mice treated orally with L-DOPA will serve as a positive control. If the therapeutic potential of the new vector is confirmed by significantly increased plasma L-DOPA levels, a biodistribution analysis of the vector in different organs such as spleen, lungs, brain, heart, liver and skeletal muscle is proposed. However, if this new strategy still does not lead to significantly increased plasma levels of L-DOPA, the project will be abandoned.

Prior to the injection of the new vector in animals, it might be well worth replacing the genes in the construct by codon-optimised sequences. Codon

optimisation is based on the codon usage bias of different organisms; because the genetic code is degenerated, the overabundance in the number of codons allows many amino acids to be encoded by more than one codon. The relative frequency of codon usage varies widely between organisms and algorithms have been developed, which convert the sequence of a given gene to one that matches the codon usage bias of the target organism without altering the amino acid sequence of the protein. Codon optimisation has been used in gene therapy strategies with AAV vectors and it has been shown to increase protein expression more than 10-fold without the necessity to increase the number of viral genome copies provided (McIntosh et al. 2013).

In conclusion, hepatic L-DOPA synthesis can be achieved using AAV vectors, however the plasma levels reached are unlikely to provide therapeutic benefit in a disease context. The reasons for the modest rise in circulating L-DOPA despite efficient hepatic transduction are currently under investigation. Nonetheless, a modification in the vector design that allows additional tissues to take part in the synthesis of L-DOPA might be enough to further increase the therapeutic potential of this gene therapy and the testing of this hypothesis will initiate once the newly designed vector has been completely validated.

Chapter 4 AAV-mediated Continuous L-DOPA Synthesis in the Central Nervous System

4.1 Introduction

The ultimate goal in translational research is to practically apply the knowledge gained from years of lab work in a way that matters to patients and the community. From bench-to-bedside projects require joint efforts from scientists, clinicians and investors to successfully translate basic science discoveries into medicine.

The early stages of this project date back to 1998 when Mandel et al. demonstrated that the gold-standard treatment for PD (i.e. systemic L-DOPA) was amenable to gene therapy. At the time, the notion that gene transfer of the *TH* and *GCH1* genes was necessary and sufficient for L-DOPA synthesis in cultured cells was already well established. The pioneer study of Mandel et al. demonstrated key aspects that strongly increased the potential of gene therapy for the treatment of PD. Recapitulating the results obtained in cultured cells, they demonstrated that AAV-mediated TH and GCH1 expression in the striatum led to *in vivo* synthesis of L-DOPA in a rat model of PD. Secondly, transgene expression was shown to be long lasting (over one year post-gene therapy) and, equally important, it was well tolerated. Finally, this study defined the striatal cell population transduced by rAAV2 as being overwhelmingly neuronal (Uchida et al. 1992; Bencsics et al. 1996; Mandel et al. 1998). In the following 14 years, additional studies provided further insight into the AAV-mediated *TH* and *GCH1* gene transfer approach, which allowed for its refinement, bringing it ever closer to translation.

In 2002, a study from Kirk et al. showed that, beyond long-term L-DOPA synthesis, AAV-mediated TH and GCH1 expression in the striatum of 6-OHDA lesioned rats was able to achieve L-DOPA synthesis at levels required for the reversal of motor impairments (Kirik et al. 2002). Soon after, an important study demonstrated that *in vivo* gene therapy using AAV-TH and AAV-GCH1 vectors promoted a significant reduction of abnormal involuntary movements induced by L-DOPA therapy and near complete reversal of motor deficits in 6-OHDA

lesioned rats (Carlsson et al. 2005). Another study complemented these previous findings by establishing a direct correlation between motor improvement after AAV-mediated TH and GCH1 expression in the striatum and the restoration of a functional dopamine pool that reached the post-synaptic dopaminergic receptors in the striatum at physiological levels (Leriche et al. 2009). Furthermore, in another important study Björklund et al. used two separate AAV5 vectors coding for either TH or GCH1 to investigate the stoichiometric ratio of both enzymes that led to optimal TH activity. By maintaining a fixed dose of the AAV5-TH vector and co-injecting increasing amounts of AAV5-GCH1 into the striatum of 6-OHDA lesioned rats, they determined a 5:1 TH:GCH1 ratio as optimal for robust TH activity and efficient L-DOPA synthesis (Björklund et al. 2009). This study also promoted a better understanding of the enzymatic processes and compartments involved in the continuous L-DOPA delivery by revealing that endogenous AADC present in serotonergic neurons participates in the conversion of ectopically delivered L-DOPA into dopamine. This was an important finding, since this strategy relies on endogenous AADC for dopamine synthesis and serotonergic neurons are affected to a lesser extent than dopaminergic neurons in PD. Furthermore, this was the first study that used AAV5 vectors for L-DOPA delivery and it demonstrated that transduction efficiency with this serotype was superior to the previously used AAV2. Finally, an AAV vector, which expresses TH and GCH1 from a single genome in the optimal 5:1 TH:GCH1 ratio was proposed. Intrastriatal delivery of this single vector to the 6-OHDA lesioned rat model of PD led to L-DOPA synthesis, which was superior to what had previously been achieved with two separate vectors. Consequent restoration of extracellular dopamine levels and complete recovery of motor function was demonstrated in a series of behavioural tests (Cederfjäll et al. 2012). These features made this bicistronic vector the first clinical candidate vector for the continuous L-DOPA synthesis approach. To translate these findings into the clinics, Prof. Anders Björklund, a world leader in PD research founded, together with other scientists and investors, the biotech company Genepod Therapeutics®, which funded the preclinical studies in the NHP model of PD discussed here.

The data presented in this chapter describe the preclinical testing of a novel gene therapy for continuous L-DOPA synthesis in the CNS. Behavioural studies on a MPTP-lesioned NHP model of PD are described as well as the progress and challenges encountered towards the translation of this therapeutic strategy into a Phase I clinical trial. The specific aim of this chapter was to test the preclinical efficacy of a candidate AAV vector for clinical trials as well as develop and test improved versions thereof.

This project involved collaborative efforts from four different teams. Our laboratory at King's College London contributed to the design, cloning, generation and the *in* vitro testing of the different viral vectors used in the animal studies. Rodent studies were performed in Dr. Tomas Björklund's laboratory in Lund where I participated in the behavioural evaluation of the animals and performed some of the post-mortem molecular analyses such as IHC assessment of vector transduction in the rat brain. The Gene Therapy Consortium at University College London manufactured the vectors used in the NHP studies; these were outsourced to Motac Neuroscience, a contract research organisation based in Manchester, UK and Bordeaux, France. Motac Neuroscience performed the NHP *in* vivo studies in Beijing, China through the Institute of Laboratory Animal Sciences (ILAS) at the China Academy of Medical Sciences and reported the behavioural data to the scientists in Manchester and Bordeaux on a regular basis. My involvement in the NHP studies included a short stay in Bordeaux where I got familiarised with the study protocols and the different behavioural tests through demonstrations of video scorings for the clinical rating of NHP as well as discussions on the techniques used for the *ex-vivo* analyses of the NHP brain. The molecular and behavioural data generated by Motac were provided to all people directly involved in the study. The generation of the graphics, the statistical analysis of the data, and the interpretation of the results presented in this thesis were done by me. Likewise, the assessment of the gene therapy in the rodent model of PD was done by me and, where necessary to ensure that the implications of my findings are clear to the reader, contributions from Dr. Björklunds's lab are included and clearly indicated in the figure legends.

4.2 Results

4.2.1 Development and Efficacy of a Bicistronic Brain Vector Tested in the MPTP-lesioned NHP Model

The AAV vector used in this study was first described by Cederfjäll et al. in 2012. Its genome codes for TH and GCH1, the two rate-limiting enzymes shown to be sufficient and necessary for L-DOPA synthesis *in vivo*. In addition, each gene is expressed from an independent cassette under the control of the human neuron-specific synapsin (SYN) promoter. The *TH* gene is followed by the WPRE sequence in order to enhance its expression and ensure the optimal TH:GCH1 ratio for *in vivo* L-DOPA synthesis. The serotype selected for this gene therapy approach was AAV5 based on its superiority in transducing the putamen and caudate nucleus (which together form the striatum) of NHP compared to other serotypes as well as on its ability to efficiently deliver L-DOPA in the rat brain in a continuous manner (Dodiya et al. 2010; Cederfjäll et al. 2013). Following successful preclinical studies by Cederfjäll et al. in the 6-OHDA-lesioned rat model, vector production was scaled up for toxicology and efficacy tests in the MPTP-lesioned NHP. MPTP (1-methyl-4-phenyl-1,2,3,6-tetrahydropyridine) is a neurotoxin that is selectively taken up by dopaminergic neurons, where it is metabolised into the toxic cation 1-methyl-4-phenylpyridinium (MPP+) leading to neuronal cell death through oxidative stress. MPTP-treated NHP have been shown to recapitulate most of the pathophysiological changes that occur in PD and are therefore used as PD model in research (Bezard et al. 1997).

For the upscaling of vector production, both GCH1 and TH transgene cassettes were synthesised as one single DNA molecule flanked by BglII endonuclease restrictions sites and subsequently cloned into an AAV-ITR containing backbone. The plasmid was named pGPT002 and used to generate a recombinant AAV vector of the AAV5 serotype (Figure 37). This vector will hereafter be referred to as GPT002.

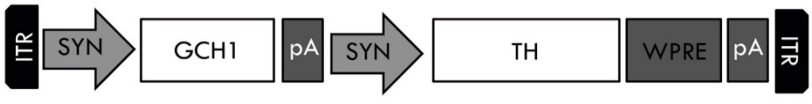

Figure 37: Schematic representation of the GPT002 genome.

4.2.1.1 MPTP Lesion, Induction of LID and Validation of NHP Model

Prior to the brain surgery for AAV vector injection, NHP were treated with the neurotoxin MPTP in order to develop parkinsonism and, after recovery, primed with L-DOPA in order to develop LID. The following data describe the validation of the lesioning (i.e. development of PD motor symptoms) as well as the development of LID. In total, forty naïve macaques (*Macaca mulatta*) were lesioned with daily MPTP injections (0.2mg/kg, i.v.) to induce parkinsonism and treatment was halted once the animals reached a parkinsonian disability score of 6 on the Benazzouz clinical scale (Benazzouz et al. 1993). This clinical rating scale measures motor behaviour in both normal and parkinsonian monkeys according to the symptoms presented in Table 14. Scores range from 0-25 and a score ≥ 15 corresponds to full parkinsonism, similarly to stage IV of the scale of Hoehn and Yahr used for humans (Hoehn & Yahr 2001).

The score of 6 corresponds to a mild degree of parkinsonism and it was chosen in order to allow for the forthcoming surgical procedures to occur with a minimal risk and not to compromise animal recovery and post-surgical health.

Benazzouz rating scale for parkinsonian disability	Score range
Tremor	0-3
Bradykinesia	0-3
Change in posture	0-3
Vocalization	0-2
Freezing	0-2
Rigidity (per arm)	(0-3) x 2
Frequency of arm movements (per arm)	(0-3) x 2
Total	0-25

Table 14: Benazzouz parkinsonian macaque clinical rating scale.

The MPTP treatment lasted on average 25 days, ranging from 17 to 47 days. The slightly longer treatment time required for some individuals might have been due to the fact that estimates for treatment time are based on the lighter primate *Macaca fascicularis* (3kg vs. 7.7kg average weight of an adult male *M.*

mulatta). After the lesioning period, the NHP were left untreated until their disabilities stabilised and remained constant for a period of 2 weeks. Animals that appeared to be unlesioned or excessively lesioned based on the Benazzouz behavioural scoring, were excluded from the subsequent phases of the study. In total, 29 NHP were selected for the next phase of the study.

Following recovery from the MPTP lesion, a two-week treatment with Madopar® (L-DOPA/benserazide, ratio 4:1, p.o., hereafter referred to as L-DOPA) was conducted in order to induce dyskinesia in the NHP. This model mimics the clinical condition of a patient who has received long-term L-DOPA therapy and has developed LID. L-DOPA was given to 29 NHP twice daily at a dose adjusted for each individual. The dose was selected to maximally reverse parkinsonian motor symptoms and cause hyperactivity in the animals, which has been associated with the development of dyskinesia. This L-DOPA treatment regimen was administered until dyskinesia stabilised. After the L-DOPA priming period, the lowest dose able to produce a complete reversal of parkinsonian symptoms was defined as “100% L-DOPA treatment” or “treatment dose” (Table 15).

	Madopar (L-DOPA + Benserazide 4:1)		
NHP ID	**Weight (kg)**	**Priming dose (mg/kg)**	**Treatment dose (mg/kg)**
S1	4.1	37	27
S2	4.5	24	18
S3	4.1	32	24
S4	5.4	46	35
S5	4.8	33	25
S7	5.7	39	29
S9	4.9	27	20
S10	5.1	35	26
S11	4.2	21	16
S13	4.5	33	25
S14	3.9	26	19
S15	4	33	24
S16	5	20	15
S17	5.3	32	24
S18	5.5	27	20
S20	4.8	46	34
S21	4.3	30	23
S23	4.6	52	39
S26	4.9	41	31
S27	6	42	31
S28	4.1	37	27
S30	3.8	58	43
S31	4	25	19
S32	6.3	25	19
S33	4.4	32	24
S35	4.6	39	29
S36	4.5	29	22
S38	4.7	28	21
S40	4.1	32	24

Table 15: L-DOPA priming and treatment doses for the 29 NHP defined post-MPTP lesion and prior to group selection for gene therapy.

Following the L-DOPA priming period, the 29 NHP were video-recorded for 1h in the OFF state (i.e. off L-DOPA medication) and for 4h over 10-min intervals following L-DOPA treatment with the "priming" and "treatment" doses. Parkinsonian disability scoring was performed post hoc on video recordings of

animals freely moving in their home cages following a slightly different rating scale adapted from the Benazzouz scale (Table 16).

Parkinsonian disability	Score range
Range of movement	0-4
Bradykinesia	0-3
Posture	0-2
Tremor	0-1
Total	0-10

Table 16: Parkinsonian disability rating scale used for NHP selection and subsequent monthly assessments post-gene therapy.

In this rating scale, "vocalisation" is not accounted for. "Freezing" and "rigidity" fall under bradykinesia, while "frequency of arm movements" falls under range of movement. The parkinsonian disability was scored by assessing the four subcategories mentioned in Table 11 and calculated by the formula: (4 – range of movement) + bradykinesia + posture + tremor. Behaviour was assessed for 4h post L-DOPA administration and scored over 10 min intervals by an observer blinded to treatment. The final scores from each 10-minute observation period were cumulative throughout the 4h observation period.

After the NHP were rated for parkinsonian disability, they were scored for the two most common features in LID: chorea and dystonia. The score for each feature ranges from 0-4 (best to worst) and the combination of both features constitutes the global dyskinesia score. For any given time point, the dyskinesia score assigned to the NHP was the highest one from either chorea or dystonia.

Figure 38 shows that both priming and treatment doses elicited dyskinesia with an expected time-course, which mirrored the anti-parkinsonian action of L-DOPA. The L-DOPA response profiles (anti-parkinsonian and pro-dyskinetic) were in agreement with previous studies using the MPTP-lesioned macaque model of PD (Bézard et al. 2003; Hill et al. 2004; Berton et al. 2009), which further supported the inclusion of the animals in the subsequent phases of the study.

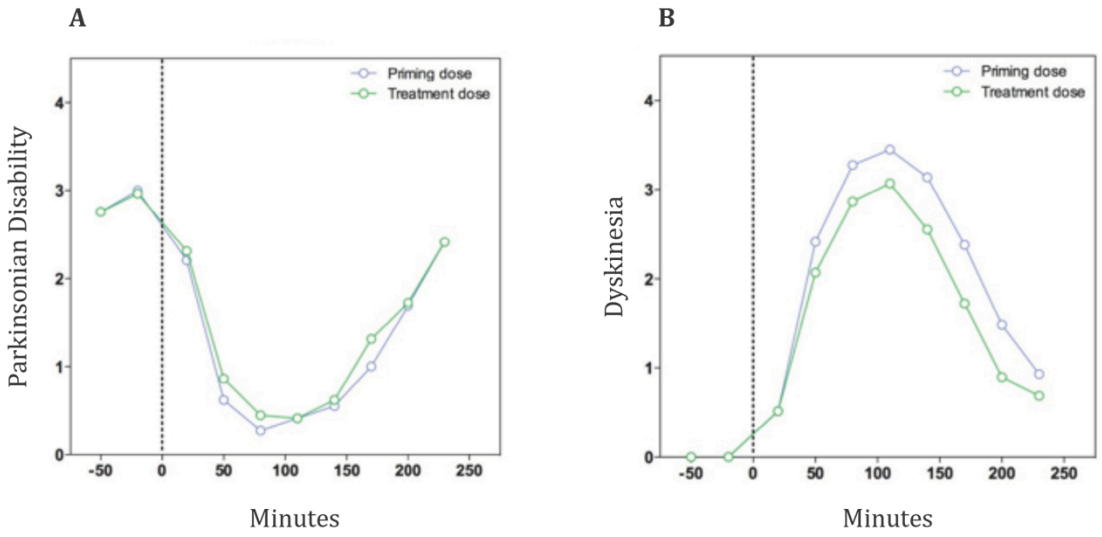

Figure 38: Mean parkinsonian disability and dyskinesia scores of primed NHP.
Acute response to L-DOPA was scored in MPTP-lesioned NHP. Parkinsonian disability (A) and dyskinesia (B) scores of the NHP selected for the study are shown.

After cessation of MPTP treatment and L-DOPA priming, animals were assessed for disability in the OFF state and for their acute response to an oral dose of L-DOPA. Eighteen animals with similar behaviour scores were selected, randomised and assigned into one of the three treatment groups: vehicle, low-dose or high-dose gene therapy. No statistical difference in parkinsonian motor symptoms was found between groups prior to gene therapy surgery. In addition to the 18 animals selected for the study, six MPTP-lesioned animals were kept as 'reserve' in case of any losses during surgery, which did not occur.

Further validation of the MPTP lesion was done *post-mortem* on the brains of the NHP. Stereological counting of TH+ cells in the SNc demonstrated that MPTP treatment caused pronounced cell loss (Mann-Whitney test, $p<0.001$; Figure 39). There was no significant difference in the number of TH+ neurons in the SNc among lesioned animals at the end of the study, indicating that AAV-mediated gene transfer to the putamen and caudate nucleus does not affect MPTP-mediated cell death in the SNc.

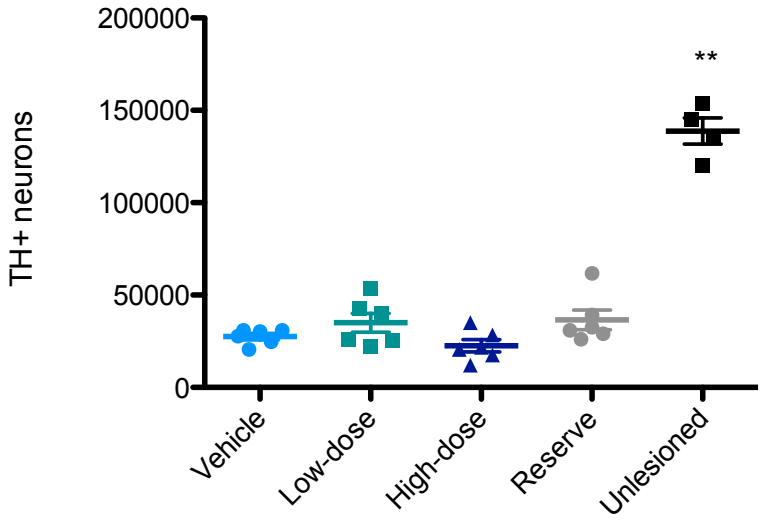

Figure 39: Stereological counting of TH+ neurons in the SNc of NHP after MPTP lesioning. NHP were given daily i.v. injections of 0.2mg/kg MPTP for ~25 days. Unlesioned NHP were used as controls. Mann-Whitney test of unlesioned vs. MPTP-treated ($p<0.01$). Mean ± SEM values are shown.

4.2.2 Behavioural Assessment of GPT002 in MPTP-lesioned NHP

To investigate if AAV-mediated delivery of TH and GCH1 to the striatum would lead to decreased parkinsonism and dyskinesia in the MPTP-lesioned NHP model of PD, behavioural studies were performed on animals treated with GPT002.

Prior to surgery for gene therapy, the behavioural responses to 50% and 100% L-DOPA treatment as well as no L-DOPA treatment (OFF state) were scored by video recording and locomotor activity assessment, measured by automatic count of infra-red beam breaks and taken as baseline values. The behavioural response to 50% L-DOPA – half the dose shown to completely reverse parkinsonism in the lesioned NHP (i.e. treatment dose, Table 15) – was used throughout the study to assess efficacy of the gene therapy treatment. The four normal non-lesioned NHP were subject to sham surgery and included in this study.

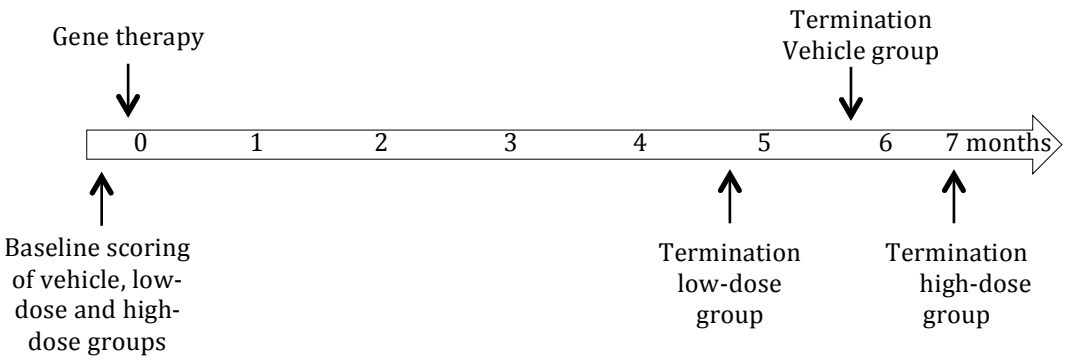

Figure 40: Timeline of NHP behavioural study to test the efficacy of GPT002.
Following MPTP-lesioning and priming with L-DOPA to induce LID, animals were scored for baseline locomotor activity, parkinsonian disability and dyskinesia. Animals were then treated with vehicle or AAV vector and scored once monthly for up to 5 months (low-dose), 6 months (vehicle) and 7 months (high-dose).

A first group (n=6) received bilateral injections of GPT002 at a titre of $1x10^{11}$ gcp/ml into the putamen (striatum) along 3 tracks per hemisphere with 2 deposits per track (6 stereotactic injections of 7.5 µl; that is 45 µl per striatum and a total of 90 µl per animal). This group was called "low-dose". A second group (n=6) received bilateral injections of the same volumes of a $1x10^{12}$ gcp/ml GPT002 preparation ("high-dose" group). A third group (n=6) received bilateral injections of the vehicle solution in the same deposit coordinates as the treatment groups.

4.2.2.1.1 Locomotor activity and Parkinsonian Disability After Gene Therapy With GPT002

In the months following gene therapy surgery, NHP were assessed OFF L-DOPA and after 50% L-DOPA treatment in order to closely mimic a future clinical scenario in which gene therapy will be given combined with oral L-DOPA pharmacotherapy to improve the treatment of PD. Animals were recorded once per month for 4h and video recordings for each individual were scored over 10-minute intervals post hoc by a rater blind to the treatment groups.

Following gene therapy, NHP treated with GPT002 demonstrated significant improvement in locomotor activity compared to the vehicle-treated group in the OFF state as well as following 50% L-DOPA treatment. In the absence of L-DOPA treatment (OFF L-DOPA), low-dose and high-dose treated animals significantly

improved their locomotor activity compared to vehicle-treated animals in the time course of 5 and 6 months, respectively (Wilcoxon signed rank test, $p<0.05$). A significant increase in locomotor counts was also seen between high-dose vs. vehicle treated animals after 50% L-DOPA treatment (Wilcoxon signed rank test, $p<0.05$). Furthermore, when compared against baseline scores, high-dose-treated animals showed a significantly higher locomotor activity at months 3 and 7 post-gene therapy OFF L-DOPA and at month 7 after 50% L-DOPA treatment (Friedman test followed by Dunn's multiple comparison, $p<0.05$) (Figure 41).

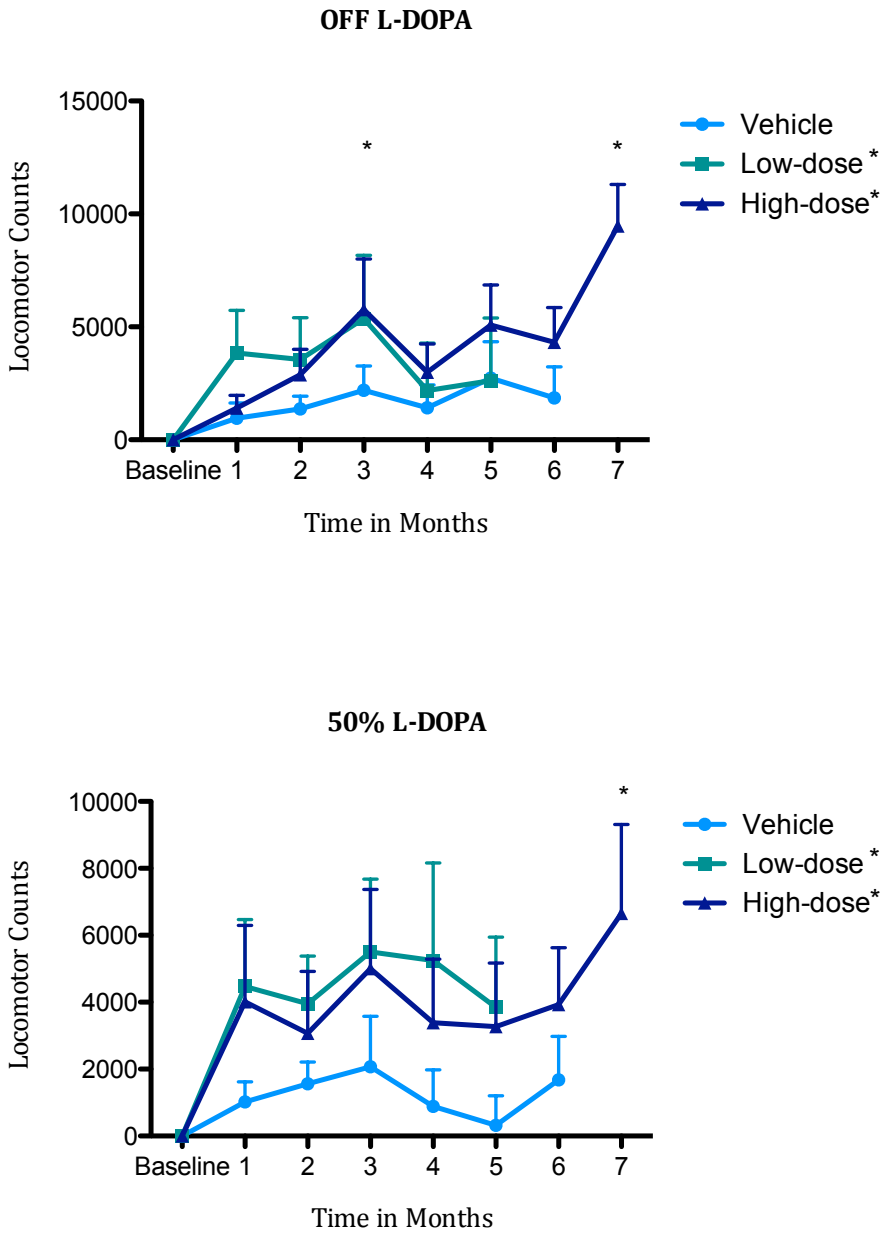

Figure 41: Locomotor activity of lesioned NHP treated with GPT002.
Comparison between treatments was done with the non-parametric Wilcoxon signed rank test, while intragroup comparison against baseline scores was done with the Friedman test (the non-parametric equivalent of the repeated measures ANOVA) followed by Dunn's multiple comparisons. Values are shown as mean ± SEM and only upper error bars are shown for clarity. All values are normalised to the baseline scores. In the absence of L-DOPA treatment both, low- and high-dose treated NHP showed an improvement in locomotor activity relative to the vehicle-treated group throughout the 5 and 6 months of the experiment, respectively ($p<0.05$). When compared to baseline scores, high-dose-treated NHP showed a significant improvement at months 3 and 7 ($p<0.05$). Significant improvement in locomotor activity relative to vehicle was also seen in both vector-treated groups after 50% L-DOPA treatment ($p<0.05$). When compared to the baseline scores, high-dose treated NHP showed a significant improvement at month 7 post-AAV injection ($p<0.05$). Asterisks behind treatment group legends indicate there was a statistical difference relative to the vehicle-treated group. A Friedman test performed on all groups up to month 5 showed a significant difference ($p<0.05$) between vehicle and vector-treated animals for the low-dose group OFF L-DOPA and for both treated groups after 50% L-DOPA treatment (results for this test are not indicated by asterisks in the figure).

However, it must be noticed that a spontaneous improvement occurred in all treatment groups at month 3 OFF and ON L-DOPA. Furthermore, at month 7, vehicle-treated NHP were not scored alongside the high-dose NHP, therefore locomotor scores for high-dose-treated animals at this time point can only be compared to the group's baseline scores. Surprisingly, MPTP-lesion did not cause a marked decrease in the locomotor counts relative to normal NHP (Kruskal-Wallis test, $p>0.05$). As seen in Figure 42, baseline levels of locomotor activity pre-gene therapy intervention show that vehicle, low-dose and high-dose groups had a decreased locomotor activity of 42%, 19% and 30% relative to unlesioned NHP, respectively. This might indicate that stopping MPTP lesion once NHP reach a score of 6 in the Benazzouz disability rating scale is not sufficient to cause a parkinsonian phenotype that can be detected by automatic counts of infra-read beam breaks.

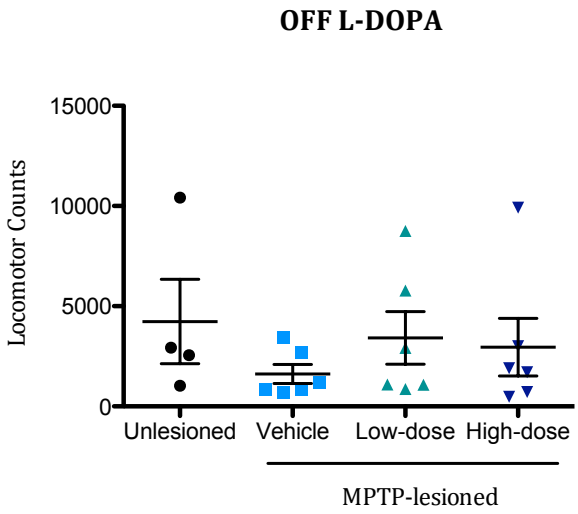

Figure 42: Baseline locomotor counts on MPTP-lesioned and unlesioned NHP. Comparison between groups was done with the Kruskal-Wallis test (the non-parametric equivalent of the non-repeated measures ANOVA). Values are shown as mean ± SEM.

Clinical rating showed an improvement in the parkinsonian disability score of the high-dose treated group throughout months 1 to 7 OFF L-DOPA. At month 7 NHP had 100% decreased parkinsonian disability relative to baseline (Friedman test, $p<0.05$). No significant effect was observed when the NHP were challenged

with 50% L-DOPA treatment, however disability decreased in both vector-treated groups (Figure 43).

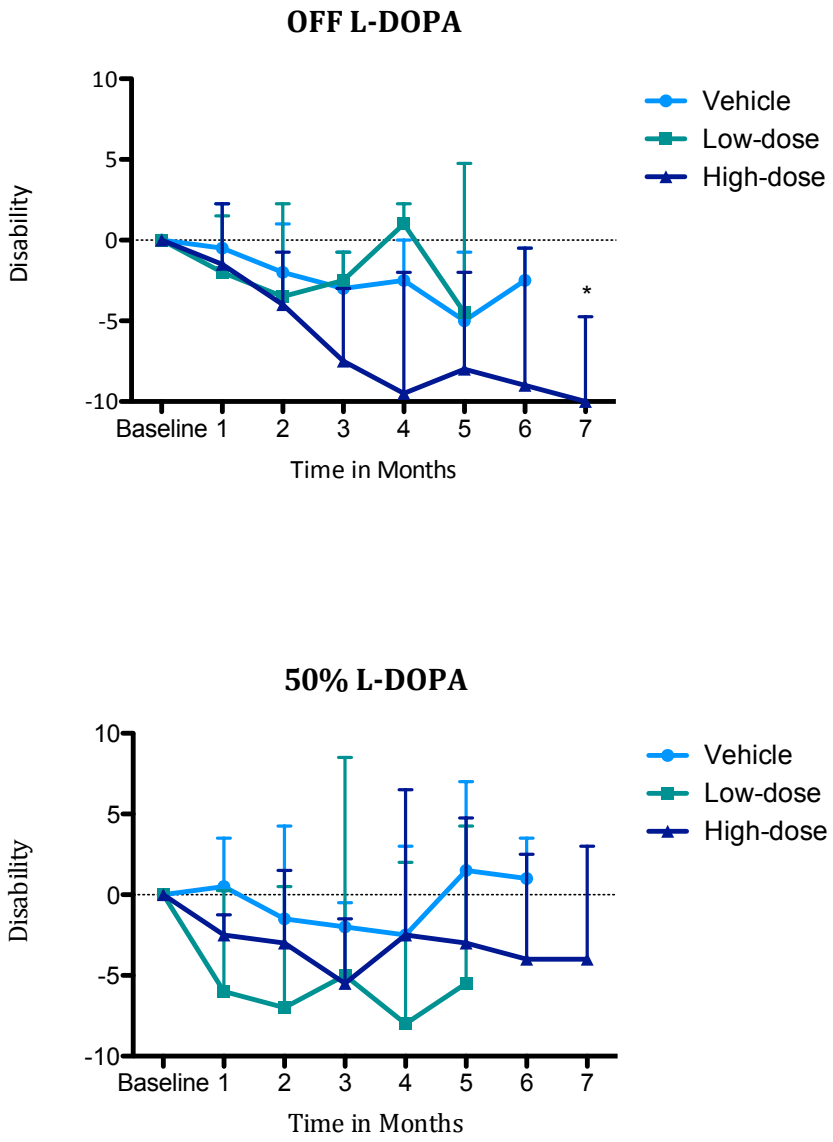

Figure 43: Disability scores of NHP treated with GPT002 OFF L-DOPA and after 50% L-DOPA treatment.
Comparison between treatments was done with the non-parametric Wilcoxon signed rank test, while intragroup comparison against baseline scores was done with the Friedman test followed by Dunn's multiple comparisons. Median ± interquartile range values are shown and only upper error bars are shown for clarity. All values are normalised to the baseline scores. Vector treatment caused symptomatic improvement in the OFF state and after 50% L-DOPA treatment. A statistically significant decrease in parkinsonian disability was detected at month 7 relative to baseline scores in the absence of L-DOPA treatment ($p<0.05$).

4.2.2.1.2 Dyskinesia and Good On-time

Because standard oral treatment with L-DOPA provides powerful relief from PD motor symptoms but also induces uncontrolled, disabling drug-induced dyskinesias, their incidence post AAV gene therapy was investigated. Administration of GPT002 alone did not induce dyskinesia in the lesioned animals without co-medication with oral L-DOPA for the entire duration of the study – i.e. dyskinesia was absent at all time points. This indicates that the gene therapy provides symptomatic relief without triggering LID.

To closely mimic a potential future clinical trial situation in dyskinetic patients, NHP were challenged with 50% L-DOPA treatment and the occurrence of chorea and dystonia was recorded for a period of 4h. Chorea and dystonia are the most common features in LID and their scores in the rating scale adopted in this study range from 0 to 4. At each time point animals were given the score that corresponded to the highest value from either feature and the global score given was representative of each 10-minute observation. Good on-time (i.e. the timespan after L-DOPA oral medication in which animals show no bradykinesia and little to no dyskinesia) was also measured to evaluate the ability of the gene therapy to ameliorate LID (Figure 44 – bottom). Groups tested with both gene therapy doses showed decreasing dyskinesia relative to baseline scores up to month 5, however, this trend was also followed by the vehicle treated group, which showed an up to 60% spontaneous reduction in dyskinesia during the experiment. This observation undermines the interpretation of a causal relationship between gene therapy and a decrease in dyskinesia.

Unlike other gene therapy preclinical trials, in which L-DOPA doses are constantly adjusted relative to the primates' locomotor scores (Jarraya et al. 2009), throughout this study the NHP received the same dose, defined as 50% treatment prior to gene therapy. Therefore, any change in weight that might have occurred during the experimental months can have affected the L-DOPA mg/kg ratio and consequently the ability of oral L-DOPA treatment to trigger LID. Nevertheless, the fact that AAV treatment did not increase previously established LID is of clinical importance.

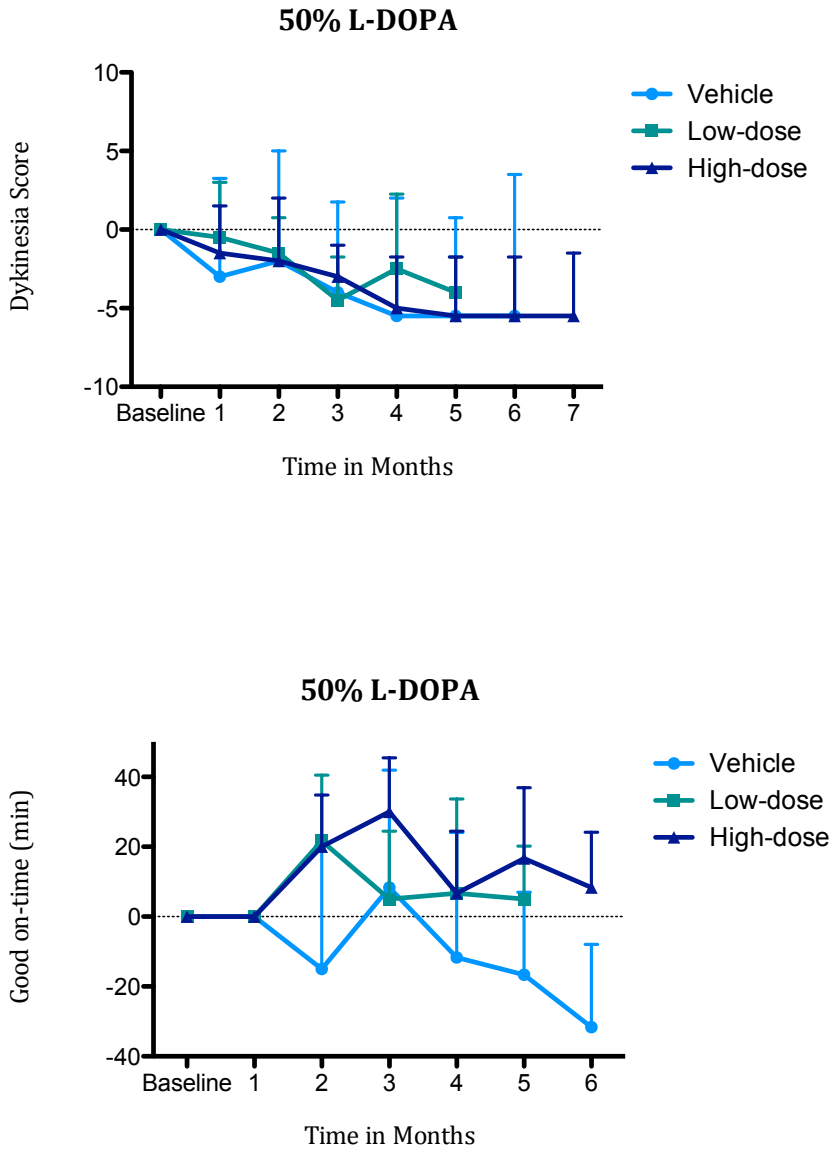

Figure 44: Dyskinesia scores and good on-time in NHP treated with GPT002.
Scores for dyskinesia (top) and good on-time (bottom) are presented as median ± interquartile range (dyskinesia) and mean ± SEM (good on-time), respectively. All values are normalised to the baseline scores. Only upper error bars are shown for clarity.

4.2.3 Efficacy of an Increased Dose of GPT002 and of its Truncated Variant

Taken together, treatment with GPT002 provides symptomatic improvement without increasing pre-established dyskinesia. However, this efficacy was considered partial and insufficient to justify clinical investigation.

We hypothesised that the gene therapy doses tested in the first NHP study possibly led to a modest increase in intrastriatal L-DOPA levels that were slightly above the threshold needed to evoke a robust behavioural response (Kirik et al.

2002). We also pondered whether enhancing TH activity would lead to an increased behavioural response i.e. less parkinsonian disability and LID. To test this possibility, we decided to enhance the catalytic activity of TH by removing its regulatory domain, thereby rendering it constitutively active. A similar strategy was adopted in another intrastriatal gene therapy approach for dopamine replacement (Jarraya et al. 2009). The removal of the TH regulatory domain also abolishes the end-product feedback inhibition mechanism, which TH is subject to (Daubner et al. 2011). Thus, a variant form of GPT002 was generated which lacked the first 155 amino acids of TH (Figure 45). The truncated variant of GPT002 was generated by deleting the first 465nt of the TH gene by overlapping PCR followed by isothermal assembly. The truncated TH used here is identical to the one used in the liver vector (Chapter 1).

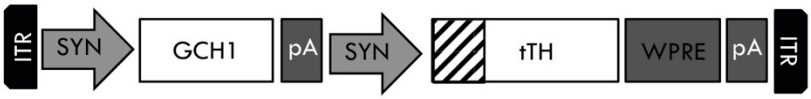

Figure 45: Schematic representation of the truncated GPT002 genome.
Dashed square in the *TH* cassette symbolises the deletion of the 155 amino acids at the N-terminus portion of the enzyme.

Efficacy assessment of this truncated variant of GPT002 was performed in NHP following an identical protocol as used in the previous study but with a 10-fold higher dose. In addition, transduction efficiency of the truncated GPT002 was compared to the full-length form in the striatum of 6-OHDA lesioned rats.

4.2.3.1 Striatal Spread of the Truncated GPT002 in the 6-OHDA Lesioned Rat

With the aim to compare striatal spread of the newly generated truncated vector with GPT002, a qualitative assessment was performed in the 6-OHDA rat model of PD prior to injection in NHP. A total dose of $2x10^9$ gcp of GPT002 and of its truncated variant was injected in the striatum of unilaterally 6-OHDA lesioned rats followed by IHC analysis of TH expression six weeks post-injection (n= 3 per vector).

Injection of 6-OHDA into the medial forebrain bundle (MFB) in one hemisphere resulted in a complete loss of the neurons located in the ipsilateral SNc, while the contralateral side remained visually unaffected. A stronger striatal transduction was observed with GPT002 vector relative to its truncated variant, as seen by the area positively stained for TH (Figure 46).

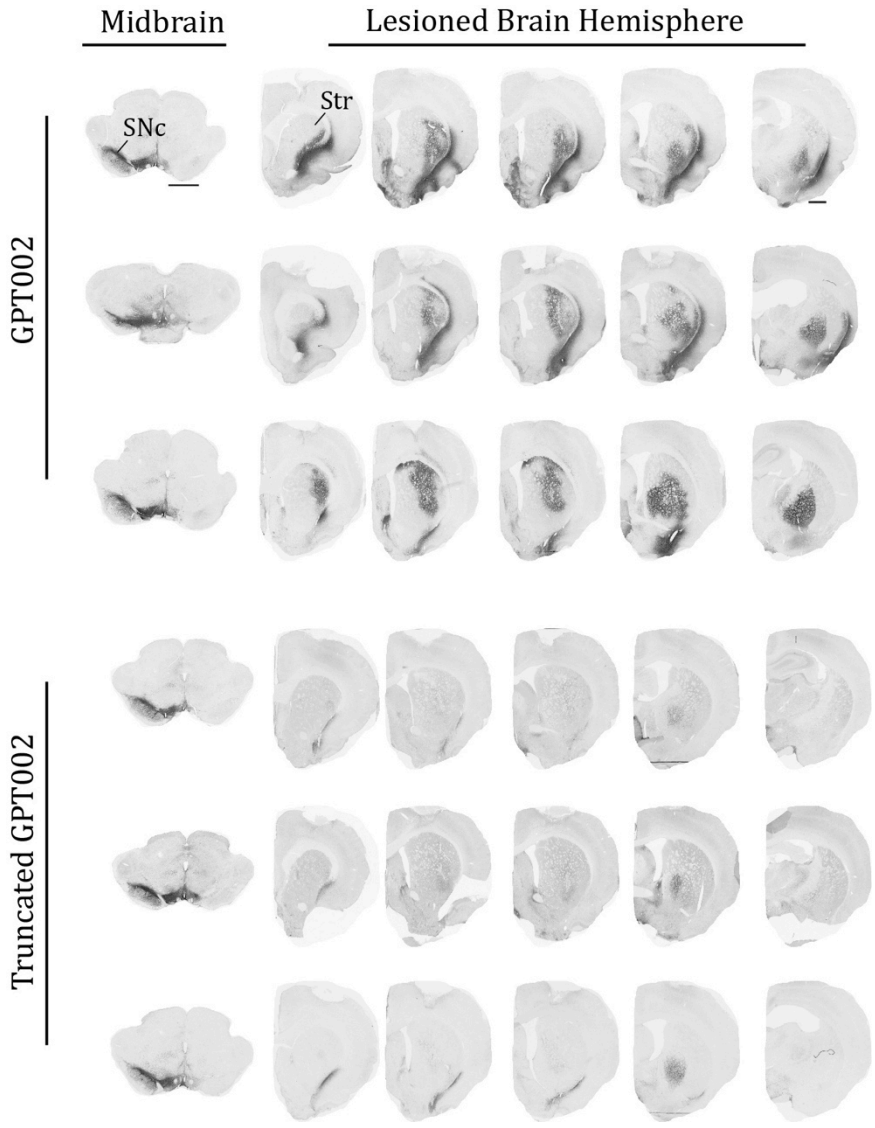

Figure 46: Transduction of AAV vectors in unilaterally 6-OHDA lesioned rats detected by IHC of TH in the striatum.
Six weeks post-AAV injection, animals treated with GPT002 (n=3) and its truncated variant (n=3) were deeply anesthetised with pentobarbital, transcardially perfused; the brains readily dissected, and then incubated in paraformaldehyde (PFA) for 2 hours. After overnight incubation in sucrose the brains were cut in 35µm coronal sections. Full-length GPT002 showed stronger transduction and broader spread in the striatum. Sections of the midbrain in the left column show the complete absence of TH+ cells in the SNc on the side ispilateral to the 6-OHDA injection, whereas on the contralateral side the dopaminergic cells were virtually unaffected. This validates the unilateral 6-OHDA lesion and indicates that any TH staining in the lesioned side of the striatum must be attributed to AAV-

mediated TH expression. Each row corresponds to a different animal. Str: Striatum; SNc: Substantia nigra pars compacta. Scale bar: 2mm midbrain and 0.2mm lesioned brain hemisphere. These stainings were performed by the staff in Dr. Björklund's lab and are reproduced here with his permission.

4.2.3.2 Behavioural Assessment of GPT002 and its Truncated Variant in MPTP-lesioned NHP

Because only a partial behavioural improvement was observed with high dose GPT002, a second study was performed with an increased vector dose. In parallel, the vector expressing the truncated TH-variant was included in order to assess whether enhanced TH catalytic activity could lead to an increased vector potency *in vivo*. In this study, the original vehicle group from study 1 was reused and the 6 reserve lesioned animals were injected with a ten-fold higher dose of GPT002 (hereafter referred to as the "full-length" group). Animals treated with the low dose in study 1 were re-injected with the truncated TH GPT002 at the same dose as the "full-length" group. The parkinsonian disability and dyskinesia scores observed for the low-dose-treated group in study 1 did not differ from the vehicle group over the duration of the study (Figure 43 and Figure 44). Therefore, the locomotor, disability and dyskinesia scores recorded for this group immediately prior to the injection with the truncated GPT002 were used as the new baseline against which the efficacy of this intervention was assessed. As in study 1, animals were assessed for their locomotor activity (automatic counts of infra-red beam breaks), parkinsonian disability (range of movement, bradykinesia, posture and tremor) and dyskinesia (chorea and dystonia) in the OFF state as well as following treatment with 50% L-DOPA for four months post gene therapy.

4.2.3.2.1 Locomotor activity and Parkinsonian disability after gene therapy with GPT002 and its truncated variant

Gene therapy with the full-length and truncated GPT002 at an increased dose led to an improvement in locomotor activity in treated animals relative to vehicle-treated during the time course of 4 months when animals were OFF L-DOPA (Friedman test followed by Dunn's multiple comparisons, $p<0.05$). Furthermore, at individual time points, locomotor activity showed a significant

increase relative to baseline scores at months 4 and 2 in the full-length and truncated vector-treated NHP OFF L-DOPA, respectively, and at months 2 and 3 in both full-length and truncated vector-treated animals on 50% L-DOPA (Friedman test followed by Dunn's multiple comparisons, $p<0.05$). However, as seen in study 1, spontaneous improvement in locomotor activity at month 3 was also observed in vehicle-treated NHP after 50% L-DOPA treatment, thus weakening any interpretation of a causal relationship between gene therapy and increased locomotor activity at this time point (Figure 47).

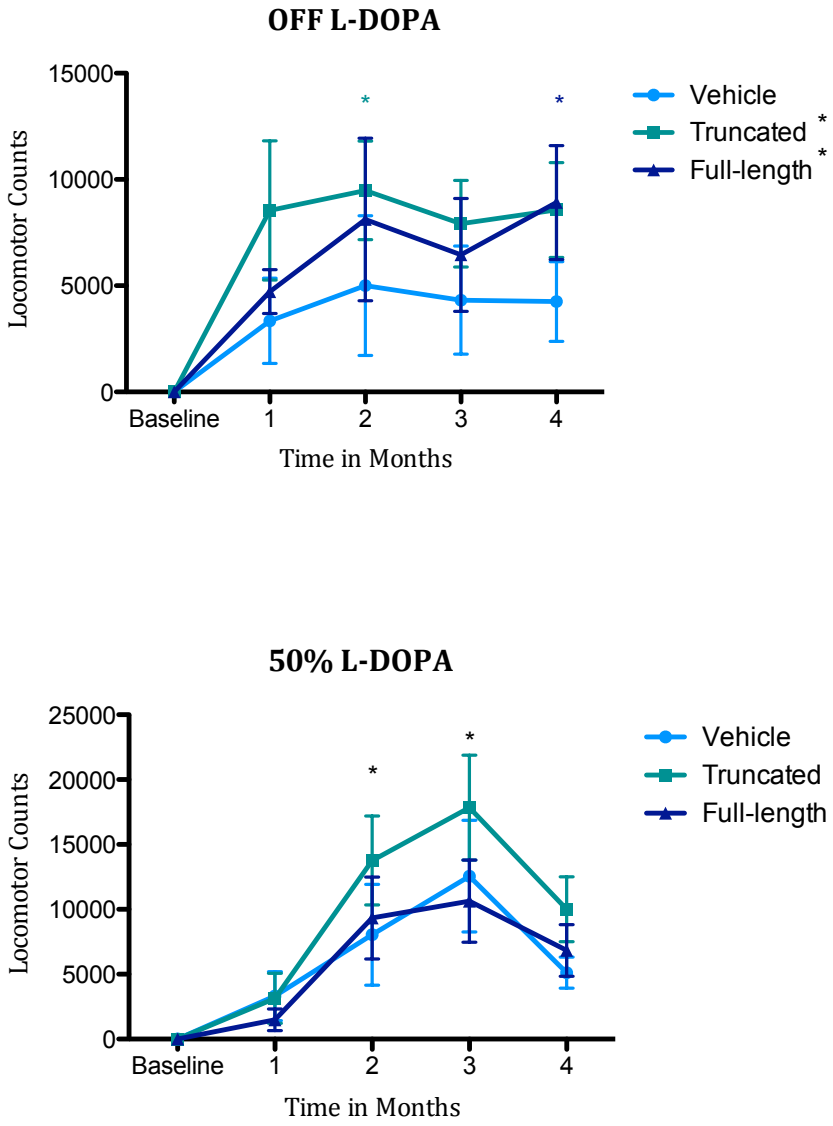

Figure 47: Locomotor activity of MPTP-lesioned NHP treated with the full-length and the truncated variant of GPT002 OFF L-DOPA and after 50% L-DOPA treatment.
Comparison between vehicle and vector-treated groups as well as at individual time-points relative to the baseline was done with the non-parametric Friedman test followed

by Dunn's multiple comparisons. Values are shown as mean ± SEM and are normalised to the baseline scores. In the absence of L-DOPA treatment, both vector-treated groups showed improved locomotor activity relative to vehicle treated animals ($p<0.05$). GPT002 showed a significant difference relative to the baseline at month 4 ($p<0.05$, blue asterisk), while the truncated vector-treated animals showed a difference to the baseline at month 2 ($p<0.05$ green asterisk). Difference at individual time points was also seen upon 50% L-DOPA treatment at months 2 and 3 for both vector-treated groups ($p<0.05$, black asterisks), however no difference was seen relative to vehicle treated animals. Asterisks behind treatment group legends indicate there was a statistical difference relative to the vehicle-treated group.

It is noteworthy that the baseline locomotor counts of the MPTP-lesioned NHP in this study did not differ significantly from the non-lesioned NHP used in study 1. It is acceptable to compare study 2 lesioned animals vs. study 1 non-lesioned animals given that the vehicle and truncated groups are the same animals used in study 1. Furthermore, the reserve animals used for treatment with the higher dose full-length GPT002 were lesioned together with the other NHP (Figure 48). As in the previous study, the extent of the MPTP lesion was probably not sufficient to cause a parkinsonian phenotype that can be detected by automatic counts of infra-read beam breaks.

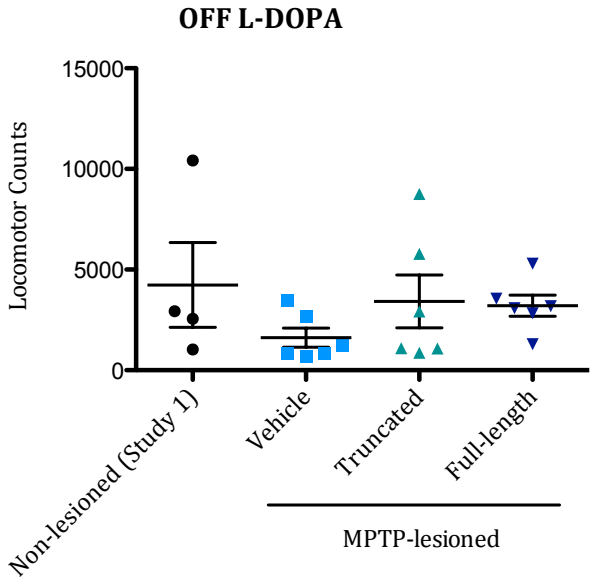

Figure 48: Locomotor activity in non-lesioned NHP from study 1 and MPTP-lesioned animals in study 2.
The severity of the MPTP lesion did not result in a significant difference in locomotor counts in lesioned vs. non-lesioned NHP (Friedman test).

Clinical rating 4 months post-gene therapy showed an effect in vector- vs. vehicle-treated NHP (Friedman test, $p<0.05$). A decrease of up to 40% in parkinsonian disability was seen in NHP treated with the truncated and the full-length vector-treated NHP OFF L-DOPA at months 4 and 2, respectively. Disability scores remained stable throughout half the duration of the study, with vector treatment leading to a clear symptomatic improvement. Upon treatment with 50% L-DOPA a numerical decrease in disability was seen in NHP treated with truncated GPT002 (Figure 49).

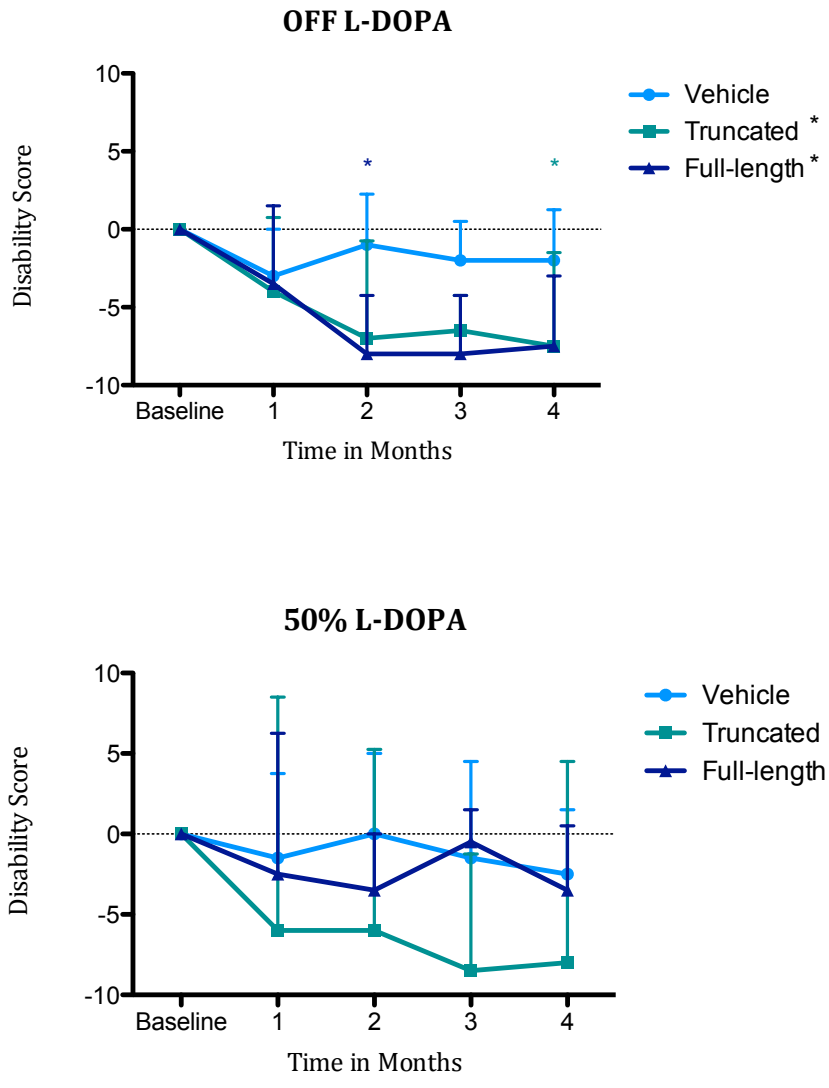

Figure 49: Disability scores in NHP treated with GPT002 and its truncated variant OFF L-DOPA and after 50% L-DOPA treatment.
Disability scores decreased after treatment with both vectors in the OFF state but only with the truncated variant after 50% L-DOPA treatment. Comparison between treatments and at individual time-points relative to the baseline was done with the non-parametric Friedman test followed by Dunn's multiple comparisons. Median ± interquartile range values are shown. Only upper error bars are shown for clarity. All values are normalised

to the baseline scores. NHP OFF L-DOPA showed decreased disability at month 2 (full-length vector, $p<0.05$, blue asterisk) and at month 4 (truncated-vector, $p<0.05$, green asterisk).

4.2.3.2.2 Dyskinesia and Good On-time

The ability of the increased dose of GPT002 and its truncated variant to prevent LID was assessed by rating chorea and dystonia for 4h after the administration of 50% L-DOPA. Improvements at individual time points vs. the baseline scores show that dyskinesia decreased by 82% at month 2 and by 44% at month 3 in truncated vector-treated NHP. This decrease was mirrored by an increase of 50min in the good on-time relative to the baseline. However, a spontaneous decrease in dyskinesia was observed in vehicle-treated animals during the first two months, which reached 47% at month 2 and was followed by an increase at months 3 and 4. These changes in the dyskinesia scores of the vehicle group did not reflect in significant alteration of good on-time (Figure 50). Nonetheless, the spontaneous improvement in dyskinesia seen in vehicle-treated animals urges for caution in the interpretation of the results from vector-treated NHP. When assessed OFF L-DOPA, dyskinesia scores remained zero at all time points for all NHP, indicating that an increased dose of GPT002 does not trigger LID by itself.

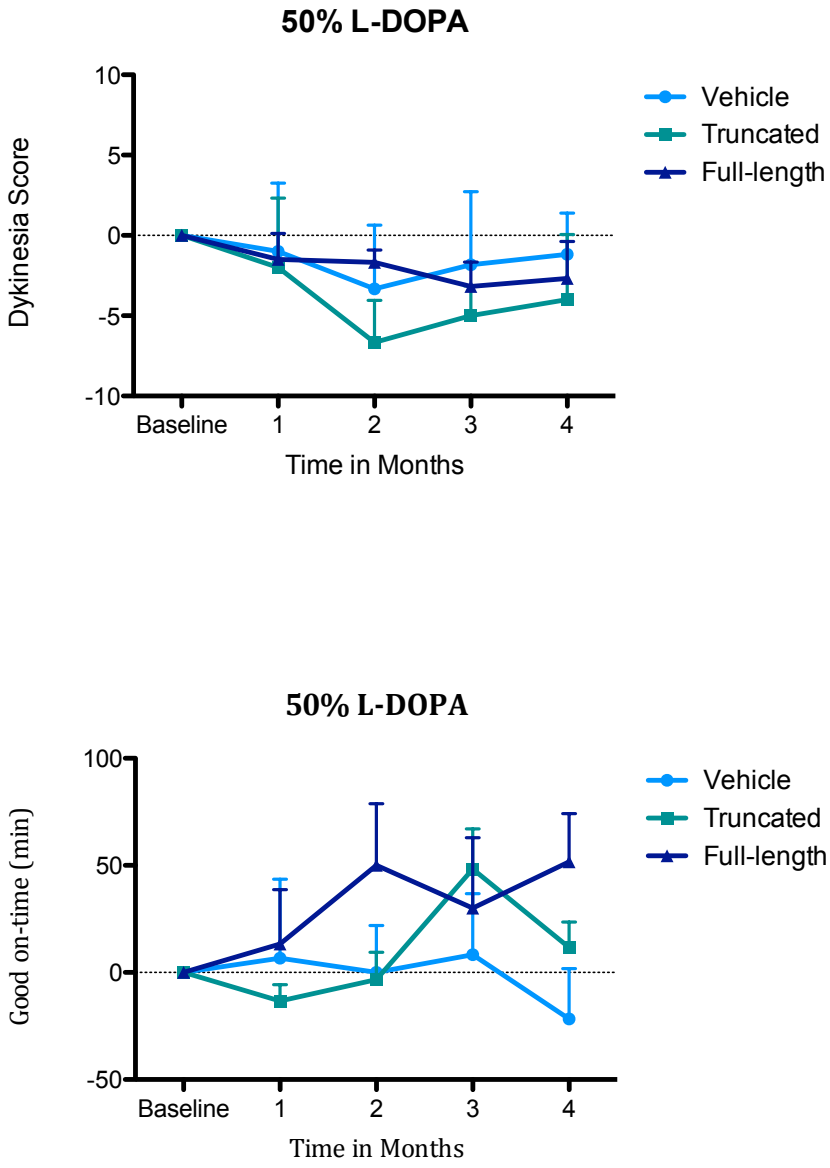

Figure 50: Dyskinesia scores and good on-time in NHP treated with GPT002 and its truncated variant.
Scores for dyskinesia (top) and good on-time (bottom) are presented as median ± interquartile range (dyskinesia) and mean ± SEM (good on-time), respectively. All values are normalised to the baseline scores. Only upper error bars are shown for clarity.

4.2.3.3 Post-mortem Detection of TH+ and GCH1+ Cells in the Putamen of NHP

To determine the transduction efficiency of the AAV vectors, *post-mortem* quantitative histological analysis of transgene expression was performed by immunofluorescence staining against TH and GCH1 in the putamen followed by optical density quantification. As seen in Figure 51, MPTP depletion of

dopaminergic cells in the SNc led to a reduced number of TH+ neurons in the putamen. Surprisingly, little to no difference in the number of TH+ neurons was observed between vehicle- and AAV-treated NHP several months post-injection. Gene therapy with GPT002 led to an increase in GCH1+ neurons in the putamen of NHP but the difference was only significant in NHP treated with full-length GPT002 (Mann-Whitney, $p<0.05$) (Figure 51).

GPT002 has previously been shown to efficiently transduce the striatum and lead to improvement in behavioural tests in the 6-OHDA lesioned rat model, attesting the ability of this vector to express TH (Cederfjäll et al. 2012). In addition, an increase in AAV-mediated GCH1 expression is observed in the brains of one group of vector-treated NHP. Furthermore, AAV-mediated TH expression in the putamen of MPTP lesioned NHP has been detected after treatment with a similar AAV dose 65 days post-injection (Muramatsu et al. 2002). This suggests possible technical issues with the TH staining. Further insight into possible reasons for the lack of TH detection could be gained through gene expression analysis. An accumulation of TH and GCH1 mRNA would indicate whether any repression is happening at the transcriptional or translational level. Finally, more sensitive analysis of tissue extracts such as western blot could complement the immunofluorescence quantification of transgene expression. However, handling of the NHP brain tissue is not allowed in our facilities due to the risk of the presence of herpes B virus in the specimens, therefore these experiments were not performed.

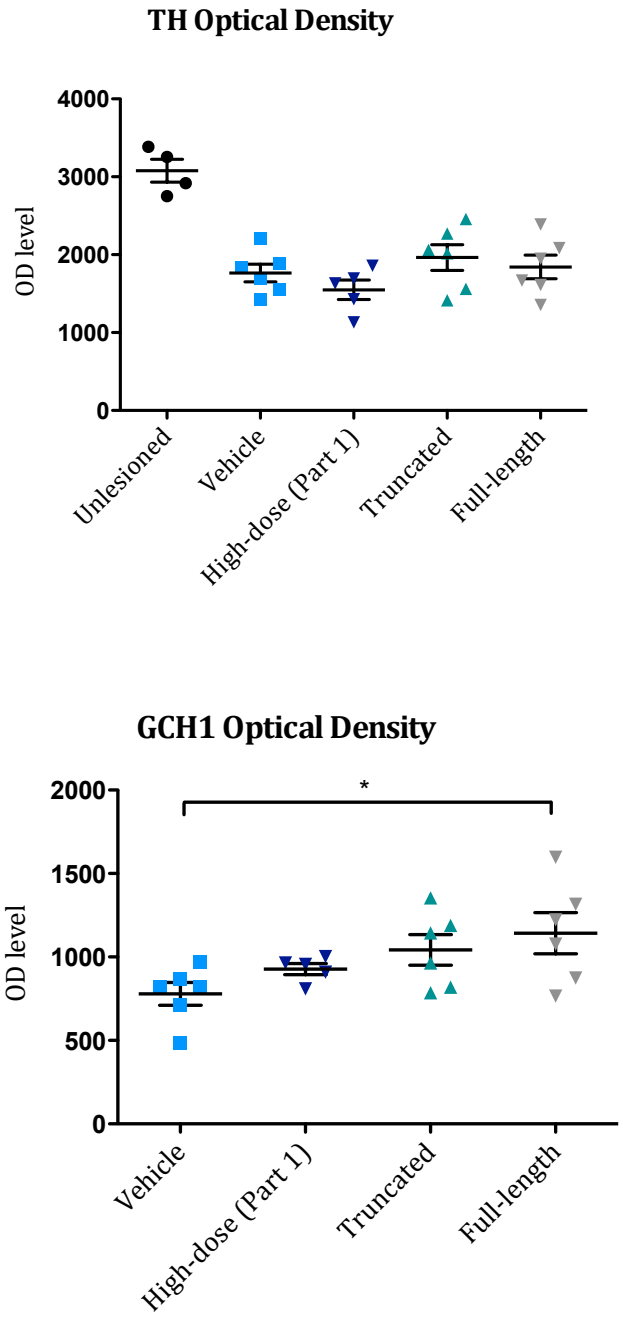

Figure 51: Optical density measurement of putamen sections stained with antibodies against TH and GCH1.
Values presented as mean ± SEM of 14 sections covering different regions of the putamen (Mann-Whitney test, $p<0.05$).

Taken together, the results of study 2 demonstrate that AAV-mediated delivery of TH (or its truncated form) and GCH1 into the putamen of dyskinetic lesioned NHP is able to decrease parkinsonism without triggering the typical L-DOPA induced side effects. When OFF L-DOPA medication, treated animals

showed less parkinsonian disability and increased locomotor activity relative to vehicle-treated NHP. The results of locomotor activity, however, must be taken with caution given that the degree of parkinsonism in these animals was not sufficiently severe to significantly affect locomotor counting baseline scores. Dyskinesia scores must also be interpreted with caution. Although a decrease was seen post-AAV gene therapy, vehicle-treated animals showed some degree of spontaneous amelioration. When comparing the efficacy of full-length vs. truncated TH, both vectors led to increased locomotor activity and decreased parkinsonism. Therefore, similar efficacy was demonstrated with both GPT002 forms and the results did not justify the replacement of the full-length TH by the truncated variant for future studies.

4.2.4 *In vivo* Assessment of the GPT002 By-product

Efficacy of AAV gene therapy in studies 1 and 2 was observed for some endpoints and, most importantly, it did not lead to LID in vector-treated NHP. By the time these studies were completed, molecular analysis of the bicistronic liver vector (Chapter 1) had shown intramolecular HR, which is triggered by the presence of two identical promoters in the vectors (Figures 18B and 19). Similarly to what occurred with the bicistronic liver vector, the presence of 2 copies of the SYN promoter in GPT002 induced the formation of a second smaller vector also occurred with GPT002 (Figure 52).

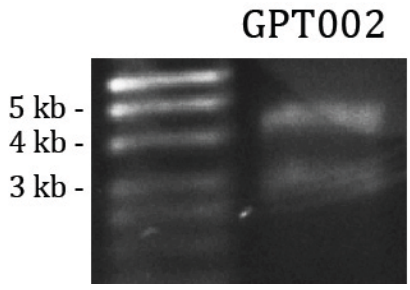

Figure 52: Alkaline gel electrophoresis showing the genomes of GPT002 and its by-product comprised by the TH expression cassette only.
The 4.6 kb band corresponds to the bicistronic GPT002 genome, while the 3.3 kb band corresponds to the by-product vector.

While HR was not a major concern for the proof-of-principle study for peripheral L-DOPA synthesis, the unexpected formation of a secondary virus

poses a potential hurdle for the translation of this therapeutic approach. Regardless of the efficacy of the brain bicistronic vector in alleviating parkinsonism without inducing LID in the NHP model of PD, from a regulatory perspective it is important to know whether the by-product vector formed upon HR is a functional virus able to express TH. The uncontrolled formation of an inactive by-product can potentially be seen as a contaminant in the AAV preparation and therefore considered not suitable for use in humans. Furthermore, whether the ratios at which each species is formed under standard GMP vector manufacturing procedures is constant or variable is critical for the reliable prediction of treatment outcome in a future PD patient. Therefore, the functionality of the GPT002 by-product virus was tested in a small-scale *in vivo* study by comparing the TH expression of different viral vectors and preparations in two MPTP-lesioned NHP. For this purpose, a vector mimicking the HR by-product of GPT002 - containing only the SYN-TH expression cassette - was constructed by removing the SYN-GCH1 cassette from GPT002. This vector was named "lower band virus" in reference to its lower molecular size on the alkaline gel (Figure 52 – lower band). Additionally, the HR by-product virus was removed by CsCl density gradient centrifugation from a GPT002 preparation in order to generate a prep containing only the bicistronic species (seen on the alkaline gel as the higher band – Figure 52). These two preparations were assessed for intrastriatal TH expression in two MPTP-lesioned NHP alongside two other preparations. One was a "complete" GPT002 prep, in which the "higher" and "lower band" virus species were present. The other was a monocistronic AAV vector expressing the TH gene from a CMV promoter previously described by Muramatsu et al. (Muramatsu et al. 2002). In this experiment, both NHP received an intracranial injection of each preparation in four different areas of the putamen - two different preparations injected into each brain hemisphere. All preparations were injected at the same dose ($7.5x10^9$ gcp/injection), except for the "lower band" virus (HR by-product), which was given at a 3-fold lower dose to mimic the estimated by-product formation ratio of higher:lower band observed in the lab. Animals were sacrificed 6 weeks post injection and IHC staining of brain sections was performed to assess vector spread in the putamen. Quantification of transduction efficiency for each vector was done by assessing

vector spread in the three histological sections closest to each needle track (Figure 53) and quantified by automatic threshold quantification of positively stained regions using the ImageJ software (Table 17).

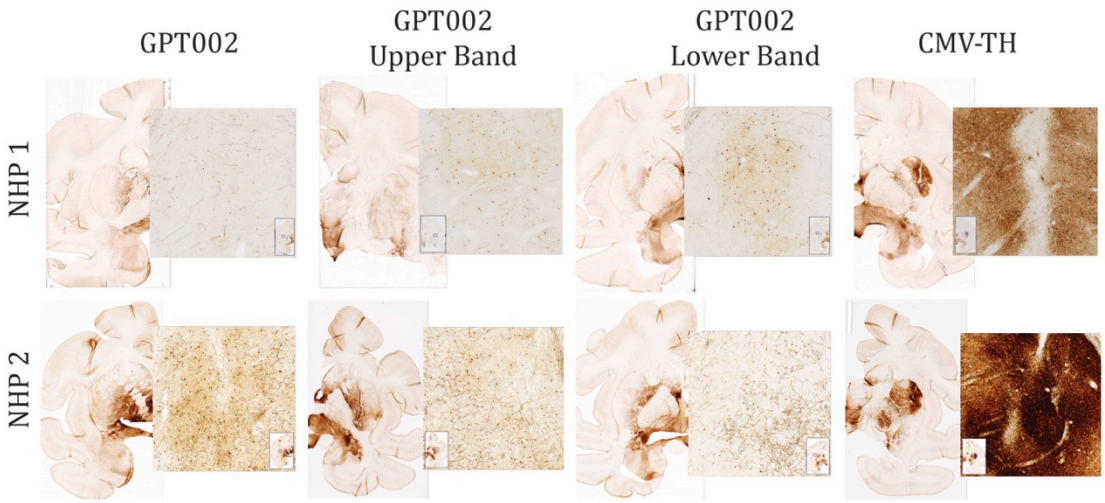

Figure 53: TH staining of the striatum of NHP used in the small-scale study to test expression of the by-product of GPT002.
TH staining of brain sections around the needle track for the different vectors tested. Each row represents one animal and columns represent the different preps injected in different areas of the putamen.

Preparation	% Putamen transduction	
	NHP1	NHP2
AAV2/5 GPT002	0.6	19.65
AAV2/5 Upper band	0.61	16.94
AAV2/5 Lower band	1.17	7.32
AAV2/5 CMV-TH	13.89	30.88

Table 17: Percentage of transduced striatum per prep per animal assessed by TH staining.

While the transduction efficiency was variable for the different preparations between both NHP, the results clearly demonstrate that the lower band virus (GPT002 by-product) is a functional virus able to express TH. It is evident that the vector containing the CMV-TH cassette had a stronger transduction than GPT002 and its isolated components.

Although the recombination by-product was shown to be functional, the observation that the CMV-TH vector had a stronger transduction led to the decision to redesign of the bicistronic brain vector. The redesign involved the replacement of the *TH* cassette in GPT002 by the CMV-TH cassette tested in the small-scale NHP study described above.

4.2.5 Redesign of the Bicistronic Brain Vector and Assessment of its *in vivo* Efficacy

Based on the bigger striatal spread and stronger TH expression from the CMV-TH vector in the small-scale NHP study, the bicistronic brain vector was redesigned. The new vector, called GPT004, still expresses GCH1 and TH from a single AAV genome and the difference between GPT002 and GPT004 is confined to the *TH* expression cassette. In the new vector, *TH* is under the control of the CMV promoter, followed by a human growth hormone intron. A further difference between both *TH* cassettes is that while GPT002 contains the *TH* coding sequence followed by the WPRE, the *TH* gene in the new vector is followed by its 3' UTR. The CMV-TH cassette in GPT004 is identical to the one from the CMV-TH virus used in the small-scale NHP study (Figure 53). A schematic representation of GPT004 is shown in Figure 54.

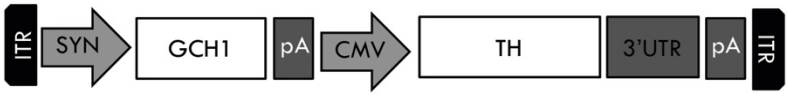

Figure 54: Schematic representation of the GPT004 genome.
The vector was constructed by modifying the *TH* expression cassette in GPT002. The SYN promoter was replaced by the CMV promoter and the WPRE was replaced by the 3' UTR of *TH*.

4.2.6 Molecular and Behavioural Assessment of GPT004 in the 6-OHDA Lesioned Rat Model

To compare the new vector GPT004 to GPT002, transduction and therapeutic efficacy was assessed in 6-OHDA-lesioned rats (n= 6 per treatment group). The motor deficits induced by the 6-OHDA lesion were assessed at 5 weeks post-lesion in the amphetamine-induced rotation test and only animals exhibiting

more than six full-body turns per minute towards the dopamine-depleted side were included in the study. Next, motor baseline scores were taken for the cylinder, corridor and stepping tests confirming that the near complete lesion of the ascending dopamine innervation by injection of 6-OHDA in the medial forebrain bundle (MFB) in the left brain hemisphere causes a severe impairment in right limb use. At 6 weeks post-6-OHDA lesion, animals received an injection of either GPT002 or GPT004 in the lesioned side; changes in motor performance in the three tests were monitored over 12 weeks.

The cylinder test was carried out to assess exploratory forelimb use asymmetry by placing the animal in a cylinder and counting the frequency of right and left forelimb touches on the glass wall. Compared to the baseline, 8 weeks post-AAV treatment GPT004 animals still showed a strong tendency towards using only the left forepaw: right forelimb use was 25.6 ± 1.86% at baseline and 27.2 ± 4.4% of total at week 8. At this time point, asymmetrical forepaw-use was restored in GPT002-treated rats: right forelimb use was 23.3 ± 3.4% at baseline vs. 47.8 ± 5% at week 8 (Figure 56A).

The corridor test was used to study the sensorimotor aspect of the lesion. In this test, the read-out variable is the animals' lateralised response selection by nose-pokes in small, equally spaced, containers filled with sugar pellets along a corridor (Figure 55).

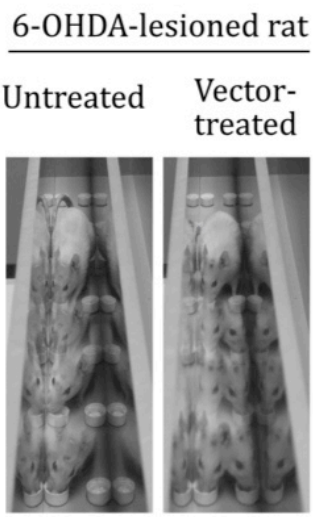

Figure 55: Schematic representation of the corridor test.
Upon unilateral depletion of dopaminergic neurons by 6-OHDA lesion, rats develop contralateral special neglect and retrieve sugar pellets from one side only (left image, untreated). Upon treatment with gene therapy, lesioned rats recover their ability to retrieve sugar pellets from both sides of the corridor (right image, vector-treated, GPT002). (From Cederfjäll E. et al. Molecular Therapy 2012 Jul;20(7):1315-26).

In the corridor test, 8 weeks post-injection animals treated with GPT004 still showed a bias towards retrieving pellets from the side ipsilateral to the lesion (right side retrievals 12.5 ± 4.1% of total) wile the GPT002 group displayed a behavioural improvement towards a symmetrical response (right retrievals 37.3 ± 6.1% of total). This behaviour remained virtually unchanged in both groups for up to 12 weeks post-AAV treatment (right retrievals 14.2 ± 4% and 38.3 ± 5.7% of total for GPT004 and GPT002, respectively) (Figure 56 B).

The stepping test was used to assess forelimb akinesia by quantifying the ability to do adjusting side steps. Eight weeks post-AAV treatment, animals in the GPT002 group showed a significant improvement in left forepaw use relative to baseline (82.2 ± 3.7% vs. 14.43 ± 4.1% forepaw steps relative to intact side at week 8 and baseline, respectively). In the GPT004 group the animals showed an increased performance with the right forepaw (contralateral to the lesion) but the improvement was not as remarkable as in GPT002-treated animals (45.9 ± 9.8% vs. 17 ± 4.2% forepaw steps relative to intact side at week 8 and baseline, respectively). This recovery was maintained up to week 12 post-AAV treatment (80.3 ± 2.5% and 47.7 ± 8.4% forepaw steps relative to intact side GPT002 and GPT004, respectively) (Figure 56 C).

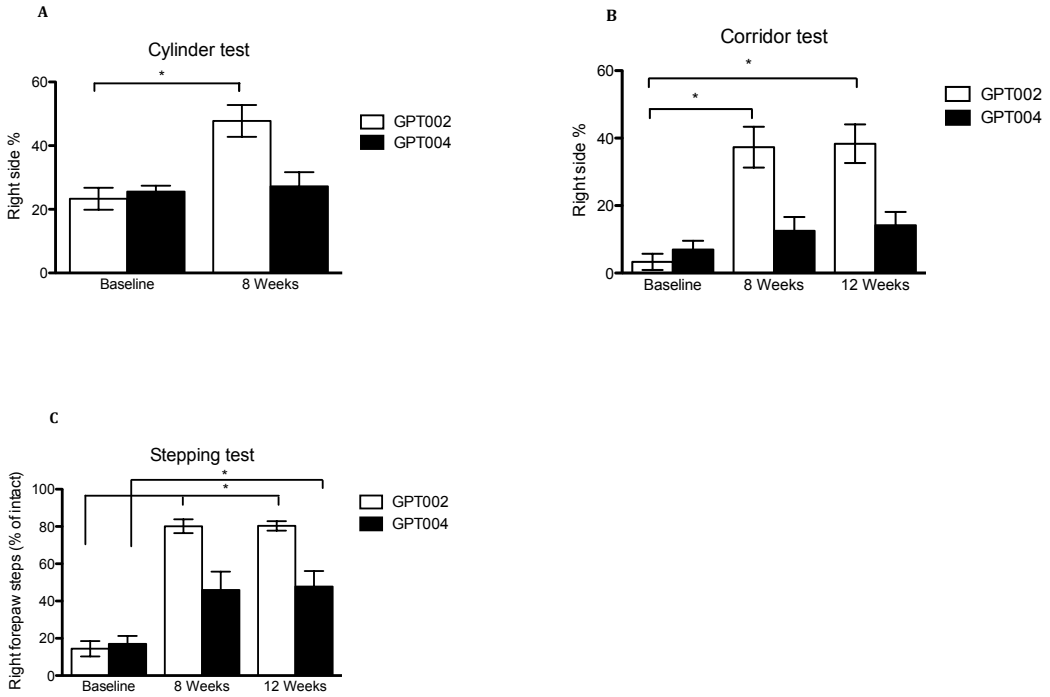

Figure 56: Behavioural tests run over a period of 12 weeks post-AAV treatment.
(A) Cylinder test; (B) corridor test; (C) stepping test (Friedman test followed by Dunn's multiple comparison, p <0.05). In the cylinder tests treatment with GPT002 led to a significant increase in the use of the right forepaw. Improvement after GPT002 treatment was also seen in the corridor test 8 weeks post-injection. Retrieval of sugar pellets from the right side remained stable up to 12 weeks post-injection. The ability to do adjusting sidesteps with the right forepaw increased after treatment with both vectors. However, while GPT002 already sowed an effect after 8 weeks, GPT004 only led to improved behaviour 12 weeks post-AAV injection.

In a separate group of rats (n=5 per group), IHC was used to qualitatively assess transgene expression 6 weeks post-AAV injection. The injection of 6-OHDA into the MFB in one hemisphere resulted in a complete loss of the dopaminergic neurons that innervate the striatum, while the contralateral side remained visually unaffected. Both, GPT002 and GPT004 vectors induced ectopic TH and GCH1 expression in the rat striatum at similar levels (Figure 57).

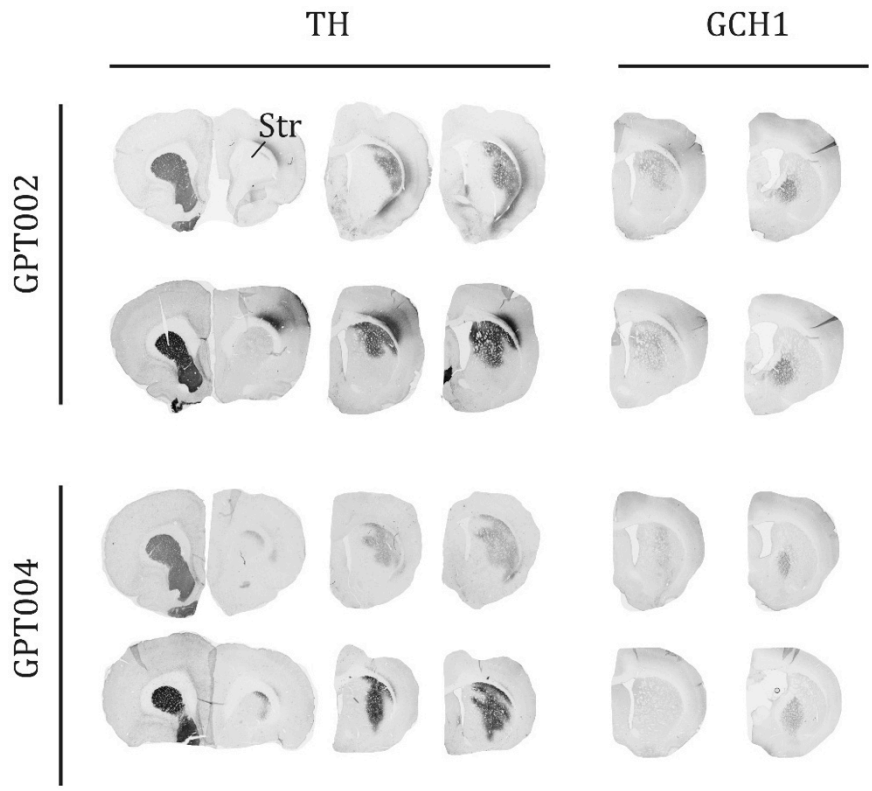

Figure 57: Transgene expression of GPT002 and GPT004 detected by IHC.
The first column shows both brain hemispheres of unilaterally 6-OHDA-lesioned rats: non-lesioned hemisphere on the left; lesioned hemisphere on the right. The other four columns show only the lesioned hemisphere six weeks post-AAV injection. Animals from both the GPT002 (n = 5) and GPT004 (n = 5) were deeply anesthetised with pentobarbital, transcardially perfused; brains were readily dissected, and then fixed in paraformaldehyde (PFA) for 2 hours. After overnight incubation in sucrose the brains were then cut in 35µm coronal sections.

4.2.7 Behavioural Assessment of GPT004 in the MPTP-lesioned NHP Model

To further investigate the ability of GPT004 to correct parkinsonism without inducing dyskinesia, 18 NHP were lesioned with daily MPTP injections and randomly assigned to one of three groups after the cessation of MTPT treatment (n=6 per group). The first group received a total volume of 90 µl of a $5x10^{11}$ gcp/ml GPT004 preparation (low-dose) and a second one received the same volume of a $5x10^{12}$ gcp/ml preparation of GPT004 (high-dose). A third group of MPTP-lesioned NHP did not receive any treatment. Injections were given bilaterally in the same areas of the putamen as in the previous two studies. Behavioural assessment of locomotor activity, parkinsonian disability and dyskinesia was carried out over 6 months once monthly in the absence of L-DOPA treatment and after a sub-threshold dose of L-DOPA, called 50% L-DOPA

treatment – half of the dose needed to completely reverse parkinsonian motor symptoms.

4.2.7.1 Locomotor Activity and Parkinsonian Disability in GPT004-treated NHP

During the study, no significant improvement in locomotor activity was observed in the absence of L-DOPA treatment (OFF L-DOPA) or after a sub-threshold dose (50% L-DOPA). Intriguingly, locomotor activity in all three groups decreased over the time course of the experiment upon treatment with 50% L-DOPA (Figure 58).

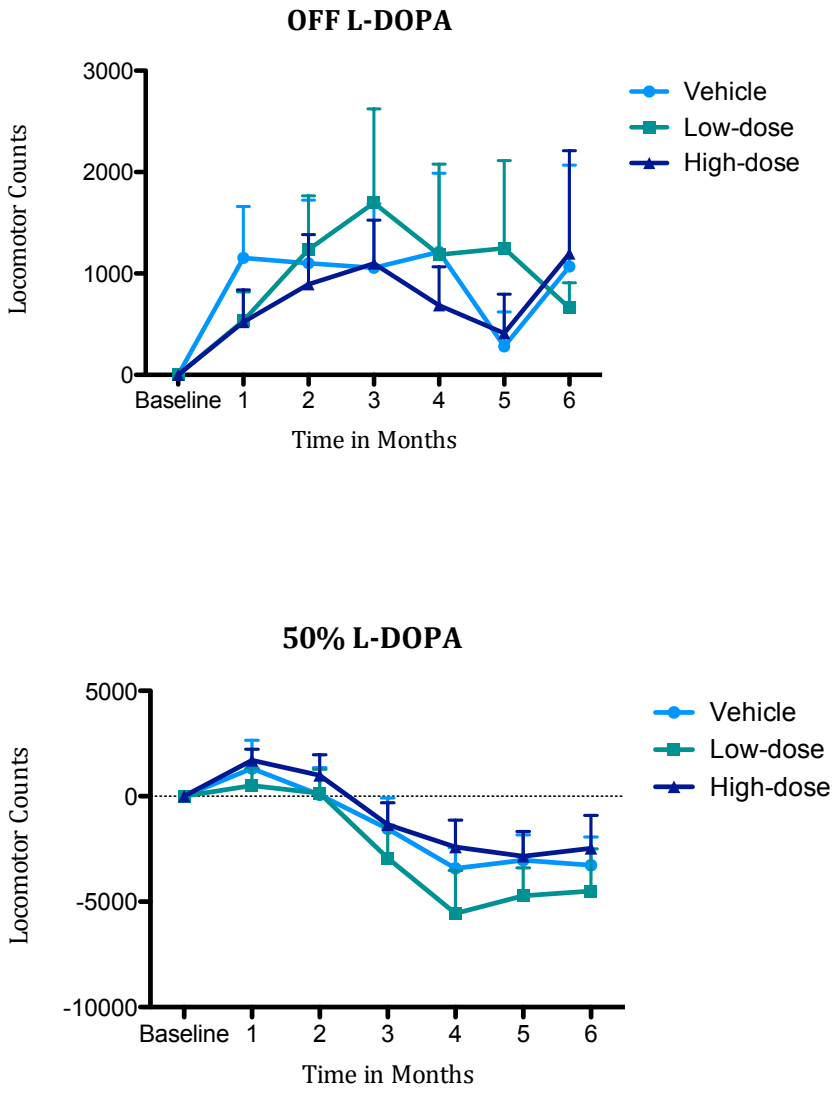

Figure 58: Locomotor activity of lesioned NHP-treated with GPT004.
Comparison between treatments and intragroup comparison against baseline scores was done with the Friedman test followed by Dunn's multiple comparisons. Values are shown as mean ± SEM and only upper error bars are shown for clarity. All values are normalised to the baseline scores.

Because non-lesioned animals were not included in this study, the baseline measurements of the MPTP-treated NHP were compared with the scores from the non-lesioned NHP from study 1. MPTP-lesioned NHP had decreased locomotor counts of 75%, 82% and 91% in the vehicle, low-dose and high-dose treated groups, respectively (Figure 59).

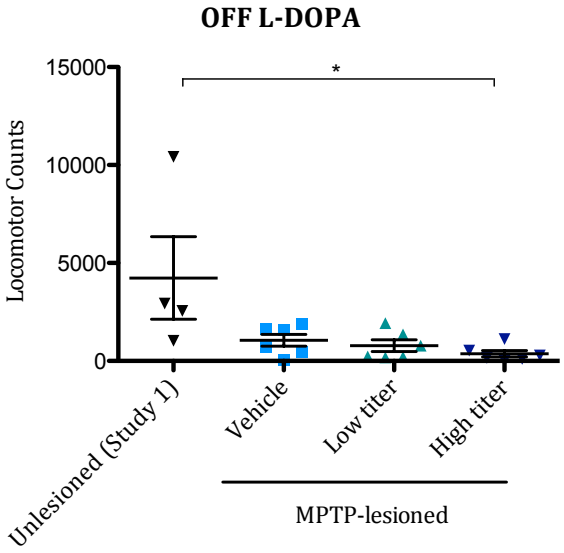

Figure 59: Locomotor activity in normal NHP from study 1 and MPTP-lesioned NHP in study 3.
The difference between groups was tested by Friedman test (*p>0.05). Mean values ± SEM are shown.

Clinical rating for parkinsonian disability demonstrated a modest decrease in the low-dose treated NHP OFF L-DOPA. However, this was not significant relative to vehicle-treated animals. Similarly, upon challenge with 50% L-DOPA, no significant decrease in parkinsonian disability was demonstrated. Likewise, high-dose treatment had no effect on parkinsonian disability either in the OFF state or after 50% L-DOPA treatment (Figure 60).

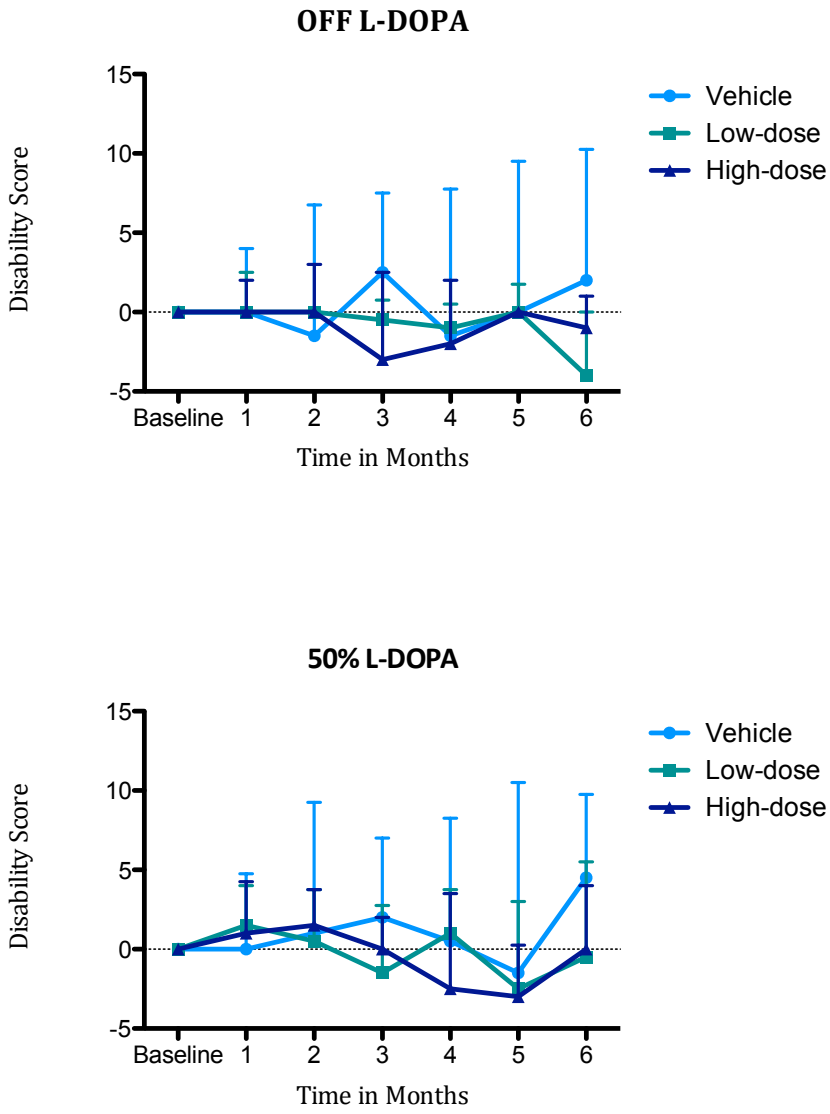

Figure 60: Disability scores of NHP treated with GPT004.
Comparison between treatments was performed with the non-parametric Friedman test, while intragroup comparison against the baseline was done with the Friedman test followed by Dunn's multiple comparisons. Median values ± interquartile range are shown. Only upper error bars are shown for clarity. All values are normalised to the baseline scores.

4.2.7.2 Dyskinesia and Good On-time

Priming L-DOPA treatment was given to NHP following MPTP-lesioning in order to induce sustained and severe dyskinesia in these animals. We assessed whether treatment with GPT004 was able to decrease the occurrence and severity of chorea and dystonia, the two hallmarks of LID. Treatment with GPT004 showed a statistically significant reduced dyskinesia in NHP that

received a low-dose of the vector (Friedman test, $p<0.05$). This result was mirrored by an increase in the good on-time – time after L-DOPA treatment in which NHP show no bradykinesia and minimal dyskinesia. However, given the lack of symptomatic improvement in the locomotor counts and parkinsonian disability scores, this observation does not have clinical significance. No effects were seen in NHP treated with high-dose of GPT004 (Figure 61).

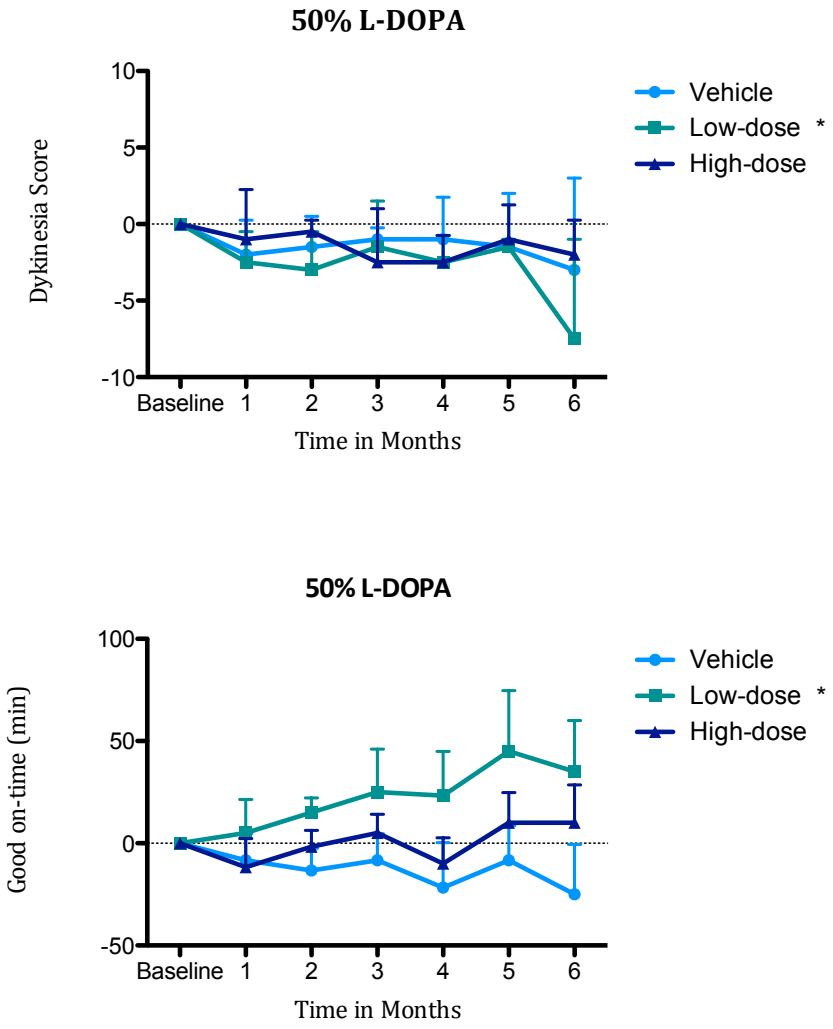

Figure 61: Dyskinesia scores and good on-time in the NHP treated with GPT004.
Scores for dyskinesia (top) and good on-time (bottom) are presented as median ± interquartile range (dyskinesia) and mean ± SEM (good on-time). All values are normalised to the baseline scores. Only upper error bars are shown for clarity. NHP treated with the low-dose of GPT004 showed a significant decrease in dyskinesia ($p<0.05$) with a concomitant increase in the on-time ($p<0.05$) relative to the vehicle treated NHP. However, this observation was not considered clinically significant.

4.2.8 *In vitro* Assessment of GPT004

The surprisingly low efficacy of GPT004 seen in both, the rat and NHP model of PD called for further analyses to elucidate the reasons for its poor outcome. Valuable insight will be gained through *post-mortem* analyses of the animals, such as confirmation and comparison of transgene and protein expression levels in the striatum, measurement of TH activity and intrastriatal levels of L-DOPA. However, at the time the rodent study was terminated, the NHP study was still ongoing and it was decided that the rodents' brains were to remain frozen until later efficacy time points were available from the NHP study. These analyses are now ongoing but at the time this thesis was being written no data was available.

Because *a post*-mortem analysis of the animals' brains was not possible, an investigation of transgene and protein expression from the brain vectors was performed *in vitro*. For this purpose, GPT002, GPT004 and the AAV-CMV-TH vector were pseudotyped in an AAV2 vector and used to infect the neuroblastoma cell line SH-SY5Y. The decision to use AAV2 in the *in vitro* experiments was made because an infection curve for this serotype in SH-SY5Y cells had been previously been performed in our lab and we knew that an MOI of 10^4 gcp would lead to 40% transduction. A transduction curve for AAV5 in the same cell line had not been done in our lab. The AAV-CMV-TH vector was used as a positive control since it had shown strong *in vivo* transduction in 2 NHP (Figure 53) and because the identical TH expression cassette was present in GPT004.

Transduction of SH-SY5Y cells led to increased *TH* gene expression from all three vectors and increased *GCH1* gene expression from GPT004 only (Figure 62 A). *TH* gene expression from GPT004 and AAV-CMV-TH was 100-fold higher than from GPT002. While a 6-fold increase in *GCH1* gene expression was observed upon infection with GPT004, its expression after GPT002 and CMV-TH infection was similar to that from uninfected cells. No DNA amplification was detected in the real time quantitative PCR in any of the -RT samples - reverse transcriptions performed in the absence of the reverse transcriptase enzyme -, confirming that the DNA detected in the test samples was cDNA that had been converted from mRNA and not contaminant genomic or viral DNA.

Western blot analysis of TH expression revealed the same pattern observed for the mRNA expression: GPT004 and CMV-TH vectors showed a much stronger expression than GPT002 (Figure 62 B).

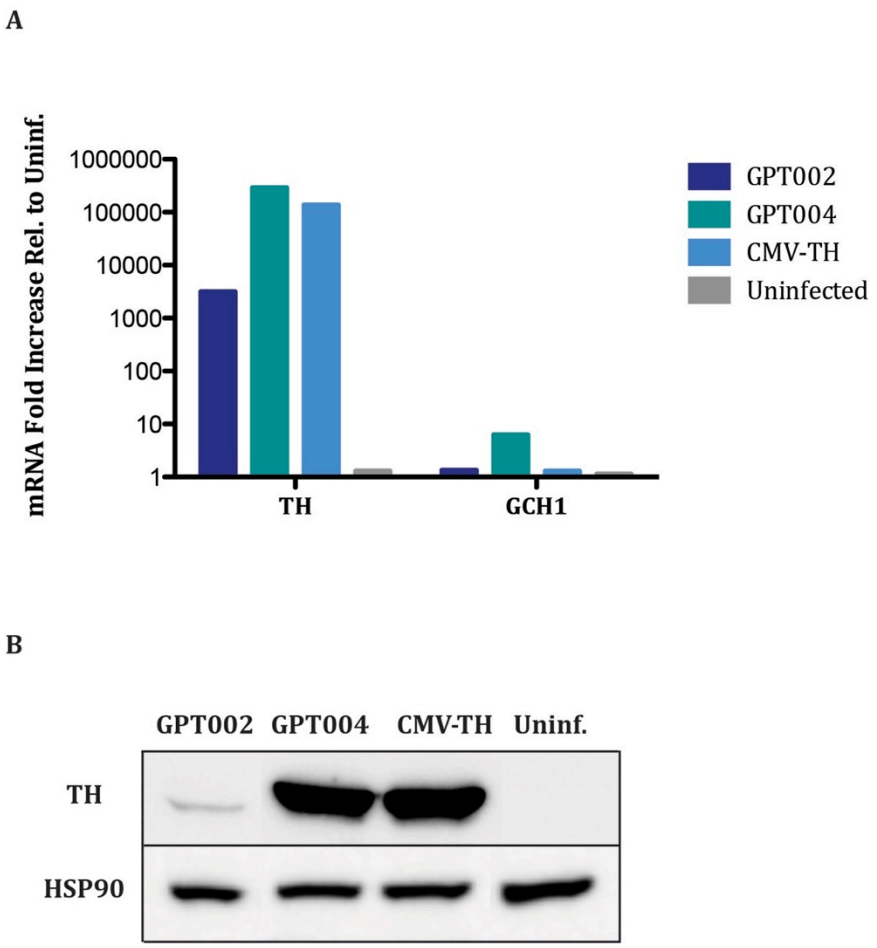

Figure 62: *In vitro* comparison of gene and protein expression of GPT002 and GPT004. Gene expression (A) and protein expression (B) of GPT002 was compared with GPT004. As a positive control, the AAV-CMV-TH vector was used. SH-SY5Y cells were transduced with GPT002, GPT004 and AAV-CMV-TH at an MOI of 10^4 gcp; mRNA and proteins were extracted 48h post-infection for gene and protein expression analyses. GPT004 and AAV-CMV-TH show higher expression than GPT002 at the gene and protein levels. Results presented are the mean of two independent experiments.

4.3 Discussion

In this chapter I investigated the efficacy of a clinical candidate AAV vector in the MPTP-lesioned NHP model of PD. The efficacy and safety studies described here represent a crucial step towards the translation of a novel gene therapy strategy following preclinical data generated in the 6-OHDA-lesioned rat model of PD (Cederfjäll et al. 2012).

In total, four NHP studies were carried out, which evaluated different vector designs, putaminal spread and doses for their ability to improve locomotor activity, parkinsonian disability and dyskinesia in the MPTP-lesioned NHP model of PD.

In the first NHP efficacy study, 18 MPTP-lesioned primates were assigned to one of three treatment groups (vehicle, low-dose and high-dose gene therapy) and submitted to behavioural tests (locomotor counts, parkinsonian disability and dyskinesia) OFF L-DOPA and after challenge with a sub-threshold dose of L-DOPA for up to 7 months. Here, a significant difference in locomotor counts was observed relative to vehicle-treated NHP in low- and high-dose-treated groups, both OFF L-DOPA and after challenge with 50% L-DOPA. Moreover, a significant improvement relative to the baseline was observed for the high-dose treated group at months 3 and 7 OFF L-DOPA and at month 3 after 50% L-DOPA treatment (Figure 41). Because the behavioural assessments stopped at different months for the three groups, the Wilcoxon matched pairs test – the non-parametric equivalent of the t-test – was performed individually on both treated groups vs. vehicle for up to months 5 and 6 with the low- and high-dose groups, respectively. The Friedman test – the non-parametric equivalent of repeated measurements ANOVA – was also performed on all groups up to month 5 in order to remain consistent in the tests run in all three NHP studies. This showed a significant difference between vehicle- and vector-treated animals for the low-dose group OFF L-DOPA and for both treated groups after 50% L-DOPA treatment. A slight improvement, although not significant, was also observed in the vehicle treated animals at month 3 both in OFF L-DOPA state and after 50% L-DOPA medication. High-dose-treated NHP also showed significantly increased locomotor activity at month 7 relative to the baseline. However, there are no

data for the vehicle control group at this time point to allow for a direct comparison between groups.

In addition to these analyses, baseline locomotor counts of MPTP-lesioned NHP were compared with normal NHP. Four non-lesioned NHP had been included in the study and it was surprising to observe that the difference in the baseline scores between normal and lesioned NHP was not significant (Figure 42). Although effective MPTP lesioning was demonstrated in the NHP through parkinsonian disability and dyskinesia scoring prior to the initiation of the study (Figure 38) and was validated by *post-mortem* stereological counting of TH+ neurons in the SNc (Figure 39), a difference in locomotor counts was also expected between normal and lesioned NHP. In this study, daily MPTP treatment to induce parkinsonism was halted when primates reached a score of 6 in the Benazzouz rating scale (Table 14), which ranges from 0 (normal) to 25 (severe parkinsonism). Although this score was used as a threshold for the cessation of MPTP treatment in order to ensure survival of the NHP in the forthcoming surgical procedures, previous studies using the Benazzouz scale to measure the extent of the MPTP lesion only halted the treatment once the NHP reached a score of 8 (Bezard et al. 1997). In addition, the degree of parkinsonian disability at which the MPTP treatment was stopped in this study corresponds to 24% of the maximum score (6 out of 25), whereas in a similar study from Jarraya et al., which also evaluated the efficacy of gene therapy for the treatment of PD, MPTP treatment was halted when 71% of the maximum disability score was achieved: ≥10 out of 14 in a rating scale adapted from Papa and Chase (Imbert et al. 2000; Jarraya et al. 2009). Finally, in the study from Jarraya et al., decrease in locomotor activity was used to decide when to stop MPTP treatment. It is therefore possible that the severity of the MPTP lesioning used in the experiments described in thesis was sufficient to cause parkinsonism and allow for the development of LID but not to significantly affect locomotor counts.

It was also noted that in the first NHP study dyskinesia scores decreased gradually in all groups, including the vehicle-treated (Figure 44 top). The reasons for this spontaneous improvement are not entirely clear but it is possible that changes in the NHP weight could be responsible for this phenomenon. The NHP were treated every month with the same sub-threshold amount of L-DOPA

established at the beginning of the experiment. Therefore, an increase in weight could have had an influence on the effective dose (mg/kg) given. In the study from Jarraya et al., the L-DOPA dose given to animals was adjusted to their weight. Despite the spontaneous improvement in the dyskinesia scores upon L-DOPA challenge seen in this study, dyskinesia was absent in GPT002-treated NHP in the OFF state at all time points measured and did not worsen when they were challenged with 50% L-DOPA.

In summary, symptomatic improvement in the first NHP study was observed for the endpoints locomotor activity in the high-dose-treated group in the OFF state and after 50% L-DOPA treatment as well as in parkinsonian disability in the OFF state. Overall, these effects were considered only partial and thus insufficient to justify clinical investigation.

Following the termination of study 1, a second study was conducted for 4 months to test the efficacy of a 10-fold higher dose of GPT002. In addition, an almost identical vector expressing a truncated form of TH was injected in a group of NHP. This vector was included in order to test whether increased TH catalytic activity was able to enhance the *in vivo* potency of the vector (Walker et al. 1994). Support for the use of a truncated TH also came from a successful preclinical study and Phase I gene therapy trial for the treatment of PD, in which a vector containing a truncated TH was used (Jarraya et al. 2009; Palfi et al. 2014). The 6 NHP injected with the truncated vector were the same “low-dose” NHP from study 1. The decision to reuse these animals was based on the observation that a low-dose treatment with GPT002 did not have any effect on the endpoints parkinsonian disability and dyskinesia for the entire duration of study 1 (Figure 43 and Figure 44). A group of reserve NHP lesioned together with those from study 1 was injected with the new dose of GPT002, while the same vehicle-treated group from study 1 was reused in study 2. After 4 months, efficacy was observed for both vectors, full-length and truncated, OFF L-DOPA for the endpoints locomotor counts and parkinsonian disability.

Since some of the NHP in this study were the same ones used in study 1 or lesioned at the same time, the lack of difference in locomotor counts between lesioned and normal NHP in study 2 remains a caveat in the measurement of this endpoint (Figure 48). Interestingly, no difference in efficacy was observed

between the full-length and the truncated vector, despite predicted increased activity of the truncated form of TH (Walker et al. 1994). Analysis of vector transduction in the rat model showed increased transduction of the full-length vector relative to the truncated variant (Figure 46). If this differential transduction is also true for the NHP, the similar efficacy of the two vectors in NHP might be attributed to the enhanced catalytic activity of the truncated TH. However, *post-mortem* analysis of the NHP brains showed no difference in the levels of ectopic TH between the full-length- and the truncated vector-treated NHP (Figure 51). The behavioural effect observed upon vector treatment in both NHP studies suggests vector-mediated L-DOPA synthesis. As the post-lesioning staining of the SNc showed, TH depletion was equivalent in all MPTP-treated NHP (Figure 39), therefore behavioural improvement seen in vehicle-treated NHP relative to vector-treated NHP is unlikely to have been caused by spared dopaminergic neurons alone. Furthermore, the lack of differential TH expression in the putamen between vector-treated and untreated NHP is unlikely to be a true reflection of a lack of transgene expression from the vector as the *post-mortem* histological data suggest. Firstly, the same GPT002 vector has been shown to efficiently express both its transgenes in the striatum of rodents (Cederfjäll et al. 2012 and Figure 36). Furthermore, an increase in GCH1+ cells was seen in NHP treated with the full-length vector. Finally, a similar gene therapy study in NHP was able to demonstrate high levels of TH expression from an AAV vector injected into the putamen at similar doses (Muramatsu et al. 2002). It can be argued that the vector used by Muramatsu et al. expressed TH from the CMV promoter, which could have led to a much stronger TH expression than a SYN-driven TH. On the other hand, the Muramatsu study used an AAV vector of serotype 2, which was shown to possess an 8- to 10-fold decreased ability to transduce the striatum relative to AAV5 (Burger et al. 2004). Based on these three facts, it is possible that technical issues in the detection of TH are the reason why no difference was seen in the number of TH+ cells between vector- and vehicle-treated NHP.

During the 4 months of study 2, dyskinesia scores showed a trend towards a decrease in both vector-treated groups and an increase in the good on-time (time in which parkinsonian disability is low and no severe dyskinesia is present).

However, these observations were not statistically significant relative to vehicle treated NHP. Nevertheless, the fact that gene therapy treatment was not able to trigger dyskinesia after oral L-DOPA treatment is of clinical relevance. In a Phase I lentiviral-based gene therapy for the treatment of PD, increased LID after L-DOPA oral medication was associated with vector treatment. However, it must be highlighted that these dyskinetic events had not been identified in the efficacy studies in MPTP-lesioned NHP and they could be resolved by decreasing the patient's L-DOPA oral medication (Jarraya et al. 2009; Palfi et al. 2014).

In summary, efficacy in study 2 was seen for the endpoints locomotor activity and parkinsonian disability for both vectors in the OFF state. Although dyskinesia did not decrease significantly, the fact that it did not increase post-gene therapy treatment is relevant.

Despite increased efficacy observed with the truncated and full-length GPT002 vectors relative to study 1, the identification of HR in these vectors posed a potential deterrent for the approval of this compound as a medicine. In order to be regarded as safe for human use, the ratio of both vector species (Figure 52) must be constant across preparations. However, this was not tested. In addition, if the by-product vector formed upon HR does not have the ability to express TH, it can be regarded as a contaminant. Therefore, to address the latter concern, the different fractions of a GPT002 preparation - i.e. complete prep, "higher band" only and "lower band" only - were injected in the striatum of 2 NHP. As positive control, the CMV-TH vector from Muramatsu et al. was included in the study (Muramatsu et al. 2002). Analysis of vector transduction in the putamen indicated that the by-product SYN-TH vector formed upon HR was able to express TH. However, expression from the CMV-TH vector was the strongest (Figure 53). This observation, added to the potential regulatory issue caused by the HR of the vector, prompted us to design a new and improved vector. The new vector, named GPT004, contained the same CMV-TH expression cassette present in Muramatsu's vector. By eliminating the first SYN promoter the intramolecular HR was abolished.

The poor efficacy of GPT004 in the rodent and NHP models of PD was unexpected given that the small-scale NHP study showed that the CMV promoter led to strong TH expression (Figure 53). Interestingly, the poor outcome of

GPT004 in the rodents was predictive for the NHP study, where efficacy was not met for any of the study's endpoints. The only effect seen in the NHP was a decrease in dyskinesia in the group treated with the low-dose of GPT004 but due to the lack of symptomatic improvement in locomotor counts and parkinsonian disability, this observation was not considered clinically significant (Figure 61).

The reasons for the unexpectedly low *in vivo* efficacy of GPT004 are not yet entirely clear. Strong expression from the CMV-TH cassette was achieved from a monocistronic vector in the small study using the 2 NHP and the study from Muramatsu et al. (Figure 43 and Muramatsu et al. 2002). Therefore, it is possible that the different vector designs (i.e. monocistronic vs. bicistronic) has an influence on transgene expression. Substantial promoter interference between internal heterologous promoters has been described to occur in a retroviral vector expressing its transgenes from the CMV and EF1α promoters, which affected the expression of both transgenes (Curtin et al. 2008). The mechanisms by which promoter interference occurs have been described as being through the formation of a read-through transcript from the upstream gene into the regulatory region of the second one, which disrupts the binding of transcription factors and other DNA-binding proteins (Greger et al. 1998). Alternatively, the formation of a read-through transcript with an abnormal 3'UTR could lead to mRNA targeted degradation by the nonsense-mediated mRNA decay pathway (Bicknell et al. 2012). Another proposed mechanism to explain bidirectional promoter interference is competition between promoters for transcription factors, enhancers or their binding proteins. Promoter interference-like effects could also occur through post-transcriptional mechanisms, such as competition between the different vector-encoded transcripts for ribosomal association. Intriguingly, these proposed interpretations for the *in vivo* data could not be confirmed by *in vitro* experiments. As seen in Figure 62, transcript stability and translation of TH are not affected in either GPT002 or GPT004. In fact, the strong TH expression observed *in vitro* does not correspond to the poor *in vivo* performance of the rats and NHP injected with GPT004. Promoter interference, however, can be suggested for the transcription of the *GCH1* cassette in GPT002, which showed similar transcript levels as uninfected cells.

The analysis of the brains of the animals used in these experiments will provide important indications on possible reasons for the poor *in vivo* performance of GPT004. Some insight was gained through the IHC analysis of a small group of rats, which demonstrated similar striatal transduction levels with both vectors. This is in contrast to the differential TH expression seen *in vitro* (Figure 57 and Figure 62). However, the animals used for the IHC analysis were not the same ones as those used for the behavioural tests.

The GPT004 efficacy study in the NHP was terminated only recently and the brains of the rodents and of the NHP are currently being analysed. The *post-mortem* analyses will allow for the comparison of transgene mRNA and protein expression levels in the striatum. This analysis will confirm whether expression levels correlate with the behavioural efficacy. Furthermore, *ex vivo* measurement of intrastriatal TH activity and L-DOPA levels will provide a readout of the activity levels of each vector.

Given the low numbers of gene therapy trials that have been able to show efficacy in double blind, placebo controlled trials, it is sensible to aim for stronger preclinical efficacy from an improved vector before tests in humans are conducted (Bartus et al. 2014). In order to accomplish this, understanding the reasons behind the poor efficacy of GPT004 is crucial. If promoter interference is suggested by the *post-mortem* analyses of the animals, the use of an IRES to allow the expression of two different transgenes without using separate promoters can be explored by redesigning the vector similarly to the tricistronic vector proposed in Chapter 3 or the vector that was used in the lentiviral gene therapy trial for intrastriatal dopamine synthesis (Figure 26 and Jarraya et al. 2009). Alternatively, transgene expression from different monocistronic AAV vectors can be considered. Although this strategy does not ensure that all neurons will be equally transduced with both vectors, there is evidence of preclinical efficacy using this approach (Muramatsu et al. 2002).

Chapter 5 Addendum

5.1 Attempt to Abolish the Intramolecular Recombination in the Bicistronic Liver Vector

The original vectors proposed for intrahepatic and intrastriatal AAV-mediated continuous synthesis of L-DOPA expressed both rate-limiting enzymes in the synthesis of L-DOPA from a single AAV genome. Each gene was driven by an identical promoter sequence, which allowed their expression from independent cassettes (Figure 17 and Figure 37). Prior to the conceptualisation of the AAV-mediated hepatic L-DOPA approach, preclinical efficacy with GPT002 had already been shown in the 6-OHDA rat model of PD (Cederfjäll et al. 2012). Therefore, the same vector design was adopted for the bicistronic liver vector.

Intramolecular HR recombination was at first identified in the liver bicistronic vector during its genome titration by alkaline agarose gel (Figure 18B and Figure 19) and subsequently in GPT002 (Figure 52). While this was not a major concern for the proof-of-principle liver approach, it was potentially problematic for the already ongoing efficacy studies in NHP. Therefore, finding a way to abolish the HR without dramatically altering the vector design was of relevance to this gene therapy strategy.

AAV has been shown to achieve relatively efficient, high-fidelity, non-mutagenic gene repair in host cells through HR following transduction with a rAAV, in which the viral genes are replaced by sequences homologous to the target chromosomal locus. Usually the modification is introduced between stretches of homology called 5' and 3' homology arms, which, upon transduction, lead to recombination with the chromosomal target. The higher targeting efficiencies achieved with AAV relative to other methods such as electroporation or other viral vectors is thought to be achieved through the recruitment of components of the HR pathway by the T-shaped ITRs.

The length of the homology arms is known to be crucial for AAV-mediated gene targeting. Furthermore, a single mismatch in these homologous sequences can dramatically decrease targeting success (Khan et al. 2011). I therefore hypothesised that insertion of point mutations along the first LP1 promoter in

the liver bicistronic vector would have the potential to dramatically decrease the chances of intramolecular HR during vector production. To test this, different nucleotides (nt) along the first LP1 promoter were mutated in pAAV-LP1-GCH1-LP1-tTH (pAA019) and vectors were subsequently produced to assess the effect of the mutations in HR (Figure 63).

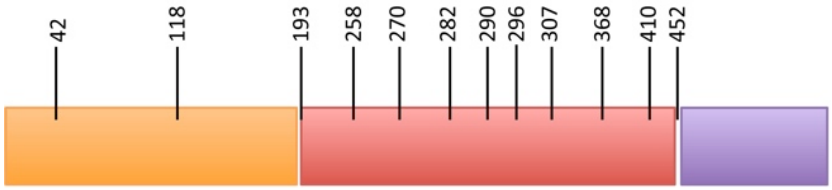

Figure 63: Schematic representation of the LP1 promoter and the 12 point mutations introduced in its sequence.
Numbers represent the nucleotide position relative to the first nucleotide in the enhancer sequence. The whole LP1 promoter comprises 545 nt. The orange region comprises nt 1-192 and corresponds to the human apolipoprotein E/C-I gene locus control region; the red region comprises nt 194-255 and corresponds to the human α1-antitrypsin promoter; the purple region comprises nucleotides 453-545 and corresponds to the modified SV40 intron.

The effect of the different mutations on HR was assessed by running viral preps containing different numbers of mutations on an alkaline agarose gel and quantifying the HR by-product (2.8kb band) relative to the full-length genome (4.4kb band). Surprisingly, the ratio between both bands remained unaffected even after 12 mutations were inserted in the first LP1 promoter sequence (Figure 64). These results indicate that point mutations do not hinder the occurrence of intramolecular HR during rAAV production of the liver bicistronic vector.

Previous reports have shown the ability of AAV to repair deletions in one ITR during viral replication (Samulski et al. 1983). To investigate whether a similar phenomenon was happening with the mutated vectors, the 2.8 kb band was isolated from the alkaline gel, purified and sent for sequencing. Sequencing results revealed that the LP1 sequence of the by-product virus was partially reverted back to the original sequence from nucleotide 258 onwards, indicating that the intact LP1 sequence served as a template for the sequence correction.

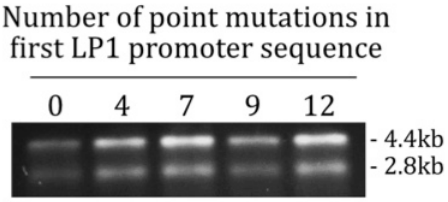

Figure 64: Effect of point mutations in the LP1 sequence.
HR-mediated formation of by-product vector (2.8kb) in the bicistronic liver vector is not affected by the insertion of point mutations in the first LP1 promoter sequence: the ratios between upper and lower bands are equal in all vector preparations.

It remains to be analysed whether the second LP1 sequence, which was not altered by mutagenesis, is also targeted by the mutated LP1 during vector production resulting in a promoter with a mutated sequence. However, these questions were put on hold once the decision was made to redesign the vectors in order to achieve higher transduction levels in both the liver and brain approach for continuous L-DOPA synthesis.

Chapter 6 General Discussion

Almost 60 years after its discovery as a powerful drug to treat the motor symptoms of PD, L-DOPA still remains the most effective antiparkinsonian medication. Virtually all patients respond to it and no other therapy has yet been shown to provide greater symptomatic relief. However, chronic oral L-DOPA therapy is associated with the development of disabling motor complications in most patients. Among them is LID, which has proven extremely difficult to manage thanks to the inconveniently short half-life of L-DOPA and its poorly understood interactions with the disease progression.

The studies presented in this thesis describe and evaluate two novel gene therapy strategies using AAV vectors to improve the treatment of PD through a constant L-DOPA supply to the brain. The first one describes the assessment of a gene therapy for continuous L-DOPA synthesis in the periphery, a strategy with compelling scientific rationale but for which feasibility had not been tested before. The second study pertains to AAV-mediated gene therapy for continuous L-DOPA synthesis in the CNS, a project that is built on solid and promising preclinical studies in a rodent model of PD (Cederfjäll et al. 2013).

In the proof-of-concept study for continuous L-DOPA delivery in the liver, I was able to show that plasma L-DOPA levels could be increased in healthy mice through AAV-mediated delivery of the essential genes involved in L-DOPA synthesis. However, the magnitude of the effect achieved with the initial vector is not likely to be of clinical significance, which led to the proposition and redesign of an optimised vector that is currently being validated. The testing and optimisation of different vectors is a process common to the early stages of a gene therapy project and, like all phases in the development of a therapy, it has to overcome several challenges. Examples of such challenges can be gathered from the development of AAV vectors for the treatment of haemophilia. The expression levels of the therapeutic protein required for a phenotype correction led to the development of the artificial LP1 liver-specific promoter. This promoter had to be tissue-specific, strong and at the same time short in length in order to accommodate its transgene in a self-complementary AAV vector. Further optimisation of the promoter - i.e. shortening without loss of strength -

was required to allow for the accommodation of even bigger transgene cassettes. In addition to modifications to the promoter, different bioengineered forms of the therapeutic protein – i.e. human clotting factor – were tested until an optimal candidate was selected for the preclinical studies (Nathwani et al. 2006; McIntosh et al. 2013). The novel concept of AAV-mediated L-DOPA synthesis in the periphery is based on the gold-standard L-DOPA pharmacotherapy given orally to patients. Once ingested, L-DOPA becomes systemically available, crosses the blood-brain-barrier and reaches the basal ganglia, where it is converted to dopamine. A novel and improved form of L-DOPA delivery to patients that further supports the rationale for the proposed gene therapy is the continuous intrajejunal infusion of L-DOPA (Olanow et al. 2014). This technology, now approved for commercialisation, provides patients with a formulation of L-DOPA and AADC inhibitor and has been shown to increase ON-time without troublesome dyskinesia. In contrast to the duodenal infusion strategy, the gene therapy approach does not provide continuous AADC inhibition and peripheral degradation of L-DOPA must be supplied alongside oral L-DOPA therapy.

Although the levels of plasma L-DOPA after hepatic targeting with the bicistronic AAV-vector increased relative to vehicle-treated animals, they may not be sufficiently high to guarantee therapeutic effect. Despite these seemingly modest results, it is important to note that the L-DOPA dose of 10mg/kg given to the orally-treated group was higher than the usual 6mg/kg given to induce behavioural improvement (Carlsson et al. 2005). Therefore, the benchmark against which the gene therapy was compared to was potentially too stringent.

In summary, the data show that peripheral L-DOPA synthesis can be achieved and further optimisations/modifications of the vector may be needed to bridge the gap necessary to achieve therapeutic levels of circulating L-DOPA. Because the proposed gene therapy aims to provide a basal and constant L-DOPA supply in the periphery, once this is achieved, a reduction in the oral dosage will be possible, thereby decreasing the side effects caused by the peaks and troughs in circulating L-DOPA.

The second gene therapy proposed in this thesis is in a more advanced stage. The studies presented here evaluated the efficacy of a vector that had already shown therapeutic potential in a small animal model of PD and here, the efficacy

and safety of the vector was assessed in the MPTP-lesioned NHP model. I was able to show that the vector was safe and led to symptomatic improvement of NHP without worsening pre-established dyskinesia. The clinical relevance of these findings and their potential benefit to patients are positive. However, the observed HR of GPT002 and the partial motor improvement observed in the study's endpoints do not support the advancement of this therapy to early phase trials.

Gene therapy strategies showing preclinical safety, symptomatic improvement and strong clinical potential have contributed immensely to the progress of the field. These studies have led, in the past decade alone, to nine gene therapy trials being conducted to treat PD, most of them using AAV vectors. All nine trials have supported the safety of targeting the CNS with viral vectors. However, so far no study was able to demonstrate robust efficacy to justify its broad application in humans (Bartus et al. 2014). In most cases, the preclinical findings in NHP were not predictive of the outcome in the early phase trials, which highlights the necessity of better and more predictive animal models (Bankiewicz et al. 2000; Emborg et al. 2007; Kaplitt et al. 2007; Jarraya et al. 2009; Mittermeyer et al. 2012; Palfi et al. 2014). The best PD models currently available do not present a similar aetiology nor do they recapitulate the stages of disease progression observed in humans. While genetic models show an accumulation of α-synuclein but fail in presenting the motor impairment seen in patients, toxin-based models, generated by the selective destruction of the nigrostriatal dopaminergic neurons, present most of the motor complications associated with PD but fail to show Lewy body inclusions, the pathological hallmark of PD. Therefore, progress in the understanding of the pathology and disease development must advance hand in hand with the improvement of the current animal models in order for preclinical results to be more reliable and predictive (Lane & Dunnett 2008; Bartus et al. 2014). Working with models that only artificially mimic the features observed in a disease can not only lead to the testing in humans of therapies bound to fail when exposed to the real context of the disease but may also prevent potentially promising therapies from entering clinical trials.

The rodent and NHP models used in these studies are the best ones available to date and approval for clinical trials still relies on efficacy data generated in these animals. Despite the fact that experience has shown poor clinical translation of treatment in these models, a more careful selection of human trial candidates could improve the chances of success of a novel therapy. For example, the success of neuroprotective gene therapy strategies for PD may come much sooner if trials select patient cohorts at earlier stages of the disease, who can potentially benefit more from neuroprotective strategies than later stage patents (Bartus et al. 2014).

The most effective therapy for LID currently available is deep brain stimulation (DBS) of the STN and the GPi. Until now, no gene therapy strategy has proven more efficacious than DBS for the treatment of LID. Similarly to the proposed gene therapy, DBS is able to improve LID by allowing a reduction in the L-DOPA dosage. Notwithstanding, DBS is a procedure prone to failure for reasons such as misplacement of the stimulating electrodes, poor programming and inadequate balancing between stimulation and pharmacological treatment, thus, this technology is only applied in patients that no longer respond satisfactorily to pharmacological treatment (Kühn & Volkmann 2016). Gene therapy for continuous L-DOPA delivery, on the other hand, once well established, will have the potential to treat the non-responsiveness to pharmacotherapy or at least significantly delay the onset of L-DOPA induced complications with a single intervention.

Transplant of foetal tissue – i.e. neuroblasts - has also been successfully used to treat the motor symptoms of PD. Clinical trials have demonstrated post-transplantation graft survival, synaptic integration of dopaminergic neurons and significant reduction in motor deficit in patients (Barker et al. 2013). Unfortunately, due to the limited availability of tissue for transplantation, foetal tissue has not become a routine treatment for PD. The problem of the limited amount of tissue for transplantation can be solved with stem cells. The rapid development of clinically-compliant strategies for stem cell maintenance and directed differentiation have brought their application closer to the clinic. The current major roadblock for their wide application to treat PD symptoms is safety, most notably graft-induced dyskinesia (GID) (Rylander Ottosson & Lane

2016) and a better understanding and control of this phenomenon is an imperative for the future application of transplantation for the treatment of PD. A recent study has shed some light in our understanding of some mechanisms underlying GID by unveiling the link between serotonin 5-HT6 receptor stimulation, dysplastic dopamine release and GID (Aldrin-Kirk et al. 2016).

PD has emerged as a prototype platform for the development of gene therapy strategies targeting the CNS due to the well-defined and targetable neuronal systems involved in the motor symptoms, the need for relatively small titres and volumes of vector needed to target those sites and the increasing demand for improved therapeutics with an aging population. However, it has become clear that PD is far more complex than once appreciated. The understanding of many aspects of the disease aetiology, pathogenesis and symptoms still remain obscure to us. These factors contribute to the uncertainty and difficulty in developing a successful therapeutic strategy. Nonetheless, gene therapy for PD has made remarkable progress in the past decade. Gene therapy strategies for other diseases such as haemophilia B did not lead to the cure of a patient before encountering obstacles not foreseen in preclinical studies and addressing a variety of other issues: design of more optimised expression cassettes, improved AAV serotypes, identification of an optimal route of vector delivery, dose and genome conformation as well as the inclusion of a short course of corticoid administration to temporarily supress a T cell-mediated immune response against the AAV capsid (George & Fogarty 2015). The treatment of haemophilia with gene therapy, although quite established and very effective, continues to undergo improvements with respect to vector design and treatment regimen. As an even more complex disease, gene therapy for PD faces more challenges on its journey towards the translation from animals to patients.

Taken together, the seemingly disappointing results achieved so far in the field of gene therapy to treat PD should not be considered discouraging. In fact they represent crucial steps that must be taken in the advancement towards its translation. Given the safety record of the use of viral vectors for the treatment of diseases that affect the CNS, the continuous advancement in our understanding of PD and the increasing awareness for the importance of more reliable and predictive animal models, it is safe to assume that gene therapy will be an

important contributor to the treatment and improvement of the quality of life of the growing number of people affected by the disease.

References

Abbott, A., 2010. Levodopa: the story so far. *Nature*, 466(7310), pp.S6–7.

Agbandje-McKenna, M. & Kleinschmidt, J., 2011. AAV capsid structure and cell interactions. *Methods in molecular biology (Clifton, N.J.)*, 807, pp.47–92.

Aldrin-Kirk, P. et al., 2016. DREADD Modulation of Transplanted DA Neurons Reveals a Novel Parkinsonian Dyskinesia Mechanism Mediated by the Serotonin 5-HT6 Receptor. *Neuron*, 90(5), pp.955–68.

Anon, 2015. The Journal of Gene Medicine - Wiley Online Library. Available at: http://www.wiley.com/legacy/wileychi/genmed/clinical/ [Accessed July 15, 2015].

Aucoin, M.G., Perrier, M. & Kamen, A.A., 2008. Critical assessment of current adeno-associated viral vector production and quantification methods. *Biotechnology advances*, 26(1), pp.73–88.

Bainbridge, J.W.B. et al., 2008. Effect of gene therapy on visual function in Leber's congenital amaurosis. *The New England journal of medicine*, 358(21), pp.2231–9.

Bajpai, P. et al., 2013. Metabolism of 1-methyl-4-phenyl-1,2,3,6-tetrahydropyridine by mitochondrion-targeted cytochrome P450 2D6: implications in Parkinson disease. *The Journal of biological chemistry*, 288(6), pp.4436–51.

Balazs, A.B. et al., 2012. Antibody-based protection against HIV infection by vectored immunoprophylaxis. *Nature*, 481(7379), pp.81–4.

Bankiewicz, K.S. et al., 2000. Convection-enhanced delivery of AAV vector in parkinsonian monkeys; in vivo detection of gene expression and restoration of dopaminergic function using pro-drug approach. *Experimental neurology*, 164(1), pp.2–14.

Bankiewicz, K.S. et al., 2006. Long-term clinical improvement in MPTP-lesioned primates after gene therapy with AAV-hAADC. *Molecular therapy : the journal of the American Society of Gene Therapy*, 14(4), pp.564–70.

Barker, R. et al., 2013. Fetal dopaminergic transplantation trials and the future of neural grafting in Parkinson's disease. *Lancet Neurology*, 12(1), pp.84–91.

Bartlett, J.S., Wilcher, R. & Samulski, R.J., 2000. Infectious entry pathway of adeno-associated virus and adeno-associated virus vectors. *Journal of virology*, 74(6), pp.2777–85.

Bartus, R.T., Weinberg, M.S. & Samulski, R.J., 2014. Parkinson's disease gene therapy: success by design meets failure by efficacy. *Molecular therapy : the journal of the American Society of Gene Therapy*, 22(3), pp.487–97.

Benazzouz, A. et al., 1993. Reversal of rigidity and improvement in motor performance by subthalamic high-frequency stimulation in MPTP-treated monkeys. *The European journal of neuroscience*, 5(4), pp.382–9.

Bencsics, C. et al., 1996. Double transduction with GTP cyclohydrolase I and tyrosine hydroxylase is necessary for spontaneous synthesis of L-DOPA by primary fibroblasts. *The Journal of neuroscience : the official journal of the Society for Neuroscience*, 16(14), pp.4449–56.

Berns, K.I. et al., 2015. Adeno-Associated Virus Type 2 and Hepatocellular Carcinoma? *Human*

gene therapy, 26(12), pp.779–81.

Berton, O. et al., 2009. Striatal overexpression of DeltaJunD resets L-DOPA-induced dyskinesia in a primate model of Parkinson disease. *Biological psychiatry*, 66(6), pp.554–61.

Bezard, E. et al., 1997. A chronic MPTP model reproducing the slow evolution of Parkinson's disease: evolution of motor symptoms in the monkey. *Brain research*, 766(1-2), pp.107–12.

Bezard, E. et al., 2001. Relationship between the appearance of symptoms and the level of nigrostriatal degeneration in a progressive 1-methyl-4-phenyl-1,2,3,6-tetrahydropyridine-lesioned macaque model of Parkinson's disease. *The Journal of neuroscience : the official journal of the Society for Neuroscience*, 21(17), pp.6853–61.

Bézard, E. et al., 2003. Attenuation of levodopa-induced dyskinesia by normalizing dopamine D3 receptor function. *Nature medicine*, 9(6), pp.762–7.

Bicknell, A.A. et al., 2012. Introns in UTRs: why we should stop ignoring them. *BioEssays : news and reviews in molecular, cellular and developmental biology*, 34(12), pp.1025–34.

Birkmayer, W. et al., 1974. [2-year experiences with a combination treatment of Parkinsonism with L-dopa and a decarboxylase inhibitor (Benserazid, Ro 4-4602)]. *Wiener medizinische Wochenschrift (1946)*, 124(22), pp.340–4.

Birkmayer, W. & Hornykiewicz, O., 1961. [The L-3,4-dioxyphenylalanine (DOPA)-effect in Parkinson-akinesia]. *Wiener klinische Wochenschrift*, 73, pp.787–8.

Björklund, A. et al., 1997. Studies on neuroprotective and regenerative effects of GDNF in a partial lesion model of Parkinson's disease. *Neurobiology of disease*, 4(3-4), pp.186–200.

Björklund, T. et al., 2009. Optimization of continuous in vivo DOPA production and studies on ectopic DA synthesis using rAAV5 vectors in Parkinsonian rats. *Journal of neurochemistry*, 111(2), pp.355–67.

Blaese, R.M. et al., 1995. T lymphocyte-directed gene therapy for ADA- SCID: initial trial results after 4 years. *Science (New York, N.Y.)*, 270(5235), pp.475–80.

Borenfreund, E. et al., 1970. Studies of DNA-induced heritable alteration of mammalian cells. *The Journal of experimental medicine*, 132(6), pp.1071–89.

Braak, H. et al., Staging of brain pathology related to sporadic Parkinson's disease. *Neurobiology of aging*, 24(2), pp.197–211.

Bradbury, A.M. et al., 2015. A review of gene therapy in canine and feline models of lysosomal storage disorders. *Human gene therapy. Clinical development*, 26(1), pp.27–37.

Brimble, M.A. et al., 2016. New and improved AAVenues: current status of hemophilia B gene therapy. *Expert opinion on biological therapy*, 16(1), pp.79–92.

Burger, C. et al., 2004. Recombinant AAV viral vectors pseudotyped with viral capsids from serotypes 1, 2, and 5 display differential efficiency and cell tropism after delivery to different regions of the central nervous system. *Molecular therapy : the journal of the American Society of Gene Therapy*, 10(2), pp.302–17.

Camargo, S.M.R. et al., 2014. The molecular mechanism of intestinal levodopa absorption and its possible implications for the treatment of Parkinson's disease. *The Journal of pharmacology and experimental therapeutics*, 351(1), pp.114–23.

Carlsson, T. et al., 2005. Reversal of dyskinesias in an animal model of Parkinson's disease by continuous L-DOPA delivery using rAAV vectors. *Brain : a journal of neurology*, 128(Pt 3), pp.559–69.

Carta, M. et al., 2007. Dopamine released from 5-HT terminals is the cause of L-DOPA-induced dyskinesia in parkinsonian rats. *Brain : a journal of neurology*, 130(Pt 7), pp.1819–33.

Cavazzana-Calvo, M. et al., 2000. Gene therapy of human severe combined immunodeficiency (SCID)-X1 disease. *Science (New York, N.Y.)*, 288(5466), pp.669–72.

Cederfjäll, E. et al., 2013. Continuous DOPA synthesis from a single AAV: dosing and efficacy in models of Parkinson's disease. *Scientific reports*, 3, p.2157.

Cederfjäll, E. et al., 2012. Design of a single AAV vector for coexpression of TH and GCH1 to establish continuous DOPA synthesis in a rat model of Parkinson's disease. *Molecular therapy : the journal of the American Society of Gene Therapy*, 20(7), pp.1315–26.

Chaudhuri, K.R. & Schapira, A.H. V, 2009. Non-motor symptoms of Parkinson's disease: dopaminergic pathophysiology and treatment. *The Lancet. Neurology*, 8(5), pp.464–74.

Chiorini, J.A. et al., 1999. Cloning and characterization of adeno-associated virus type 5. *Journal of virology*, 73(2), pp.1309–19.

Chiorini, J.A. et al., 1997. Cloning of adeno-associated virus type 4 (AAV4) and generation of recombinant AAV4 particles. *Journal of virology*, 71(9), pp.6823–33.

Chiti, F. & Dobson, C.M., 2006. Protein misfolding, functional amyloid, and human disease. *Annual review of biochemistry*, 75, pp.333–66.

Christine, C.W. et al., 2009. Safety and tolerability of putaminal AADC gene therapy for Parkinson disease. *Neurology*, 73(20), pp.1662–9.

Curtin, J.A. et al., 2008. Bidirectional promoter interference between two widely used internal heterologous promoters in a late-generation lentiviral construct. *Gene therapy*, 15(5), pp.384–90.

Daubner, S.C., Le, T. & Wang, S., 2011. Tyrosine hydroxylase and regulation of dopamine synthesis. *Archives of biochemistry and biophysics*, 508(1), pp.1–12.

Davidoff, A.M. et al., 2003. Sex significantly influences transduction of murine liver by recombinant adeno-associated viral vectors through an androgen-dependent pathway. *Blood*, 102(2), pp.480–8.

Davidson, B.L. et al., 2000. Recombinant adeno-associated virus type 2, 4, and 5 vectors: transduction of variant cell types and regions in the mammalian central nervous system. *Proceedings of the National Academy of Sciences of the United States of America*, 97(7), pp.3428–32.

Degkwitz, R. et al., 1960. Über die Wirkungen des L-Dopa beim Menschen und deren Beeinflussung durch Reserpin, Chlorpromazin, Iproniazid und Vitamin B6. *Klinische Wochenschrift*, 38(3), pp.120–123.

Dethy, S. et al., 1997. Microdialysis-HPLC for plasma levodopa and metabolites monitoring in parkinsonian patients. *Clinical chemistry*, 43(5), pp.740–4.

Ding, W. et al., 2005. Intracellular trafficking of adeno-associated viral vectors. *Gene therapy*,

12(11), pp.873–80.

Ding, Z. et al., 2008. Correction of murine PKU following AAV-mediated intramuscular expression of a complete phenylalanine hydroxylating system. *Molecular therapy : the journal of the American Society of Gene Therapy*, 16(4), pp.673–81.

Dodiya, H.B. et al., 2010. Differential transduction following basal ganglia administration of distinct pseudotyped AAV capsid serotypes in nonhuman primates. *Molecular therapy : the journal of the American Society of Gene Therapy*, 18(3), pp.579–87.

Doehmer, J. et al., 1982. Introduction of rat growth hormone gene into mouse fibroblasts via a retroviral DNA vector: expression and regulation. *Proceedings of the National Academy of Sciences of the United States of America*, 79(7), pp.2268–72.

Doherty, K.M. et al., 2013. Parkin disease: a clinicopathologic entity? *JAMA neurology*, 70(5), pp.571–9.

Donnelly, M.L. et al., 2001. Analysis of the aphthovirus 2A/2B polyprotein "cleavage" mechanism indicates not a proteolytic reaction, but a novel translational effect: a putative ribosomal "skip". *The Journal of general virology*, 82(Pt 5), pp.1013–25.

Dowd, E. et al., 2005. The Corridor Task: a simple test of lateralised response selection sensitive to unilateral dopamine deafferentation and graft-derived dopamine replacement in the striatum. *Brain research bulletin*, 68(1-2), pp.24–30.

Drouin, L.M. & Agbandje-McKenna, M., 2013. Adeno-associated virus structural biology as a tool in vector development. *Future virology*, 8(12), pp.1183–1199.

Duan, D., Sharma, P., et al., 1998. Circular intermediates of recombinant adeno-associated virus have defined structural characteristics responsible for long-term episomal persistence in muscle tissue. *Journal of virology*, 72(11), pp.8568–77.

Duan, D., Yue, Y., et al., 1998. Polarity influences the efficiency of recombinant adenoassociated virus infection in differentiated airway epithelia. *Human gene therapy*, 9(18), pp.2761–76.

Duque, S.I. et al., 2015. A large animal model of spinal muscular atrophy and correction of phenotype. *Annals of neurology*, 77(3), pp.399–414.

Eiden, L.E. et al., 2004. The vesicular amine transporter family (SLC18): amine/proton antiporters required for vesicular accumulation and regulated exocytotic secretion of monoamines and acetylcholine. *Pflügers Archiv : European journal of physiology*, 447(5), pp.636–40.

Elsworth, J.D. & Roth, R.H., 1997. Dopamine synthesis, uptake, metabolism, and receptors: relevance to gene therapy of Parkinson's disease. *Experimental neurology*, 144(1), pp.4–9.

Emborg, M.E. et al., 2007. Subthalamic glutamic acid decarboxylase gene therapy: changes in motor function and cortical metabolism. *Journal of cerebral blood flow and metabolism : official journal of the International Society of Cerebral Blood Flow and Metabolism*, 27(3), pp.501–9.

Fabbrini, G. et al., 2007. Levodopa-induced dyskinesias. *Movement disorders : official journal of the Movement Disorder Society*, 22(10), pp.1379–89; quiz 1523.

Fagone, P. et al., 2011. Systemic Errors in Quantitative Polymerase Chain Reaction Titration of

Self-Complementary Adeno-Associated Viral Vectors and Improved Alternative Methods. *Human gene therapy*, 8, pp.1–8.

Faravelli, I. et al., 2015. Spinal muscular atrophy--recent therapeutic advances for an old challenge. *Nature reviews. Neurology*, 11(6), pp.351–9.

Feng, L. & Maguire-Zeiss, K., 2011. Gene therapy in Parkinson's disease: rationale and current status. *CNS drugs*, 24(3), pp.177–192.

Festing, M.F.W., 2010. Improving toxicity screening and drug development by using genetically defined strains. *Methods in molecular biology (Clifton, N.J.)*, 602, pp.1–21.

François, C., Yelnik, J. & Percheron, G., 1996. A stereotaxic atlas of the basal ganglia in macaques. *Brain research bulletin*, 41(3), pp.151–8.

Freed, C.R. et al., 2001. Transplantation of Embryonic Dopamine Neurons for Severe Parkinson's Disease. *New England Journal of Medicine*, 344(10), pp.710–719.

Friedmann, T., 1992. A brief history of gene therapy. *Nature genetics*, 2(2), pp.93–8.

Gao, G. et al., 2004. Clades of Adeno-associated viruses are widely disseminated in human tissues. *Journal of virology*, 78(12), pp.6381–8.

Gao, G.-P. et al., 2002. Novel adeno-associated viruses from rhesus monkeys as vectors for human gene therapy. *Proceedings of the National Academy of Sciences of the United States of America*, 99(18), pp.11854–9.

Gaspar, H.B. et al., 2004. Gene therapy of X-linked severe combined immunodeficiency by use of a pseudotyped gammaretroviral vector. *Lancet*, 364(9452), pp.2181–7.

Gaspar, H.B. et al., 2011. Long-term persistence of a polyclonal T cell repertoire after gene therapy for X-linked severe combined immunodeficiency. *Science translational medicine*, 3(97), p.97ra79.

Gehl, J., 2003. Electroporation: theory and methods, perspectives for drug delivery, gene therapy and research. *Acta physiologica Scandinavica*, 177(4), pp.437–47.

Gelsinger, P. & Shamoo, A.E., 2008. Eight years after Jesse 's death, are human research subjects any safer? *The Hastings Center report*, 38(2), pp.25–7.

Geoffroy, M.-C. & Salvetti, A., 2005. Helper functions required for wild type and recombinant adeno-associated virus growth. *Current gene therapy*, 5(3), pp.265–71.

George, L.A. & Fogarty, P.F., 2015. Gene Therapy for Hemophilia: Past, Present and Future. *Seminars in Hematology*, 53(1), pp.46–54.

Ghosh, A. & Duan, D., 2007. Expanding adeno-associated viral vector capacity: a tale of two vectors. *Biotechnology & genetic engineering reviews*, 24, pp.165–77.

Gibson, D.G. et al., 2009. Enzymatic assembly of DNA molecules up to several hundred kilobases. *Nature methods*, 6(5), pp.343–5.

Gil-Farina, I. et al., 2016. Recombinant AAV integration is not associated with hepatic genotoxicity in non-human primates and patients. *Molecular Therapy*.

Goins, W.F. et al., 2014. Engineering HSV-1 vectors for gene therapy. *Methods in molecular biology (Clifton, N.J.)*, 1144, pp.63–79.

Graham, F.L. & van der Eb, A.J., 1973. A new technique for the assay of infectivity of human

adenovirus 5 DNA. *Virology*, 52(2), pp.456–67.

Greger, I.H. et al., 1998. Transcriptional interference perturbs the binding of Sp1 to the HIV-1 promoter. *Nucleic acids research*, 26(5), pp.1294–301.

Grieger, J.C. & Samulski, R.J., 2012. Adeno-associated virus vectorology, manufacturing, and clinical applications. *Methods in enzymology*, 507, pp.229–54.

Grieger, J.C., Soltys, S.M. & Samulski, R.J., 2015. Production of Recombinant Adeno-associated Virus Vectors Using Suspension HEK293 Cells and Continuous Harvest of Vector From the Culture Media for GMP FIX and FLT1 Clinical Vector. *Molecular therapy : the journal of the American Society of Gene Therapy*, 24(2), pp.287–97.

Hacein-Bey-Abina, S. et al., 2010. Efficacy of gene therapy for X-linked severe combined immunodeficiency. *The New England journal of medicine*, 363(4), pp.355–64.

Hacein-Bey-Abina, S. et al., 2008. Insertional oncogenesis in 4 patients after retrovirus-mediated gene therapy of SCID-X1. *The Journal of clinical investigation*, 118(9), pp.3132–42.

Handa, A. et al., 2000. Adeno-associated virus (AAV)-3-based vectors transduce haematopoietic cells not susceptible to transduction with AAV-2-based vectors. *The Journal of general virology*, 81(Pt 8), pp.2077–84.

Hauck, B. & Xiao, W., 2003. Characterization of tissue tropism determinants of adeno-associated virus type 1. *Journal of virology*, 77(4), pp.2768–74.

Hauswirth et al., 2008. Treatment of leber congenital amaurosis due to RPE65 mutations by ocular subretinal injection of adeno-associated virus gene vector: short-term results of a phase I trial. *Human gene therapy*, 19(10), pp.979–90.

Hauswirth, W.W. & Berns, K.I., 1977. Origin and termination of adeno-associated virus DNA replication. *Virology*, 78(2), pp.488–99.

Heintz, C. et al., 2012. Quantification of phenylalanine hydroxylase activity by isotope-dilution liquid chromatography-electrospray ionization tandem mass spectrometry. *Molecular genetics and metabolism*, 105(4), pp.559–65.

Henckaerts, E. & Linden, R.M., 2010. Adeno-associated virus: a key to the human genome? *Future virology*, 5(5), pp.555–574.

High, K.H. et al., 2014. Current status of haemophilia gene therapy. *Haemophilia : the official journal of the World Federation of Hemophilia*, 20 Suppl 4, pp.43–9.

Hill, M.P. et al., 2004. Levetiracetam potentiates the antidyskinetic action of amantadine in the 1-methyl-4-phenyl-1,2,3,6-tetrahydropyridine (MPTP)-lesioned primate model of Parkinson's disease. *The Journal of pharmacology and experimental therapeutics*, 310(1), pp.386–94.

Hoehn, M.M. & Yahr, M.D., 2001. Parkinsonism: onset, progression, and mortality. 1967. *Neurology*, 57(10 Suppl 3), pp.S11–26.

Hoggan, M. D., Thomas, G. F. and Johnson, F.B., 1973. Continuous carriage of adenovirus-associated virus genome in cell culture in the absence of helper adenovirus. In *Proceedings of the Fourth Lepetit Colloquium*. pp. pp. 41–47.

Hohen, M.M. & Yahr, M.D., 1967. Parkinsonism: onset, progression and mortality. *Neurology*, 17(5), pp.427–442.

Horger, B.A. et al., 1998. Neurturin exerts potent actions on survival and function of midbrain dopaminergic neurons. *The Journal of neuroscience : the official journal of the Society for Neuroscience*, 18(13), pp.4929–37.

Horowitz, E.D. et al., 2013. Biophysical and ultrastructural characterization of adeno-associated virus capsid uncoating and genome release. *Journal of virology*, 87(6), pp.2994–3002.

Howe, S.J. et al., 2008. Insertional mutagenesis combined with acquired somatic mutations causes leukemogenesis following gene therapy of SCID-X1 patients. *The Journal of clinical investigation*, 118(9), pp.3143–50.

Hüser, D. et al., 2014. Adeno-associated virus type 2 wild-type and vector-mediated genomic integration profiles of human diploid fibroblasts analyzed by third-generation PacBio DNA sequencing. *Journal of virology*, 88(19), pp.11253–63.

Im, D.S. & Muzyczka, N., 1990. The AAV origin binding protein Rep68 is an ATP-dependent site-specific endonuclease with DNA helicase activity. *Cell*, 61(3), pp.447–57.

Imbert, C. et al., 2000. Comparison of eight clinical rating scales used for the assessment of MPTP-induced parkinsonism in the Macaque monkey. *Journal of neuroscience methods*, 96(1), pp.71–6.

Inagaki, K. et al., 2006. Robust systemic transduction with AAV9 vectors in mice: efficient global cardiac gene transfer superior to that of AAV8. *Molecular therapy : the journal of the American Society of Gene Therapy*, 14(1), pp.45–53.

Jackson, D.A., Symons, R.H. & Berg, P., 1992. Biochemical method for inserting new genetic information into DNA of simian virus 40: circular SV40 DNA molecules containing lambda phage genes and the galactose operon of Escherichia coli. 1972. *Biotechnology (Reading, Mass.)*, 24, pp.11–6.

Jarraya, B. et al., 2009. Dopamine gene therapy for Parkinson's disease in a nonhuman primate without associated dyskinesia. *Science translational medicine*, 1(2), p.2ra4.

Jenner, P., 2008. Molecular mechanisms of L-DOPA-induced dyskinesia. *Nature reviews. Neuroscience*, 9(9), pp.665–77.

Kageyama, T. et al., 2000. The 4F2hc/LAT1 complex transports L-DOPA across the blood-brain barrier. *Brain research*, 879(1-2), pp.115–21.

Kaludov, N. et al., 2001. Adeno-associated virus serotype 4 (AAV4) and AAV5 both require sialic acid binding for hemagglutination and efficient transduction but differ in sialic acid linkage specificity. *Journal of virology*, 75(15), pp.6884–93.

Kaplitt, M.G. et al., 2007. Safety and tolerability of gene therapy with an adeno-associated virus (AAV) borne GAD gene for Parkinson's disease: an open label, phase I trial. *Lancet*, 369(9579), pp.2097–105.

Kerr, J., Cotmore, S. & Bloom, M.E., 2005. *Parvoviruses*, CRC Press.

Khan, I.F., Hirata, R.K. & Russell, D.W., 2011. AAV-mediated gene targeting methods for human cells. *Nature protocols*, 6(4), pp.482–501.

Kirik, D. et al., 2001. Delayed infusion of GDNF promotes recovery of motor function in the partial lesion model of Parkinson's disease. *The European journal of neuroscience*, 13(8), pp.1589–

99.

Kirik, D. et al., 2002. Reversal of motor impairments in parkinsonian rats by continuous intrastriatal delivery of L-dopa using rAAV-mediated gene transfer. *Proceedings of the National Academy of Sciences of the United States of America*, 99(7), pp.4708–13.

Kish, S.J. et al., 2008. Preferential loss of serotonin markers in caudate versus putamen in Parkinson's disease. *Brain : a journal of neurology*, 131(Pt 1), pp.120–31.

Kish, S.J., Shannak, K. & Hornykiewicz, O., 1988. Uneven pattern of dopamine loss in the striatum of patients with idiopathic Parkinson's disease. Pathophysiologic and clinical implications. *The New England journal of medicine*, 318(14), pp.876–80.

Koenekoop, R.K., An overview of Leber congenital amaurosis: a model to understand human retinal development. *Survey of ophthalmology*, 49(4), pp.379–98.

Kohlbrenner, E. et al., 2012. Quantification of AAV particle titers by infrared fluorescence scanning of coomassie-stained sodium dodecyl sulfate-polyacrylamide gels. *Human gene therapy methods*, 23(3), pp.198–203.

Kordower, J.H. & Goetz, C.G., 1999. The first miracle in neurodegenerative disease: the discovery of oral levodopa. *Brain research bulletin*, 50(5-6), pp.377–8.

Kotin, R. & Siniscalco, M., 1990. Site-specific integration by adeno-associated virus. *Proceedings of the …*, 87(March), pp.2211–2215.

Kotin, R.M. et al., 1991. Mapping and direct visualization of a region-specific viral DNA integration site on chromosome 19q13-qter. *Genomics*, 10(3), pp.831–4.

Kühn, A.A. & Volkmann, J., 2016. Innovations in deep brain stimulation methodology. *Movement disorders : official journal of the Movement Disorder Society*.

Kurlan, R. et al., 1988. Erratic gastric emptying of levodopa may cause "random" fluctuations of parkinsonian mobility. *Neurology*, 38(3), pp.419–21.

Landsberg, L., 1972. L-dopa and cardiac arrhythmia. *N.Engl.J Med*, 286(0028-4793), p.218.

Lane, E. & Dunnett, S., 2008. Animal models of Parkinson's disease and L-dopa induced dyskinesia: how close are we to the clinic? *Psychopharmacology*, 199(3), pp.303–12.

de Lau, L.M.L. & Breteler, M.M.B., 2006. Epidemiology of Parkinson's disease. *Lancet neurology*, 5(6), pp.525–35.

Laughlin, C.A. et al., 1983. Cloning of infectious adeno-associated virus genomes in bacterial plasmids. *Gene*, 23(1), pp.65–73.

Leblois, A. et al., 2006. Competition between feedback loops underlies normal and pathological dynamics in the basal ganglia. *The Journal of neuroscience : the official journal of the Society for Neuroscience*, 26(13), pp.3567–83.

Lechardeur, D., Verkman, A.S. & Lukacs, G.L., 2005. Intracellular routing of plasmid DNA during non-viral gene transfer. *Advanced drug delivery reviews*, 57(5), pp.755–67.

Leonard, B.E., 1993. Principles of neural science, third edition. By E. R. Kandel, J. H. Schwartz and T. M. Jessell. Appleton & Lange, 1991. pp. 1135 + xxxvii. ISBN 0-8385-8068-8. *Human Psychopharmacology: Clinical and Experimental*, 8(4), pp.294–294.

Leriche, L. et al., 2009. Positron emission tomography imaging demonstrates correlation between

behavioral recovery and correction of dopamine neurotransmission after gene therapy. *The Journal of neuroscience : the official journal of the Society for Neuroscience*, 29(5), pp.1544–53.

Li, J.-Y. et al., 2008. Lewy bodies in grafted neurons in subjects with Parkinson's disease suggest host-to-graft disease propagation. *Nature medicine*, 14(5), pp.501–3.

Lin, D. et al., 2005. AAV2/5 vector expressing galactocerebrosidase ameliorates CNS disease in the murine model of globoid-cell leukodystrophy more efficiently than AAV2. *Molecular therapy : the journal of the American Society of Gene Therapy*, 12(3), pp.422–30.

Lin, L.F. et al., 1993. GDNF: a glial cell line-derived neurotrophic factor for midbrain dopaminergic neurons. *Science (New York, N.Y.)*, 260(5111), pp.1130–2.

Lisowski, L. et al., 2014. Selection and evaluation of clinically relevant AAV variants in a xenograft liver model. *Nature*, 506(7488), pp.382–6.

Lusby, E., Fife, K.H. & Berns, K.I., 1980. Nucleotide sequence of the inverted terminal repetition in adeno-associated virus DNA. *Journal of virology*, 34(2), pp.402–9.

Lux, K. et al., 2005. Green fluorescent protein-tagged adeno-associated virus particles allow the study of cytosolic and nuclear trafficking. *Journal of virology*, 79(18), pp.11776–87.

Maeda, H. et al., 2016. Re-evaluation of hepatocyte replacement by recipient-derived cells after allogenic liver transplantation: Discrepancy between clinical observations and a rat model. *Hepatology Research*, p.n/a–n/a.

Maguire, A.M. et al., 2008. Safety and efficacy of gene transfer for Leber's congenital amaurosis. *The New England journal of medicine*, 358(21), pp.2240–8.

Mandel, R.J. et al., 1998. Characterization of intrastriatal recombinant adeno-associated virus-mediated gene transfer of human tyrosine hydroxylase and human GTP-cyclohydrolase I in a rat model of Parkinson's disease. *The Journal of neuroscience : the official journal of the Society for Neuroscience*, 18(11), pp.4271–84.

Maniatis, T. et al., 1976. Amplification and characterization of a beta-globin gene synthesized in vitro. *Cell*, 8(2), pp.163–82.

Mann, R., Mulligan, R.C. & Baltimore, D., 1983. Construction of a retrovirus packaging mutant and its use to produce helper-free defective retrovirus. *Cell*, 33(1), pp.153–9.

Manno, C.S. et al., 2003. AAV-mediated factor IX gene transfer to skeletal muscle in patients with severe hemophilia B. *Blood*, 101(8), pp.2963–72.

Manno, C.S. et al., 2006. Successful transduction of liver in hemophilia by AAV-Factor IX and limitations imposed by the host immune response. *Nature medicine*, 12(3), pp.342–7.

Marcus, C.J., Laughlin, C.A. & Carter, B.J., 1981. Adeno-associated virus RNA transcription in vivo. *European journal of biochemistry / FEBS*, 121(1), pp.147–54.

Markowitz, D., Goff, S. & Bank, A., 1988. A safe packaging line for gene transfer: separating viral genes on two different plasmids. *Journal of virology*, 62(4), pp.1120–4.

Marks, W.J. et al., 2008. Safety and tolerability of intraputaminal delivery of CERE-120 (adeno-associated virus serotype 2-neurturin) to patients with idiopathic Parkinson's disease: an open-label, phase I trial. *Lancet neurology*, 7(5), pp.400–8.

Marks, W.J., Baumann, T.L. & Bartus, R.T., 2016. Long-Term Safety of Patients with Parkinson's Disease Receiving rAAV2-Neurturin (CERE-120) Gene Transfer. *Human gene therapy*.

Matheson, N.J. et al., 2015. Cell Surface Proteomic Map of HIV Infection Reveals Antagonism of Amino Acid Metabolism by Vpu and Nef. *Cell host & microbe*, 18(4), pp.409–23.

Matsushita, T. et al., 1998. Adeno-associated virus vectors can be efficiently produced without helper virus. *Gene therapy*, 5(7), pp.938–45.

Matsushita, T. et al., 2004. The adenovirus E1A and E1B19K genes provide a helper function for transfection-based adeno-associated virus vector production. *The Journal of general virology*, 85(Pt 8), pp.2209–14.

McCarty, D.M., 2008. Self-complementary AAV vectors; advances and applications. *Molecular therapy : the journal of the American Society of Gene Therapy*, 16(10), pp.1648–56.

McIntosh, J. et al., 2013. Therapeutic levels of FVIII following a single peripheral vein administration of rAAV vector encoding a novel human factor VIII variant. *Blood*, 121(17), pp.3335–44.

McLaughlin, S.K. et al., 1988. Adeno-associated virus general transduction vectors: analysis of proviral structures. *Journal of virology*, 62(6), pp.1963–73.

Meadows, A.S. et al., 2015. A GLP-Compliant Toxicology and Biodistribution Study: Systemic Delivery of an rAAV9 Vector for the Treatment of Mucopolysaccharidosis IIIB. *Human gene therapy. Clinical development*, 26(4), pp.228–42.

Mendell, J.R. et al., 2010. Dystrophin immunity in Duchenne's muscular dystrophy. *The New England journal of medicine*, 363(15), pp.1429–37.

Mendell, J.R. et al., 2009. Limb-girdle muscular dystrophy type 2D gene therapy restores alpha-sarcoglycan and associated proteins. *Annals of neurology*, 66(3), pp.290–7.

Miller, A.D., Law, M.F. & Verma, I.M., 1985. Generation of helper-free amphotropic retroviruses that transduce a dominant-acting, methotrexate-resistant dihydrofolate reductase gene. *Molecular and cellular biology*, 5(3), pp.431–7.

Mingozzi, F. et al., 2003. Induction of immune tolerance to coagulation factor IX antigen by in vivo hepatic gene transfer. *The Journal of clinical investigation*, 111(9), pp.1347–56.

Mittermeyer, G. et al., 2012. Long-term evaluation of a phase 1 study of AADC gene therapy for Parkinson's disease. *Human gene therapy*, 23(4), pp.377–81.

Mori, S. et al., 2004. Two novel adeno-associated viruses from cynomolgus monkey: pseudotyping characterization of capsid protein. *Virology*, 330(2), pp.375–83.

Morrison, C., 2015. $1-million price tag set for Glybera gene therapy. *Nature biotechnology*, 33(3), pp.217–8.

Moskovitz, C., Moses, H. & Klawans, H.L., 1978. Levodopa-induced psychosis: a kindling phenomenon. *The American journal of psychiatry*, 135(6), pp.669–75.

Mulligan, R.C., Howard, B.H. & Berg, P., 1979. Synthesis of rabbit beta-globin in cultured monkey kidney cells following infection with a SV40 beta-globin recombinant genome. *Nature*, 277(5692), pp.108–14.

Muramatsu et al., 2010. A phase I study of aromatic L-amino acid decarboxylase gene therapy for

Parkinson's disease. *Molecular therapy : the journal of the American Society of Gene Therapy*, 18(9), pp.1731–5.

Muramatsu, S. et al., 1996. Nucleotide sequencing and generation of an infectious clone of adeno-associated virus 3. *Virology*, 221(1), pp.208–17.

Muramatsu, S.-I. et al., 2002. Behavioral recovery in a primate model of Parkinson's disease by triple transduction of striatal cells with adeno-associated viral vectors expressing dopamine-synthesizing enzymes. *Human gene therapy*, 13(3), pp.345–54.

Nakai, H. et al., 2001. Extrachromosomal recombinant adeno-associated virus vector genomes are primarily responsible for stable liver transduction in vivo. *Journal of Viorology*, 75(15), pp.6969–6976.

Nakai, H. et al., 2005. Unrestricted hepatocyte transduction with adeno-associated virus serotype 8 vectors in mice. *Journal of virology*, 79(1), pp.214–24.

Nam, H.-J. et al., 2011. Structural studies of adeno-associated virus serotype 8 capsid transitions associated with endosomal trafficking. *Journal of virology*, 85(22), pp.11791–9.

Napolitano, A. et al., 1999. Pharmacokinetics and pharmacodynamics of L-Dopa after acute and 6-week tolcapone administration in patients with Parkinson's disease. *Clinical neuropharmacology*, 22(1), pp.24–9.

Nathwani, A.C. et al., 2012. Adenovirus-Associated Virus Vector-Mediated Gene Transfer in Hemophilia B. , 365(25), pp.2357–2365.

Nathwani, A.C. et al., 2011. Adenovirus-associated virus vector-mediated gene transfer in hemophilia B. *The New England journal of medicine*, 365(25), pp.2357–65.

Nathwani, A.C. et al., 2014. Long-term safety and efficacy of factor IX gene therapy in hemophilia B. *The New England journal of medicine*, 371(21), pp.1994–2004.

Nathwani, A.C. et al., 2006. Self-complementary adeno-associated virus vectors containing a novel liver-specific human factor IX expression cassette enable highly efficient transduction of murine and nonhuman primate liver. *Blood*, 107(7), pp.2653–61.

Nault, J.-C. et al., 2015. Recurrent AAV2-related insertional mutagenesis in human hepatocellular carcinomas. *Nature genetics*, 47(10), pp.1187–93.

Negre, O. et al., 2016. Gene Therapy of the β-Hemoglobinopathies by Lentiviral Transfer of the β(A(T87Q))-Globin Gene. *Human gene therapy*, 27(2), pp.148–65.

Niemeyer, G.P. et al., 2009. Long-term correction of inhibitor-prone hemophilia B dogs treated with liver-directed AAV2-mediated factor IX gene therapy. *Blood*, 113(4), pp.797–806.

Nonnenmacher, M. & Weber, T., 2011. Adeno-associated virus 2 infection requires endocytosis through the CLIC/GEEC pathway. *Cell host & microbe*, 10(6), pp.563–76.

Nutt, J.G. et al., 1984. The "on-off" phenomenon in Parkinson's disease. Relation to levodopa absorption and transport. *The New England journal of medicine*, 310(8), pp.483–8.

Nutt, J.G., Obeso, J.A. & Stocchi, F., 2000. Continuous dopamine-receptor stimulation in advanced Parkinson's disease. *Trends in neurosciences*, 23(10 Suppl), pp.S109–15.

Nutt, J.G. & Woodward, W.R., 1986. Levodopa pharmacokinetics and pharmacodynamics in fluctuating parkinsonian patients. *Neurology*, 36(6), pp.739–44.

Nutt, J.G., Woodward, W.R. & Anderson, J.L., 1985. The effect of carbidopa on the pharmacokinetics of intravenously administered levodopa: the mechanism of action in the treatment of parkinsonism. *Annals of neurology*, 18(5), pp.537–43.

Nyholm, D. et al., 2005. Duodenal levodopa infusion monotherapy vs oral polypharmacy in advanced Parkinson disease. *Neurology*, 64(2), pp.216–23.

O'Connor, D.M. & Boulis, N.M., 2015. Gene therapy for neurodegenerative diseases. *Trends in molecular medicine*, 21(8), pp.504–12.

Obeso, J.A. et al., 2000. Pathophysiology of the basal ganglia in Parkinson's disease. *Trends in neurosciences*, 23(10 Suppl), pp.S8–19.

Olanow, C., Schapira, A. & Rascol, O., 2000. Continuous dopamine-receptor stimulation in early Parkinson's disease. *Trends in neurosciences*, 23(10), pp.117–126.

Olanow, C.W. et al., 2003. A double-blind controlled trial of bilateral fetal nigral transplantation in Parkinson's disease. *Annals of neurology*, 54(3), pp.403–14.

Olanow, C.W. et al., 2014. Continuous intrajejunal infusion of levodopa-carbidopa intestinal gel for patients with advanced Parkinson's disease: a randomised, controlled, double-blind, double-dummy study. *The Lancet. Neurology*, 13(2), pp.141–9.

Olsson, M. et al., 1995. Forelimb akinesia in the rat Parkinson model: differential effects of dopamine agonists and nigral transplants as assessed by a new stepping test. *The Journal of neuroscience : the official journal of the Society for Neuroscience*, 15(5 Pt 2), pp.3863–75.

Orth, G., Vielle, F. & Changeux, J.P., 1967. On the arginase of the Shope papillomas. *Virology*, 31(4), pp.729–32.

Palfi, S. et al., 2014. Long-term safety and tolerability of ProSavin, a lentiviral vector-based gene therapy for Parkinson's disease: a dose escalation, open-label, phase 1/2 trial. *Lancet (London, England)*, 383(9923), pp.1138–46.

Pañeda, A. et al., 2009. Effect of adeno-associated virus serotype and genomic structure on liver transduction and biodistribution in mice of both genders. *Human gene therapy*, 20(8), pp.908–17.

Parkinson, J., 2002. An Essay on the Shaking Palsy. *The Journal of Neuropsychiatry and Clinical Neurosciences*.

Pastores, G.M. & Hughes, D.A., 2015. Non-neuronopathic lysosomal storage disorders: Disease spectrum and treatments. *Best practice & research. Clinical endocrinology & metabolism*, 29(2), pp.173–82.

Pedroso de Lima, M.C. et al., 2001. Cationic lipid-DNA complexes in gene delivery: from biophysics to biological applications. *Advanced drug delivery reviews*, 47(2-3), pp.277–94.

Petri, K. et al., 2015. Presence of a trs-Like Motif Promotes Rep-Mediated Wild-Type Adeno-Associated Virus Type 2 Integration. *Journal of virology*, 89(14), pp.7428–32.

Pierce, E.A. & Bennett, J., 2015. The Status of RPE65 Gene Therapy Trials: Safety and Efficacy. *Cold Spring Harbor perspectives in medicine*, 5(9), p.a017285.

Piguet, F. et al., 2012. Correction of brain oligodendrocytes by AAVrh.10 intracerebral gene therapy in metachromatic leukodystrophy mice. *Human gene therapy*, 23(8), pp.903–14.

Pillay, S. et al., 2016. An essential receptor for adeno-associated virus infection. *Nature*, 530(7588), pp.108–12.

Pilz, I.H. et al., 2012. Mutation in the platelet-derived growth factor receptor alpha inhibits adeno-associated virus type 5 transduction. *Virology*, 428(1), pp.58–63.

Pinxos, G. & Watson, C., 1986. The Rat Brain: In Stereotaxic Coordinates: George Paxinos, Charles Watson. , p.264. Available at: http://www.amazon.com/The-Rat-Brain-Stereotaxic-Coordinates/dp/0125476213 [Accessed March 27, 2016].

Prasad, K.M. & Trempe, J.P., 1995. The adeno-associated virus Rep78 protein is covalently linked to viral DNA in a preformed virion. *Virology*, 214(2), pp.360–70.

Qing, K. et al., 1999. Human fibroblast growth factor receptor 1 is a co-receptor for infection by adeno-associated virus 2. *Nature medicine*, 5(1), pp.71–7.

Qiu et al., 2006. Parvovirus RNA processing strategies. , pp.253–273.

Rabotti, G.F., 1963. INCORPORATION OF DNA INTO A MOUSE TUMOR IN VIVO AND IN VITRO. *Experimental cell research*, 31, pp.562–5.

Rafii, M.S. et al., 2014. A phase1 study of stereotactic gene delivery of AAV2-NGF for Alzheimer's disease. *Alzheimer's & dementia : the journal of the Alzheimer's Association*, 10(5), pp.571–81.

Raper, S.E. et al., 2003. Fatal systemic inflammatory response syndrome in a ornithine transcarbamylase deficient patient following adenoviral gene transfer. *Molecular genetics and metabolism*, 80(1-2), pp.148–58.

Reardon, S., 2015. Leukaemia success heralds wave of gene-editing therapies. *Nature*, 527(7577), pp.146–147.

Rivière, C., Danos, O. & Douar, A.M., 2006. Long-term expression and repeated administration of AAV type 1, 2 and 5 vectors in skeletal muscle of immunocompetent adult mice. *Gene therapy*, 13(17), pp.1300–8.

Roudaut, C. et al., 2013. Restriction of calpain3 expression to the skeletal muscle prevents cardiac toxicity and corrects pathology in a murine model of limb-girdle muscular dystrophy. *Circulation*, 128(10), pp.1094–104.

Ruottinen, H.M. & Rinne, U.K., 1996. A double-blind pharmacokinetic and clinical dose-response study of entacapone as an adjuvant to levodopa therapy in advanced Parkinson's disease. *Clinical neuropharmacology*, 19(4), pp.283–96.

Rutledge, E.A., Halbert, C.L. & Russell, D.W., 1998. Infectious clones and vectors derived from adeno-associated virus (AAV) serotypes other than AAV type 2. *Journal of virology*, 72(1), pp.309–19.

Rylander Ottosson, D. & Lane, E., 2016. Striatal Plasticity in L-DOPA- and Graft-Induced Dyskinesia; The Common Link? *Frontiers in cellular neuroscience*, 10, p.16.

Sambrook, J. et al., 1968. The integrated state of viral DNA in SV40-transformed cells. *Proceedings of the National Academy of Sciences of the United States of America*, 60(4), pp.1288–95.

Samulski, R.J. et al., 1982. Cloning of adeno-associated virus into pBR322: rescue of intact virus from the recombinant plasmid in human cells. *Proceedings of the National Academy of*

Sciences of the United States of America, 79(6), pp.2077–81.

Samulski, R.J. et al., 1983. Rescue of adeno-associated virus from recombinant plasmids: gene correction within the terminal repeats of AAV. *Cell*, 33(1), pp.135–43.

Samulski, R.J. et al., 1991. Targeted integration of adeno-associated virus (AAV) into human chromosome 19. *The EMBO Journal*, 10(12), pp.3941–3950.

Samulski, R.J., Chang, L.S. & Shenk, T., 1987. A recombinant plasmid from which an infectious adeno-associated virus genome can be excised in vitro and its use to study viral replication. *Journal of virology*, 61(10), pp.3096–101.

Samulski, R.J., Chang, L.S. & Shenk, T., 1989. Helper-free stocks of recombinant adeno-associated viruses: normal integration does not require viral gene expression. *Journal of virology*, 63(9), pp.3822–8.

San Sebastian, W. et al., 2012. Safety and tolerability of magnetic resonance imaging-guided convection-enhanced delivery of AAV2-hAADC with a novel delivery platform in nonhuman primate striatum. *Human gene therapy*, 23(2), pp.210–7.

Sanlioglu, S. et al., 2000. Endocytosis and nuclear trafficking of adeno-associated virus type 2 are controlled by rac1 and phosphatidylinositol-3 kinase activation. *Journal of virology*, 74(19), pp.9184–96.

Sarkar, R. et al., 2006. Long-term efficacy of adeno-associated virus serotypes 8 and 9 in hemophilia a dogs and mice. *Human gene therapy*, 17(4), pp.427–39.

Schallert, T. et al., 1979. Excessive bracing reactions and their control by atropine and L-DOPA in an animal analog of Parkinsonism. *Experimental neurology*, 64(1), pp.33–43.

Schmidt, M., Voutetakis, A., et al., 2008. Adeno-associated virus type 12 (AAV12): a novel AAV serotype with sialic acid- and heparan sulfate proteoglycan-independent transduction activity. *Journal of virology*, 82(3), pp.1399–406.

Schmidt, M. et al., 2006. Identification and characterization of novel adeno-associated virus isolates in ATCC virus stocks. *Journal of virology*, 80(10), pp.5082–5.

Schmidt, M., Govindasamy, L., et al., 2008. Molecular characterization of the heparin-dependent transduction domain on the capsid of a novel adeno-associated virus isolate, AAV(VR-942). *Journal of virology*, 82(17), pp.8911–6.

Schmittgen, T.D. & Livak, K.J., 2008. Analyzing real-time PCR data by the comparative C(T) method. *Nature protocols*, 3(6), pp.1101–8.

Schuh, L.A. & Bennett, J.P., 1993. Suppression of dyskinesias in advanced Parkinson's disease. I. Continuous intravenous levodopa shifts dose response for production of dyskinesias but not for relief of parkinsonism in patients with advanced Parkinson's disease. *Neurology*, 43(8), pp.1545–50.

Seeberger, L.C. & Hauser, R.A., 2015. Carbidopa levodopa enteral suspension. *Expert opinion on pharmacotherapy*, 16(18), pp.2807–17.

Seisenberger, G. et al., 2001. Real-time single-molecule imaging of the infection pathway of an adeno-associated virus. *Science (New York, N.Y.)*, 294(5548), pp.1929–32.

Sheridan, C., 2011. Gene therapy finds its niche. *Nature biotechnology*, 29(2), pp.121–128.

Shimotohno, K. & Temin, H.M., 1981. Formation of infectious progeny virus after insertion of herpes simplex thymidine kinase gene into DNA of an avian retrovirus. *Cell*, 26(1 Pt 1), pp.67–77.

Snyder, Richard O., Moullier, P., 2011. Adeno-Associated Virus - Methods and Protocols | Richard O. Snyder | Springer. , p.462. Available at: http://www.springer.com/us/book/9781617793691 [Accessed February 16, 2016].

Sonntag, F. et al., 2006. Adeno-associated virus type 2 capsids with externalized VP1/VP2 trafficking domains are generated prior to passage through the cytoplasm and are maintained until uncoating occurs in the nucleus. *Journal of virology*, 80(22), pp.11040–54.

Sonntag, F., Schmidt, K. & Kleinschmidt, J.A., 2010. A viral assembly factor promotes AAV2 capsid formation in the nucleolus. *Proceedings of the National Academy of Sciences of the United States of America*, 107(22), pp.10220–5.

Srivastava, A., Lusby, E.W. & Berns, K.I., 1983. Nucleotide sequence and organization of the adeno-associated virus 2 genome. *Journal of virology*, 45(2), pp.555–64.

Stefanis, L., 2012. α-Synuclein in Parkinson's disease. *Cold Spring Harbor perspectives in medicine*, 2(2), p.a009399.

Sterneckert, J.L., Reinhardt, P. & Schöler, H.R., 2014. Investigating human disease using stem cell models. *Nature Reviews Genetics*, 15(9), pp.625–639.

Stieger, K. et al., 2009. Detection of intact rAAV particles up to 6 years after successful gene transfer in the retina of dogs and primates. *Molecular therapy : the journal of the American Society of Gene Therapy*, 17(3), pp.516–23.

Streck, C.J. et al., 2005. Adeno-associated virus vector-mediated systemic delivery of IFN-beta combined with low-dose cyclophosphamide affects tumor regression in murine neuroblastoma models. *Clinical cancer research : an official journal of the American Association for Cancer Research*, 11(16), pp.6020–9.

Summerford, C., Bartlett, J.S. & Samulski, R.J., 1999. AlphaVbeta5 integrin: a co-receptor for adeno-associated virus type 2 infection. *Nature medicine*, 5(1), pp.78–82.

Summerford, C. & Samulski, R.J., 1998. Membrane-associated heparan sulfate proteoglycan is a receptor for adeno-associated virus type 2 virions. *Journal of virology*, 72(2), pp.1438–45.

Sun, M., 1982. Martin Cline loses appeal on NIH grant. *Science (New York, N.Y.)*, 218(4567), p.37.

Surosky, R.T. et al., 1997. Adeno-associated virus Rep proteins target DNA sequences to a unique locus in the human genome. *Journal of virology*, 71(10), pp.7951–9.

Tabebordbar, M. et al., 2015. In vivo gene editing in dystrophic mouse muscle and muscle stem cells. *Science (New York, N.Y.)*, 351(6271), pp.407–11.

Tardieu, M. et al., 2014. Intracerebral administration of adeno-associated viral vector serotype rh.10 carrying human SGSH and SUMF1 cDNAs in children with mucopolysaccharidosis type IIIA disease: results of a phase I/II trial. *Human gene therapy*, 25(6), pp.506–16.

Tatham, A.L. et al., 2009. GTP cyclohydrolase I expression, protein, and activity determine intracellular tetrahydrobiopterin levels, independent of GTP cyclohydrolase feedback regulatory protein expression. *The Journal of biological chemistry*, 284(20), pp.13660–8.

Terheggen, H.G. et al., 1975. Unsuccessful trial of gene replacement in arginase deficiency. *Zeitschrift für Kinderheilkunde*, 119(1), pp.1–3.

Tseng, J.L. et al., 1998. Neurturin protects dopaminergic neurons following medial forebrain bundle axotomy. *Neuroreport*, 9(8), pp.1817–22.

Uchida, K. et al., 1992. Tetrahydrobiopterin-dependent functional recovery in 6-hydroxydopamine-treated rats by intracerebral grafting of fibroblasts transfected with tyrosine hydroxylase cDNA. *Developmental neuroscience*, 14(2), pp.173–80.

Ungerstedt, U. & Arbuthnott, G.W., 1970. Quantitative recording of rotational behavior in rats after 6-hydroxy-dopamine lesions of the nigrostriatal dopamine system. *Brain research*, 24(3), pp.485–93.

Ustione, A., Piston, D.W. & Harris, P.E., 2013. Minireview: Dopaminergic regulation of insulin secretion from the pancreatic islet. *Molecular endocrinology (Baltimore, Md.)*, 27(8), pp.1198–207.

Valstar, M.J. et al., 2010. Mucopolysaccharidosis type IIIA: clinical spectrum and genotype-phenotype correlations. *Annals of neurology*, 68(6), pp.876–87.

Vaughan, R.A. & Foster, J.D., 2013. Mechanisms of dopamine transporter regulation in normal and disease states. *Trends in pharmacological sciences*, 34(9), pp.489–96.

Vila, M. et al., 1997. Consequences of nigrostriatal denervation on the functioning of the basal ganglia in human and nonhuman primates: an in situ hybridization study of cytochrome oxidase subunit I mRNA. *The Journal of neuroscience : the official journal of the Society for Neuroscience*, 17(2), pp.765–73.

Vila, M. et al., 1996. Metabolic activity of the basal ganglia in parkinsonian syndromes in human and non-human primates: a cytochrome oxidase histochemistry study. *Neuroscience*, 71(4), pp.903–12.

Vogel, R. et al., 2013. Viral and Cellular Components of AAV2 Replication Compartments. *The open virology journal*, 7, pp.98–120.

Wade, D.N., Mearrick, P.T. & Morris, J.L., 1973. Active transport of L-dopa in the intestine. *Nature*, 242(5398), pp.463–5.

Walker, S.J., Roskoski, R. & Vrana, K.E., 1994. Catalytic core of rat tyrosine hydroxilase: terminal deletion analysis of bacterially expressed enzymes. *Biochimica et Biophysica Acta*, 1206, pp.113–119.

Walters, R.W. et al., 2001. Binding of adeno-associated virus type 5 to 2,3-linked sialic acid is required for gene transfer. *The Journal of biological chemistry*, 276(23), pp.20610–6.

Wang et al., 2003. Rapid and highly efficient transduction by double-stranded adeno-associated virus vectors in vitro and in vivo. *Gene therapy*, 10(26), pp.2105–11.

Wang, B.-W. et al., 2014. MicroRNA-208a increases myocardial fibrosis via endoglin in volume overloading heart. *PloS one*, 9(1), p.e84188.

Wang, K. et al., 2015. Angelica sinensis polysaccharide attenuates concanavalin A-induced liver injury in mice. *International immunopharmacology*, 31, pp.140–148.

Wang, Z. et al., 2005. Adeno-associated virus serotype 8 efficiently delivers genes to muscle and

heart. *Nature biotechnology*, 23(3), pp.321–8.

Warren Olanow, C. et al., 2015. Gene delivery of neurturin to putamen and substantia nigra in Parkinson disease: A double-blind, randomized, controlled trial. *Annals of neurology*, 78(2), pp.248–57.

Wigler, M. et al., 1978. Biochemical transfer of single-copy eucaryotic genes using total cellular DNA as donor. *Cell*, 14(3), pp.725–31.

Wistuba, A. et al., 1995. Intermediates of adeno-associated virus type 2 assembly: identification of soluble complexes containing Rep and Cap proteins. *Journal of virology*, 69(9), pp.5311–9.

Wolf, D.A. et al., 2015. Gene therapy for neurologic manifestations of mucopolysaccharidoses. *Expert opinion on drug delivery*, 12(2), pp.283–96.

Wong, F.F. et al., 2015. Effective Gene Delivery to Valvular Interstitial Cells Using Adeno-Associated Virus Serotypes 2 and 3. *Tissue engineering. Part C, Methods*, 21(8), pp.808–15.

Wong, S.Y., Pelet, J.M. & Putnam, D., 2007. Polymer systems for gene delivery—Past, present, and future. *Progress in Polymer Science*, 32(8-9), pp.799–837.

Xiao, W. et al., 2002. Adenovirus-facilitated nuclear translocation of adeno-associated virus type 2. *Journal of virology*, 76(22), pp.11505–17.

Yan, Z. et al., 2000. Trans-splicing vectors expand the utility of adeno-associated virus for gene therapy. *Proceedings of the National Academy of Sciences of the United States of America*, 97(12), pp.6716–21.

Yang, J. et al., 1999. Concatamerization of Adeno-Associated Virus Circular Genomes Occurs through Intermolecular Recombination Concatamerization of Adeno-Associated Virus Circular Genomes Occurs through Intermolecular Recombination. *Journal of Viorology*, 73(11), pp.9468–9477.

Ylä-Herttuala, S., 2012. Endgame: glybera finally recommended for approval as the first gene therapy drug in the European union. *Molecular therapy : the journal of the American Society of Gene Therapy*, 20(10), pp.1831–2.

Zanta-Boussif, M.A. et al., 2009. Validation of a mutated PRE sequence allowing high and sustained transgene expression while abrogating WHV-X protein synthesis: application to the gene therapy of WAS. *Gene therapy*, 16(5), pp.605–19.

Zigmond, R.E., Schwarzschild, M.A. & Rittenhouse, A.R., 1989. Acute regulation of tyrosine hydroxylase by nerve activity and by neurotransmitters via phosphorylation. *Annual review of neuroscience*, 12, pp.415–61.

Zincarelli, C. et al., 2008. Analysis of AAV serotypes 1-9 mediated gene expression and tropism in mice after systemic injection. *Molecular therapy : the journal of the American Society of Gene Therapy*, 16(6), pp.1073–80.

Zinn, E. & Vandenberghe, L.H., 2014. Adeno-associated virus: fit to serve. *Current opinion in virology*, 8, pp.90–7.

Appendix A. List of Primers

Primer Name	Sequence 5'->3'
AA01	CCAAGCTGAGCCCCTAAAATGGGCAAACATTG
AA02	CCAACCTGCAGGTCAGTTCCAAAGGTTGGAATC
AA03	CACCAACCTGCAGGATGGAGAAGGGCCCTGTG
AA004	CACCAAGACAAGGTCGGTCGACTAAAAAACCTC C
AA006	CCAAGACAAGGTCCCCTAAAATGGGCAAACATTG
AA07	CCCAATTCGAATCAGTTCCAAAGGTTGGAATC
AA09	TTCAAGTCCCACCACTCGCG
AA10	AGCTGGTCGGGTGGCTCGT
AA16	CCAAGCTAGCATGGAGAAGGGCCCTGTG
AA17	CCAAGCTAGCGGTCGACTAAAAAACCTCC
AA33	CCAAGCTAGCATGAGCCCCGCGGGGCCCAAG
AA34	CCAAGCTAGCGGGGGATCTTCGATGCTAGAC
AA37	CCAATCTAGAGCTGAGCCCCTAAAATGGGCAAACATTG
AA38	CCAATCTAGAGCATGCCCAATTCGAAGACAAGGTCGGTCGACTAAAAAACCTCCCACAC
AA39	AAGACTACAAGTTCAGGAGCG
AA40	ACACCTCGCATTACCATACAC
AA41	TCCCAAGAAAAGTGTCAGAGC
AA42	AAGGCGATCTCAGCAATCAG
AA60	GTACCAGTCAGTCTACTTCGT
AA65	GATTCCAACCTTTGGAACTGATTCGAAATTCAAGCTGCTAGCAAGGATC
AA73	CACCAA CCTGCAGGATTCAAGCTGCTAGCAAGG
AA84	CAATGTTTGCCCATTTTAGGGGACCTTGTCAGATCTGGTCGACTAAAAAACCTCC
AA85	GGAGGTTTTTTAGTCGACCAGATCTGACAAGGTCCCCTAAAATGGGCAAACATTG
AA133	CCAACAATTGCATTCATTTTATGTTTCAGGTTCAGGGGGAGGTGTGGGAGGTTTTT TAGTCGACCGAATTGGCCGCTACGCGTACTAGTTATTAATAGTAATCAATTACGG
AA134	CCAAAGATCTGGGGGATCTTCGATGCTAGACGATCCAGACATGATAAGATACATTG ATGAGTTTG
AA150	CCAAGCTGAGCTATCGATTGGCTCCGGTGC
AA151	CCAACCTGCAGGCCGCGTCACGACACCTGTG
AA152	CCAACCTGCAGGATTCAAGCTCGTAGCAAGGATCC
AA153	CCAAAGATCTTTAGCCAATGGCACTCAGCG
AA154	TCGAGGTTTAAACGCGG
AA155	CCAATTCGAATGTGGCCATATTATCATCGTG
AA156	CCAATTCGAAATGAGCACGGAAGGTGG
AA157	CCAAACTAGTTAGCTCCTAATGAGAGTCAGG
AA158	CCAAGTCGACATAAGACGAGCAAAAGCTTGTATAAG
LA43	CCAAAGATCTGGGCTGCAGGAATTGGCCGCT
LA44	CTTGGGCCCCGCGGGGCTCATGGTGACCGGTGGATCCTT
LA45	AAGGATCCACCGGTCACCATGAGCCCCGCGGGGCCCAAG
LA46	CCAAAGATCTGGGGGATCTTCGATGCTAGAC
LA47	CCAAATGCATCCCCATCGATGATCC
LA48	CCAACCTCAGACAGGCAGTGCAGG

Appendix B. List of Clones

Name	Genotype
pAA001	pTRUF11::*LP1*
pAA002	pTRUF11::*LP1-GCH1*
pAA003	pSUB201::*LP1-GCH1*
pAA004	pUC18::*LP1-GCH1*
pAA005	pUC18::*LP1-GCH1-LP1*
pAA006	pBluescript::*LP1-GCH1-LP1*
pAA009	sc-backbone::*LP1-GCH*1
pAA010	sc-backbone::*LP1*-Δ155TH
pAA016	sc-backbone::*HLP-Δ155TH*
pAA017	pBluescript::*LP1-GCH1-LP1-tTH*
pAA018	pBluescript::*LP1-GCH1-LP1-tTH*
pAA019	pSUB201::*LP1-GCH1-LP1-tTH*
pAA020	pBluescript::LP1-PTS-2A-GCH1-LP1-tTH
pAA056	sc-backbone::*EF1a-Δ155TH-miR208aT*
pAA057	pBluescript::*EF1a-GCH1-LP1-tTH-WPRE*
pAA058	pBluescript::*EF1a-tTH-LP1-tTH-WPRE*
pAA059	pBluescript::*EF1a-tTH-IRES-tTH-WPRE*
pAA060	pSUB201::*EF1a-tTH-IRES-tTH-WPRE*
pAA061	pSUB201::*EF1a-tTH-IRES-PTPS-GCH1-WPRE*
pAA062	pSUB201::*EF1a-tTH-IRES-PTPS-GCH1-WPRE-miR208aT*
pAA063	pSUB201::*EF1a-TH-IRES-PTPS-GCH1-WPRE-miR208aT*
pGPT002	pTRUF11::*SYN-GCH1-SYN-TH-WPRE*
pLA109	pTRUF11::*SYN-GCH1-SYN-tTH-WPRE*
pGPT004	pTRUF11::*SYN-GCH1-CMV-TH*